Visual cortical alpha rhythms: Function and relation to other dynamic signatures in local networks

Karen Hawkins

Thesis submitted for the degree of Doctor of Philosophy

The University of Hull and the University of York

Hull York Medical School

January 2016

Abstract

The alpha rhythm (8-12Hz) was the first EEG rhythm recorded by Hans Berger in 1929. Despite being the earliest rhythm discovered, alpha rhythms remain the most mysterious in terms of mechanism and function. In the visual system, post-stimulus alpha oscillations are observed upon closing of the eyes or removal of visual stimulus. Alpha rhythms have been implicated in functional inhibition and short term memory.

This thesis presents a rat *in vitro* model of the cortical alpha rhythm. This was achieved by mimicking the neuromodulatory changes that occur upon the removal of visual stimulus. Beta oscillations were induced by excitation of the visual cortex slice using the glutamate agonist kainate [800nM] to mimic sensory stimulation. This excitatory drive was then reduced using the AMPA and KA receptor antagonist NBQX [5μM], followed by the blocking of neuronal I_h current with DK-AH269 [10μM] to produce alpha frequency oscillations.

Alpha activity was seen throughout all cortical laminae, with alpha power predominating in layer IV of the V1. The rhythm was found to be critically dependent upon NMDA receptor-mediated connections between neurons which required the need to be potentiated in the prior excitation phase leading to beta frequency oscillations. Alpha activity was also dependent upon gap junctional coupling and had neuromodulatory effects similar to the human profile of alpha.

Alpha oscillations were generated by pyramidal neurons found in layer IV of the V1 which elicited burst discharges. The alpha rhythm was not dominated by synaptic inhibition despite the functional inhibition role it is thought to play. Instead, the alpha rhythm appeared to dynamically uncouple activity in the primary thalamorecipient neurons (layer IV regular spiking cells) from down-stream activity in both supragranular and infragranular layers. In this manner, the alpha rhythm appears to be ideally constructed to prevent ascending visual information from both passing on to higher order visual areas, and also being influenced by top-down signal from these areas.

Publications

Hawkins K, Simon A, Whittington MA. Gamma and Beta oscillations control stellate neuron output in layer IV of the rat primary visual cortex [abstract]. In: British Neuroscience Association; 2015 Apr 12-15; Edinburgh, UK.

Hawkins K, Simon A, Whittington MA. Alpha rhythms in the rat visual cortex are generated by local networks in layer 4 [abstract]. In: Fens featured regional meeting; 2015 Oct 7-10; Thessaloniki, Greece.

Hawkins K, Simon A, Whittington MA. Physiological mechanisms responsible for generating alpha frequency oscillations in the rat visual cortex [abstract]. In: Fens featured regional meeting; 2016 Nov 12-16; San Diego, USA.

Table of contents

List of Illustrations

Chapter 1 General Introduction

Chapter 2 Methods

Chapter 3 The generation of alpha oscillations in the primary visual cortex

Chapter 4 Results – Pharmacological Studies

Chapter 5 Results – Intracellular Recordings

Chapter 6 General Discussion

List of abbreviations

ABC kit (Avidin-Biotin Horseradish peroxidase complex)

ACh acetylcholine

ACSF artificial cerebrospinal fluid

AHDH attentional deficit hyperactivity disorder

ADP after depolarisation

AHP after hyperpolarisation

AMPA α-amino-3-hydroxy-5-methyl-4-isoxazolepropionic acid

ANOVA analysis of variance

ASD autism spectrum disorders

Biocytin (N^6-[5-[(3a*S*,4*S*,6a*R*)-Hexahydro-2-oxo-1*H*-thieno[3,4-*d*]imidazol-4-yl]-1-oxopentyl]-L-lysine),

BOLD blood oxygen level dependent

Ca^{2+} calcium ion

cAMP cyclic adenosine monophosphate

CBX Carbenoxolone ((3β,20β)-3-(3-Carboxy-1-oxopropoxy)-11-oxoolean-12-en-29-oic acid disodium)

CCH Carbachol (2-Hydroxyethyl)trimethylammonium chloride carbamate

CIQ (3-Chlorophenyl) [3,4-dihydro-6,7-dimethoxy-1-[(4-methoxyphenoxy)methyl]-2(1*H*)-isoquinolinyl]methanone

CNS central nervous system

Co 101244 ((1-[2-(4-Hydroxyphenoxy)ethyl]-4-[(4-methylphenyl)methyl]-4-piperidinol hydrochloride)),

COMT catechol-o-methyl transferase

CPP (3-((*R*)-2-Carboxypiperazin-4-yl)-propyl-1-phosphonic acid)

CSD current source density

DHPG (*RS*)-3,5-Dihydroxyphenylglycine

DMN default mode network

DMSO dimethyl sulfoxide

DK-AH 269 ((S)-(+)-7,8-Dimethoxy-3-[[1-(2-(3,4-dimethoxyphenyl)ethyl)-3-piperidinyl]methyl]-1,3,4,5-tetrahydro-2H-3-benzazepin-2-one hydrochloride)

EEG encephalogram

EPSP excitatory postsynaptic potential

ETOH ethanol

FFT fast Fourier transform

fMRI functional magnetic resonance imaging

FRB fast rhythmic bursting

GABA gamma-aminobutyric acid

GP globus pallidus

HFO high frequency oscillations

HTB high threshold bursts

HTC high threshold bursting thalamocortical neurons

Ifenprodil ((1*R**,2*S**)-*erythro*-2-(4-Benzylpiperidino)-1-(4-hydroxyphenyl)-1-propanol hemitartrate),

I_h hyperpolarisation activated current

ING interneuron network gamma

IPSP inhibitory postsynaptic potential

Isopentane (2-Methylbutane),

K^+ potassium

KA Kainate ((2*S*,3*S*,4*S*)-Carboxy-4-(1-methylethenyl)-3-pyrrolidineacetic acid),

LFP local field potential

LGN lateral geniculate nucleus

LTD long term depression

LTP long term potentiation

mAChR muscarinic acetylcholine receptors

MEG magnetoencephalogram

Mg^{2+} magnesium

mGLUR1 metabotropic glutamate receptor type 1

MT middle temporal

MUA Multiunit activity

Na^{2+} sodium ion

NaF fast voltage dependent sodium channels

NGS Normal Goat Serum

Nicotine ((*S*)-(-)-1-Methyl-2-(3-pyridyl)pyrrolidine (+)-ditartrate salt),

Noradrenaline (4-[(1*R*)-2-Amino-1-hydroxyethyl]-1,2-benzenediol (L-(+))-bitartrate salt),

NBQX (2,3-Dioxo-6-nitro-1,2,3,4-tetrahydrobenzo[*f*]quinoxaline-7-sulfonamide disodium salt),

NMDA N-methyl-D-aspartate

NNC 55-0396 ((1*S*,2*S*)-2-[2-[[3-(1*H*-Benzimidazol-2-yl)propyl]methylamino]ethyl]-6-fluoro-1,2,3,4-tetrahydro-1-(1-methylethyl)-2-naphthalenyl cyclopropanecarboxylate dihydrochloride),

NREM non-rapid eye movement

O-LM oriens-lacunosum moleculare

PA Picric acid

PB phosphate buffer

PFA Paraformaldehyde

PG persistent gamma

PING pyramidal interneuron network gamma

PND postnatal day

PPDA ((2*S**,3*R**)-1-(Phenanthren-2-carbonyl)piperazine-2,3-dicarboxylic acid),

RE reticular cells

REM rapid eye movement

RMP resting membrane potential

RSA rhythmic slow activity

sACSF sucrose artificial cerebrospinal fluid

SEM standard error of the mean

SKF 81297 ((±)-6-Chloro-2,3,4,5-tetrahydro-1-phenyl-1*H*-3-benzazepine hydrobromide),

Gabazine (6-Imino-3-(4-methoxyphenyl)-1(6*H*)-pyridazinebutanoic acid hydrobromide),

Sucrose (β-D-Fructofuranosyl α-D-glucopyranoside),

SWO slow wave oscillations

SYM 2206 ((±)-4-(4-Aminophenyl)-1,2-dihydro-1-methyl-2-propylcarbamoyl-6,7-methylenedioxyphthalazine),

TBS TRIS buffer solution

TC thalamocortical

TCN 213 (N-(Cyclohexylmethyl)-2-[(5-[(phenylmethyl)amino]-1,3,4-thiadiazol-2-yl}thio]acetamide),

UBP 301 ((α*S*)-α-Amino-3-[(4-carboxyphenyl)methyl]-3,4-dihydro-5-iodo-2,4-dioxo-1(2*H*)-pyrimidinepropanoic acid),

V1 primary visual cortex

V2 secondary visual cortex

VFO very fast oscillations

ZD-7288 (4-Ethylphenylamino-1,2-dimethyl-6-methylaminopyrimidinium chloride),

Acknowledgements

First and foremost, a huge thanks to Miles for being the best supervisor. Thank you for the opportunity, your continued support, your patience, encouragement and enthusiasm and for remembering my hollow legs. I would like to give a special mention to Roger Traub for all your hard work with the modelling and Anna Simon for your help and amazing work with the immuno saving me from my chopped ham slices!

Thanks to the members of the lab, firstly Steve, thanks for being the best big brother a girl could ask for, and for remembering me those 3 long years ago. You have been a huge help to me over the years on top of being a good friend, and thanks for reading my thesis. Thanks to Nat for being you! Iain for helping me through the long days of writing up and always accompanying me to the pub when I needed it. Thanks to Mark for all of your advice and showing me your *in vivo* work.

Big thanks to my mum and dad for supporting me my whole life and always pushing me to reach my goals, you're the best! Thanks to my grandma and grandad for being fabulous and my second mum and dad. My late Granny and Grandpa for the financial support throughout my education, my 2 sisters Jo and Rach for listening to me moan, taking the mic and being my best friends and the newest addition; my little Lily who brightens up my days. Need to thank my best friends in no particular order: Lauren for being the most wonderful housemate, you've made York a much better place and thank you for the weekend you spent helping me with my click click clicks, thanks to both Aimee and Vicky for always being at the other end of the phone on a daily basis, that group message has been my saving grace, thanks to Nicole, Jenny and Tess, you've all made the past few years amazing. I'm running out of space now and to be quite honest, I'm sick of writing…enjoy!

I confirm that this work is original and that if any passage(s) or diagram(s) have been copied from academic papers, books, the internet or any other sources these are clearly identified by the use of quotation marks and the reference(s) is fully cited. I certify that, other than where indicated, this is my own work and does not breach the regulations of HYMS, the University of Hull or the University of York regarding plagiarism or academic conduct in examinations. I have read the HYMS Code of Practice on Academic Misconduct, and state that this piece of work is my own and does not contain any unacknowledged work from any other sources.

Chapter 1: General Introduction

Over the last century huge advances in our understanding of brain function have occurred. Out of these advances two general principles arise: Firstly specific functions are, to a large extent, anatomically compartmentalised in the central nervous system (CNS). Distinct areas of the CNS are activated during certain motor, affective and cognitive tasks as revealed by functional magnetic resonance imaging (fMRI) (Huettel SA, 2014), and through selective loss of function following spatially localised stroke damage (Calautti and Baron, 2003). Secondly, the coordination of activity of neurons within discrete brain areas, and coordination of neurons across areas with different primary functions, is performed in the time dimension (Lopes da Silva, 1991).

The timing of activity in neuronal populations has been shown to be intrinsically linked to certain aspects of brain function (Gray and Singer, 1989; O'Keefe and Recce, 1993). The time at which one neuron generates an output (action potential) relative to the average activity in the population of neurons around it appears to be most important. Such average activity is readily recorded, non-invasively, as brain waves via the encephalogram (EEG or MEG). However, the most common and earliest brain wave to be discovered (the alpha rhythm (for history see (Gastaut, 1974)) is still the most mysterious in terms of function and underlying mechanism.

The aim of this section is to provide the background used to shape the experiments performed in this thesis to try and address the mechanism and function of the alpha rhythm.

1.1 The visual cortex

The alpha rhythm (8-12 Hz) occurs in many brain regions such as sensorimotor and temporal cortices (where it is known as the mu and tau rhythm respectively), the frontal lobes and the visual cortex (see below). In mammals the largest magnitude alpha rhythm is observed in the visual cortex. It was therefore decided to focus on this area of the brain to try and generate a model that would allow further understanding of alpha rhythm mechanism and function. In doing so it is necessary to consider what may be 'special' anatomically and cytoarchitectonically to give rise to the very large observed alpha rhythms there.

1.1.1 Structure

The visual cortex is one of the most specialised sensory structures in the brain. It is located at the back of the brain in the occipital lobe and consists of the primary visual cortex (V1) – also called the striate cortex - and extrastriate areas (V2-V5). Almost all visual information reaches the brain through the primary visual cortex. In humans, the V1 contains 6 layers of cells; the main input layer from the visual thalamus is the highly developed and heterogeneous layer IV. Its laminar structure is completely different from all other brain regions; layer IV contains a strip of white matter visible under light microscopy. This consists of a vast amount of myelinated axons (Funkhouser, 1915), lending it the alternative name 'striate cortex'. Interlaminar vertical connections allow the relay of cortical inputs and outputs. Horizontal connections allow for information to be transferred adjacently and to other cortical areas.

Neurons in supragranular and infragranular layers resemble cytoarchitectonically those reported in other primary sensory areas. Layer 2/3 neurons tended to be regular spiking pyramids with excitatory and inhibitory synaptic inputs similar to those seen for somatosensory and auditory cortices (Jang et al., 2012). Layer 5 neurons were generally classified as regular spiking and burst firing (Zarrinpar and Callaway, 2014) as seen for auditory and parietal layer 5 neurons (Roopun et al., 2006; Roopun et al., 2010).

Similarly, the large layer IV in the V1 contained a mixture of spiny stellate (multipolar) excitatory neurons and small pyramidal neurons as seen in the primary input layer in other sensory areas (Feldman and Peters, 1978). Inputs to these layer IV cells from visual thalamus were seen to be large and rapidly adapting (MacLean et al., 2006; Kloc and Maffei, 2014) relative to, for example, the auditory thalamocortical pathway (Richardson et al., 2009). The pyramidal cells contain long axons which project out of the cortex as well as locally. There are two types of stellate cells: spiny stellate cells and smooth stellate cells containing spiny or smooth dendrites respectively. They are small cells with axons which terminate within the V1. Pyramidal and spiny stellate cells are excitatory and utilize excitatory neurotransmitters such as acetylcholine and glutamate. Smooth stellate cells are inhibitory and contain GABA (Lund, 1973; Lund and Yoshioka, 1991; Peters and Sethares, 1991).

From the above, other than the larger, more overtly sublaminated nature of layer IV in the V1 there appears to be little in the literature that points to a putative mechanism for the large-amplitude alpha rhythm generation in this area. However, very little is known about the intrinsic and synaptic properties of V1 layer IV neurons during rhythmic activity and so this was investigated in this thesis.

1.1.2 Connections of the Primary Visual Cortex

Another possibility for the large-scale presence of the alpha rhythm in the V1 is that it manifests through the convergence of inputs from other brain regions. We therefore need to consider the connections to this area in more detail.

The lateral geniculate nucleus (LGN) is found in the thalamus of the brain and is the main receiver of visual information from the retina, with around 90% of axons from the retina terminating here. The LGN contains 6 layers; neurons within the different layers are segregated according to size. Magnocellular (M) cells (responsible for contrast, depth and movement) are large cells found in layers 1 and 2 of the LGN. Parvocellular (P) cells (critical for colour and position) are smaller cells found in

layers 3-6 (Livingstone MS, 1988). Inputs from the LGN terminate mainly in layer IV of the V1 (Nauta, 1954).

As mentioned above, layer IV in the V1 is highly specialised. It is subdivided into four different layers: 4A, 4B, 4Cα and 4Cβ (figure 1.1). The different neurons of the LGN terminate in different sublayers of layer 4; M cells primarily terminating in 4Cα and 4B and P cells terminating in 4Cβ and 4A (Hubel and Weisel, 1972; Fitzpatrick et al., 1983; Blasdel, 1983). Between the M and P layers of the LGN there are intralaminar (koniocellular) layers (Kaas et al., 1978). K cells (concerned with short wavelength colour) terminate in superficial layers 2 and 3 of the primary visual cortex in structures known as 'blobs'.

Information from the retina enters the lateral geniculate nucleus and is transmitted to the primary visual cortex by the above described geniculate neurons. Information flows through the layers of the cortex starting with spiny stellate cells which distribute the input to supra- and infragranular layers whose pyramidal cells project back subcortically and out to other regions of the brain.

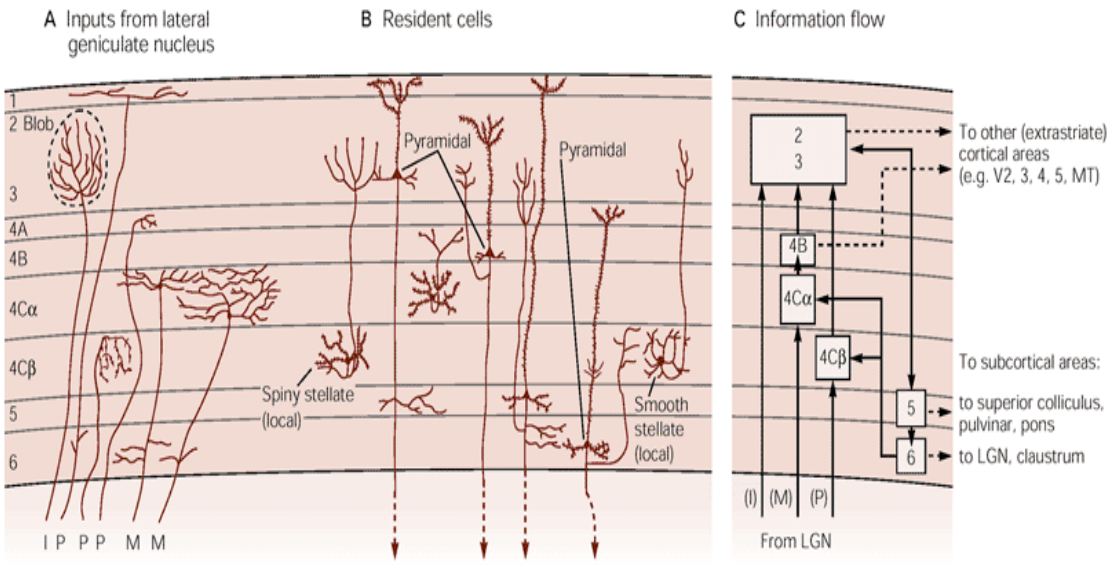

Figure 1.1 Connections and layers of the primary visual cortex. Adapted from Kandel ER (2000) (A) Inputs from the lateral geniculate nucleus terminate mostly in layer IV. The intralaminar (I) cells terminate in blobs in layers 2 and 3. Parvocellular (P) neurons end in layer 4Cβ with minor inputs to 4A and 1. Magnocellular (M) neurons end in layer 4Cα. Both M and P pathways have axons terminating in layer 6. (B) Resident cells of the primary visual cortex. Pyramidal and stellate cells are contained within the visual cortex. Pyramidal cells are excitatory with long, spiny dendrites and axons that project out of the cortex. Spiny stellate cells are excitatory and smooth stellate cells inhibitory; these cells are local. (C) Inputs from M and P cells terminate on spiny stellate cells in 4C layer subtypes, these project to layer 4B and 2/3. Inputs from I cells terminate in layers 2 and 3. Layers 2 and 3 contain axons from pyramidal cells in layers 5 and 6. Layer 6 pyramidal cells feedback to smooth stellate cells in layer 4C. Cells in layers 2, 3 and 4B project to other extrastriate cortical areas. Cells in layers 5 and 6 project to subcortical areas (i.e. LGN).

1.1.3 Function

The primary function of the visual cortex is the processing of visual information. While performing visual cognitive tasks, this area is seen to be the source of a rich array of brain rhythms (in addition to the alpha rhythm), which have been the focus of much study for over a century. It has been shown to generate gamma rhythms (Gray and Singer, 1989; Oke et al., 2010) and was the source of the original work linking these 30–80 Hz rhythms with primary sensory processing theories. It also

generates beta rhythms (12-30Hz) (Tallon-Baudry et al., 2001) and, most famously, alpha rhythms (8-12 Hz) (Berger, 1929).

Work linking brain function to rhythmic changes in the electrical activity of populations of neurons began with the invention of the electroencephalogram (EEG), though recently more invasive and *in vitro* techniques have been used to great effect to expand on this relationship. The next section considers a general overview of brain rhythm subtypes, their mechanisms (where known) and their relation to visual cortical function.

1.2 The EEG

The electroencephalogram (EEG) is a non-invasive method of recording electrical activity from the brain. Populations of neurons give rise to synchronised neural activity, known as neuronal oscillations which can be recorded by placing electrodes over the scalp. The first discovery of the electrical nature of the brain was by Richard Caton in 1875, who observed electrical impulses from the surface of the skull in living animals. Hans Berger then went on to develop the EEG in 1929. Using the EEG he was able to describe the different brain rhythms present in the brain, most famously the alpha rhythm (8-12Hz) in the occipital cortex, and its suppression upon opening of the eyes. Since this early work, EEG studies have shown oscillations occur at a range of distinct frequencies depending on the subject's behavioural state. Rhythmic activity is constantly ongoing throughout the brain with activity being most obvious in a state of sleep, with very large amplitude rhythms occurring at a low frequency. In contrast during a state of attentiveness, higher frequency rhythms occur at a lower amplitude suggesting the frequency of these rhythms are related to behavioural states.

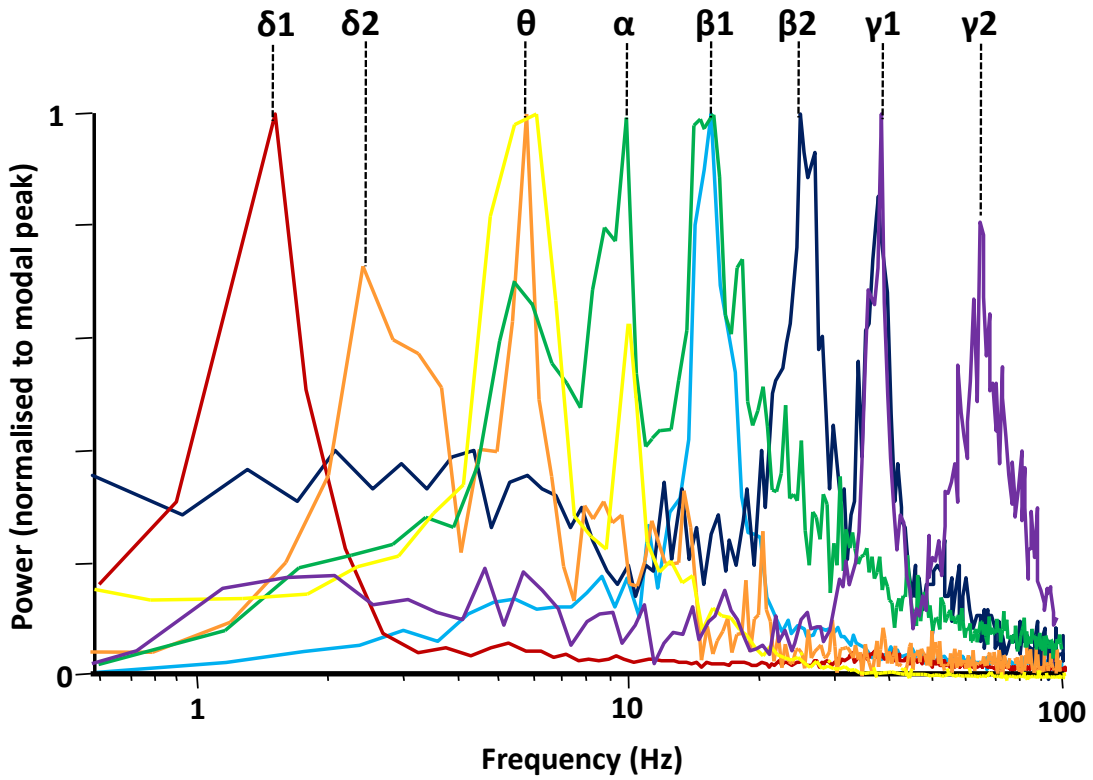

Figure 1.2. Multiple EEG-like oscillations generated from brain slices *in vitro*. The figure shows a montage of spectra derived from different brain slices (frontal cortex, parietal cortex, and auditory cortex) in different physiological and neuromodulatory conditions. All rhythms were 'persistent' in that they were generated continuously and all were recorded as local field potentials. Whittington, unpublished figure.

1.3 Neuronal oscillations

As previously mentioned, neuronal oscillations are critical in understanding how the electrical activity of the brain is associated with the behavioural state. Network oscillations of frequencies equivalent to those seen in EEG studies can be generated *in vitro,* from isolated sections of rodent brain. They show very similar characteristics to human EEG recordings, sharing the same frequency bands (alpha, beta and gamma). The exception is theta oscillations which have been shown to be slower in humans (1-4Hz) than rodents (4-10Hz), in *in vivo* recordings from the hippocampus (Watrous et al., 2013; Jacobs, 2014). The reproduction of a broad spectrum of EEG-like oscillations in very small, isolated sections (figure 1.2) of brain strongly suggests that their underlying mechanisms involve local neuronal circuits.

Thus, these models are useful in studying and understanding the mechanisms underlying the generation of these rhythms in many ways: at a cellular level i.e. what cell types are involved, the synaptic connectivity of each rhythm and their local network function in terms of shaping cortical inputs, outputs and horizontal interactions.

1.4 Classification of oscillations

Neuronal oscillations are typically classified into distinct frequency bands to help quantify their involvement in determining the behavioural state. However, for the most part, this frequency classification also reflects the different mechanisms underlying each of the rhythms (Kopell et al., 2010). Below is an introduction to the various forms of EEG rhythm that can be recorded. Rhythms that are not explored experimentally in this thesis are mentioned only briefly. Those that feature in chapter 3 are dealt with in more detail, with specific reference to visual cortical function.

1.4.1 Slow wave oscillations

Slow wave oscillations (SWO) (<1Hz) dominate the EEG during deep sleep and anaesthesia (Steriade et al., 1993b) and are thought to represent a sleep state involved in declarative memory consolidation (Steriade et al., 1993a; Sirota and Buzsaki, 2005). They are large amplitude oscillations, suggesting robust local synchrony, and are thought to be generated intracortically with the involvement of vast cortical connections. SWO have been observed in the cortex of anaesthetised cats and can survive thalamic lesions (Steriade et al., 1993a).

SWO have been modelled *in vitro* using brain slice preparations from ferret neocortex (Sanchez-Vives and McCormick, 2000). They were found to originate in layer V of the cortex, propagating up to layer IV and layers II/III, generated from interplay between excitatory pyramidal cells and inhibitory interneurons. The depolarising ‘up’ phase and a hyperpolarising ‘down’ phase allows a self-maintained circuit.

1.4.2 Delta oscillations

Delta oscillations (1-4Hz) are also high amplitude oscillations associated with sleep, predominating during stages 3-4 of non-rapid eye movement (NREM) sleep and, again, are associated with memory consolidation and formation (Huber et al., 2004). The delta oscillation has 2 components, one which originates in the cortex and one in the thalamus.

Delta oscillations generated in the thalamus are thought to be mediated by intrinsic cellular conductances: hyperpolarization activated current (I_h) and low-threshold calcium current (I_t) (Crunelli et al., 2006). There are delta oscillations which are cortical in origin (Fell et al., 2002) and can persist without the thalamus (Steriade et al., 1993b). As with slow waves, cortical delta was also observed originating in layer V of rat neocortex (Carracedo et al., 2013) generated by interplay between excitatory NMDA receptor-mediated recurrent connections between layer 5 intrinsic bursting pyramids and $GABA_B$ mediated inhibition.

1.4.3 Theta oscillations

The theta rhythm (4-8Hz) is most commonly seen in the CA1 region of the hippocampus. It is seen in the hippocampus nested in gamma oscillations during exploratory behaviour (Bragin et al., 1995). It is also observed during rapid eye movement (REM) sleep (Jouvet, 1969). Initially the theta rhythm was thought to be involved with arousal as it occurs together with a desynchronised EEG in the neocortex. It has been implicated in locomotor activity (Vanderwolf, 1969) and learning and memory (Hasselmo and Eichenbaum, 2005).

Theta rhythms are thought to be generated by rhythmic firing from excitatory principal cells and fast-spiking inhibitory interneurons acting via dendritic $GABA_A$ receptors with slow postsynaptic kinetics (Banks et al., 2000; Rotstein et al., 2005). It is proposed that theta rhythms, co-expressed with gamma oscillations, are involved in the coding and retrieval of episodic memories by allowing for interactions between cortical structures and the hippocampus (Nyhus and Curran, 2010).

Theta rhythms have also been observed in the thalamus of cats during slow wave sleep, drowsiness and relaxed wakefulness (Kanamori, 1993). Interestingly, their occurrence in thalamus may be related to the alpha rhythms that form the main topic of this thesis: Alpha rhythms during wakefulness have been shown to be gradually replaced by theta rhythms before the onset of slow wave sleep (Nieldermeyer, 1993). Whether or not theta and alpha rhythms, at least in thalamus, are mechanistically related remains to be seen. However, this is a distinct possibility given the overlap between the two rhythm bands often seen in hippocampus: Both EEG bands are commonly joined together and are collectively termed 'rhythmic slow activity (RSA)' (Klemm, 1976).

1.4.4 Very fast oscillations (VF0s)

Very fast oscillations (VFOs) are oscillations greater than 80Hz. They occur over a broad range of frequencies and, in physiological conditions, are seen transiently, nested within slower frequency rhythms like delta, beta II, gamma and transient events like physiological sharp waves. In these cases they are also variously known as high frequency oscillations (HFO) (Hunt et al., 2006), ripples (Csicsvari et al., 1999) and 'high gamma' (Canolty et al., 2006). When associated with sharp waves they appear to represent the time-compressed replay of sequences of place-cell activation during prior exploratory epochs (Gerrard et al., 2008). When associated with gamma or beta II rhythms they appear to represent the background, stochastic activity present in networks of electrically-coupled axons on principal cells (Whittington and Traub, 2003).

Mechanistically, the available data strongly suggest they are generated by ectopic action potential generation in excitatory neuronal axons. When these axons are randomly connected via gap junctions these action potentials percolate through a purely axonal network, in a manner whereby the modal frequency of the VFO corresponds to the mean path length in the axonal plexus (Traub et al., 1999b; Traub et al., 2004). As a consequence of this apparent origin, VFO can be recorded in local field potentials when back propagation of axonally–generated action potentials leads to brief bursts of activity in principal cell somata, as in beta II

rhythms (Roopun et al., 2006). In addition, when action potential back propagation is limited VFO can still be see 'down-stream' from principal cell axons as compound excitatory postsynaptic potentials onto local interneurons (Gloveli et al., 2005). VFO are also prominent in the cerebellum where the principal cells are GABAergic. Here gap junctions between principal cells (Purkinje cells) and local interneurons are suggested by dye-coupling data (Middleton et al., 2008).

VFO are associated with epileptiform activity. In epileptic patients VFO (80>200 Hz) occur at the onset of some seizures and are thought to contribute to the initiation of the full seizures themselves (Traub et al., 2001).

1.4.5 Beta oscillations

In the EEG literature there are generally two sub-categories of beta oscillations, beta I (12-20Hz) and beta II (20-30Hz). Beta I oscillations are prominent in areas involved in inputs and outputs of the motor system (Baker et al., 1999). Beta II oscillations are observed prior to motor function but not throughout the task itself (MacKay and Mendonca, 1995). In general, beta rhythms (12-30Hz) appear to be specifically involved in higher cognitive functions such as motor tasks, longer range cortical interactions i.e. neuronal synchronization associated with co-ordination of different cortical areas; and visuomotor integration (Roelfsema et al., 1997; Classen et al., 1998; Baker et al., 1999). Beta rhythms are prominent in the motor cortex; they are seen to decrease with movement suggesting they are involved with a disengagement of the motor cortex (Salmelin and Hari, 1994; Murthy and Fetz, 1996). Beta is also thought to be involved in memory formation (Traub et al., 1999b) and in the maintenance of sensory representations over a short period of time as seen in delayed match to sample tests (Tallon-Baudry et al., 2001; Tallon-Baudry et al., 2004).

An *in vitro* model for beta II rhythms was established in layer V of the somatosensory cortex using kainic acid as a general activator of excitatory synaptic communication (Roopun et al., 2006). A gamma rhythm was also observed concurrently in the superficial layers of the neocortex; however, the beta II rhythm

survived a cut through layer IV proving it to be independent of the gamma rhythm. This form of beta rhythm was found to be generated by networks of intrinsically bursting pyramidal cells in LV of neocortex and is thought to be generated by non-synaptic mechanisms as it survived blockade of synaptic transmission, but depended upon gap-junctional mediated coupling. However, the mechanisms behind the generation of beta II rhythms have been shown to vary in primary sensory areas and polymodal association areas (Roopun et al., 2010). This study modelled a beta II rhythm *in vitro* in the rat primary auditory cortex that did not occur in the polymodal association area. Glutamatergic excitation induced a beta II oscillation in LV association cortex whereas cholinergic neuromodulation generated this rhythm in LV primary auditory cortex. It was suggested the cholinergic modulation allowed for communication between the primary and secondary cortices.

The beta I rhythm is seen *in vivo* after gamma rhythms, in the detection of novel stimuli (Haenschel et al., 2000) and visual short-term memory (Tallon-Baudry et al., 1999; Tallon-Baudry et al., 2004). *In vitro* studies in hippocampus suggested that this 'post-gamma' beta I rhythm was manifested through the potentiation of recurrent excitatory synapses between pyramidal cells (Traub et al., 1999a). Such a plastic change in the local network connectivity is highly reminiscent of a substrate for memory (Bliss and Collingridge, 1993) and has been shown to have computational advantages in that it allows the local network rhythm to respond preferentially to inputs selected on the basis of their relative strengths (Olufsen et al., 2003).

Further evidence for a role for beta I rhythms in memory and higher-order cognitive processes comes from computational modelling work using data from a different *in vitro* model of this rhythm (Roopun et al., 2006). This study found that reducing synaptic excitation following a period of concurrent beta II and gamma rhythm generation caused the two independent rhythms (manifested in deep and superficial cortical layers respectively) to merge into a single beta I rhythm which was co-ordinated between the different layers. The authors suggested the function of this may be to allow for the combination of information processed at two

different sites (Kramer et al., 2008; Roopun et al., 2008). The plastic nature of the transformation from beta II to beta I rhythms allowed the subsequent 'build-up' of further temporally coordinated patterns of neuronal activity – thus a cortical representation of a sensory input could be modified and expanded as further sensory information was received (Kopell et al., 2011).

Beta rhythms may also be involved in attentional processing. It is known that beta rhythms 'carry' information down from higher order cortical areas to primary sensory areas (Buschman and Miller, 2007; Iversen et al., 2009) where they may influence the processing of sensory information through a process termed 'biased competition' (Reynolds et al., 1999). The transition from beta II to beta I rhythms in higher-order cortical areas, coupled with the generation of a cholinergic beta rhythm in primary sensory areas (see above) is predicted to provide the substrate for such biased competition (Lee et al., 2013).

1.4.6 Beta rhythms in the visual cortex

Given the proposed general role of beta rhythms in attention and short term memory it is perhaps not surprising that beta frequency oscillations are associated with an attentive state in the visual system. Wrobel et al. (1994) found an enhanced beta activity in the LGN and primary visual cortex of cats when attending to visual stimuli. Similarly, (Güntekin et al., 2013) showed that EEG evoked beta oscillations had increased power upon presentation of visual stimuli in human subjects. Beta oscillations are thought to enhance perceptive performance (Hanslmayr et al., 2007). Higher amplitude, synchronised beta activity was generated in receipt of visual stimuli more likely to be related to prior stimuli in a sequence (Piantoni et al., 2010; Quentin et al., 2014).

The situation is perhaps more complex than a simple 1:1 relationship between beta and visual attention. During high cognitive load two distinct frequencies of beta are seen in visual cortex-projecting thalamic areas (Wrobel et al., 2007) and with very high loads an overall decrease in beta power has been reported (Rouhinen et al., 2013). This ambiguity is also seen for the correlation between beta rhythms and

short-term memory. The original demonstration by Tallon-Baudry (see above) has been validated by many researchers: Memorised visual images are associated with significantly greater generation of beta I rhythms than ignored images (Onton et al., 2005). Beta rhythms are larger when reward anticipation is associated with successful memory formation (Bunzeck et al., 2011) and visual beta rhythm power decreases with age concurrently with memory performance (Krause et al., 2010)). Despite this there are also reports of decreases in beta power under certain visual memory conditions (Park and Rugg, 2010; Waldhauser et al., 2012).

Much of the confusion in the literature appears to arise from relationships between beta rhythms and alpha rhythms (see below). Many visual researchers do not find functional differences between the alpha rhythm and the lower beta rhythm band (Liang et al., 2005; Buffalo et al., 2011). This confusing relationship will be explored experimentally in chapter 3.

1.4.7 Gamma oscillations

Gamma oscillations (30-80Hz) as seen throughout the whole brain, are implicated in a range of higher cognitive functions such as attention and memory (Jensen et al., 2007). Gamma rhythms have been shown to be important in the processing of sensory information (Jokeit and Makeig, 1994), selective attention (Tiitinen et al., 1993), short term memory (Tallon-Baudry et al., 1998) and for the execution of motor commands (Szurhaj et al., 2005). There is a very large amount of evidence implicating them in forming the primary cortical representation of sensory input. This has been seen in a modality-specific manner with olfactory cortical gamma being generated by smell (Freeman, 1978), somatosensory gamma by touch (Pfurtscheller and Neuper, 1992) and auditory cortex gamma by sound (Pantev et al., 1991). But by far the most studied sensory modality has been vision and the role of gamma rhythms here will be introduced below in section 1.4.11. In addition, gamma oscillations are not exclusively confined to wakefulness when information processing is expected to happen, they are seen during REM sleep and during phases of slow sleep oscillations (Steriade et al., 1996).

Gamma oscillations can be readily generated *in vitro* through a range of different models of local circuit activation: Metabotropic glutamate receptor activation (Whittington et al., 1995); Kainate receptor activation via application of kainic acid (KA) (Cunningham et al., 2003); activation of the cholinergic pathway with application of carbachol (Traub et al., 2000). Each of these different models generates gamma rhythms with different properties in different brain regions. From all the evidence from *in vitro* studies, there appear to be 3 different mechanisms which are thought to underlie the generation of gamma rhythms. These are interneuron network gamma (ING), pyramidal-interneuron network gamma (PING) and persistent gamma (PG).

1.4.8 Interneuron network gamma

The ING mechanism was first generated in hippocampus *in vitro.* This mechanism is the mechanistically simplest form of the rhythm and states that only networks of mutually interconnected inhibitory interneurons contribute to the gamma rhythm with no input needed from excitatory pyramidal cells. The generation of ING comes from networks of inhibitory interneurons connected by synapses using $GABA_A$ receptors. In this model of local network function the activation of inhibitory interneurons is caused by tonic depolarisation by metabotropic glutamate receptors. This causes interneurons to fire action potentials which over time, become synchronised. The inhibitory post-synaptic potentials (IPSPs) impinging on each interneuron by the action potentials generated by other connected interneurons in the network effectively silence each interneuron. As a consequence each interneuron can only generate an action potential when the inhibitory input is at a minimum.

Such a network has a single stable state: Stochastic activity generates a barrage of IPSPs which effectively silences all the interneurons in the network. Under tonic depolarisation they can only generate outputs again when the barrage of IPSPs has decayed. Thus, the network self-organises such that all outputs are generated on the tail of a population IPSP, which in turn silences the network with a subsequent population IPSP. Further outputs are only possible when that subsequent IPSP has

decayed. This iterative behaviour synchronises the interneuron population and sets a maximum frequency of action potential generation inversely proportional to the decay constant of the population IPSP (Whittington et al., 1995).

1.4.9 Pyramidal-interneuron network gamma

The above demonstration of ING is conceptually useful but not practically so. In local circuits throughout the brain (with the exception of cerebellar cortex (Middleton et al., 2008)) reciprocal connectivity between interneurons and principal cells is both dense and very strong. Interplay between the interneuron network, described in the previous section, and excitatory projection neurons therefore needs to be considered. The PING mechanism does just this, being dependent on both excitatory pyramidal cells and inhibitory interneurons.

Pyramidal cells have long projections so the involvement of these cells enables PING to synchronise over long distances and spatially distributed regions (Traub et al., 1996). The PING mechanism builds upon the ING mechanism with the addition of pyramidal cells; it involves phasic excitation of interneurons following the firing of pyramidal cells. There is a convergence of pyramidal cells to a single interneuron with, in hippocampus, one basket cell receiving inputs from ca. 5000 pyramidal cells. Action potentials from these pyramidal cells produce large EPSPs which causes the interneuron to fire (Whittington et al., 1995). Conversely these interneurons have locally divergent outputs, synapsing onto a large number of pyramidal cells (again, several thousand), providing inhibition which in turn silences interneurons and pyramidal cells together (Gulyas et al., 1993).

PING is thought to be more stable than ING in terms of its frequency as the entrainment of pyramidal cells improves the response to changes in excitation (Whittington et al., 1997). In addition, recruitment of long-range projection neurons allows an interplay between local circuits which, evidence suggests, is ideal for forming highly synchronous action potential generation in brain regions despite long conduction delays (Kopell et al., 2000). The interplay between local circuit feedback activation of interneurons and the projection neuron feedforward

activation of target-region interneurons (with conduction delay) interact at the level of inhibitory inputs to principal cells. Paired pulse interactions between inhibitory synaptic events is not linear, thus the delay in generating a spike in principal cells is coded in the delay-time manifest in the conduction delay between brain areas.

1.4.10 Persistent gamma

The ING and PING mechanisms are both predominantly transient and are believed to mimic intense neuronal stimulation *in vivo*. In contrast, persistent gamma (PG) can be generated in a highly stable fashion *in vitro* which lasts for hours. Such activity may represent background gamma rhythms seen during wakefulness but may also mimic ongoing activity that is seen during cognitive tasks *in vivo.*

PG was first discovered in hippocampus (Fisahn et al., 1998) and it has since been observed in regions such as entorhinal cortex, cerebellar cortex and neocortex (Cunningham et al., 2004). PG is dependent upon both the excitatory chemical synaptic inputs to interneurons and their inhibitory synaptic outputs. However, an additional factor is required to drive the network persistently. Clues to this additional factor came from work showing that PG was sensitive to drugs which block neuronal gap junctions such as carbenoxolone (Traub et al., 2000). Gap junctions are thought to connect axons of pyramidal cells to form the axonal plexus (Traub et al., 1999a) which is capable of generating high frequency oscillations even though the pyramidal cells fire rarely during the oscillation. Action potentials from pyramidal cells can propagate through gap junctions to other cells producing activity in these cells without direct synaptic input, producing large, compound EPSPs in interneurons; this gives a means of maintaining the network.

In terms of frequency, PG generates the most stable gamma. ING, which is driven by depolarisation of interneurons alone, demonstrates a marked frequency change upon increased network drive, until the frequency reaches a maximum. PING, which is generated by principal cell spiking giving a phasic drive to interneurons, shows its frequency is less sensitive to the degree of excitation and changes over a

more broad dynamic range. PG, which is generated by phasic drive to interneurons from the axonal plexus, demonstrates a frequency which is almost inert to network drive (Whittington et al., 2011).

1.4.11 Gamma rhythms in the visual cortex

Work on gamma oscillations has been on-going since the middle of the last century but was enormously boosted by the observations linking the rhythm to the temporal coordination of spike (action potential) generation in populations of visual cortical neurons in response to patterned visual stimuli (Gray and Singer, 1989). In the visual cortex, gamma oscillations are readily seen in response to visual sensory stimuli in the V1 and have been implicated in multiple processes related to Gestalt psychology such as feature binding, scene segmentation and figure ground separation (Singer, 1999; Fries et al., 2001; Thilo et al., 2006; Uhlhaas et al., 2006; Womelsdorf et al., 2007). The key feature of visual gamma rhythms, revealed experimentally, is that they provide the temporal signature for establishing synchrony between simple cells responding to different features (primal sketch lines) of a sensory object (Fries et al., 1997; Melloni et al., 2007). This basic, but conceptually very powerful idea has had its detractors (Shadlen and Movshon, 1999) but has also formed the basis for more general hypotheses for cortical communication which are standing up well to experimental testing (Fries, 2005).

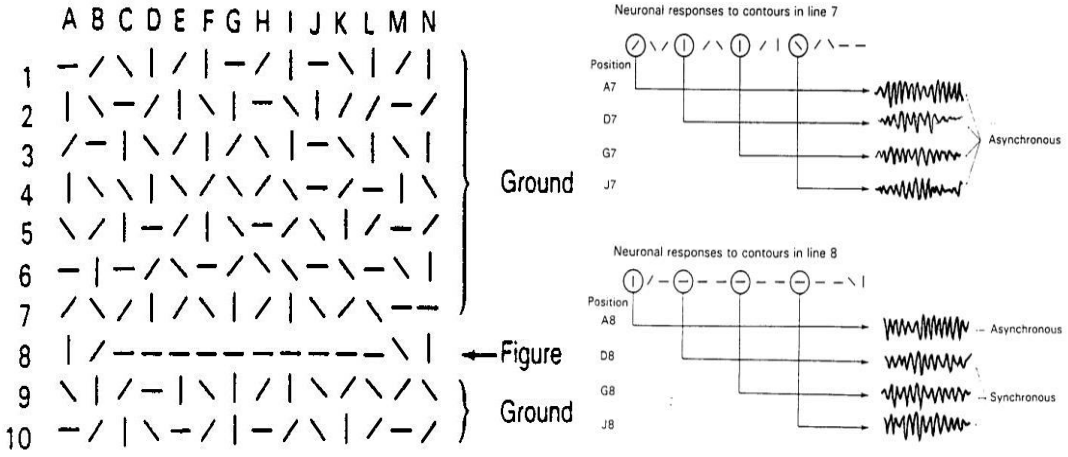

Figure 1.3. Synchrony, via gamma rhythms, 'binds' features of a perceived object. The grid of orientation lines contains 'random' orientations except for line 8. The Binding hypothesis states that activity in simple cells in the V1 coding for each component of the perceived 'line' should be synchronous, whereas the activity in cells coding for randomly distributed orientation lines should be asynchronous. Adapted from Singer, 1989.

Little is known about the mechanism underlying visual neocortical gamma rhythms to date. Studies in other sensory modalities have demonstrated that gamma rhythms are generated almost exclusively in supragranular layers (Cunningham et al., 2004). This study confirmed the role of fast rhythmic bursting neurons in generating this form of gamma rhythm, with the transient bursts generated by this cell type feeding into an axonal plexus to provide the background drive – i.e. it is a PG rhythm (see section 1.4.10 above). However, high levels of glutamatergic network activation can also generate an additional gamma rhythm, at higher frequencies, specifically in layer IV (Ainsworth et al., 2011). In this case the rhythm was insensitive to gap junction blockers and was associated with intense spike-generation in layer IV principal cells – i.e. it is a PING rhythm (see section 1.4.9). Only one *in vitro* model of gamma rhythms in the V1 exists to date and this also showed both high and low frequencies of gamma rhythm (Oke et al., 2010). However, these authors needed to excite the visual cortex with intense glutamatergic and cholinergic excitation to generate rhythmic activity so it remains to be seen whether this model reflects the physiological situation. This issue is examined further in chapter 3.

In addition to a role in the formation of primary sensory representations, gamma rhythms have been implicated in visual attention. In the V4, gamma synchrony has been shown to be enhanced by attention (Tallon-Baudry et al., 2005; Taylor et al., 2005; Fries et al., 2008; Chaumon et al., 2009). Buffalo et al. (2011) showed gamma oscillations came from the superficial layers of the V1, V2 and V4 and the gamma synchrony was enhanced by attention.

1.5 The alpha rhythm

Alpha rhythms (8-12Hz), despite being the historically earliest rhythm discovered, remain the most mysterious in terms of both the physiological mechanism behind the generation of alpha and its function, as currently, no cortical *in vitro* models exist. As such, the role of alpha in visual perception remains unknown, although many theories exist. It was initially discovered by Hans Berger in 1929 (Berger, 1929) who carried out EEG recordings from human subjects with their eyes closed and observed rhythmic activity in the alpha frequency band. He noted the blocking of these upon eye opening or certain types of mental activity. Alpha rhythms are prevalent in a relaxed but wakeful state, Berger's work was confirmed later and alpha rhythms were considered initially as an idling state of the brain (Adrian and Matthews, 1934). Alpha is suppressed upon eye opening and visual stimuli and also in the transition to sleep. Roelfsema et al. (1997) observed a decrease in frequency (20-25Hz vs. 7-13Hz) when animals switched from a focused to a resting state, along with a decrease in synchrony and increase in power in the alpha band. Today however, there is a lot of evidence against the idling hypothesis as new research has brought new theories to light, suggesting that the function of alpha has been underestimated.

In non-invasive human studies alpha is seen as the dominant frequency of oscillation in the parieto-occipital region (Shaw, 2003) and most of the studies to date on this rhythm involve the visual system. However, it is now clear that there is an alpha generator in thalamus (see below) and in other – but not all - neocortical regions. In somatosensory cortex alpha rhythms form the dominant spectral component of the 'mu' rhythm (along with transient packets of beta oscillation) – a

temporal signature associated with resting state and motor preparedness (Koshino and Niedermeyer, 1975). Similarly, in auditory areas a weaker ca. 10 Hz rhythm is seen during rest. Functional and mechanistic aspects of alpha-frequency rhythms are considered below separately for the thalamus and neocortical areas.

1.5.1 Alpha rhythms along the thalamocortical axis

The thalamus is thought to be involved in the co-ordination and generation of alpha rhythms. Originally the rhythm was thought to be related to sleep spindles but this connection has more recently been discounted (Lorincz et al., 2009). It has been suggested that the thalamus acts as a pacemaker for alpha rhythms observed over the occipital cortex. Initial studies showed the disorganisation up to total elimination of the alpha rhythm following thalamic lesions (Ohmoto et al., 1978; Lukashevich and Sazonova, 1996). Further evidence supporting the hypothesis that the generator for alpha rhythms lies in the thalamus is shown in functional magnetic resonance imaging (fMRI) studies which show an increase in oxygenated areas in the thalamus during certain types of alpha oscillations (Goldman et al., 2002; Feige et al., 2005). In addition, control of cortical alpha rhythms in response to attentional demand (see below) critically involves the pulvinar – a highly specialised thalamic subregion seen in higher mammals (Saalmann et al., 2012).

Other studies have also demonstrated a difficulty in defining the thalamus as a unique generator of alpha. While some studies suggest this to be the case (see above) and (Isaichev et al., 2001; Schreckenberger et al., 2004), others place the origin in the thalamic reticular nuclei and cortical areas that are known to project back down to this thalamic specialisation (Isaichev et al., 2003). In addition, depth electrode studies and detailed current source density analysis of EEG signals suggest a specific neocortical generator as well (Lopes da Silva et al., 1980; Bollimunta et al., 2008). These studies suggest that the thalamus may not be the only generator of alpha rhythms, there may be interactions between the thalamus and cortical areas underlying alpha oscillations in a similar manner to that seen for delta rhythms (Carracedo et al., 2013). Along such a thalamocortical axis, with global rhythms observed as a consequence of spatially distinct but functionally

coupled oscillators, it is possible to observe the rhythm of interest in either area or both. For example, alpha rhythms have been shown to occur in the thalamus even when they are not observed in the occipital cortex (da Silva et al., 1973a). This suggests that alpha oscillations can be generated locally in the thalamus.

In vivo studies have also confirmed the role of both the thalamus and cortical areas in alpha rhythm generation. Recordings of alpha oscillations were taken from dogs in a resting state i.e. eyes closed with a maximum amplitude over the occipital cortex. These were shown to occur in synchrony with alpha oscillations in the lateral geniculate nucleus (LGN) which is situated in the thalamus (da Silva et al., 1973b, a). In addition, while a visual cortical alpha rhythm can be readily observed in cortex during eyes closed state (Chatila et al., 1992), it was shown that activities in the cortex of the same frequency and synchrony were present in the LGN suggesting the LGN perhaps playing a prominent role in the driving of the cortical alpha oscillations (Chatila et al., 1993).

Localising a source of a brain rhythm is a perennial problem for whole-brain and non-invasive studies. In these cases the use of isolated *in vitro* brain slice models can be very useful. Following from the suggestion that thalamus contains its own alpha generator (Hughes et al., 2004), *in vitro* brain slice preparations of the LGN in cats have been investigated. In this isolated LGN preparation, alpha oscillations could be induced by mimicking cortico-thalamic feedback, by pharmacologically activating metabotropic glutamate receptors (mGLUR1a) (Hughes et al., 2004; Hughes and Crunelli, 2005). Intracellular studies identified a subset of thalamacortical (TC) neurones; these elicited burst discharges which fired during episodes of alpha waves at the alpha frequency. Increasing glutamate receptor activation gave alpha frequency oscillations. This caused an increased depolarisation therefore increased firing. More moderate mGLUR1a activation gave theta frequency oscillations due to decreased depolarisation and therefore decreased frequency of firing. This suggests there is a shift which occurs from relaxed wakefulness to early sleep. The alpha rhythms observed were reliant on gap-junctional coupling proposing that the thalamocortical bursting neurons are coupled by gap junctions. The neurons critical for this process were identified as

high-threshold bursting neurons that project strongly up to neocortex, perhaps at least in part explaining the strong coupling between thalamically observed alpha rhythms and their neocortical counterparts.

1.5.2 Alpha rhythms in the visual cortex

Despite the apparent dominance of the thalamus as a source of alpha rhythms, a number of features of neocortical alpha rhythms don't fit a hypothesis where all alpha seen is projected up from thalamus. The neocortical alpha rhythm is thought to be a predominantly inhibitory rhythm (see below). The emergence of alpha in neocortical recordings is associated with a net reduction in unit activity strongly suggesting a decrease in cortical neuronal excitability (Haegens et al., 2011). Whether this is a causal or casual relationship is highly debatable – alpha being most prominent during absences of sensory input. However, a specific inhibitory interneuron circuit has been identified that is capable of generating alpha frequency population rhythms (Connors and Amitai, 1997). In a similar manner to the mechanism of generation of ING (see section 1.4.8), a subset of neocortical interneurons are coupled by mutual inhibitory synapses and gap junctions. These interneurons are termed low threshold spiking (LTS) cells and generate brief bursts of action potentials when activated from depolarised levels. Burst discharges generate longer-lasting, compound inhibitory synaptic potentials which lead to an output rhythm from the LTS cell network around alpha frequency. It has been suggested that alpha functional inhibition may be a result of just such an output from GABAergic interneurons (Lorincz et al., 2009; Jensen and Mazaheri, 2010).

Some proposed forms of neocortical alpha rhythm do seem to fit with a general excitatory input from high threshold thalamocortical projection neurons. In particular the so-called 'augmenting response' involved the transient potentiation of responses of layer 5 pyramidal cells to thalamocortical input arriving at alpha frequency (Castro-Alamancos and Connors, 1996). Alpha rhythms had been thought to originate from layer V of the neocortex and to be derived from pyramidal cells previously (Lopes Da Silva and Storm Van Leeuwen, 1977). The Castro-Alamancos study implicated intrinsic dendritic conductances as critical for this augmenting

response and this has been expanded upon in computational studies: Modelling experiments carried out by (Jones et al., 2000b) suggest that pyramidal cells in LV of the neocortex produce and regulate the alpha rhythm due to interplay between I_h and I_t currents. They further predicted that this form of alpha could lead to spatial asynchrony, perhaps explaining the lateral inhibition hypothesis for alpha rhythm generation (Belov et al., 2009). However, an involvement of I_h in alpha rhythm generation does not seem to fit its occurrence in the sleep-wake cycle. I_h levels are highest during sleep and lowest during wakefulness where cholinergic neuromodulation serves to inhibit this intrinsic conductance (Griguoli et al., 2010).

In general, while a mechanism for thalamic alpha rhythm generation is well established, this cannot be said for a neocortical generator. The cell types involved in the dominance or absence of synaptic inhibition and the consequences for local circuit activity levels and temporal properties are confused rather than consolidated by the little information available to date. The main aim of this thesis is to address this issue.

1.5.3 Alpha, attention and 'inhibition' in visual processing

The most common proposal on the functional role of alpha in the visual cortex is the gating of neuronal processes. This 'attentional' role in cognition has been subdivided into two mutually interacting processes: The suppression or 'functional inhibition' of irrelevant or distracting components of a visual stimulus, and the selection of the 'attended' component (Klimesch, 2012). Many researchers consider alpha rhythms to be a vital component of the mechanism the brain uses to segregate certain responses to sensory input. In general an increase in the power of the alpha rhythm is thought to underlie the functional inhibition (suppression) aspect of attention and the specific phase of the alpha rhythm is thought to be important for the selection process. These two phenomena will be considered separately below.

1.5.3.1 Attention and changes in alpha rhythm power

Perhaps the simplest, and earliest, connection between the alpha rhythm and visual cognition was the observation that opening the eyes decreases the power of the on-going alpha rhythm (so called 'event related desynchronization', (Pfurtscheller et al., 1994)). This phenomenon is not directly related to input of sensory information however, as it occurs even in complete darkness (Adrian and Matthews, 1934). Instead, evidence appears to suggest that alpha is inversely correlated with visual attention – the more a component of the visual field is salient to the viewer the less alpha is generated in regions of visual cortex responsible for processing that component. This idea is supported by experiments that show 'active' enhancement of alpha power ('event related synchronisation') in visual areas processing information irrelevant or distracting to the cued image (Pfurtscheller et al., 1996).

This 'attend away' form of the alpha rhythm has been reported within the visual cortices, across the hemispheres (Sauseng et al., 2009) and even across different modalities of concurrent sensory input. For example, when a subject is given both auditory and visual information, but asked to attend to only the visual information, alpha power is seen to increase in auditory cortex alone (Foxe et al., 1998). Similarly, alpha amplitude was found to increase in visual regions during attention to motor tasks, and was also enhanced in sensorimotor regions during visual tasks (Pfurtscheller, 1992).

Ahveninen et al. (2012) proposed that visual alpha activity changes induced by auditory tasks represented a form of visual pathway inhibition. The generation of alpha rhythms is thought to represent a form of lateral inhibition; the silencing of neighbouring cortical areas by generation of alpha rhythms through projections from a non-alpha-generating, adjacent active area. It is suggested that this locally elevated alpha power is associated with inhibition of task irrelevant areas, routing information to task relevant areas, and is therefore necessary for internal mental operations (Cooper et al., 2003; Klimesch et al., 2007; Jensen and Mazaheri, 2010;

Mathewson et al., 2011). There is an enhanced processing of visual stimuli at a cued location at which attention has been directed, along with attenuated processing of competing stimuli at other locations (Desimone and Duncan, 1995).

In support of the above idea that elevated alpha power suppresses information processing in a region-specific manner, general excessive alpha rhythm generation is correlated with loss of consciousness (Supp et al., 2011) – so-called 'alpha coma' (Iragui and McCutchen, 1983). More subtle evidence comes from observations suggesting that active sensory processing is temporally quantised in intervals of approximately 100ms (10 Hz). Presenting images that flicker to one eye suppresses the processing of images presented to the other eye, with a peak effect seen with flicker rates of 10Hz (Tsuchiya and Koch, 2005). In addition, using an optical illusion in which rotating 'wagon wheel' images are presented at frequencies around the alpha, 10Hz modal peak, it has been shown that subjects can be made to see the direction of rotation reverse depending on the image flicker rate relative to each subjects peak alpha frequency (VanRullen et al., 2005). The authors argue that the visual sensory information is discretely sampled at ca. 10 Hz, and deviations of presentation frequency around that endogenous sampling frequency can result in a precession-like phenomenon.

It is hard to reconcile the bodies of evidence linking alpha rhythms with attention, and the evidence for quantising of sensory input. In fact it has been shown that the 'wagon wheel' illusion described above occurs independently of any attentional processes – the flicker and reversed rotation even persist in the after-image maintained following stimulus presentation (Sokoliuk and VanRullen, 2013). In addition, it is hard to understand how an active area of visual cortex, responding to an attended image with gamma and beta rhythms (see above), could generate a different, alpha frequency, rhythm in inactive areas as proposed by the lateral inhibition hypothesis. In the absence of clear evidence for any inhibitory role for alpha rhythms at the neuronal network level researchers have proposed a different role for the rhythm, bringing together the above ideas of a temporal organisation of sensory awareness with longer-range brain interactions involved in forming and interrogating memory.

1.5.3.2 Attention and alpha rhythm phase

In attempts to examine the contradictory nature of the large amount of evidence implicating changes in the alpha rhythm power with selective attentional processes, some researchers see alpha rhythms as a way to coordinate network activity in a similar manner to that known for gamma rhythms (see section 1.4.11). All brain rhythms are an effective way to control the relative phase of activity in different neurons and even different brain areas. Precise synchrony and antisynchrony (the identical timing of outputs from neurons despite physical separation, or the exact opposite timing of outputs in a train respectively), arise from combinations of synaptic inputs and intrinsic properties of neurons (Whittington et al., 2011). Neuronal synchronisation is advantageous as it increases the likelihood of enhanced effects on convergent target neurons (Ainsworth et al., 2012). If alpha rhythms behave in a similar manner then the phase relationships they set-up in various brain regions may be functionally more important than changes in power alone.

Alpha rhythms have been shown to temporally coordinate visual neuronal responses across multiple spatial scales (Doesburg et al., 2009) with these authors suggesting this represents an enhanced mechanism for visual processing. The amplitude of alpha oscillations would increase ipsilateral to the attended location and decrease contralateral which fits with the inhibition framework. The long-range synchronisation would decrease in the ipsilateral hemisphere and increase in the contralateral respectively, fitting with the co-ordination idea. This idea formulates an “active processing hypothesis” for optimal processing of visual information. In addition, task performance has been shown to be critically dependent on the precise timing of visual inputs relative to the on-going cortical alpha rhythm (Mathewson et al., 2009). Other than this there is little work directly showing a role for phase relationships established by alpha rhythms in visual processing and this deficit is, in part, addressed (on a local network scale) in chapter 3.

1.5.4 Alpha and memory

In general there is quite a lot of evidence linking alpha rhythms with visual short-term memory. Alpha oscillations were found to increase with memory load during retention tasks (Jensen et al., 2002; Jensen et al., 2007; Tuladhar et al., 2007) and certain types of memory retrieval (Palva and Palva, 2007; Palva and Palva, 2011). Freunberger et al. (2008) reported that during long term memory tasks, alpha oscillations decreased in power, but increased in phase synchronisation implying alpha-mediated temporal coordination is needed for the accessing of semantic information. Data from recall tasks have led to the suggestion that alpha rhythms form an 'attentional buffer' – effectively maintaining cued features of the visual stimulus in short term memory for rapid retrieval (MacLean et al., 2012; Zauner et al., 2012).

It is now established that the power of alpha oscillations increases in occipital regions ipsilateral to the attended visual field and decreases in the contralateral regions (Ergenoglu et al., 2004; Kelly et al., 2009; Foxe and Snyder, 2011). However, rather than suggesting a suppression (inhibitory) role for this alpha, Klimesch et al. (2011), have suggested that the alpha rhythms seen are needed for accessing of mnemonic information necessary for stimulus recognition. Other studies involving a short-term memory component have found that the degree of cognitive processing and feature extraction is linked to the amount of alpha rhythm modulation after visual stimulation (Schürmann and Başar, 2001; Klimesch et al., 2007). These studies mark the importance of alpha oscillations in directing attention to task relevant areas and visual processing.

Interestingly, in working memory and long term memory studies, it was found that the highest power alpha oscillations were associated with the most successful performance on the memory tasks, and a lower power oscillation was associated with an unsuccessful performance i.e. when more errors were made (Haegens et al., 2010; Meeuwissen et al., 2011). These studies suggest that a high power alpha oscillation in task irrelevant areas gives an optimal brain state for memory task execution. However, a positive correlation between the alpha rhythm and memory tasks has been reported specifically when the task involves an 'internal' attentional

component (Cooper et al., 2003; Palva and Palva, 2007). Such introspective tasks involve activation of the default mode network (DMN) – a collection of brain areas involved in memory formation, particularly of the autobiographical variety (Raichle et al., 2001). Temporal coordination of activity within the DMN is critically dependent on the generation of alpha rhythms (Fingelkurts and Fingelkurts, 2011; Fingelkurts et al., 2012). These observations may support the hypothesis of Klimesch et al. (2011), suggesting that alpha rhythms are generated in order to compare new visual sensory input with long-term memories of past visual experiences.

Further evidence for a connection between alpha rhythms and memory comes from the psychophysical correlates of the large increase in alpha power immediately on closing the eyes (terminating a visual sensory input). The current hypothesis for this form of alpha rhythm states that it is involved in 'echoic' memory – the short term maintenance of a visual scene in the cortical code (VanRullen and Macdonald, 2012). Interestingly, this has been suggested for other brain rhythms e.g. beta rhythms (Kopell et al., 2000). However, this particular function of alpha seems to be region-specific in cortex: Van Rullen and co-workers have reported an echoic memory function for alpha in the visual system but not found any evidence for it in the auditory system (İlhan and VanRullen, 2012). This is stark contrast to the alpha rhythm seen in auditory cortex during visual attention tasks with concurrent auditory input (above). This dichotomy strongly suggests that different origins and mechanisms of the alpha rhythm may exist. While this may simply reflect different levels of cortical and thalamic alpha generation it may also indicate different mechanisms and roles for alpha generation in different cortical areas.

1.5.5 Alpha interactions with other frequencies

In the visual cortex, laminar differences in oscillations were shown in visual areas V1, V2 and V4 of rhesus monkeys. Gamma oscillations originated from the superficial layers and alpha from the deep layers (Buffalo et al., 2011). The gamma synchrony between each of these visual areas was enhanced by attention and the alpha synchrony reduced, showing that different frequency oscillations play

different roles in attention. (Spaak et al., 2012) went on to show the existence of interlaminar cross-frequency coupling between gamma and alpha in the V1 of the awake macaque, suggesting processing in the visual cortex is modulated in a top down manner by alpha oscillations. This suggests alpha plays an important role in the optimisation of visual processing. Jensen et al. (2012) propose that cross-frequency, phase-locked gamma and alpha oscillations create a cycle with a time gap ideally suited to keep apart unattended stimuli and process visual stimuli in order of relevance, further implying that alpha plays a key role in visual processing.

Other studies have also demonstrated that gamma activity is modulated by alpha phase (Daria et al., 2008; Voytek et al., 2010). These observations suggest that there is an inhibition of the visual system during the alpha cycle until a phase of excitable gamma activity occurs i.e. the gamma oscillations are phase locked to the alpha cycle. The gamma/alpha coupling has been shown to increase in visual areas during visual stimulation, potentially reflecting a mechanism of communication between neuronal networks.

The above evidence strongly suggests that alpha and gamma rhythms can coexist in the visual cortex and that the temporal organisation of this coexistence has implications for visual sensory processing. This does not appear to be the case for alpha and beta rhythms. In general alpha and low-beta rhythms tend to be lumped together as a single entity (Killian and Buffalo, 2014). Both alpha and beta bands are implicated in top-down processing (Jensen et al., 2015). However, anticipatory tasks show a different, even contrasting role for beta and alpha rhythms (Buchholz et al., 2014). Similarly, selection tasks also show differential roles for alpha and beta rhythms: For intra- and extradimensional set shifting tasks learning the correct rule was correlated by increased frontal cortical beta synchronisation whereas suppression of prior learned rules on set-shifting was correlated with synchrony in the alpha band.

1.5.6 Alpha rhythms and brain neurological illness

There is a correlation between excessive alpha rhythm generation and the minimally conscious state (above). However, more subtle changes in alpha rhythm generation are also seen in disorders associated with attentional deficits.

As previously mentioned, alpha has been shown to be involved in attention. Attentional deficit hyperactivity disorder (ADHD) is characterised by a short attention span/distraction, restlessness or over activity and includes problems in directing or sustaining attention. Alpha oscillations have shown to be important in the directing of information to relevant brain regions when allocating attention.

It has been proposed that ADHD could be associated with problems in modulating alpha activity. The resting state of subjects with ADHD possesses different electrocortical activities than control subjects. The theory is that an increased alpha and decreased theta during the resting state gives high levels of theta and low levels of alpha throughout task performance, enabling optimal cognitive performance. There is an increased theta and decreased beta band activity in ADHD, which has been related to a slow alpha peak frequency (Lansbergen et al., 2011). Increased alpha and theta power at rest has been shown to impair cognitive performance in children with ADHD (Hermens et al., 2005). MEG scans of patients with ADHD that were known responders to pharmacotherapy showed increased levels of alpha activity in the prefrontal cortex after pharmacotherapy (Wilson et al., 2013)

Alpha band oscillations have been shown to undergo event-related desynchronization in task relevant areas and event-related synchronisation in task-irrelevant areas (Klimesch et al., 2011) therefore, inhibiting processing in task irrelevant areas and dis-inhibiting processing in task relevant areas, giving an optimal brain state in the processing of information. In subjects with ADHD, it has been shown that alpha oscillations possess a deviant pattern of activity. There has been shown to be significantly less post-cue suppression of alpha activity in the visual cortex (Mazaheri et al., 2010; Mazaheri et al., 2014) which could act to reduce attention and therefore diminish visual processing.

The degree of lateralized alpha has been shown to be modulated in visual attention tasks in subjects with ADHD. There is an inability to sustain alpha lateralization before cued targets thus reducing performance on the attention task (Vollebregt et al., 2015). It has also been shown in ADHD subjects that there is a significant bias to the right visual hemisphere due to the inability to sustain alpha lateralization in the left hemisphere compared with healthy children (ter Huurne et al., 2013; Vollebregt et al., 2015). These modulations of alpha activity could reflect some of the attention related problems in ADHD and diminish visual processing.

Finally, a connection between disrupted alpha rhythm generation and autism spectrum disorders (ASD) has also been proposed. The sensorimotor alpha rhythm (the mu rhythm) is directly related to the recruitment of mirror neurons in humans (Pineda et al., 2000) and specific decreases in this rhythm are seen in high-functioning ASD patients when observing movement of others rather than self-performed movements (Oberman et al., 2005). In the visual system ASD patients have greater 'eyes-open' alpha rhythms and less visual alpha suppression which correlated strongly with the degree of pathological attention to detail demonstrated in this patient group (Mathewson et al., 2012).

1.6 Aims and objectives

The current understanding of neuronal oscillations in the visual cortex have been outlined and, given the dominance of the alpha signal in EEG from occipital cortex, my thesis will concentrate on *in vitro* models of local circuit dynamics in visual cortex (V1 and V2 specifically). I will attempt to address the following basic aims:

1) To determine whether a purely visual neocortical alpha generator exists or whether all cortical alpha rhythms represent alpha-frequency input from thalamus.

2) To characterise the local circuit, synaptic and cellular properties of the visual alpha rhythm.

3) To establish the consequences of the alpha rhythm for activity in the V1 – is the alpha rhythm really inhibitory and if so how is this inhibition generated.

4) To quantify the relationship between alpha rhythm generation and 'memory' processes as manifested in synaptic plastic changes.

5) To investigate the apparent differential relationship between the alpha rhythm and gamma or beta rhythms.

To attempt to address these aims the following objectives are set:

1) To establish an *in vitro* model of the physiological alpha rhythm in isolated brain slice preparations and map its occurrence throughout the laminar column and across the primary visual cortex.

2) To establish the pharmacological properties of the alpha rhythm and identify the key cellular mechanisms, synaptic connectivity and network substrates.

3) To study the individual neurons involved in alpha oscillations and their specific contributions in order to determine the cellular basis of the rhythm.

4) To map the consequences of the alpha rhythm, for local network function in terms of temporally shaping cortical inputs, outputs and horizontal interactions.

Chapter 2: Methods

2.1 Animal provision

All experiments were performed *in vitro* using brain slice preparations from young adult male Wistar rats aged between 35-80 days weighing 150-300g. Animals were obtained from Charles River Laboratories Inc. and were housed in the Biology Service Facility (BSF) at the University of York. Animals were left to acclimatise in-house for at least 7 days before experiments were performed and were maintained in a 12 hour light dark cycle and provided with food and water *ad libitum.*

2.2 Anaesthesia and animal procedures

All procedures performed in this thesis conformed to the UK Animals (Scientific Procedures) Act, 1986, and were covered by personal and project licenses awarded by the UK Home Office, EU directive and ARRIVE guidelines.

Animals were firstly placed into a bell jar and approximately 5ml of the gaseous anaesthetic isofluorane (Abbott Laboratories, Illinois, U.S.A) was added until a loss of the righting reflex was observed. Animals were than intramuscularly injected with 0.2ml xylazine (10mg.kg^{-1}, Bayer Healthcare AG, Germany) and 0.4ml ketamine (100mg.kg^{-1}, Vetoquinol, Buckingham, UK) into the gluteal area of the hind leg and left until there was a loss of the pedal withdrawal and corneal reflex. Once these pain reflexes were abolished, the abdominal cavity and ribcage were cut open to reveal the heart. The left ventricle was pierced with a catheter and a small incision was made into the right atrium so the rats could be intracardially perfused with around 60ml of oxygenated, ice cold, sucrose artificial cerebrospinal fluid (sACSF) at a rate of approximately 1ml/s (see section 2.6). The modified sACSF replaces NaCl with sucrose and has been shown to improve the viability of neurons, alleviating the neurotoxic effects of swelling and cell lysis associated with re-entry of chloride ions into the neurons (Aghajanian and Rasmussen, 1989).

2.3 Preparation of visual cortex slices

Following intracardial perfusion, an incision was made along the midline of the animal's head to expose the skull and the spinal cord was severed. From the point where the spinal cord was severed, the animal's skull was cut along the sagittal

suture from the caudal to rostral plane. The skull and dura matter were then peeled away to expose the brain and the brain was excised and immersed in a petri dish containing oxygenated, ice cold sACSF. The cerebellum, brain stem and frontal cortex were then trimmed from the brain using a blade cutting along the coronal plane. The remaining brain tissue was superglued on the rostral plane to the chuck of a Leica VT1000 Vibratome (Leica Microsystems, Nussloch, Germany) against a block of agar for support so the visual cortex at the back of the brain was revealed. The chuck was then placed into the cutting chamber of the microtome containing oxygenated, ice cold sACSF.

Coronal sections containing visual cortex were cut to 450μm in thickness. This thickness maintains the local circuitry in the brain needed to generate oscillatory activity and is also thin enough to maintain sufficient oxygenation. Once slices were cut they were transferred to a petri dish again containing continuously oxygenated, ice cold sACSF, where they were trimmed from both hemispheres of the brain to produce sections containing V1 and V2 structures of the visual cortex (see figure 2.1). The area of the visual cortex that was required was identified using a rat brain atlas (Paxinos and Watson, 1998) with respect to bregma, the anatomical point on the skull at which the coronal and sagittal sutures intersect. The visual cortex slices used were approximately 6.3mm-7.04mm.

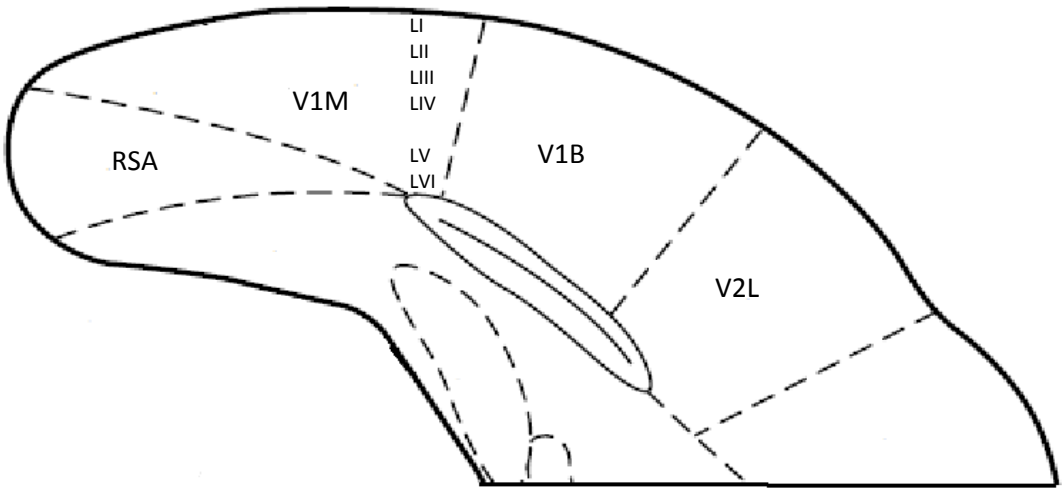

Figure 2.1 Illustration of a visual cortex coronal brain slice at the level and orientation used throughout this thesis.

2.4 Maintenance of visual cortical slices

Upon preparation of visual cortical slices, tissue was transferred to a holding chamber containing continuously oxygenated artificial cerebrospinal fluid (ACSF) and allowed to equilibrate at room temperature for approximately 1 hour for use up to 8 hours after their preparation. After at least 1 hour, 2 of the slices were transferred to an interface recording chamber upon 2 layers of lens cleaning tissue (Whatman International Ltd. Maidstone, UK). Tissue was maintained at the interface between humidified carbogen gas (95% O_2, 5% CO_2) and continuously oxygenated, circulating ACSF at a temperature of 30-34°C using a flow heater (Grant Instruments Ltd., Cambridge, UK). The circulating ACSF was maintained using a peristaltic pump (Watson-Marlow, UK) at the rate of 1-2ml per minute. Pharmacological agents could then be added to the circulating ACSF to produce and modulate oscillatory activity.

2.5 Drugs and solutions

The sucrose artificial cerebrospinal fluid was composed of 252mM sucrose, 3mM KCl, 1.25mM NaH_2PO_4, 24mM $NaHCO_3$, 2mM $MgSO_4$, 2mM $CaCl_2$ and 10mM glucose. The artificial cerebrospinal fluid was composed 126mM NaCl, 3mM KCl, 1.25mM NaH_2PO_4, 24mM $NaHCO_3$, 1mM $MgSO_4$, 1.2mM $CaCl_2$ and 10mM glucose. Drugs were stored in their solid forms at temperatures instructed from their suppliers until they were needed. The drugs were made up in stock solutions dissolved in distilled water, or, if insoluble in water, dimethyl sulfoxide (DMSO) or ethanol and kept either refrigerated or frozen according to supplier instructions. If made up in DMSO or ethanol, stock concentrations were made up so the final concentration of DMSO was less than 0.1% v/v. The drugs made up in DMSO or ethanol were: CIQ, PPDA, SYM 2206, TCN 213 and UBP 301. When needed, drugs were bath applied to the recording chamber at appropriate concentrations via the circulating, oxygenated ACSF. The concentration of each drug applied was determined based on previous research using these compounds, along with the EC50 and IC50 values. This determined concentration was chosen as it had the optimal effect on each drug's preferred target with minimal interaction with others.

List of drugs and chemicals

Drug/Chemical and supplier

- ABC kit (Avidin-Biotin Horseradish peroxidase complex), Vector Labs
- Agar, Fisher Scientific UK Ltd., Loughborough, UK
- Biocytin (N^6-[5-[(3a*S*,4*S*,6a*R*)-Hexahydro-2-oxo-1*H*-thieno[3,4-*d*]imidazol-4-yl]-1-oxopentyl]-L-lysine), Santa Cruz Biotechnology, Inc., Germany
- Calcium chloride, Fisher Scientific UK Ltd., Loughborough, UK
- Carbenoxolone disodium salt ((3β,20β)-3-(3-Carboxy-1-oxopropoxy)-11-oxoolean-12-en-29-oic acid disodium), Sigma-Aldrich Ltd., Dorset, UK
- Carbachol (2-Hydroxyethyl)trimethylammonium chloride carbamate, Tocris Biosciences Ltd., Bristol, UK
- CIQ (3-Chlorophenyl) [3,4-dihydro-6,7-dimethoxy-1-[(4-methoxyphenoxy)methyl]-2(1*H*)-isoquinolinyl]methanone, Tocris Biosciences Ltd., Bristol, UK
- Co 101244 ((1-[2-(4-Hydroxyphenoxy)ethyl]-4-[(4-methylphenyl)methyl]-4-piperidinol hydrochloride)), Tocris Biosciences Ltd., Bristol, UK
- *(R)*- CPP (3-((*R*)-2-Carboxypiperazin-4-yl)-propyl-1-phosphonic acid), Tocris Biosciences Ltd., Bristol, UK
- D-Glucose anhydrous, Fisher Scientific UK Ltd., Loughborough, UK
- (*RS*)-3,5-DHPG (*RS*)-3,5-Dihydroxyphenylglycine, Tocris Biosciences Ltd., Bristol, UK
- DMSO, Sigma-Aldrich Ltd., Dorset, UK
- DK-AH 269 ((S)-(+)-7,8-Dimethoxy-3-[[1-(2-(3,4-dimethoxyphenyl)ethyl)-3-piperidynyl]methyl]-1,3,4,5-tetrahydro-2H-3-benzazepin-2-one hydrochloride), Santa Cruz Biotechnology, Inc., Germany
- Ethanol, Sigma-Aldrich Ltd., Dorset, UK
- Gelatine, Sigma-Aldrich Ltd., Dorset, UK
- Goat anti-mouse IgG(H+L) Secondary antibody, Alexa Fluor 488 conjugate, Catalog#: A-11001, ThermoFisher Scientific Inc., MA, USA
- Ifenprodil hemitartrate ((1*R**,2*S**)-*erythro*-2-(4-Benzylpiperidino)-1-(4-hydroxyphenyl)-1-propanol hemitartrate), Tocris Biosciences Ltd., Bristol, UK

- Isopentane (2-Methylbutane), Sigma-Aldrich Ltd., Dorset, UK
- Kainic acid ((2*S*,3*S*,4*S*)-Carboxy-4-(1-methylethenyl)-3-pyrrolidineacetic acid), Tocris Biosciences Ltd., Bristol, UK
- Magnesium sulphate, Fisher Scientific UK Ltd., Loughborough, UK
- Nicotine ditartrate ((*S*)-(-)-1-Methyl-2-(3-pyridyl)pyrrolidine (+)-ditartrate salt), Tocris Biosciences Ltd., Bristol, UK
- Noradrenalin bitartrate (4-[(1*R*)-2-Amino-1-hydroxyethyl]-1,2-benzenediol (L-(+))-bitartrate salt), Tocris Biosciences Ltd., Bristol, UK
- NBQX disodium salt (2,3-Dioxo-6-nitro-1,2,3,4-tetrahydrobenzo[*f*]quinoxaline-7-sulfonamide disodium salt), Sigma-Aldrich Ltd., Dorset, UK
- NNC 55-0396 ((1*S*,2*S*)-2-[2-[[3-(1*H*-Benzimidazol-2-yl)propyl]methylamino]ethyl]-6-fluoro-1,2,3,4-tetrahydro-1-(1-methylethyl)-2-naphthalenyl cyclopropanecarboxylate dihydrochloride), Tocris Biosciences Ltd., Bristol, UK
- PPDA ((2*S**,3*R**)-1-(Phenanthren-2-carbonyl)piperazine-2,3-dicarboxylic acid), Tocris Biosciences Ltd., Bristol, UK
- Potassium acetate, Fisher Scientific UK Ltd., Loughborough, UK
- Potassium chloride, Fisher Scientific UK Ltd., Loughborough, UK
- SKF 81297 hydrobromide ((±)-6-Chloro-2,3,4,5-tetrahydro-1-phenyl-1*H*-3-benzazepine hydrobromide), Tocris Biosciences Ltd., Bristol, UK
- Sodium bicarbonate, Fisher Scientific UK Ltd., Loughborough, UK
- Sodium chloride, Fisher Scientific UK Ltd., Loughborough, UK
- Sodium dihydrogen phosphate, Fisher Scientific UK Ltd., Loughborough, UK
- Sodium phosphate monobasic anhydrous, Fisher Scientific UK Ltd., Loughborough, UK
- SR 95531 hydrobromide (6-Imino-3-(4-methoxyphenyl)-1(6*H*)-pyridazinebutanoic acid hydrobromide), Santa Cruz Biotechnology, Inc., Germany
- Streptavidin Alexa Flour 568 conjugate, Catalog#:S-11226
- Sucrose (β-D-Fructofuranosyl α-D-glucopyranoside), Fisher Scientific UK Ltd., Loughborough, UK

- SYM 2206 ((±)-4-(4-Aminophenyl)-1,2-dihydro-1-methyl-2-propylcarbamoyl-6,7-methylenedioxyphthalazine), Tocris Biosciences Ltd., Bristol, UK
- TCN 213 (N-(Cyclohexylmethyl)-2-[(5-[(phenylmethyl)amino]-1,3,4-thiadiazol-2-yl}thio]acetamide), Tocris Biosciences Ltd., Bristol, UK
- UBP 301 ((α*S*)-α-Amino-3-[(4-carboxyphenyl)methyl]-3,4-dihydro-5-iodo-2,4-dioxo-1(2*H*)-pyrimidinepropanoic acid), Tocris Biosciences Ltd., Bristol, UK
- ZD-7288 (4-Ethylphenylamino-1,2-dimethyl-6-methylaminopyrimidinium chloride), Tocris Biosciences Ltd., Bristol, UK

2.6 Recording techniques

Extracellular local field potentials were recorded using microelectrodes with a resistance less than 5MΩ pulled from standard walled borosilicate glass capillaries (1.2mm O.D. x 0.69mm I.D., Harvard Apparatus Ltd., Kent, UK) filled with normal ACSF of the same composition used in the experiments. Sharp microelectrodes were used for intracellular recordings, also pulled from standard walled borosilicate glass capillaries. These electrodes had a higher resistance (70MΩ– 150MΩ) and were filled with potassium acetate solution [2M] containing dissolved Biocytin hydrochloride [4-6%]. All electrodes were pulled using a Flaming/Brown type Horizontal puller (Sutter Instruments Co., California, U.S.A).

Approximately half an hour after the slices were placed in the interface chamber, extracellular electrodes were placed in the V1 or V2 of the visual cortical slices. Control recordings were then taken prior to the addition of any pharmacological agents to ensure any oscillatory activity was due to the addition of pharmacological agents. Electrodes were inserted using a Narishige MX4 manipulator and a microscope to enable accurate positioning of the electrodes.

2.7 Pharmacological induction of the alpha rhythm *in vitro*

Kainate (800nM) was the pharmacological agent used to produce initial oscillatory activity in the slices. The kainate was bath applied to the circulating ACSF and the slices were perfused with kainate for approximately 1 hour to produce persistent oscillatory activity in the beta and/or gamma frequency band. Extracellular

electrodes recorded the local field potentials (LFP's), the sum of the electrical current from multiple surrounding neurons, and once oscillations had stabilised i.e. there was a less than 10% difference in the amplitude of oscillations in three consecutive recordings, further experiments could be carried out. To induce oscillations in the alpha frequency band, NBQX (5μM) and DK-AH (10μM) were added to reduce both extrinsic and intrinsic neuronal excitability. Previous experiments have shown that a small concentration of NBQX is enough to partially antagonise AMPA and KA receptors to reduce a beta II frequency to beta I ((Roopun et al., 2006) see chapter 3 for more detail). This concentration of NBQX was used as preliminary experiments showed it to be the optimum concentration for reducing excitation without abolishing rhythmicity in the slice (see chapter 3). Once persistent oscillations in the gamma, beta, or alpha frequency were determined, further pharmacological experiments, laminar and horizontal profiles, and intracellular recordings could be carried out to study the properties of the rhythms.

2.8 Data acquisition

Extracellular signals detected by the slices were recorded in current clamp mode and band pass filtered at 3-200Hz. Signals were amplified and filtered using an Axoclamp 900A amplifier (Molecular Devices LLC., CA, U.S.A). Intracellular signals were recorded in DC mode and low pass filtered at 2 kHz. Any electrical line noise was filtered using 'Humbug' adaptive filters (Quest Scientific Instruments Inc., North Vancouver, Canada). Signals were then digitized at 10 kHz by an Instrutech ITC-18 A/D Converter (Instrutech Corp., NY, U.S.A) and transferred to either a Mac (Apple Computer Inc.) or Windows PC (Microsoft Corporation). Axograph X software version 1.5.4 (Axon Instruments) was used to visualise and store recordings, along with initial frequency analysis.

2.9 Data analysis

Analysis and presentation of data was done using a number of programs. The raw data was collected using Axograph X version 1.5.4 (Axon Instruments). Analysis of the traces was carried out using bespoke programmes written in Matlab 8.3

software (The Maths Works Inc., Natick, MA, U.S.A). Statistical analysis was carried out using Sigmaplot (Systat Inc.) and the data was presented using Microsoft PowerPoint and Microsoft Word (Microsoft Corporation).

2.9.1 Analysis of oscillation frequency

Extracellular LFP recordings were quantified based on the peak frequency of the oscillation and the amplitude of the modal peak of the oscillation. Power spectra were produced from 60 second time epochs of raw data using a fast fourier transform (FFT) algorithm. This converts the time domain to a frequency domain by deconstructing the waveform of an oscillation into a series of pure sine and cosine functions within pre-defined frequency bands. The phase information inherent in this analysis was discarded and the magnitude squared value for each frequency component used to calculate the power distribution. This is then expressed as a sum of the voltage squared in a particular frequency band (μV^2/Hz). The power is therefore representative of the power at the particular frequency band of interest, which in this thesis were alpha (8-12Hz), beta (12-30Hz) and gamma (30-80Hz). The amplitude and frequency of the modal peak can then be measured directly off the peak. Spectrograms were also used to illustrate any time-dependent changes in frequency content of raw traces using Matlab version 8.3. This is a visual representation of the spectrum of frequencies in the signal with the amplitude of the oscillation represented via colormap transformation.

The rhythmicity of oscillations was measured using autocorrelation analysis of 60 second epochs of the raw extracellular data. This compares a trace with itself over multiple time intervals, resulting in a plot of the degree of correlation against time, which takes on a sinusoidal form. The plot is normalised and the correlation is determined by calculating the difference in amplitude as measured on the Y-axis between the central peak to the first side trough. This gives information about the synchrony of an oscillation; the greater the level of correlation of an oscillation with itself over time, the more synchronous it is.

2.9.2 Analysis of individual neuronal properties.

Cells were characterized from intracellular recordings using a range of depolarising steps (0.1-1nA). Electrophysiological properties of the cells were used to determine the cell type, these included cells responses to depolarising current, post step after hyperpolarisation (AHP) (see figure 2.2), action potential width at half height, AHP and after depolarisation (ADP) of individual spikes (see figure 2.3), resistance (see figure 2.4), average spike rate and inhibitory postsynaptic potential (IPSP) and excitatory postsynaptic potential (EPSP), rise time, amplitude and decay time (see figure 2.5). ADP is defined as a period of depolarisation after an action potential which increases the likelihood of the neuron firing again, for the purpose of this thesis, ADP was quantified as described below (see figure 2.3). Analyses of neuronal properties were carried out by randomly selecting portions of the data and taking measurements of individual properties i.e. single spikes. Measurements were carried out manually, directly from the raw data as described below (figure 2.2-2.5). For analysis of each of these properties from individual neurons, ≥20 measurements were taken from each cell and then averaged to produce an N of 1, where N=number of cells, and n=number of measurements taken. These measurements were taken in order to determine neuronal cell types and identify any differences in the properties of the neuronal subtypes recorded from during intracellular experiments.

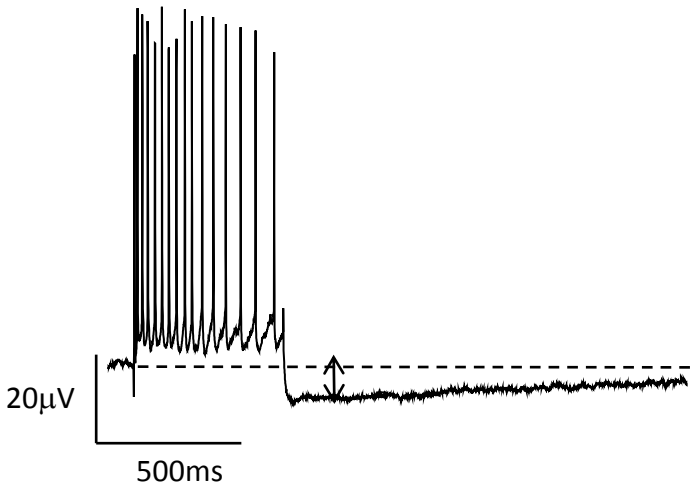

Figure 2.2 Response to 0.5nA depolarising step illustrating the response of the cell. Post step AHP was quantified by measuring the maximum amplitude, which was taken between resting membrane potential and the trough of the AHP indicated by an arrow.

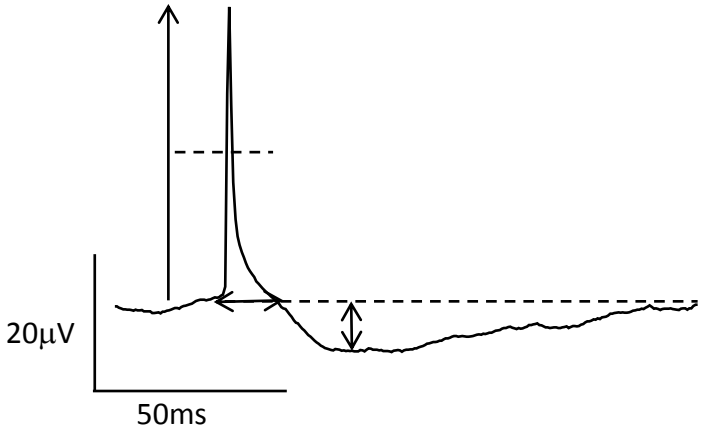

Figure 2.3 Intracellular recording of single spike of cell at resting membrane potential. Action potential width was quantified by measuring width at half height; AHP was quantified by measuring the amplitude which is taken between resting membrane potential and the trough of the AHP indicated by an arrow. ADP was quantified by measuring the time from the start of the action potential until the end indicated by an arrow.

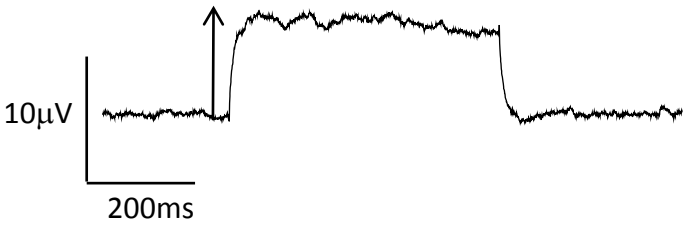

Figure 2.4 Response to 0.2nA depolarising step. The resistance of cells was calculated by injecting cells with a depolarising current and dividing the voltage (indicated by arrow) by the amount of current injected.

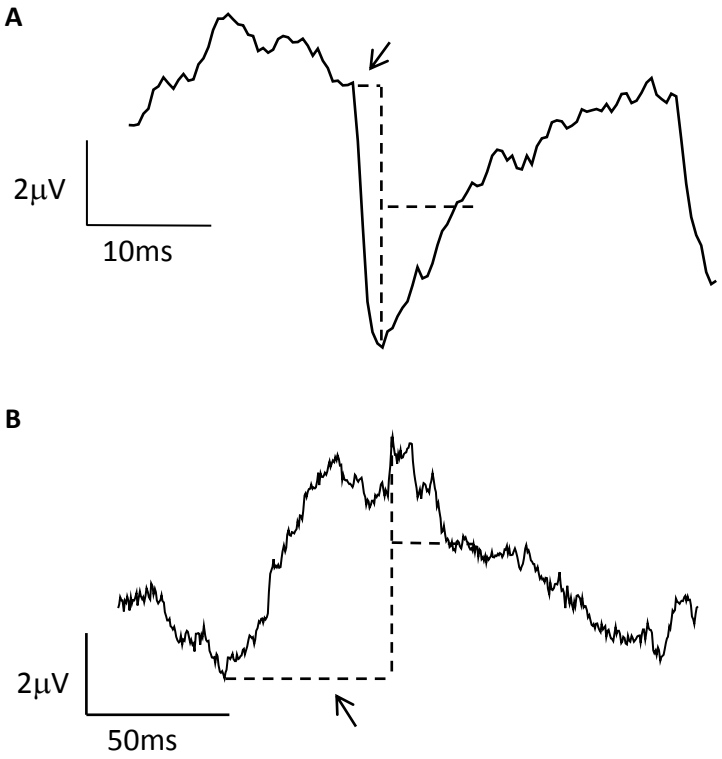

Figure 2.5 A. IPSP recorded by depolarising the cell to -30mV. **B.** EPSP recorded by hyperpolarising the cell to -70mV (resting membrane potential -60mV). The amplitude of IPSPs and EPSPs was calculated by measuring the voltage of the peak or trough. The rise time was the time it took for the IPSP or EPSP to reach its maximum amplitude indicated by an arrow. The decay time was quantified using the time constant (τ), this was measured from the peak or trough of the IPSP or EPSP to the time it took to decay to 63.2% of its final value.

For each cell type, EPSPs and IPSPs were optimised by tonically hyperpolarising or depolarising the cell to a membrane potential of -70mV or -20mV respectively, in the presence of an oscillation. From the intracellular recordings, cell firing, EPSPs and IPSPs during gamma, beta or alpha rhythms could be cross correlated with the oscillation to measure phase synchrony and spike triggered average of the field to determine which cell types were actively or passively involved in the particular rhythms using Matlab version 8.3. Briefly, for spike-triggered LFP averages spike peaks were detected via simple thresholding of intracellular waveforms and rasterised. Each spike was used as a 'time zero' reference point for splitting concurrently recorded LFP waveforms into 1s epochs (+/- 500 ms from the spike reference point). The LFP epochs were then summed to give the average LFP waveform, occurring at the point of the spike. For wave (LFP)-triggered averaging the LFP waveform was tightly band-pass filtered according to the modal peak frequency (30 – 50 Hz for gamma, 14-30 Hz for beta, 8-12 Hz for alpha). Maximal trough deflections were detected using a simple 'local minimum' routine and the time point for these minima used to construct 1s epochs of intracellular waveform data. Field-triggered spike histograms were found by taking a 1s time-course of the spikes found for each wave-trigger and summing them in bins of 200ms. For EPSP and IPSP analysis these epochs were averaged, for spike/LFP coherence the 1s epochs were divided into 5 ms bins and the total number of spikes occurring in each bin for every epoch (relative to time zero – the LFP local minimum) plotted as a histogram.

2.9.3 Statistical analysis

Statistical analysis of the data for the pharmacological experiments was conducted using Sigmaplot 12.3 software (Systat software Inc.) and Microsoft Excel (Microsoft Corp.). The data was presented in the text and graphical representations as the mean of the data +/- the standard error of the mean (SEM). Primary analysis was done to determine the distribution of the data set. If the data displayed a normal distribution paired t-tests were carried out to compare data which had been derived from the same slice or cell i.e. before and after addition of pharmacological

agents. For data which did not contain a normal distribution, Mann-Whitney Rank Sum Tests were used. The median value plus the interquartile range (Q1-Q3) was expressed for data which did not display a Gaussian distribution, and a Mann-Whitney Rank Sum Test was used to compare the median values of data sets rather than their mean values.

Alternatively, where the analysis was concerned with more than one treatment groups, repeated measures tests were used. A One-Way Analysis of Variance (ANOVA) Test was carried out on parametric data to compare the mean values from data of the same entity which were normally distributed. For non-parametric data, a Kruskal-Wallis ANOVA Test was used e.g. to compare differences in power across the laminar column. A confidence interval of 95% ($P<0.05$) was employed for all statistical analyses, data was confirmed as statistically significant if the difference between groups exceeded this value. If data exceeded this confidence interval, the difference was greater than what would be expected by chance and the null hypothesis could then be rejected.

Correlation statistics were used to test how strongly a pair of variables were related e.g. when comparing preceding beta power with alpha power. The correlation coefficient or R value ranges from +1 to -1, giving information on how closely the two variables are related. By squaring the R value, the percent of the variation in one variable to the other is given, for example an R^2 value of 0.5 means 25% of the variation is related.

2.10 Immunohistochemistry techniques

2.10.1 Fixation and sectioning of slices

Slices were maintained at 4°C in 4% Paraformaldehyde (PFA) and 15% Picric acid (PA) for >24 hours. Slices were then washed in 0.1M phosphate buffer (PB) and 10-20% sucrose and embedded in a solution of 10% gelatine in distilled water which dissolved at around 40°C after 10 minutes. Slices were submerged in gelatine and left to set on ice before being excised and stored in fixative (4% PF, 15%PA) for 1

hour. Gelatine-containing slices were then removed from the fixative and cut in 40-60μm thick sections using a vibratome to ensure successful visualisation of immunohistochemically stained cells.

2.10.2 Staining techniques

Re-sectioned slices were again washed in 0.1M PB followed by 0.01M Sodium Citrate at 100°C for 10 minutes then rinsed with PBS at room temperature for 20 minutes. Slices were then washed in TRIS buffer solution (TBS) followed by 10% Normal Goat Serum (NGS) in TBS containing 0.5% TWEEN for 60 minutes. They were then left to incubate at room temperature overnight with the primary antibody anti-GAD-67, raised in mouse (Millipore, UK) made up in 2% NGS-TBS TWEEN. After overnight incubation, slices were washed in TBS then incubated with secondary antibodies: AF488 goat anti mouse IgG(H+L) and AF568 streptavidin (ThermoFisher Scientific, MA, U.S.A) made up in TBS at room temperature for 2 hours in the dark. Slices were then mounted onto slides with vectashield to be visualised using confocal microscopy.

2.10.3 Staining of Biocytin filled cells

After confocal microscopy, the sections were carefully removed from the slides and washed with TBS; they were then left to incubate overnight with the ABC elite kit (Vector labs, Peterborough) in a cold room on a shaker. Sections were again washed in TBS followed by TB before being placed in 0.05% DAB and the sections were observed for a colour change to a dark brown. Once this was achieved, the reaction of the DAB was stopped by washing in PB and distilled water. The sections were then mounted onto a glass slide to be viewed under the light microscope.

Chapter 3: Results - Generation of alpha oscillations in the primary visual cortex

3.1 Introduction

3.1.1 Models of alpha rhythms

Alpha frequency activity was first described *in vitro* in slice preparations of rat sensorimotor neocortex by Silva et al. (1991). They recorded from 2 types of pyramidal cells, some that elicited single spikes and others which fired rhythmic bursts, in layer V and observed rhythmic firing patterns between 5-12Hz. The authors increased activation of NMDA receptors by reducing extracellular magnesium ion concentration. This facilitates NMDA gated currents in most subtypes of NMDA-gated channel by removing the open channel block afforded by this ionic species (Jahr and Stevens, 1990). Bathing slices in zero magnesium concentrations led to the observation of rhythmic synchronised activity at 4-10Hz. The pyramidal neurons were phase locked to the rhythmic field potentials.

Whether this type of alpha-frequency network behaviour is of physiological relevance is debatable. Alpha rhythms in sensorimotor cortex are seen concurrently with beta frequency spectral content (the 'mu' rhythm (Pfurtscheller et al., 1997)) but the above study demonstrated only theta and alpha frequency activity. In addition, reducing magnesium ion content of the bathing solution for slices maintained *in vitro* is a well-established model of epileptiform activity in neocortex (Straub et al., 1992). Slow (theta/alpha) bursting is a characteristic feature of a number of epilepsies in humans, with 'alpha seizures' being typically associated with epilepsies secondary to anoxia and localised encephalopathies (Gelety et al., 1985)

A more physiological model of alpha rhythms has been reported in thalamic tissue. Alpha oscillations have been generated *in vitro* in cat brain slices of the lateral geniculate nucleus (LGN). This was done by strong activation of the metabotropic glutamate receptor (mGLUR1) mimicking cortico-thalamic feedback (Hughes et al., 2004). This study showed alpha rhythms to be driven by high threshold bursting thalamaocortical neurons (HTC) and synchronised by gap junctions.

A computational model of thalamic alpha oscillations has been devised by Vijayan and Kopell (2012). Here they adapted a thalamic model from previous studies (Destexhe et al., 1996) consisting of a network of reticular nucleus cells and TC cells. They incorporated the HTC cells connected by gap junctional coupling discovered by previous work by Hughes et al. as described above, which burst at the alpha frequency at a depolarised membrane potential. Their model generated alpha activity by the activation of muscarinic acetylcholine receptors (mAChR) or the mGluR1 subtype of glutamate receptors. They found that, consistent with *in vitro* experiments, TC cells fire during any phase of alpha with the mGLuR1-induced alpha model. In the mAChR model of alpha, TC cells fire phase locked to the alpha field. They suggest that the mAChR-induced alpha, when there is strong alpha power, inhibits layer IV pyramidal cell firing in the neocortex. When alpha power is weak, TC cell firing is strong and this could drive layer IV pyramidal cells in the neocortex in a tonic manner, suggesting the mAchR model may group TC cell activity into perceptual units for processing. On the other hand, the mGluR1 induced alpha model may be involved in functional inhibition, and due to the irregular spike-field coherence, may block the inputs from thalamus reaching the cortex.

Large scale computational modelling has reproduced the alpha rhythm, without involving the thalamus, in a manner based on excitatory lateral interactions between coupled cortical macrocolumns serving as alpha generators (Naruse et al., 2010). Freyer et al. (2011) were able to produce a model incorporating thalamocortical activity. In addition, computational models of purely neocortical alpha rhythms have been proposed. A model by Jones et al. (2000a) suggested that h- and T- currents present in layer V pyramidal cells produce and regulate alpha frequency rhythms and promote spatially asynchronous firing patterns.

While the thalamic alpha generator is well established mechanistically *in vitro*, very little is known about the possibility of a purely neocortical generator. The model of Jones et al. (above) was critically dependent on h-current, but levels of activity of this intrinsic conductance are low in the awake state (see chapter 1). In addition, none of the models described above address the apparent interplay between alpha

and beta rhythms (Killian and Buffalo, 2014), nor do they consider any role for synaptic plasticity in the formation of this rhythm.

3.1.2 Kainate induced beta oscillations

Beta rhythms are a very common feature of cortical dynamics and a number of *in vitro* models have established their underlying mechanism and its relation to synaptic plasticity (e.g. see (Roopun et al., 2008)). Most of these models use network activation *in vitro* via kainate receptors (KA) (Roopun et al., 2006) so this approach will be used as a starting point in attempts to generate a useful *in vitro* model of alpha rhythms in this thesis.

KA receptors are ionotropic receptors which respond to the binding of glutamate and contribute to glutamatergic excitation at the synapse. They were first identified through their activation upon application of the agonist KA to frog spinal cord *in vitro* (Evans, 1980). There are 5 different subunits of KA receptors: GluR5, GluR6, GluR7, KA1 and KA2. KA receptors are tetrameric; the subunits can be arranged in different ways to form a four-subunit receptor. Glu5-7 can form homomers, a receptor consisting entirely of one subunit, or heteromers, a receptor consisting of two or more subunits. KA1 and KA2 can only form functional receptors with the GluR5-7 subunits (for review see (Carta et al., 2014)). KA receptors are distributed throughout the brain, they modulate synaptic transmission and neuronal excitability as well as playing a role in synaptic plasticity (Contractor et al., 2011). KA receptors have pre- and post-synaptic actions, post-synaptic activation is involved with excitatory neurotransmission and pre-synaptic activation is involved in inhibitory neurotransmission via modulating the release of GABA.

The role of KA receptors in rhythm generation appears to involve at least three mechanisms: In the hippocampus they can directly excite axons of interneurons in a manner that has been linked to gamma rhythm generation (Fisahn et al., 2004) and they can alter the intrinsic potassium current in principal cells, increasing spike rates and decreasing accommodation (Melyan et al., 2002), thus favouring recruitment into fast (beta/gamma) network activity. In somatosensory cortex they

can tonically depolarise certain subtypes of principal cells – particularly intrinsically bursting neurons – facilitating burst-dependent beta rhythms (Roopun et al., 2006). In cortex, both post and pre-synaptic kainite receptors have been shown to contribute to thalamocortical transmission (Kidd and Isaac, 1999; Kidd et al., 2002). However, all these mechanisms have been characterised in brain regions other than visual cortex. It is uncertain what effect KA receptor activation has in the V1, nor is it known how KA receptors modulate functional network activity in the visual cortices.

Not much is known about the mechanisms underlying the generation of beta oscillations in the visual system either. Chemical activation of KA and/or muscarinic cholinergic receptor subtypes has been shown to generate beta oscillations in the somatosensory cortex (Roopun et al., 2006), auditory cortex (Roopun et al., 2010) and medial prefrontal cortex (mPFC) (Glykos et al., 2015). While these *in vitro* studies strongly suggest that an excitatory glutamatergic or cholinergic drive is needed to generate these oscillations, it is not known how they contribute to beta rhythms in the visual system. At a phenomenological level the primary visual cortex is thought to contribute to beta oscillations in extra-striate areas. During visual stimulation, beta oscillations in the V4 are replaced by gamma oscillations. A lesion in the primary visual cortex reverses this suppression of beta rhythms in the V4, suggesting beta responses in extra-striate areas are controlled by the V1 (Schmiedt et al., 2014). Thus the origin of both alpha and beta rhythms appears to lie in the V1.

3.1.3 Aims and objectives

Alpha oscillations have been shown to follow beta oscillations in the human visual cortex after the removal of a visual stimulus or an “eyes closed” state; there have been no attempts made to replicate these findings in *in vivo* recordings from rodents. In order to generate a model for this type of alpha rhythm in the visual system the main aim was therefore to mimic this sequence of network activity (eyes open) followed by relative inactivity (eyes closed). The main objective in this respect was to establish a beta/gamma rhythm state in visual cortex and then use

pharmacological manipulation to attempt to selectively reduce the level of excitation in a manner that gives rise to alpha rhythms. Once established the remaining two aims for the body of work in this chapter were to spatially characterise the alpha rhythm and to quantify any relationship between the alpha rhythm and prior beta/gamma rhythms.

Previous pilot studies have shown that alpha oscillations *can* be generated in the visual cortex *in vitro* using exclusively cortical interactions, without the need for thalamic input. These preliminary experiments showed post-response alpha in the primary visual cortex upon layer IV activation with microdrop application of a small volume of glutamate (1mM, 70nL) (Figure 3.1). This manipulation alone generated a transient epoch of gamma/beta rhythms which faded, in both power and frequency, rapidly with time. When the same manipulation was repeated with nicotinic cholinergic neuromodulation the initial, transient gamma/beta response transformed into a prolonged alpha rhythm. This showed the possible validity of a purely neocortical alpha rhythm model *in vitro*. However, such transient, rapidly time-variant events are very hard to explore mechanistically so a more 'persistent' model system was needed. This chapter describes how such a model was produced.

3.2 methods

All experiments described in this chapter were carried out using *in vitro* brain slice preparations (450μM slice thickness) from adult male Wistar rats (150-200g). Visual cortex containing slices were cut coronally and were prepared and maintained as described in chapter 2.1-2.4. n reflects the number of slices. All drugs were applied to the bathing medium. All data obtained from experiments from this chapter was via extracellular field recordings outlined in chapter 2.6 and all data acquisition and analysis are described in chapter 2.7-2.8.

3.3 Results

3.3.1 Generation of beta oscillations in the primary visual cortex

Persistent beta oscillations (14-30Hz) were generated in the primary visual cortex by bath application of the kainate receptor agonist KA [400-800nM] to the circulating ACSF. Control recordings were taken prior to addition of KA to ensure the slices contained no intrinsic oscillatory activity, thus, upon addition of KA, any oscillatory activity observed could be connected to the activation of KA receptors. Preliminary investigations showed that beta activity was highest in layer IV of the V1, so initial extracellular field recordings were obtained from there before a more thorough quantification of laminar distribution was attempted (see 3.3.8 below).

Application of KA to the slices generated oscillations in the beta frequency range (14-30Hz). Figure 3.2A shows examples of extracellular beta activity at two different concentrations of KA [400 and 800nM]. Figure 3.2.B shows example power spectra produced from FFT analysis of a 60 second epoch of extracellular data. The power spectra produced provided a quantitative measurement from which the peak power and frequency of oscillations could be determined. Increasing the concentration of KA caused no significant difference in the mean frequency of the oscillation: 30.1Hz $\pm$ 0.9Hz vs. 29.0Hz $\pm$ 0.5Hz for 400 and 800nM KA respectively ($P>0.05$, n=43 for 400nM KA n=93 for 800nM KA, Mann-Whitney Rank Sum Test, Figure 3.2D). Doubling the concentration did however cause a significant increase in the power of the oscillation from 7.0μV^2 $\pm$ 1.8μV^2 to 11.4μV^2 $\pm$ 1.0μV^2, ($P<0.001$, n=43 for 400nM KA n=93 for 800nM KA, Mann-Whitney Rank Sum Test, Figure 3.2D).

Figure 3.2C shows a measure of the rhythmicity of oscillations by auto-correlation analysis of 60 second epochs of extracellular data. From this it was determined that the temporal organisation of the beta rhythm seen was qualitatively similar at each of the two concentrations used. From these initial experiments, it was decided

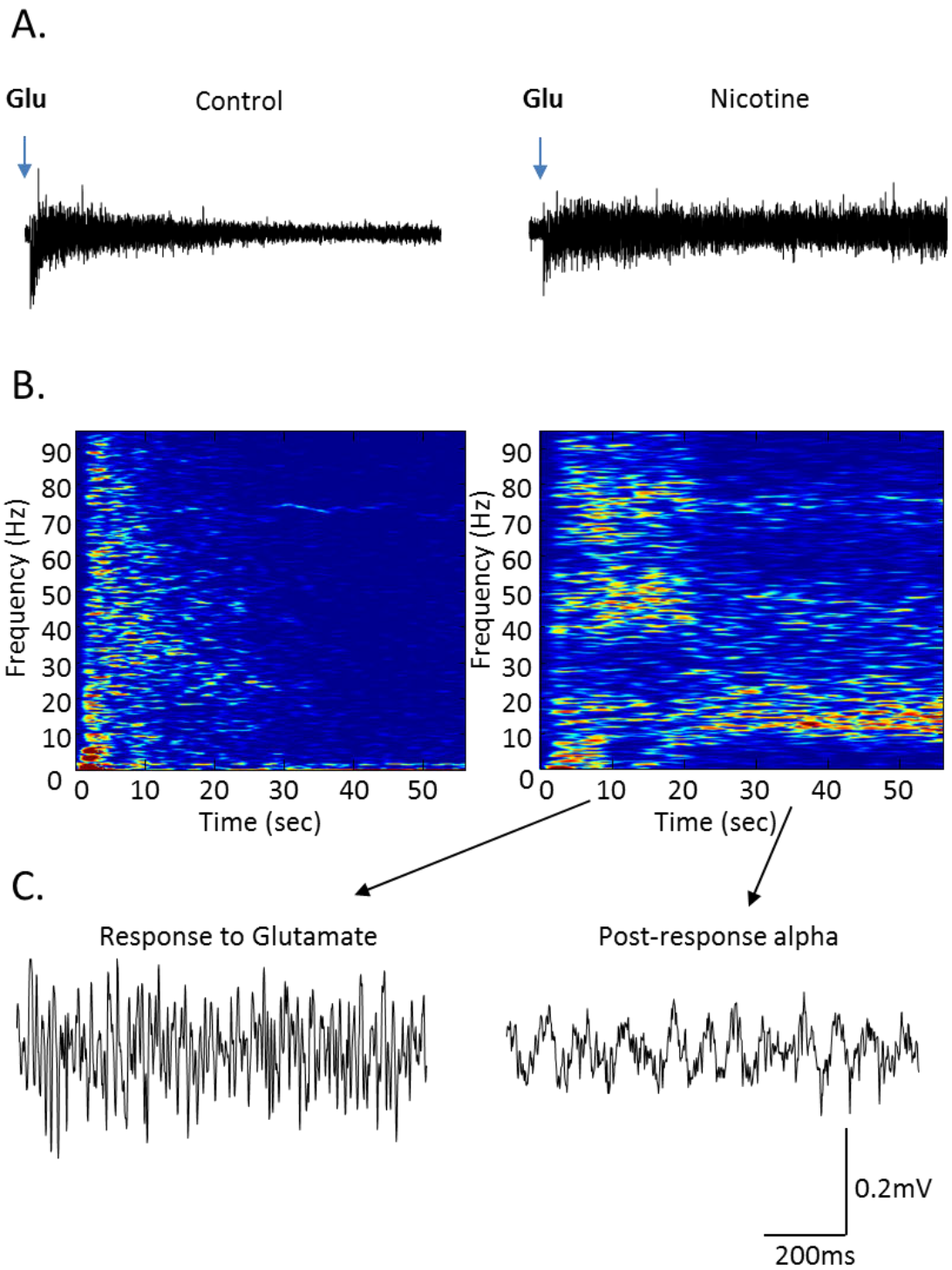

Figure 3.1 Post-stimulus alpha oscillations are observed after spritzing with glutamate in the presence of Nicotine in layer IV of the primary visual cortex. A. One minute example traces of extracellular activity after spritzing of glutamate [1mM] before and after the addition of Nicotine [10μM]. **B.** Example spectrogram produced from traces in A. **C.** One second example traces of extracellular activity produced from the traces shown in A showing the response to glutamate approximately 10 seconds after spritzing and post-stimulus alpha approximately 30 seconds after glutamate spritzing (n=4).

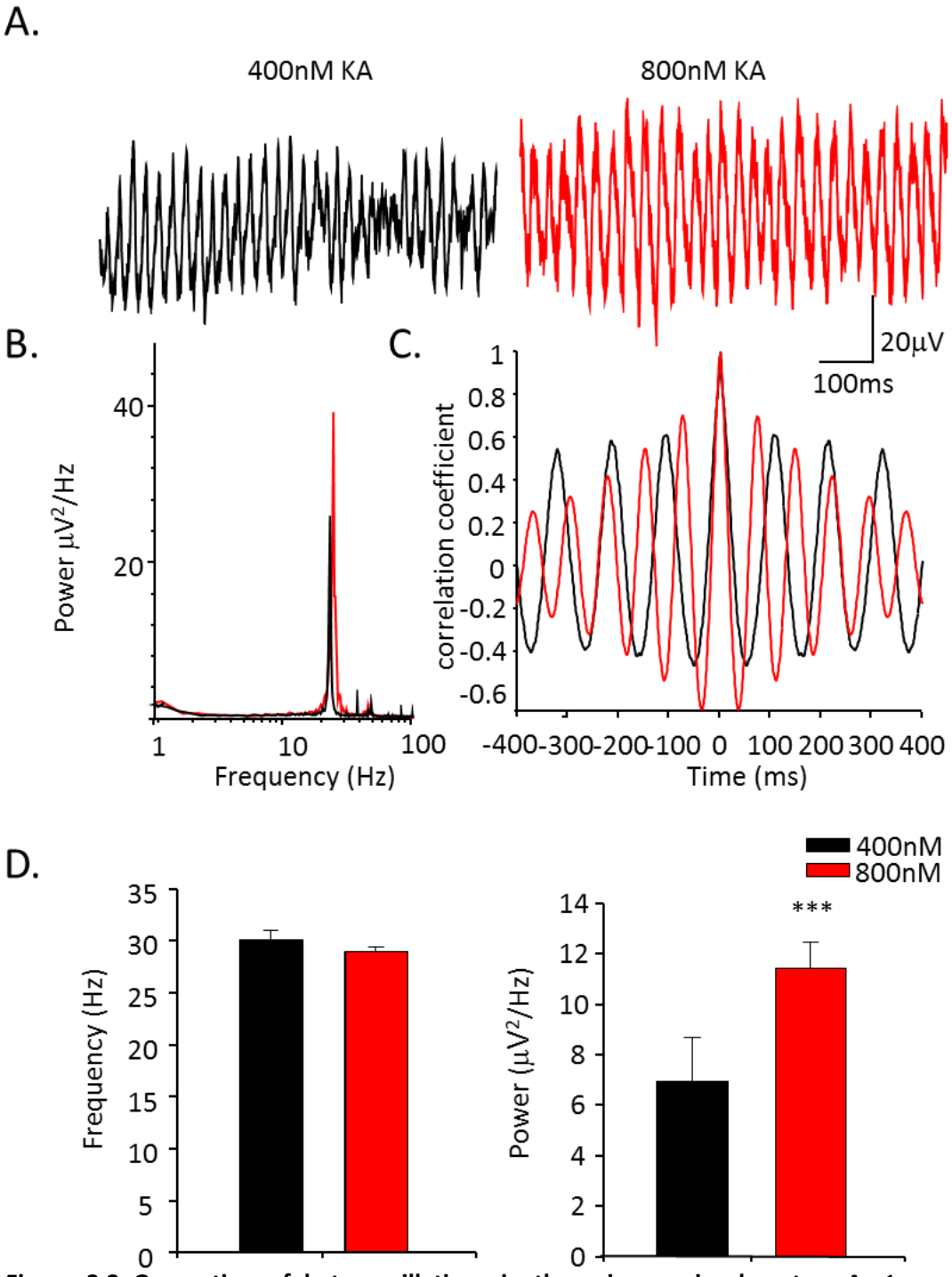

Figure 3.2 Generation of beta oscillations in the primary visual cortex. A. 1 second example traces of extracellular activity induced by Kainate [KA, 400nM] (black trace) and [800nM] (red trace). **B.** Example power spectra produced from traces in A. **C.** Example auto-correlations produced from 60 second epochs of extracellular data showing rhythmicity after application of 400nM KA (in black) and 800nM KA (in red). **D.** Graphs showing the change in frequency and amplitude between 400nM and 800nM of KA (frequency, $P>0.05$, amplitude $P<0.001$, both Mann-Whitney Rank Sum Test, n=43 black, n=93 red. n=number of slices).

800nM KA would be the optimum concentration to use for generation of persistent beta oscillations in the primary visual cortex.

3.3.2 Variations in the effects of KA

The beta rhythm, as described in 3.3.1 above, was evoked in coronal sections of the primary visual cortex. On some occasions however only a gamma rhythm or a dual gamma and beta rhythm was observed after application of 800nM KA (Figure 3.3A and 3.3B). No overt pattern to the change in the spectral content of KA-induced rhythms was immediately obvious, but it was decided to see whether subtle alterations in the slice orientation or surface damage may underlie the variability; it is possible that cutting the slices in different orientations can have an effect on the connections and local circuitry, therefore affecting oscillation frequency. It was found that changing the blade orientation during coronal slicing of the brain (Figure 3.3C) changed the incidence and frequency of oscillations seen. Figure 3.3D shows graphical representations of these changes. Cutting with a forwards facing blade gave oscillations in the beta frequency (14-30Hz) at the highest incidence of 76 vs. 49 occasions when comparing to gamma frequency oscillation alone (30-50Hz). In contrast a dual gamma and beta spectrum was seen on 19 occasions. A back facing blade gave oscillations in the gamma frequency the highest number of times at 33, with only 10 observed in the beta frequency and 8 at dual gamma beta frequencies. A sideways facing blade gave the highest incidence of dual gamma beta oscillations at 6 occasions vs. 4 incidences of beta and only 1 at gamma frequency. These results were not statistically significant (P=0.062, One Way Analysis of Variance). However, for beta oscillations, a front facing orientation of the blade was used primarily in cutting. For gamma oscillations a back facing orientation of the blade was used to optimise the chance of seeing each of these spectral components for further experimentation.

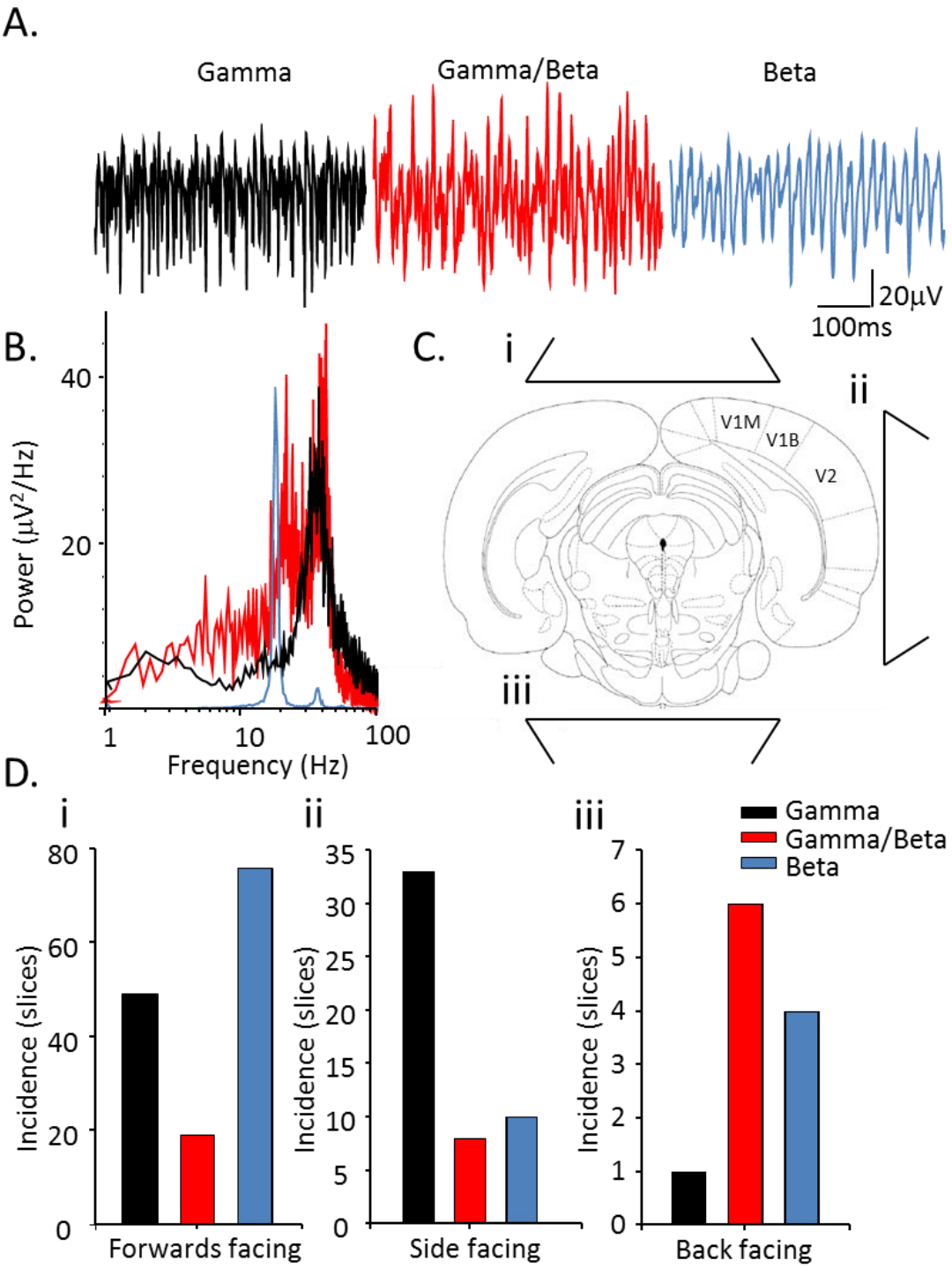

Figure 3.3 Variations in the effects of KA. A. 1 second example traces of extracellular activity after application of 800nM KA **i**. example gamma oscillation **ii.** example gamma/beta oscillation and **iii.** example beta oscillation**. B.** Example power spectra produced from traces in A. **C.** Diagram showing the orientation of the blade during slicing **i.** forward facing **ii.** side facing **iii.** back facing. **D.** Graphs showing the incidence and frequency of oscillations depending on slice orientation during cutting after application of KA [800nM] ($P>0.05$, One Way Analysis of Variance).

3.3.3 Generation of alpha oscillations in the primary visual cortex

From the above section it was clear we could reliably model visual cortical activation persistently using KA. The next step was therefore to investigate how we could reduce the level of network excitation to see if this activated state could be transformed into one showing alpha rhythms. The following subsections describe different strategies used to achieve this. In each case slices were left to oscillate in KA alone for a minimum of 30 minutes before further drugs were added.

3.3.3.1 Antagonism of KA or AMPA receptors alone did not reduce the frequency of beta oscillations in the primary visual cortex

The first step was to see whether the selective antagonism of either α-amino-3-hydroxy-5-methyl-4-isoxazolepropionic acid receptor (AMPA) or the KA receptors used to generate the network activation in the first place was necessary and sufficient to reduce the frequency of oscillations to that in the alpha range.

The selective (ca. 30-fold over AMPA receptors (More et al., 2003) antagonism of KA receptors with (αS)-α-Amino-3-[(4-carboxyphenyl)methyl]-3,4-dihydro-5-iodo-2,4-dioxo-1(2H)-pyrimidinepropanoic acid (UBP301 [15μM]) caused no change in the frequency of the beta rhythm 31.1Hz ± 2.8Hz vs. 31.2Hz ± 3.6Hz (P= 0.818, KA alone vs. KA followed by KA+UBP301, n=6 Mann-Whitney Rank Sum Test, figure 3.4). UBP301 also failed to change the rhythmicity of the observed beta rhythm: 0.6 ± 0.1 vs. 0.4 ± 0.1 for KA or KA + UBP301 respectively (P=0.145, n=5, Two-Tailed T-Test). However, reduction in KA receptor function did cause a decrease in the power of the beta rhythm: 5.4μV^2 ± 1.0μV^2 vs. 2.0μV^2 ± 0.5μV^2 for KA and KA+UBP301 respectively (P<0.05, n=6, Two-Tailed T-Test).

Selectively antagonising AMPA receptors alone with the non-competitive agent (±)-4-(4-Aminophenyl)-1,2-dihydro-1-methyl-2-propylcarbamoyl-6,7-methylenedioxy-phthalazine (SYM2206 [10μM]) caused no significant difference in the power, frequency or rhythmicity of the beta rhythm (figure 3.5). Mean oscillation

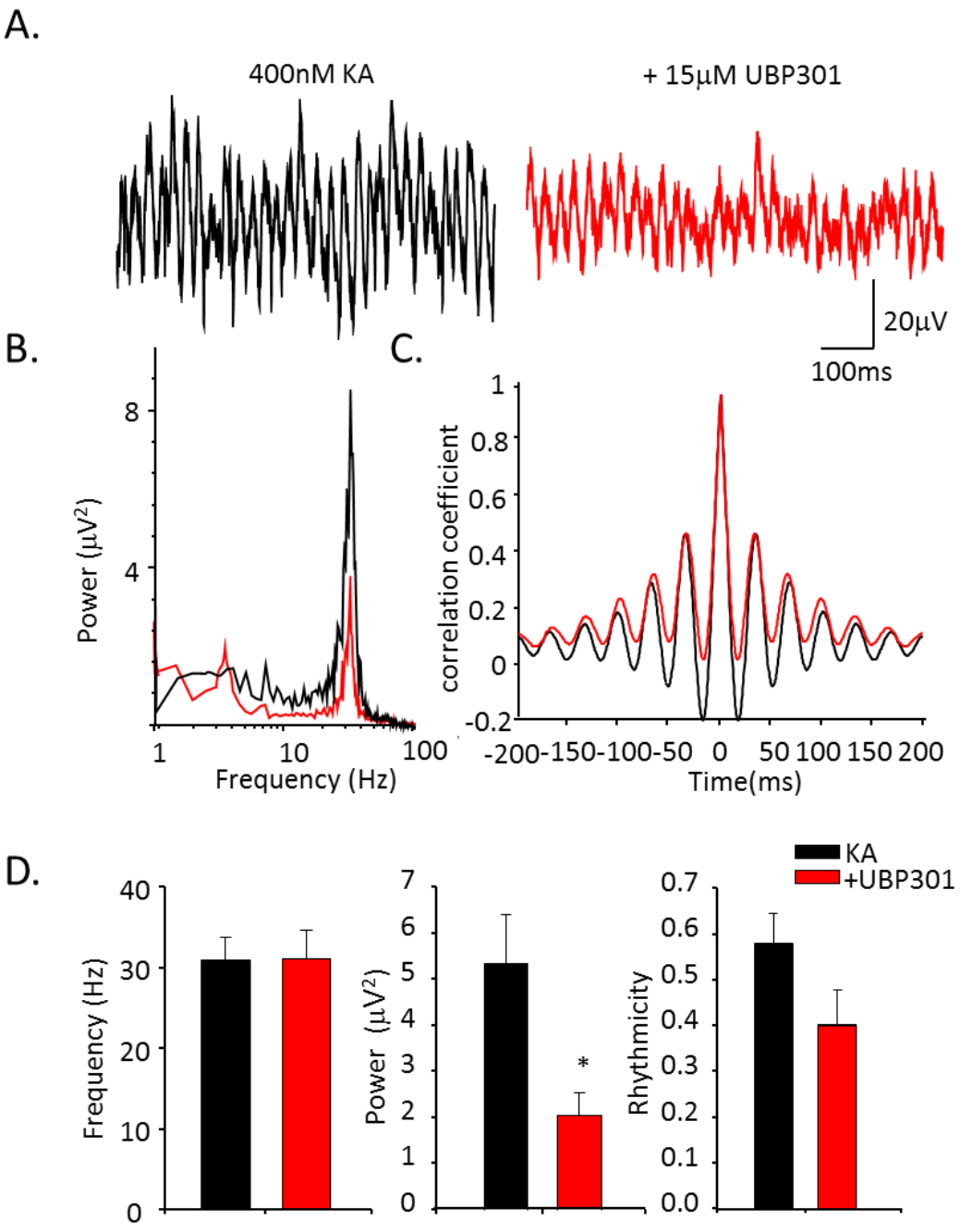

Figure 3.4 Blocking KA receptors alone reduced power but not frequency of beta oscillations. A. 1 second example traces of extracellular activity induced by Kainate [400nM] (black trace) and 30 minutes after addition of UBP301 [15µM] (red trace). **B.** Example power spectra produced from traces in A showing the effect of UBP301 on beta oscillations. **C.** Example auto-correlations produced from 60 second epochs of extracellular data showing rhythmicity before (in black) and after (in red) application of UBP. **D.** Graphs showing the change in frequency, amplitude and rhythmicity of oscillations before and after application of UBP (frequency $P>0.05$, n=6, Mann-Whitney Rank Sum Test, amplitude $P<0.05$, n=6, Two-tailed T-Test, rhythmicity $P>0.05$, Two-Tailed T-Test, n=5).

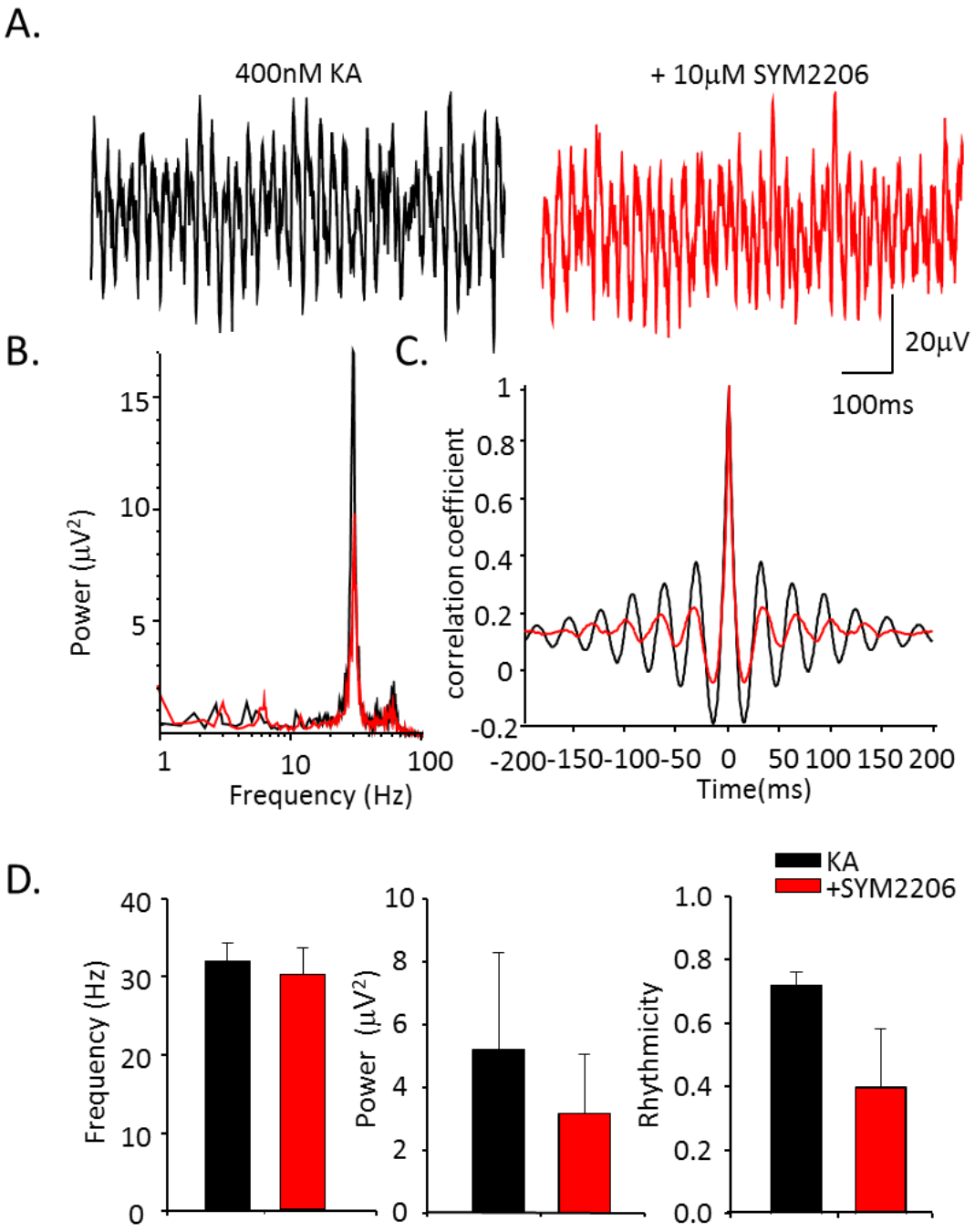

Figure 3.5 Blocking AMPA receptors alone did not reduce the frequency of the beta rhythm. A. 1 second example traces of extracellular activity induced by Kainate [400nM] (black trace) and 30 minutes after addition of SYM2206 [10µM] (red trace). **B.** Example power spectra produced from traces in **A** showing the effect of SYM2206 on beta oscillations. **C.** Example auto-correlations produced from 60 second epochs of extracellular data showing rhythmicity before (in black) and after (in red) application of SYM2206. **D.** Graphs showing the change in frequency, power and rhythmicity of oscillations before and after application of SYM2206 (frequency $P>0.05$, amplitude $P>0.05$, rhythmicity $P>0.05$, all Mann-Whitney Rank Sum Test, n=6).

frequencies with KA or KA followed by SYM 2206 were 32.0Hz ± 2.3Hz and 30.3Hz ± 2.4Hz respectively (P = 0.485, n=6, Mann-Whitney Rank Sum Test). Mean peak powers were 5.2μV^2 ± 3.0μV^2 and 3.1μV^2 ± 1.9μV^2 (P = 0.394, n=6, Mann-Whitney Rank Sum Test), and mean rhythmicities were 0.72 ± 0.04 vs. 0.40 ± 0.19 (P=0.180, n=6, Mann-Whitney Rank Sum Test). The above data showed that reducing the original activation of the network by KA reduced the power of the rhythm generated. However, this was not associated with a reduction to alpha frequencies. Reducing AMPA receptor activity alone also did not cause a reduction to alpha frequencies and had only subtle (non-significant) effects on mean power and rhythmicity. We therefore next tried a reduction in both glutamate receptor systems together.

3.3.3.2 Partial antagonism of KA and AMPA receptors together reduced the frequency of beta oscillations in the primary visual cortex

Once beta oscillations were established in the V1, the non-selective KA and AMPA receptor antagonist 2,3-Dioxo-6-nitro-1,2,3,4-tetrahydrobenzo[f]quinoxaline-7-sulfonamide (NBQX) was added. Different concentrations (2-10μM) of NBQX were applied to determine the optimum amount required to potentially reduce the frequency without abolishing power or rhythmicity of the beta oscillation (Figure 3.6A). A gradual decrease in peak oscillation frequency was seen as NBQX concentration was increased. At the highest concentration tested (10μM) the control frequency of 27.6Hz ± 0.9Hz was significantly reduced to 11.8Hz ± 0.7Hz (P<0.001, n=5, Two-Tailed T-Test, figure 3.6). Interestingly, an Inverted U Function relationship was seen between NBQX concentration and oscillation power (Figure 3.6A), with beta oscillation power increasing from control levels around an NBQX concentration of ca. 5μM. 6.8μV^2 ± 1.2μV^2 vs. 16.7 μV^2 ± 6.8μV^2 (P=0.259, n=5, Two-Tailed T-Test) then decreasing to 3.9μV^2 ± 1.5μV^2 (P=0.157, n=5, Two-Tailed T-Test) at a concentration of 10μM, however these results were not significant.

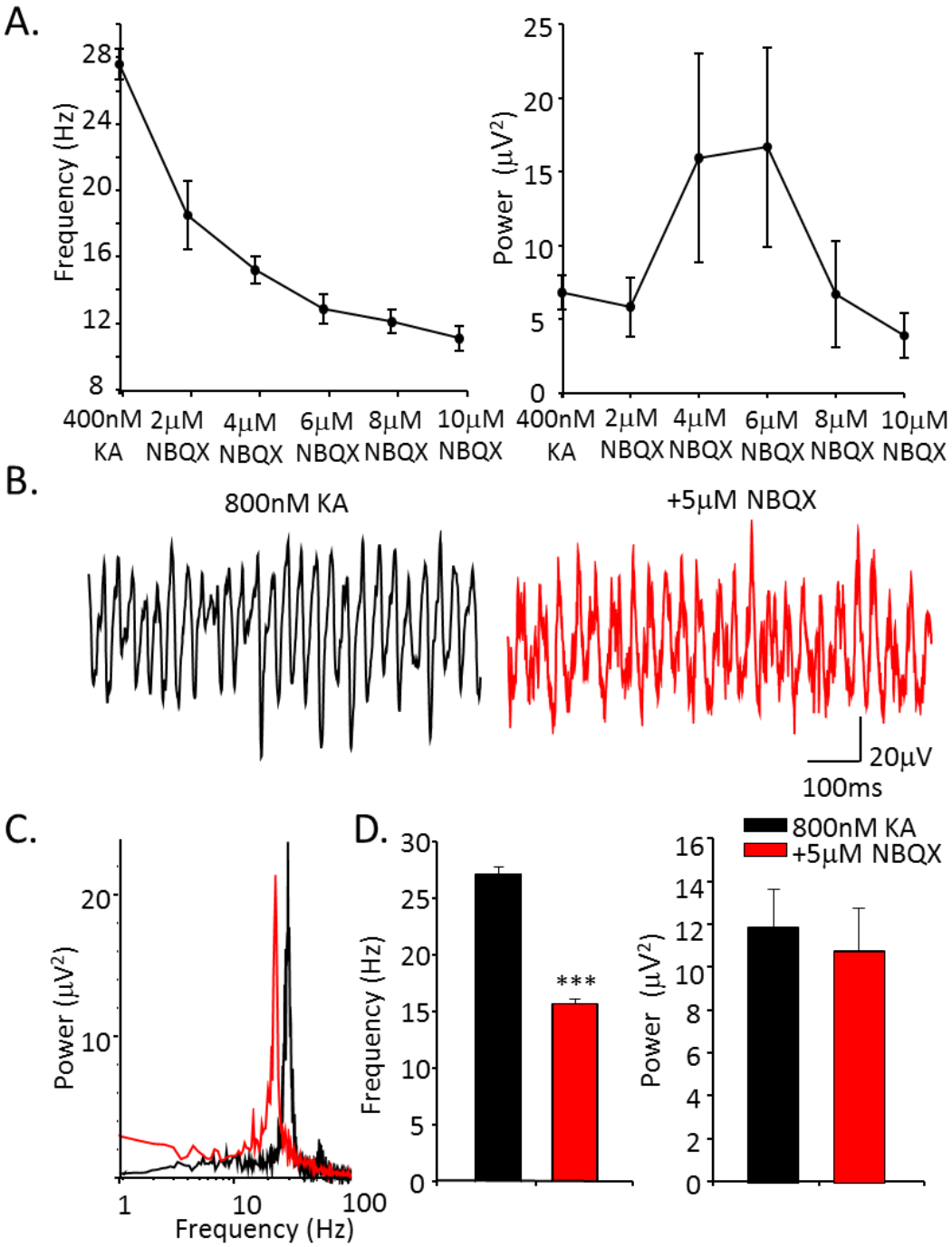

Figure 3.6 Partial antagonism of both KA and AMPA receptors reduced the frequency but not the power of beta oscillations. A. Concentration response curves showing the effects of increasing concentrations of NBQX (2-10μM) on the frequency and power of beta oscillations induced by 400nM KA (n=5)**. B.** 1 second example traces of extracellular activity induced by Kainate [800nM] (black trace) and NBQX [5μM] (red trace). **C.** Example power spectra produced from traces in B. **D.** Graphs showing the change in frequency and peak power of beta oscillations after addition of 5μM NBQX (frequency $P<0.001$, amplitude $P>0.05$, both Mann-Whitney Rank Sum Test, n=52).

Application of 5μM NBQX to the beta rhythms generated by the higher KA concentration of 800nM also caused a reduction in the frequency of the rhythm by approximately 12Hz (27.3Hz ± 0.6Hz vs. 15.8Hz ± 0.4Hz P<0.001, n=51, Mann-Whitney Rank Sum Test, figure 3.6B,C). However, with beta rhythm power already high, there was no significant decrease in the power 11.9μV^2 ± 1.8μV^2 vs. 10.8μV^2 ± 8.2μV^2 (P=0.287, n=51, Mann-Whitney Rank Sum Test). These data demonstrated that concurrent reduction in KA and AMPA receptor-mediated network excitability could reduce network peak frequency. However, this manipulation of activity levels did not reduce frequencies down to alpha rhythm levels. We therefore built on the network effects of NBQX, using the concentration of 5μM from now on, and looked at further reductions in excitability at the single cell level.

3.3.3.3 Blocking I_h current reduced the frequency of oscillations to alpha and caused an increase in power

Application of the I_h channel blocker 4-Ethylphenylamino-1,2-dimethyl-6-methylaminopyrimidinium chloride (ZD7288 [10μM]) to the beta rhythm prior to its reduction in drive with NBQX together caused a reduction of frequency to that in the alpha range 15.6Hz ± 1.3Hz vs. 11.7Hz ± 0.3Hz (P<0.001, n=22, Mann-Whitney Rank Sum Test, figure 3.7D) and a 4 fold increase in the power 11.6μV^2 ± 5.6μV^2 vs. 55.4μV^2 ± 5.9μV^2 (P<0.01, n=22, Mann-Whitney Rank Sum Test). The rhythmicity of this resultant alpha rhythm was also significantly larger than the beta rhythm generated by KA and NBQX alone: 0.59 ± 0.15 vs. 1.00 ± 0.14 (P<0.05, n=10, Two-Tailed T-Test).

ZD7288 has also been reported to affect GABAergic synaptic inhibition at the concentration used (Lupica et al., 2001), so to confirm the above observed effects were mediated by I_h suppression we used a different, more selective blocker. Subsequent blocking of I_h channels, following NBQX application to KA-induced beta rhythms, with (S)-(+)-7,8-Dimethoxy-3-[[1-(2-(3,4-dimethoxyphenyl)ethyl)-3-piperidinyl]methyl]-1,3,4,5-tetrahydro-2H-3-benzazepin-2-one hydrochloride (DK-

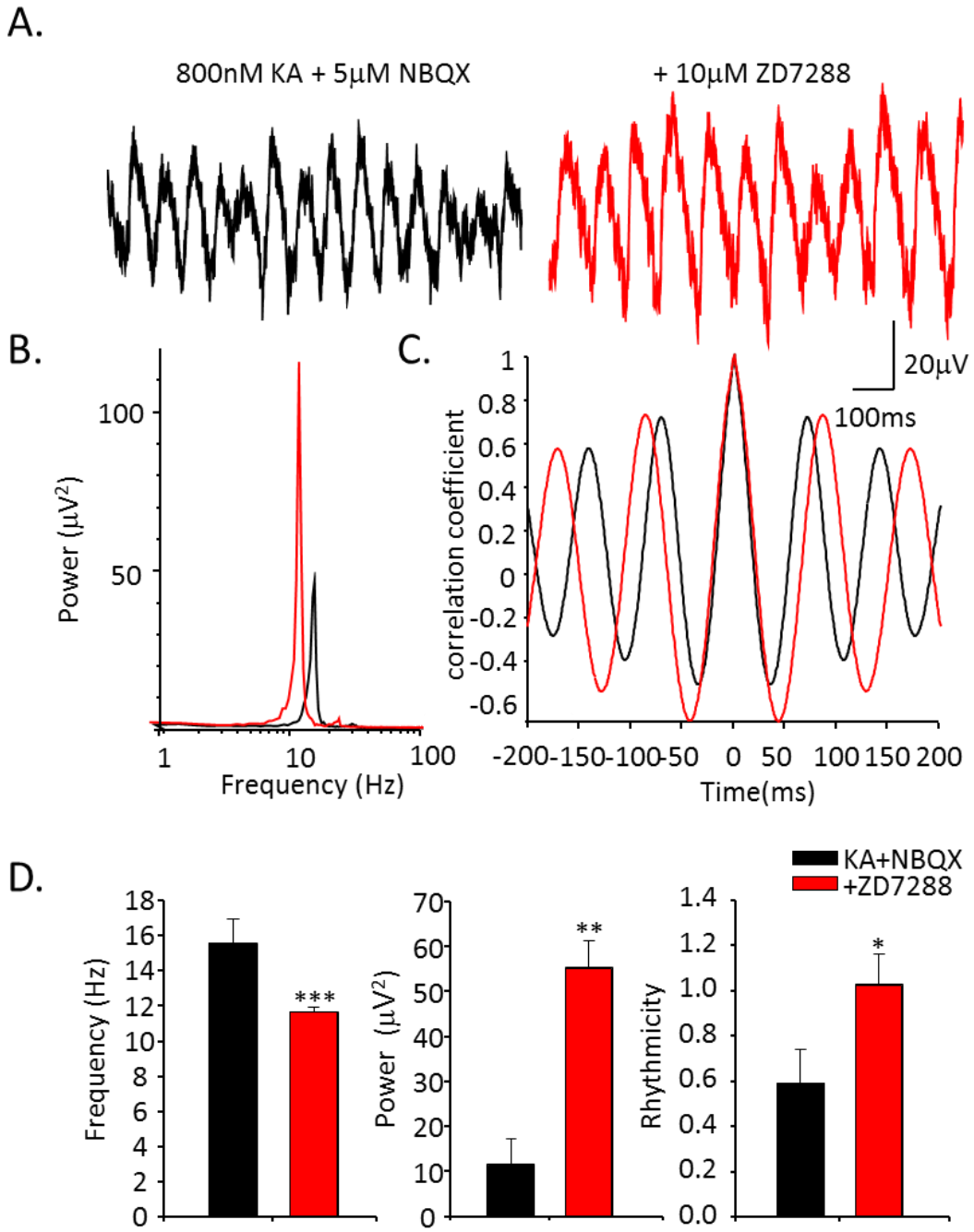

Figure 3.7 Subsequent blocking of I_h channels produced alpha frequency oscillations: effects of ZD7288. A. 1 second example traces of extracellular activity induced by Kainate [800nM] and NBQX [5µM] (black trace) and 30 minutes after addition of ZD7288 [10µM] (red trace). **B.** Example power spectra produced from traces in A. **C.** Example auto-correlations produced from 60 second epochs of extracellular data showing rhythmicity before (in black) and after (in red) application of ZD7288. **D.** Graphs showing the change in frequency ($P<0.001$, n=22, Mann-Whitney Rank Sum Test), power ($P<0.01$, n=22, Mann-Whitney Rank Sum Test) and rhythmicity ($P<0.05$, n=10, Two-Tailed T-Test) of oscillations after addition of ZD7288.

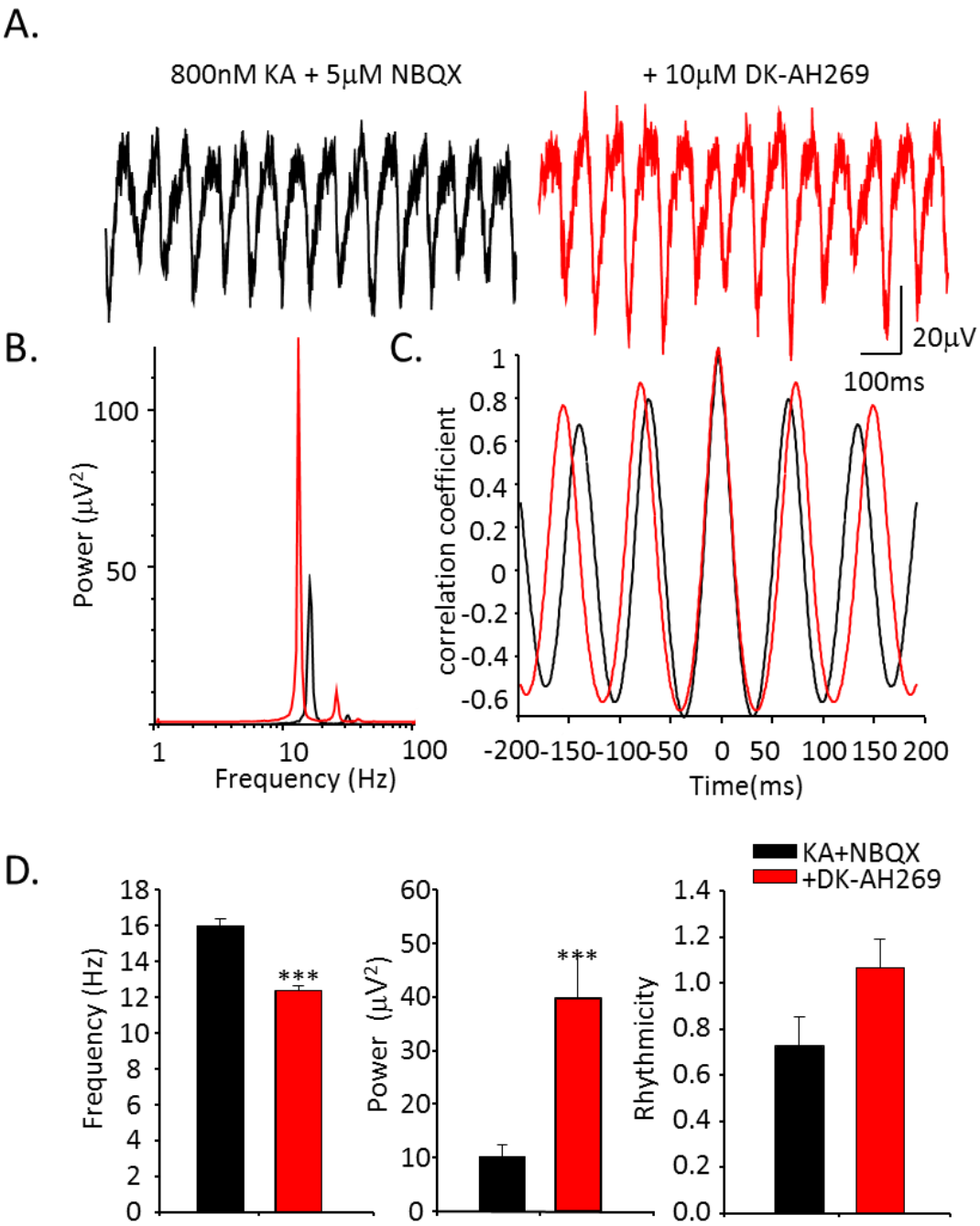

Figure 3.8 Subsequent blocking of I_h channels produced alpha frequency oscillations: effects of DK-AH269. A. 1 second example traces of extracellular activity induced by Kainate [800nM] and NBQX [5µM] (black trace) and 30 minutes after addition of DK-AH269 [10µM] (red trace). **B.** Example power spectra produced from traces in A. **C.** Example auto-correlations produced from 60 second epochs of extracellular data showing rhythmicity before (in black) and after (in red) application of DK-AH269. **D.** Graphs showing the change in frequency ($P<0.001$, n=30, Mann-Whitney Rank Sum Test), power ($P<0.001$, n=30, Mann-Whitney Rank Sum Test) and rhythmicity ($P>0.05$, n=10, Two-Tailed T-Test) of oscillations after addition of DK-AH269.

AH269 [10μM]) also produced a reduction in frequency to that in the alpha range: 16Hz ± 0.5Hz vs. 12.4Hz ± 0.3Hz (P<0.001, n=30, Mann-Whitney Rank Sum Test, figure 3.8) and, again, a 4 fold increase in power from 10.3μV^2 ± 2.2μV^2 to 39.8μV^2 ± 8.0μV^2 (P<0.001, n=30, Mann-Whitney Rank Sum Test). It also caused an increase in the mean rhythmicity of the oscillation, however this was not statistically significant: 0.73 ± 0.13 vs. 1.00 ± 0.12 (P=0.069, n=10, Two-Tailed T-Test).

Once alpha oscillations had been established, recordings were taken at 15 minute intervals to follow the temporal stability of this rhythm. It was determined that alpha oscillations reach their maximum amplitude 105 minutes after application of DK-AH [10μM] (Figure 3.9). There is a gradual increase in power concurrent with small decreases in frequency after application of DK-AH [10μM]. After the peak in power at approximately 105 minutes, the frequency and amplitude of oscillations slowly decreased until all rhythmicity had died away. These data suggest that alpha rhythms are a response to reduced network and cellular excitability following a prior period of network activation. We therefore needed to address the relationship between the alpha rhythm and the properties of this prior activated network. To do this we took advantage of the variable expression of gamma and beta rhythms inherent in the slice model used (3.3.2 above).

3.3.4 Robust alpha rhythms could not be generated from gamma rhythms alone in the primary visual cortex

Excitation of the primary visual cortex with KA [800nM] has already been shown to generate both beta and gamma oscillations (3.3.2). By using slices that generated only gamma rhythms, and not beta rhythms, it was shown that a preceding gamma rhythm did not lead to strong alpha frequency oscillations when network and cellular excitation was reduced. Application of NBQX [5μM] and DK-AH269 [10μM]

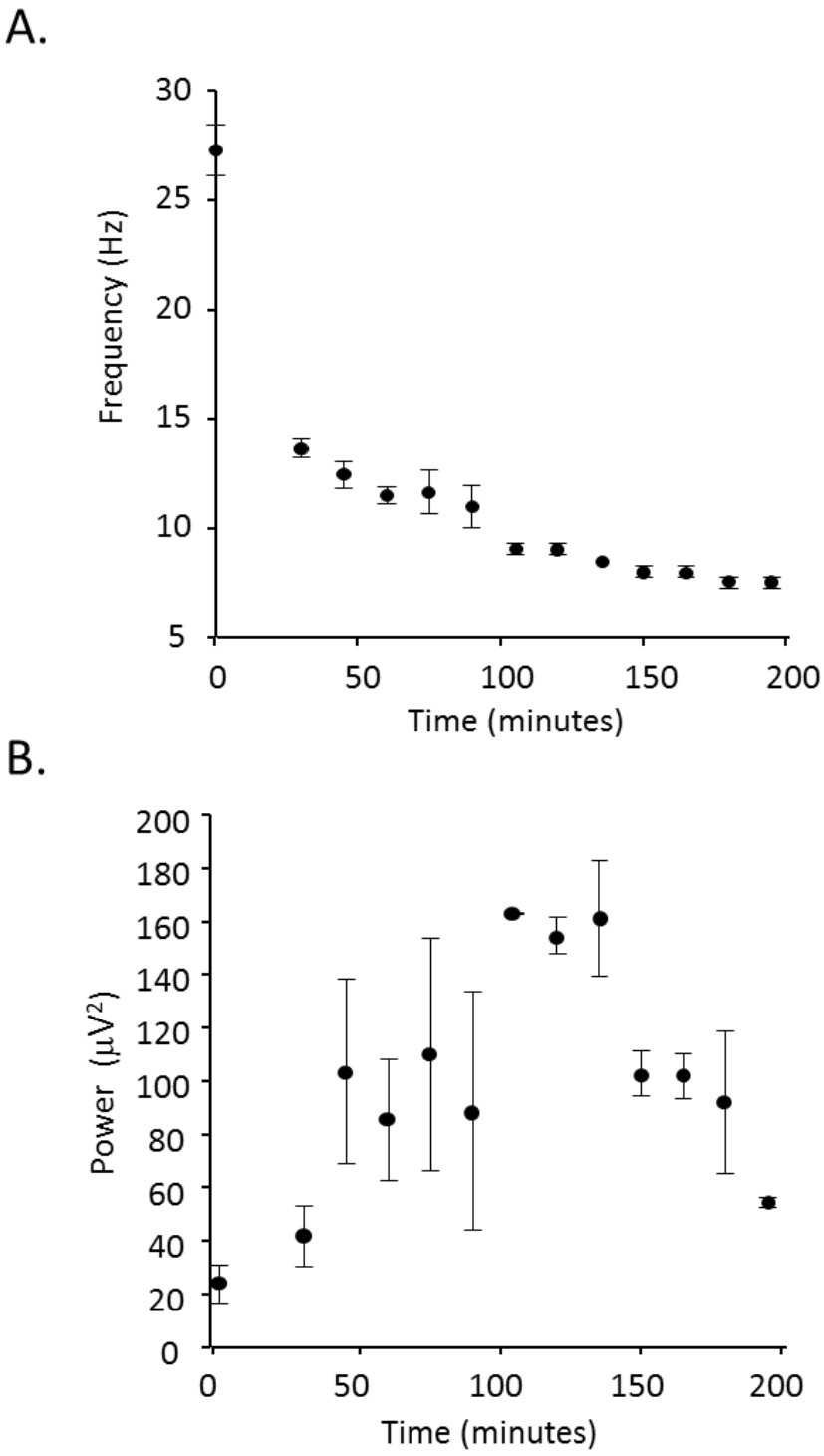

Figure 3.9 The alpha rhythm reached its maximum amplitude 105 minutes after application of NBQX and DK-AH in the visual cortex. A. Graph showing the effect of time on the frequency of alpha oscillations. **B.** Graph showing the effect of time on the power of alpha oscillations produced from 60 second epochs of extracellular data. The beta rhythm is generated with application of KA [800nM], at 0 minutes NBQX [5μM] and DK-AH269 [10μM] were added to generate alpha frequency oscillations (n=14 0-60 minutes, n=4 90-120 minutes, n=2 150-200 minutes).

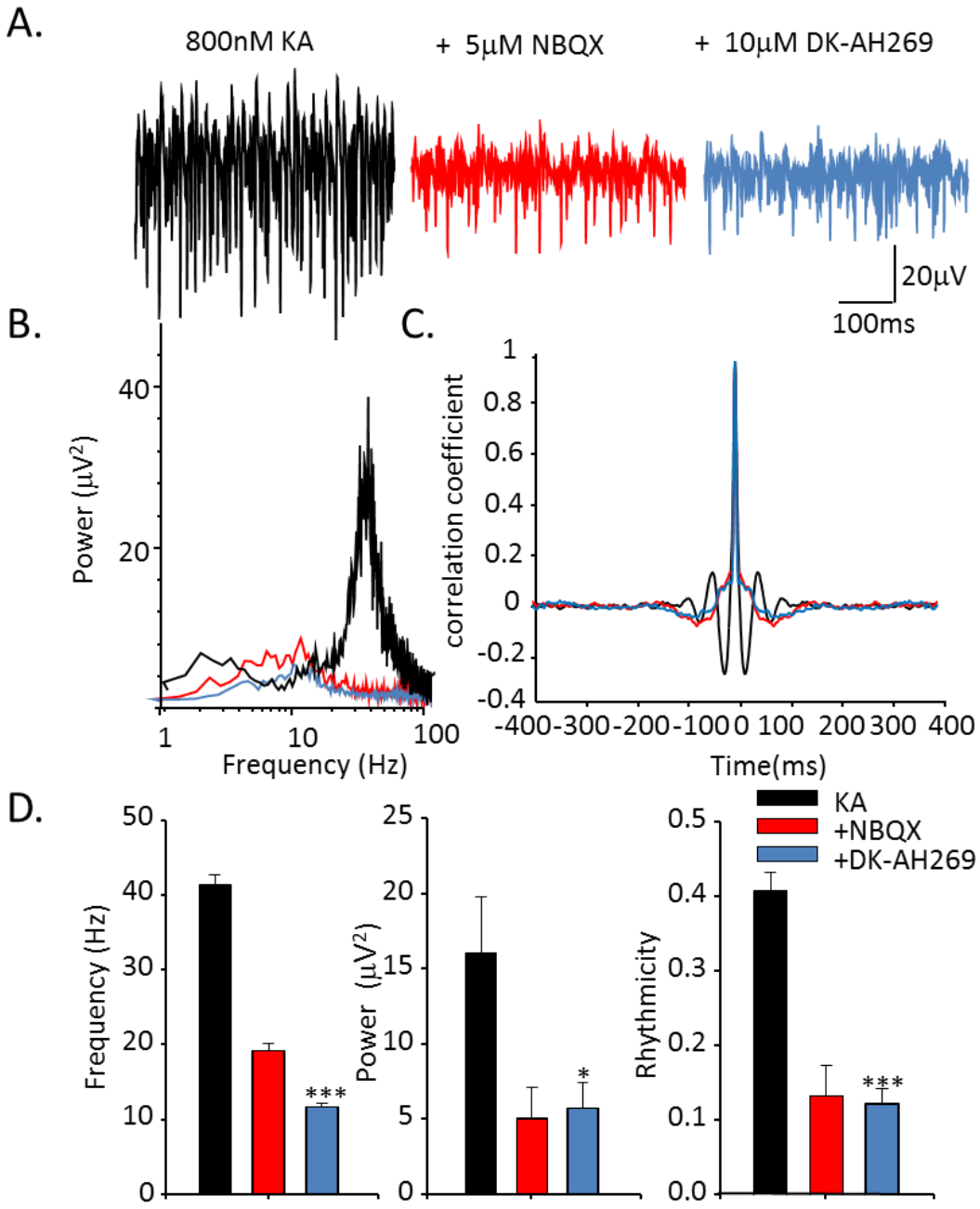

Figure 3.10 A preceding gamma rhythm alone did not generate alpha frequency oscillations in the visual cortex. A. 1 second example traces of extracellular activity induced by Kainate [800nM] (black trace) in a slice showing only gamma rhythms (see Fig.3.3), 30 minutes after addition of NBQX [5µM] (red trace) and 30 minutes after addition of DK-AH269 [10µM] (blue trace). **B.** Example power spectra produced from traces in A. **C.** Example auto-correlations produced from 60 second epochs of extracellular data showing rhythmicity after addition of 800nM KA (in black), NBQX [5µM] (in red) and DK-AH269 [10µM] (in blue). **D.** Graphs showing the change in frequency ($P<0.001$, $n=27$), power ($P<0.05$, $n=27$) and rhythmicity ($P<0.001$, $n=9$, all Mann-Whitney Rank Sum Test) of oscillations after excitation with KA [800nM], application of NBQX [5µM] and subsequent application of DK-AH269 [10µM].

to an existing gamma rhythm caused a reduction in frequency of the rhythm from 41.4Hz ± 1.3Hz to the alpha frequency: 11.8Hz ± 0.5Hz (P<0.001, n=27, Mann-Whitney Rank Sum Test, Figure 3.10). However the power of the rhythm was also significantly reduced from 16.1μV^2 ± 3.7μV^2 to 5.7μV^2 ± 1.7μV^2 (P<0.05, n=27, Mann-Whitney Rank Sum Test), with the abolition of any clear modal peak in the alpha band (Figure 3.10B). The absence of a modal peak was accompanied by a near abolition of rhythmicity: 0.40 ± 0.02 at gamma frequency vs. 0.10 ± 0.02 for the residual alpha frequency (P<0.001, n=9, Mann-Whitney Rank Sum Test). These observations were in stark contrast to the elevated power and rhythmicity on transition to alpha rhythms from beta rhythms described above (compare figure 3.10 with figures 3.7 and 3.8).

3.3.5 Dual gamma/beta oscillations could generate low power alpha oscillations in the primary visual cortex

It has also been noted that dual gamma/beta rhythms may be generated in the primary visual cortex upon application of KA [800nM] (3.3.2). These rhythms produced 2 peaks in power spectra (Figure 3.11B) and had frequencies both between 12-30Hz and 30-50Hz. The mean frequencies of these rhythms were 46.1Hz ± 1.8Hz vs. 27.2Hz ± 0.8Hz and the differences were statistically significant (P<0.001, n=21, Mann-Whitney Rank Sum Test). The mean beta power was also greater than the power of gamma oscillations 3.8μV^2 ± 1.0μV^2 vs. 11.0μV^2 ± 5.1μV^2 (P<0.05, n=21, Mann-Whitney Rank Sum Test).

Application of NBQX [5μM] and DK-AH269 [10μM] to the dual gamma/beta rhythm caused a reduction in frequency of the rhythm from 46.1Hz ± 1.8Hz and 27.2Hz ± 0.8Hz to a single peak at 11.3Hz ± 0.6Hz (P<0.001, n=21, Mann-Whitney Rank Sum Test). It also caused a slight increase in power of the rhythm from 3.8μV^2 ± 1.0μV^2 (beta) and 11.0μV^2 ± 5.1μV^2 (gamma) to 15.3μV^2 ± 5.7μV^2 (alpha) with the difference in gamma to alpha power being statistically significant (P<0.01, n=21, Mann-Whitney Rank Sum Test) but beta to alpha not (P=0.546, n=21, Mann-Whitney Rank Sum Test). There was also an apparent reduction in mean

rhythmicity, however this was not statistically significant 0.6 ± 0.1 vs. 0.4 ± 0.1 (P=0.335, n=10, Mann-Whitney Rank Sum Test).

These data demonstrated that generation of a high-power alpha rhythm on reducing network and intrinsic excitation appeared to be associated with prior manifestation of the beta rhythm in the V1. With beta rhythms alone alpha power was, on average, 40-60μV^2, with lower power beta rhythms manifested concurrently with gamma rhythms the subsequent alpha power was approximately 10-20μV^2. Without beta rhythms, but with prior gamma rhythm generation subsequent alpha power was 0-10μV^2 with no clear modal peak in this frequency band. We therefore next attempted to see if there was a significant relationship between beta and alpha power or whether just the presence of a prior beta rhythm was sufficient.

3.3.6 No significant relationship between the power of alpha oscillations and the prior power of beta oscillations

Attempts to generate alpha oscillations did not always succeed; approximately 75% of slices gave alpha oscillations once the pharmacological agents as described above had been applied. These alpha oscillations however were not always the high power alpha as seen *in vivo*, we therefore needed to look at a possible relationship between the beta and alpha rhythms. The previous results suggested that power of the alpha rhythm may be determined by the power of the preceding beta rhythm. Data from all experiments where a clear beta spectral peak was seen prior to reducing network and intrinsic neuronal drive was pooled to see if such a relationship was quantifiable. Figure 3.12A shows the relationship between prior beta power and subsequent alpha power had an R squared value of 0.08 (n=126, P=0.397). This is a very poor fit, indicating that, while beta rhythms may be a prerequisite for alpha rhythm generation (previous sections above), there was no direct, numerical correlation. There was a similarly poor correlation with pooled data from slices in which only gamma rhythms were seen prior to reduced network and cellular excitability (Figure 3.12B). The mean power of alpha oscillations generated from a preceding gamma rhythm was much lower than that from a

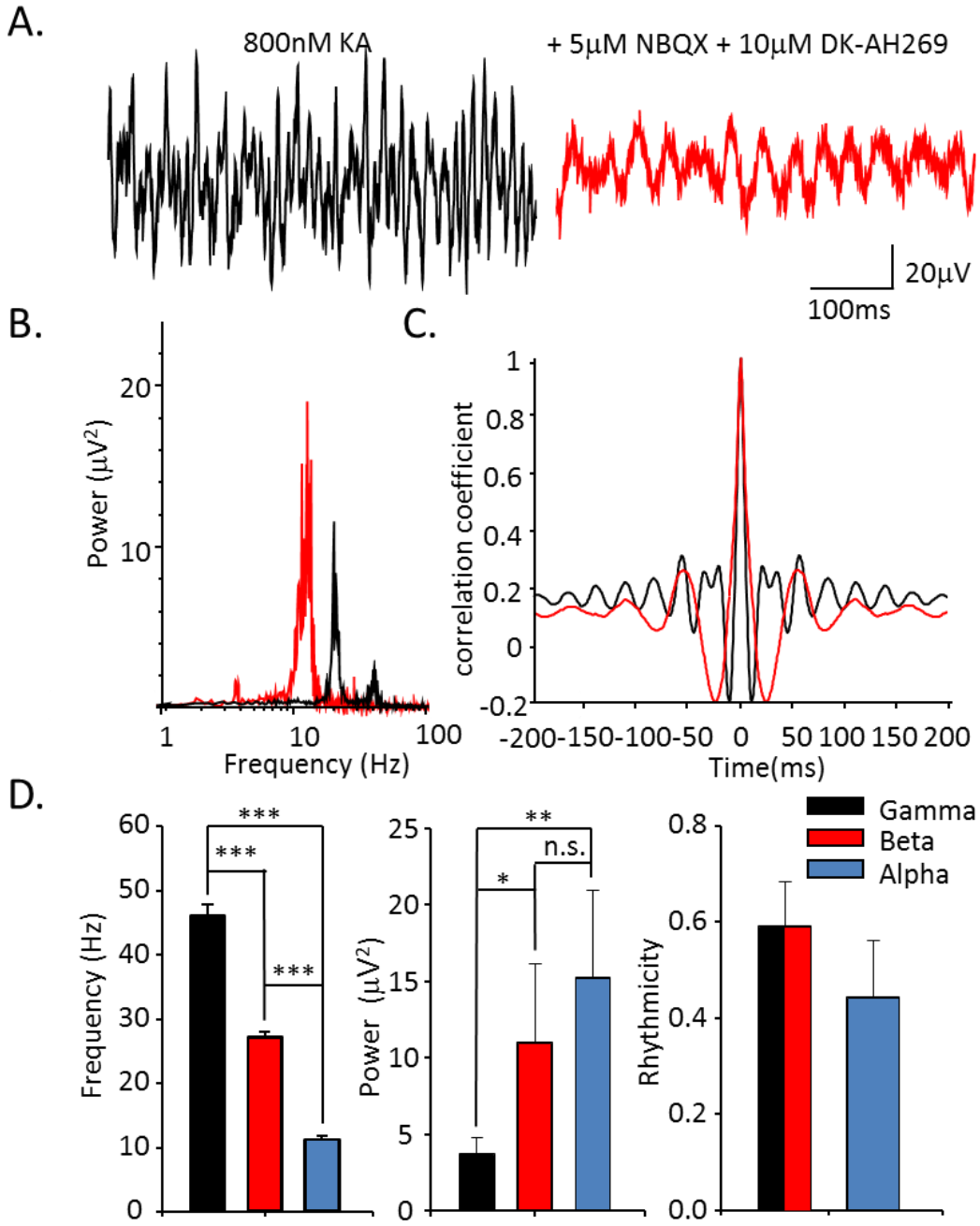

Figure 3.11 A preceding gamma/beta rhythm could generate low amplitude alpha frequency oscillations in the visual cortex. A. 1 second example traces of extracellular activity induced by Kainate [800nM] (black trace) and 30 minutes after addition of NBQX [5µM] and DK-AH [10µM] (red trace). **B.** Example power spectra produced from traces in A. **C.** Example auto-correlations produced from 60 second epochs of extracellular data showing rhythmicity after addition of 800nM KA (in black), and NBQX [5µM] and DK-AH [10µM] (in red). **D.** Graphs showing frequency ($P<0.001$, $n=21$), power ($P<0.01$ for gamma-alpha, $P<0.05$ gamma-beta, $P>0.05$ for beta-alpha, $n=21$) and rhythmicity ($P>0.05$, $n=10$, all Mann-Whitney Rank Sum Test) of gamma and beta oscillations after excitation with KA [800nM], and subsequent application of NBQX [5µM] and DK-AH [10µM].

preceding beta rhythm: 5.7μV^2 $\pm$ 1.7μV^2 vs. 42.6μV^2 $\pm$ 4.4μV^2 respectively (P<0.001, n=27 gamma, n=148 beta, Mann-Whitney Rank Sum Test) and, again, R squared values (0.16) indicated a weak, if any, causal relationship (n=26, P=0.434). For the purpose of all experiments performed and presented in the subsequent two results chapters it was necessary to be able to predict the generation of a strong alpha rhythm prior to reducing excitation levels. This was because we probed the nature of the network changes during activation that lead to alpha rhythms in more detail using addition of pharmacological agents during this activation stage. With such a poor correlation between preceding beta power and subsequent alpha power this was difficult. However, we subjectively determined that a good alpha power was one over 10μV^2. With this threshold set, any experiment with alpha power below this had a mean power of 3.8μV^2 $\pm$ 0.4μV^2 with a mean preceding beta power of 6.8μV^2 $\pm$ 0.9μV^2 (P<0.05, n=64, Mann-Whitney Rank Sum Test). Any alpha oscillations with a power over 10μV had a mean power of 48.5μV^2 $\pm$ 5.7μV^2 with a mean preceding beta power of 15.0μV^2 $\pm$ 1.8μV^2 (P<0.001, n=77, Mann-Whitney Rank Sum Test). The difference in the beta power between those experiments showing above- and below-threshold alpha power was 15.0μV^2 $\pm$ 1.8μV^2 vs. 6.8μV^2 $\pm$ 0.9μV^2 respectively (P<0.001, n=77, n=64 respectively, Mann-Whitney Rank Sum Test). The difference in the alpha power above and below threshold was 48.5μV^2 $\pm$ 5.7μV^2 vs. 3.8μV^2 $\pm$ 0.4μV^2 respectively (P<0.001, n=77, n=64 respectively, Mann-Whitney Rank Sum Test). The effects of thresholding and dividing the dataset are shown graphically in Figure 3.12C.

3.3.7 The generation of alpha rhythms required prior excitation in the visual cortex

While the absolute level of beta power did not correlate well with subsequent alpha activity levels, the above experiments did suggest that beta rhythms were an essential prerequisite. To test this, further experiments were carried out to see if alpha rhythms can be generated without any prior overtly rhythmic activity at all. Application of KA [800nM], NBQX [5μM] and DK-AH269 [10μM] all at the same time produced no detectable spectral peaks before or after addition of pharmacological

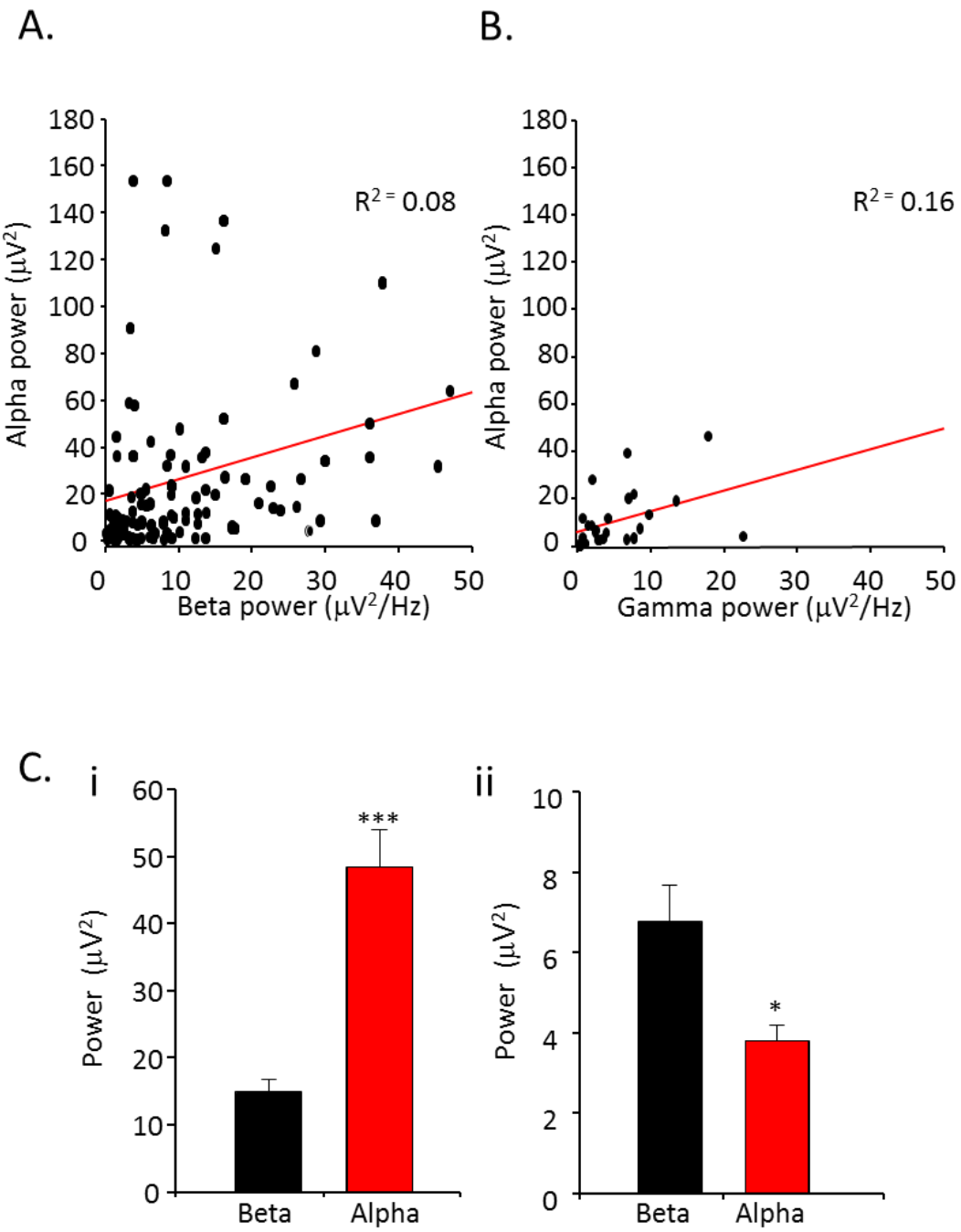

Figure 3.12 Relationship between alpha and beta or gamma power. A. Diagram with regression line showing the relationship between alpha power and the preceding beta power produced from 60 second epochs of extracellular recordings in slices showing beta rhythms only (n=143). **B.** Diagram with regression line showing the relationship between alpha power and the preceding gamma power produced from 60 second epochs of extracellular recordings in slices showing gamma rhythms only (n=27). **C.** Graphs showing the power of the preceding beta **i.** when alpha power exceeds 10μV ($P<0.05$, n=64) and **ii**. When alpha power is below 10μV ($P<0.001$, all Mann-Whitney Rank Sum Test, n=77).

agents. However, this spectral signature was not significantly different from that seen in slices with no drugs added. Frequency was 17.4Hz $\pm$ 0.6Hz in drug-free slices vs. 19.5Hz $\pm$ 1.5Hz in the presence of all the above agents needed to generate the alpha rhythm (P = 0.465, n=10, Two-Tailed T-Test, Figure 3.13). Similarly, the power at this frequency was 0.20μV^2 $\pm$ 0.04μV^2 in drug-free conditions and 0.20μV^2 $\pm$ 0.05μV^2 in the presence of all drugs (P = 0.447, n=10, Mann-Whitney Rank Sum Test).

This stark difference in behaviour of the slice when comparing to a sequential addition of drugs to first enhance then reduce network and cellular activity demanded further investigation. Blocking I_h current *prior* to reducing synaptic excitation did not produce overt alpha frequency oscillations. Application of ZD7288 to the beta rhythm caused no change in the frequency or power of the beta rhythm itself: 26.6Hz $\pm$ 1.7Hz vs. 24.8Hz $\pm$ 2Hz (P=0.488, n=11, Two-Tailed T-Test), 4.7μV^2 $\pm$ 2.0μV^2 vs. 4.8μV^2 $\pm$ 1.5μV^2 (P=0.818, n=11, Mann-Whitney Rank Sum Test, Figure 3.14). Subsequent application of NBQX [5μM] to the rhythm caused a reduction of frequency to that in the alpha range: 24.8Hz $\pm$ 2.0Hz vs. 9.3Hz $\pm$ 1Hz (P<0.001, n=11, Two-Tailed T-Test). However it also almost abolished the power of the local field potential rhythm, reducing it from 4.8μV^2 $\pm$ 1.5μV^2 to 0.9μV^2 $\pm$ 0.3μV^2 (P<0.01, n=11, Mann-Whitney Rank Sum Test).

In contrast, concurrent reduction in both synaptic (network) and intrinsic (I_h-mediated) excitation by co-application of NBQX [5μM] and DK-AH269 [10μM] following a period of excitation with KA [800nM] alone, readily produced alpha frequency oscillations. Frequencies were reduced from 30.0Hz $\pm$ 0.7Hz to 12.5Hz $\pm$ 0.2Hz (P<0.001, n=26, Mann-Whitney Rank Sum Test), and powers enhanced from 11.7μV^2 $\pm$ 1.4μV^2 to 31μV^2 $\pm$ 4.0μV^2 (P<0.001, n=26, Mann-Whitney Rank Sum Test, Figure 3.15).

The model for alpha predicted that there may be a form of synaptic plasticity occurring, as prior excitation of the slice must occur before alpha rhythms can be generated. This plasticity appeared to be associated with beta rhythm generation in the V1 and not gamma rhythm generation. However, whatever potential plastic

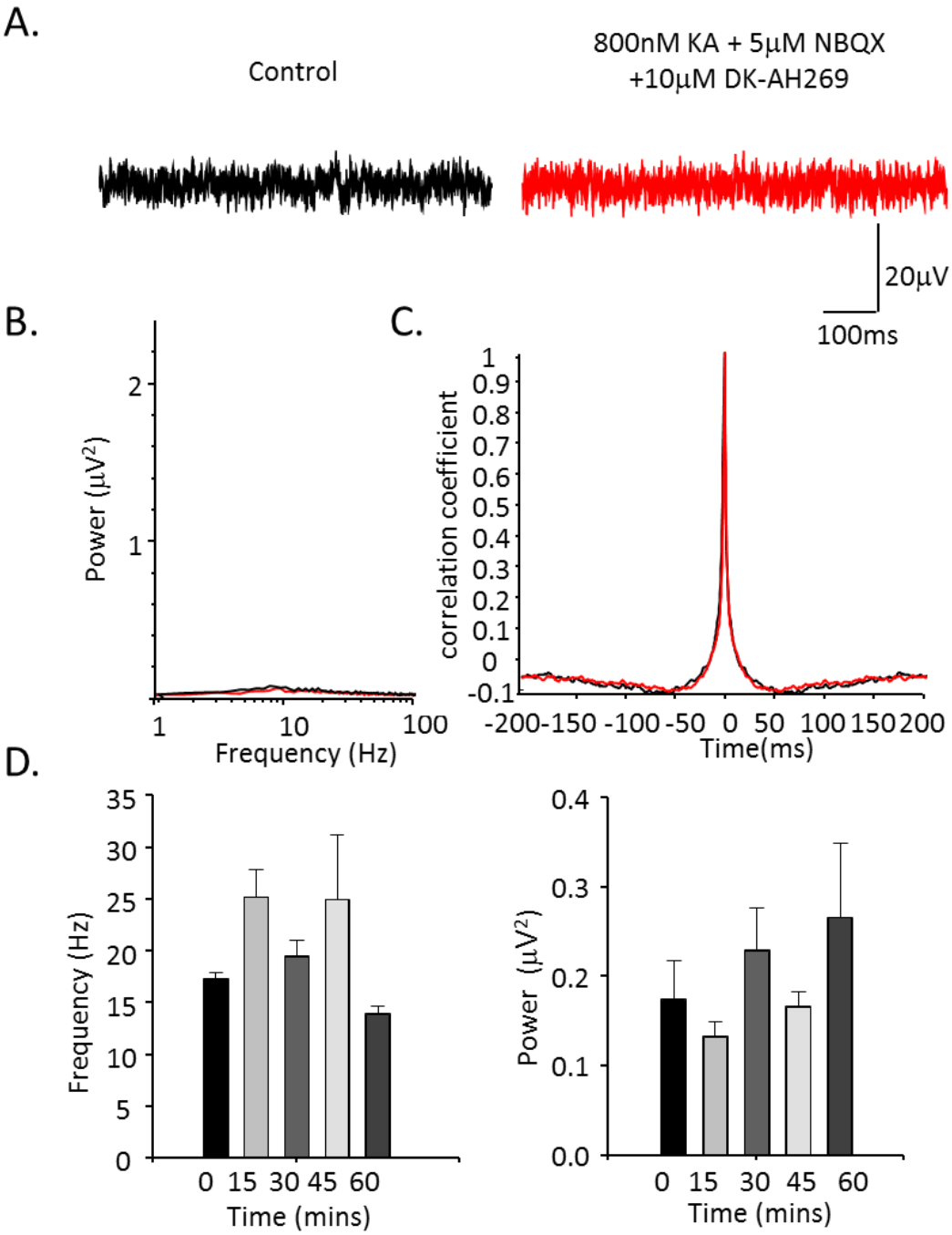

Figure 3.13 Alpha rhythms could not be generated in the visual cortex without prior excitation. A. 1 second example traces of extracellular activity prior to the addition of any pharmacological agents (black trace) and after simultaneous addition of Kainate [800nM], NBQX [5µM] and DK-AH269 [10µM] (red trace). **B.** Example power spectra produced from traces in A. **C.** Example auto-correlations produced from 60 second epochs of extracellular data showing rhythmicity before (in black) and after (in red) addition of KA [800nM], NBQX [5µM] and DK-AH269 [10µM]. **D.** Graphs showing the change in frequency and amplitude of oscillations before addition of pharmacological agents and 15, 30, 45 and 60 minutes after (frequency $P>0.05$, Two-Tailed T-Test, amplitude $P>0.05$, Mann-Whitney Rank Sum Test, n=10).

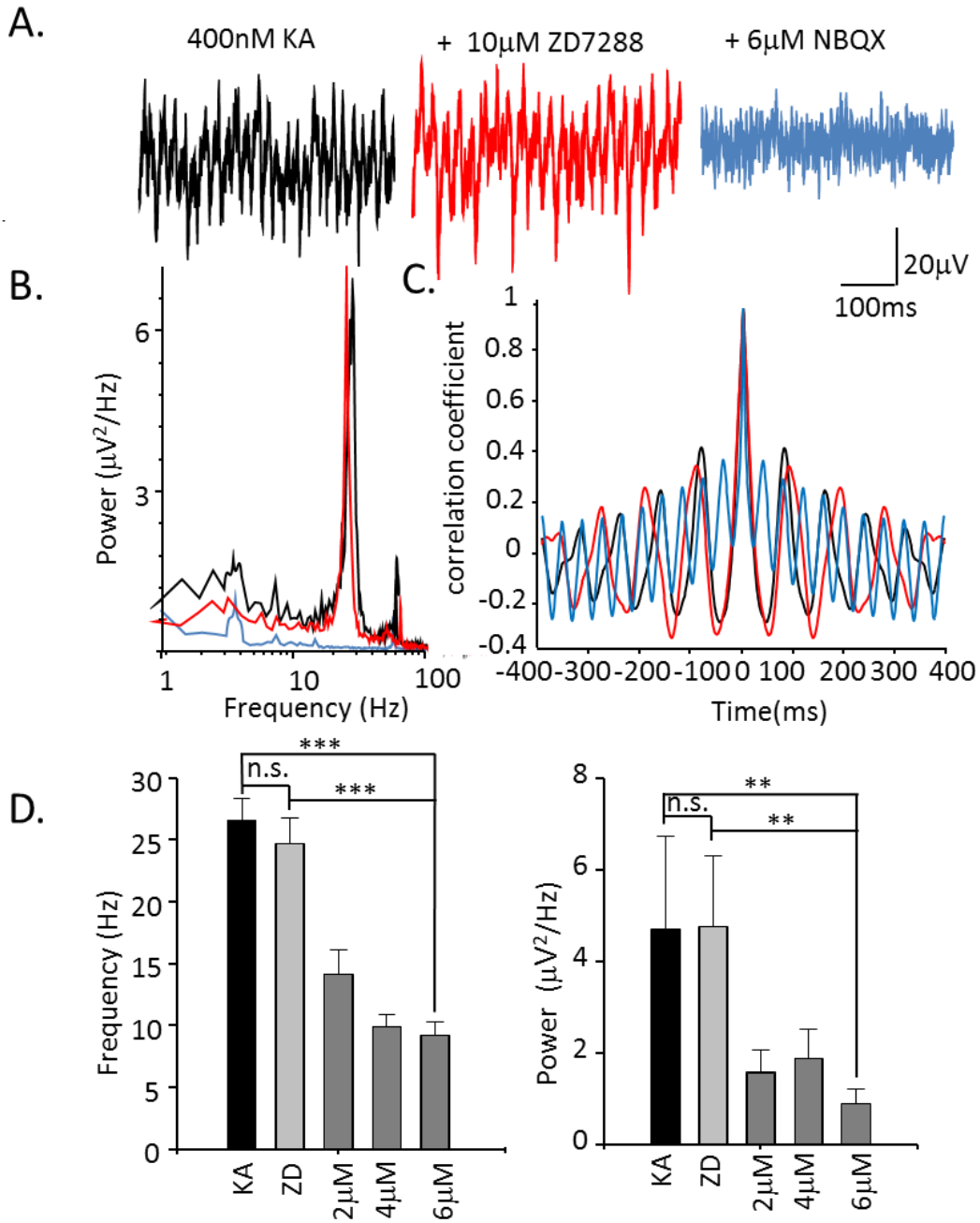

Figure 3.14 Blocking I_h current before reducing synaptic excitation did not produce alpha frequency oscillations in the visual cortex. A. 1 second example traces of extracellular activity induced by Kainate [800nM] (black trace), 30 minutes after addition of ZD7288 [10μM] and 30 minutes after addition of NBQX [6μM] (blue trace). **B.** Example power spectra produced from traces in A. **C.** Example auto-correlations produced from 60 second epochs of extracellular data showing rhythmicity after addition of 800nM KA (in black), ZD7288 [10μM] (in red) and NBQX [6μM] (in blue). **D.** Graphs showing the change in frequency (KA-ZD P>0.05, KA-NBQX P<0.001, ZD-NBQX P<0.001, n=11, all Two-Tailed T-Test) and power (KA-ZD P>0.05, KA-NBQX P<0.01, ZD-DK-AH P<0.01, all Mann-Whitney Rank Sum Test, n=11) after excitation with KA [800nM], application of ZD [10μM] and subsequent application of NBQX [2-6μM].

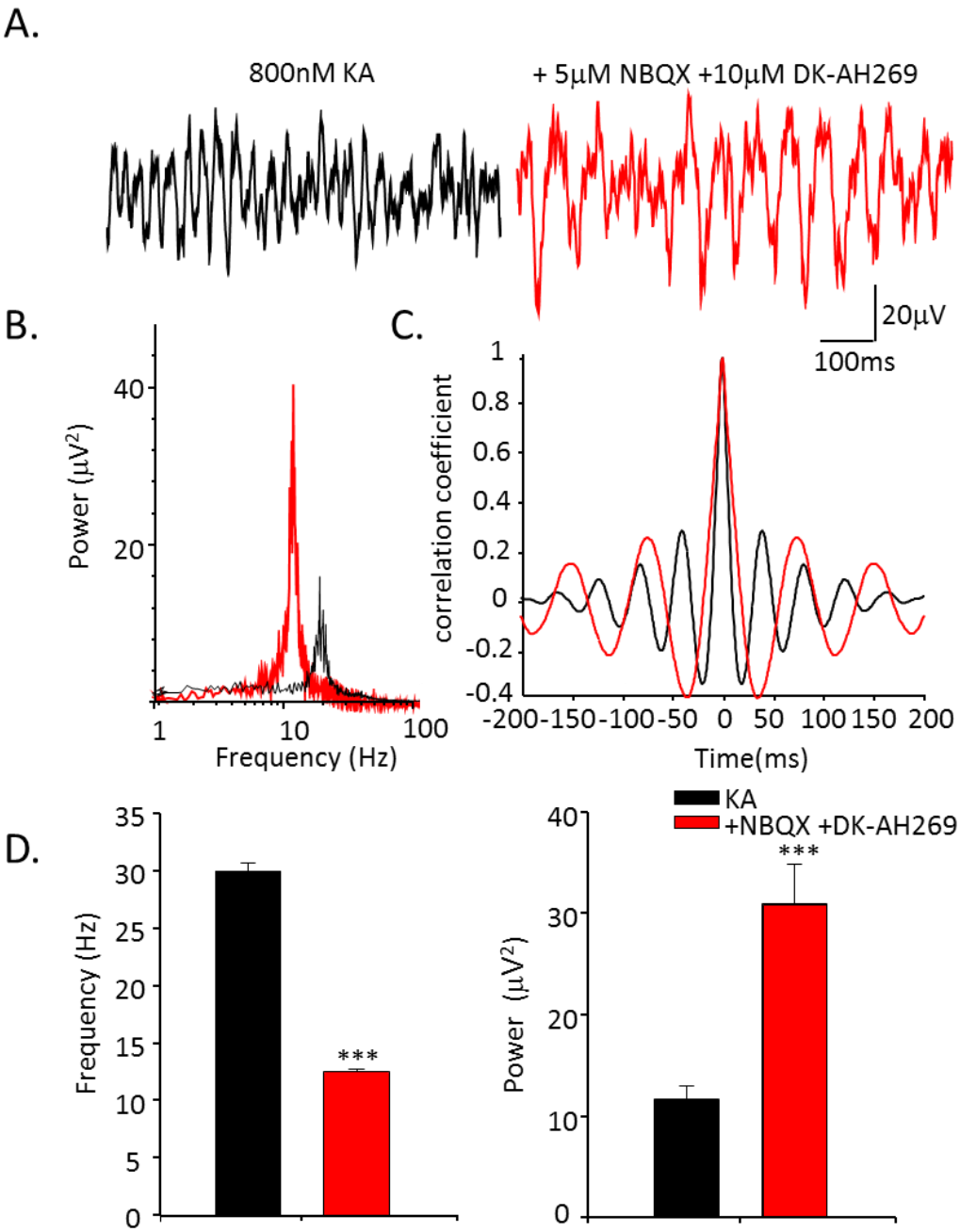

Figure 3.15 Concurrent reduction in both synaptic and intrinsic excitation generated alpha rhythms following a period of prior excitation. A. 1 second example traces of extracellular activity induced by Kainate [800nM] (black trace), and 30 minutes after simultaneous addition of DK-AH269 [10µM] and NBQX [5µM] (red trace). **B.** Example power spectra produced from traces in **A**. **C.** Example auto-correlations produced from 60 second epochs of extracellular data showing rhythmicity after addition of 800nM KA (in black) and 30 minutes after simultaneous addition of DK-AH269 [10µM] and NBQX [5µM] (in red). **D.** Graphs showing the change in frequency and power after excitation with KA [800nM] and after subsequent addition of DK-AH269 [10µM] and NBQX [5µM] (frequency and amplitude $P<0.001$, Mann-Whitney Rank Sum Test, n=26).

process was occurring during the excitation manifest as a beta rhythm, it clearly needed the activity of I_h conductance to modify the network so that alpha rhythms could be generated subsequently. This potential plasticity aspect to alpha rhythm generation is explored in more detail in the next results chapter. However, before we could delve deeper into these mechanisms we needed to make sure we looked in the right place and at the right cortical neuronal subtypes, so we proceeded to map spatially the extent of the alpha rhythm produced by the model described above.

3.3.8 Laminar and horizontal profiles of activity in the primary visual cortex

In order to determine the spatial origins of each rhythm found in the primary visual cortex, extracellular field recordings were taken from each layer of the cortical column, and horizontally across the brain slice. This was carried out during beta, gamma and alpha oscillations.

3.3.8.1 Laminar and horizontal profiles of beta activity in visual and adjacent areas

Beta activity was detected throughout layers I-VI of the V1 and was found to predominate in layer IV (Figure 3.16) with a median power of 13.8μV^2 (1.5-31.9μV^2). The differences in the median power of oscillations through layers I-VI were statistically significant with values ranging from 0.4-13.8μV^2 ($P<0.01$, n=9, Kruskal-Wallis ANOVA on Ranks). The frequency of beta oscillations throughout layers I-VI did not differ significantly with median values ranging from 23.9-25.0Hz across the cortical column ($P=0.684$, n=9, Kruskal-Wallis ANOVA on Ranks).

As beta power was found to be highest in layer IV, horizontal profiles were carried out with the extracellular recordings taken from layer IV (as defined as distance from pial surface) across 9 evenly spaced points starting in the retrosplenial agranular cortex (RSA) area of the slice, throughout the V1 and ending in the secondary visual cortex (V2) (See figure 3.17B for illustration). The highest strength

beta rhythm was found to be in position 2 in this scheme (corresponding to the V1M) with a median value of 17.9μV^2 (1.7-32.3μV^2) (Figure 3.17). The power of beta oscillations were found to be significantly different across different areas of the visual cortex slice with a median value ranging from 0.4-17.9μV^2 ($P<0.05$, n=5, Kruskal-Wallis ANOVA on Ranks). The frequency of beta oscillations across the visual cortex again did not differ significantly with median values ranging from 24.9-25.4Hz ($P=0.633$, n=5, Kruskal-Wallis ANOVA on Ranks).

3.3.8.2 Laminar and horizontal profiles of gamma activity in visual and adjacent areas

Gamma activity was detected throughout layers I-VI of area V1 and was also found to predominate in layer IV (Figure 3.18) with a median power of 16.0μV^2 (10.5-20.5μV^2). The differences in the median power of gamma oscillations through layers I-VI were statistically significant with values ranging from 0.9-16.0μV^2 ($P<0.01$, n=6, Kruskal-Wallis ANOVA on Ranks). The frequency of gamma oscillations throughout layers I-VI did not differ significantly with median values ranging from 36.5-38.7Hz across the cortical column ($P=0.962$, n=6, Kruskal-Wallis ANOVA on Ranks).

Gamma power was found to be highest in layer IV, therefore, horizontal profiles were carried out with the extracellular recordings taken from layer IV, or equivalent distance from pial surface, across 9 evenly spaced points as described above (3.3.7.1) (See figure 3.19B for illustration). The highest strength gamma rhythm was, found to be in position 4 (also V1M in this scheme) at 24.4μV (Figure 3.19) with powers ranging from 1.5-24.4μV^2. Similarly, the frequency of gamma oscillations across the visual cortex did not differ much with frequencies ranging from 32.9-44.2Hz (n=1).

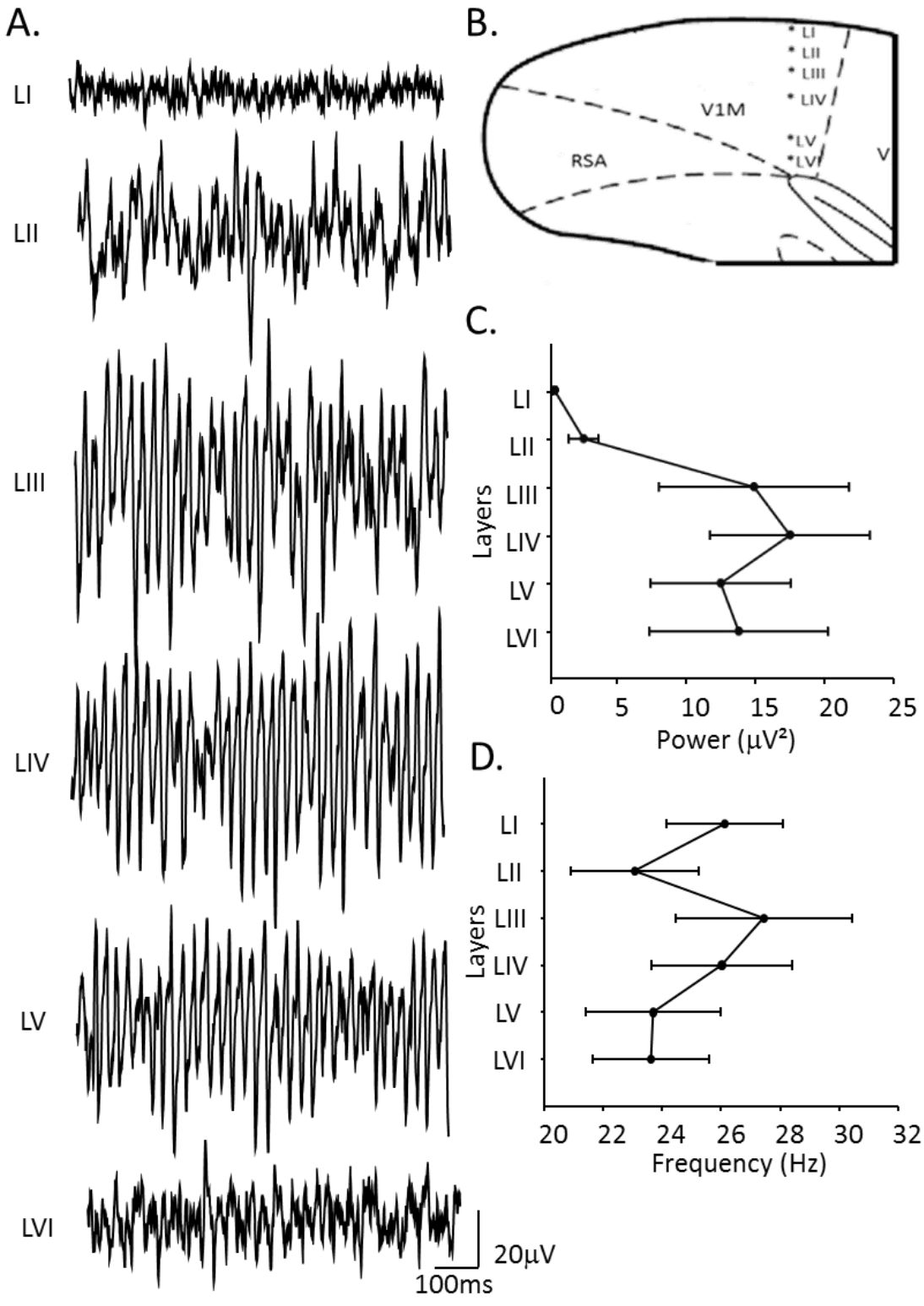

Figure 3.16 Laminar profiles of beta activity in the primary visual cortex. A. 1 second example traces of extracellular activity recorded from layers I to VI of a single cortical column. **B.** Illustration of the brain slice and position of the electrodes from which extracellular field recordings were obtained across the different layers**. C** and **D.** Mean amplitude and frequency of beta activity from layers I to VI from pooled 60 epochs of extracellular data (n=9).

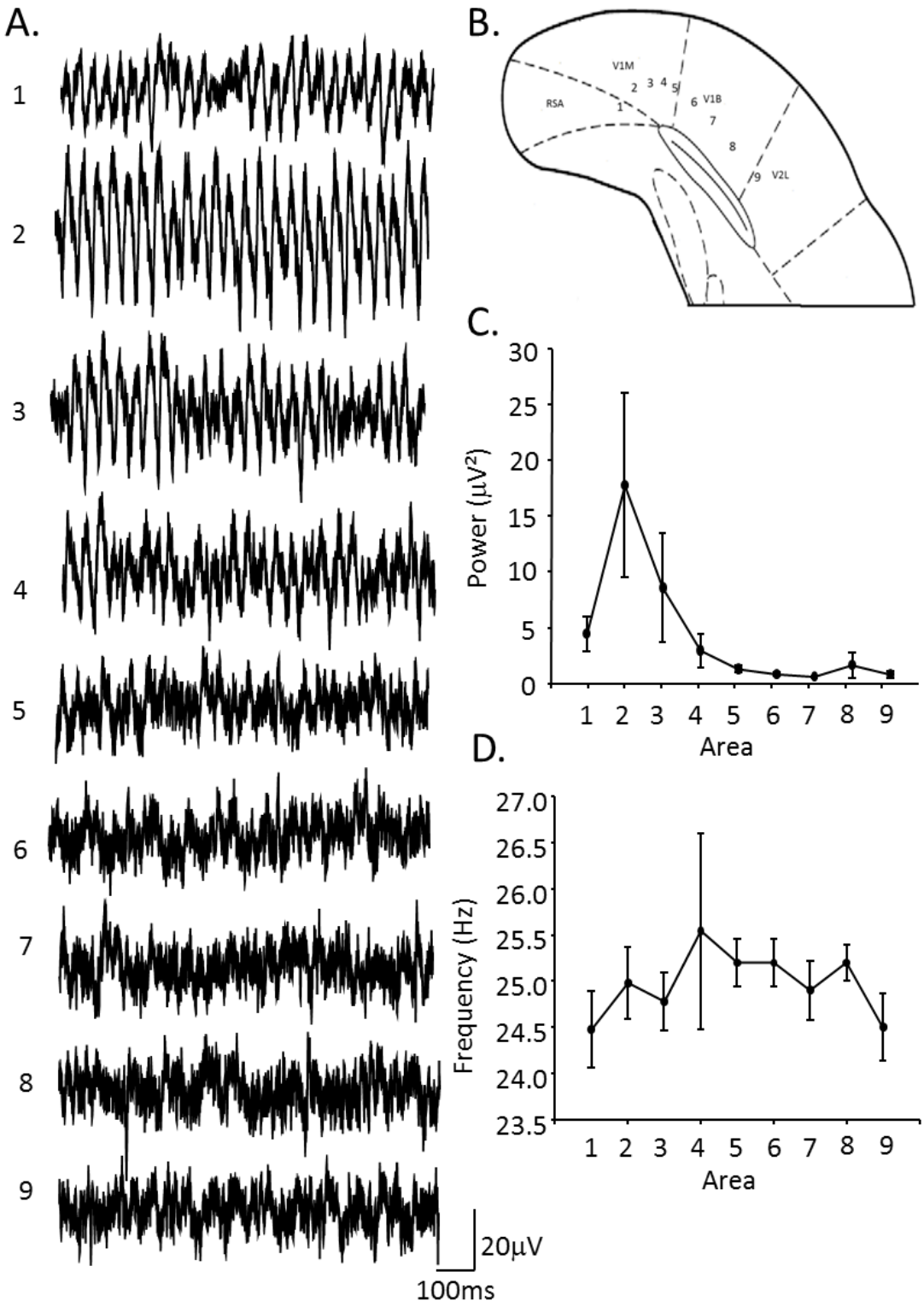

Figure 3.17 Horizontal profiles of beta activity in visual and adjacent areas. A. 1 second example traces of extracellular activity recorded across the visual cortex. **B.** Illustration of the brain slice and position of the electrodes from which extracellular field recordings were obtained from layer IV or equivalent distance from pial surface across different areas of the visual cortex. **C** and **D.** Mean amplitude and frequency of beta activity recorded from layer IV across the visual cortex from pooled 60 epochs of extracellular data (n=5).

3.3.8.3 Laminar and horizontal profiles of alpha activity in visual and adjacent areas

Alpha activity was detected through layers I-VI of the V1 and was found to be largest in layer IV with a median value of 88.5μV^2 (34.6-174.6μV^2) (Figure 3.20). The differences in power across the cortical layers I-VI were statistically significant with median values ranging from 1.2-88.5μV^2 ($P<0.001$, n=6, Kruskal-Wallis ANOVA on Ranks). The frequency of alpha oscillations throughout layers I-VI did not differ significantly with median values ranging from 10.6-11.8Hz (P=0.107, n=9, Kruskal-Wallis ANOVA on Ranks).

Horizontal profiles were carried out in layer IV as this is where alpha power was found to be highest. Horizontal profiles were carried out as described above (3.3.7.1) (See figure 3.21B for illustration). Alpha power was shown to be highest in position 3 (as with beta and gamma rhythms, also V1M) (Figure3.21C), however, the overall differences in power of alpha oscillations across the visual cortex were not significant, with median values ranging from 1.3-26.3μV^2 (P=0.204, n=5, Kruskal-Wallis ANOVA on Ranks). This statistic may have been generated owing to uniformly low alpha rhythm power at all locations except 2 and 3. Similarly the frequency of alpha oscillations across the visual cortex were not found to be statistically significant with median frequencies ranging from 11.9-12.8Hz (P=0.965, n=5, Kruskal-Wallis ANOVA on Ranks).

The results showed that alpha oscillations were most dominant in LIV of the V1M – the same layer and region that gave rise to the strongest gamma and beta rhythms prior to lowering excitation. We therefore attempted again to correlate alpha power with preceding beta and gamma power, but this time pairing values according to layer (Figure 3.22) or region (Figure 3.23). There was a moderate positive correlation between alpha and beta power when considering laminar occurrence (R squared=0.45, n=54, $P<0.001$) this was considerably higher than for the pooled, unsorted data (R squared=0.08, figure 3.12A). The correlation was poor between alpha and beta power when considering regional occurrence (R squared=0.12, n=45, P=0.422). The correlation between prior gamma rhythm

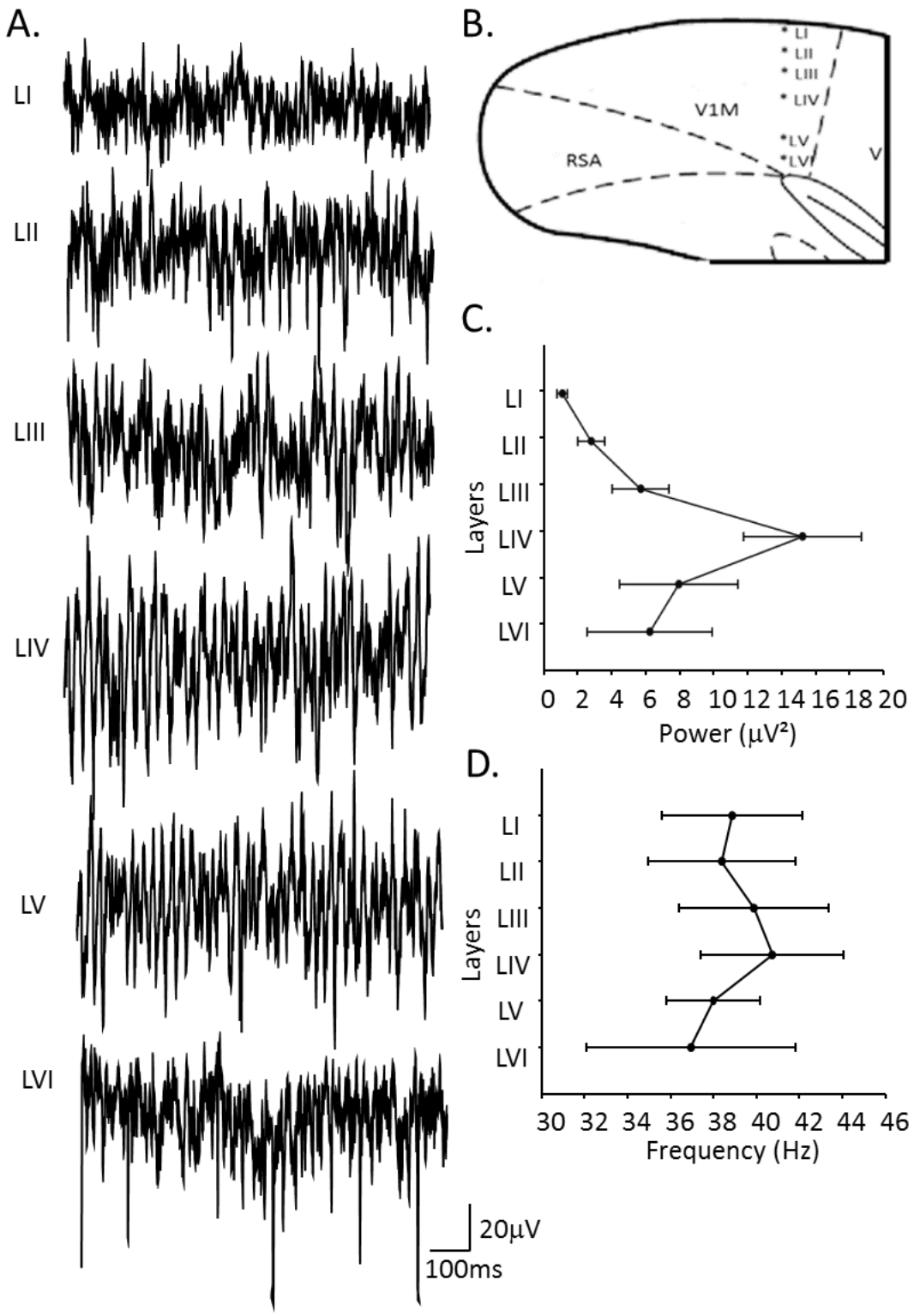

Figure 3.18 Laminar profiles of gamma activity in the primary visual cortex. A. 1 second example traces of extracellular activity recorded from layers I to VI of a single cortical column. **B.** Illustration of the brain slice and position of the electrodes from which extracellular field recordings were obtained across the different layers**. C and D.** Mean amplitude and frequency of gamma activity from layers I to VI from pooled 60 epochs of extracellular data (n=6).

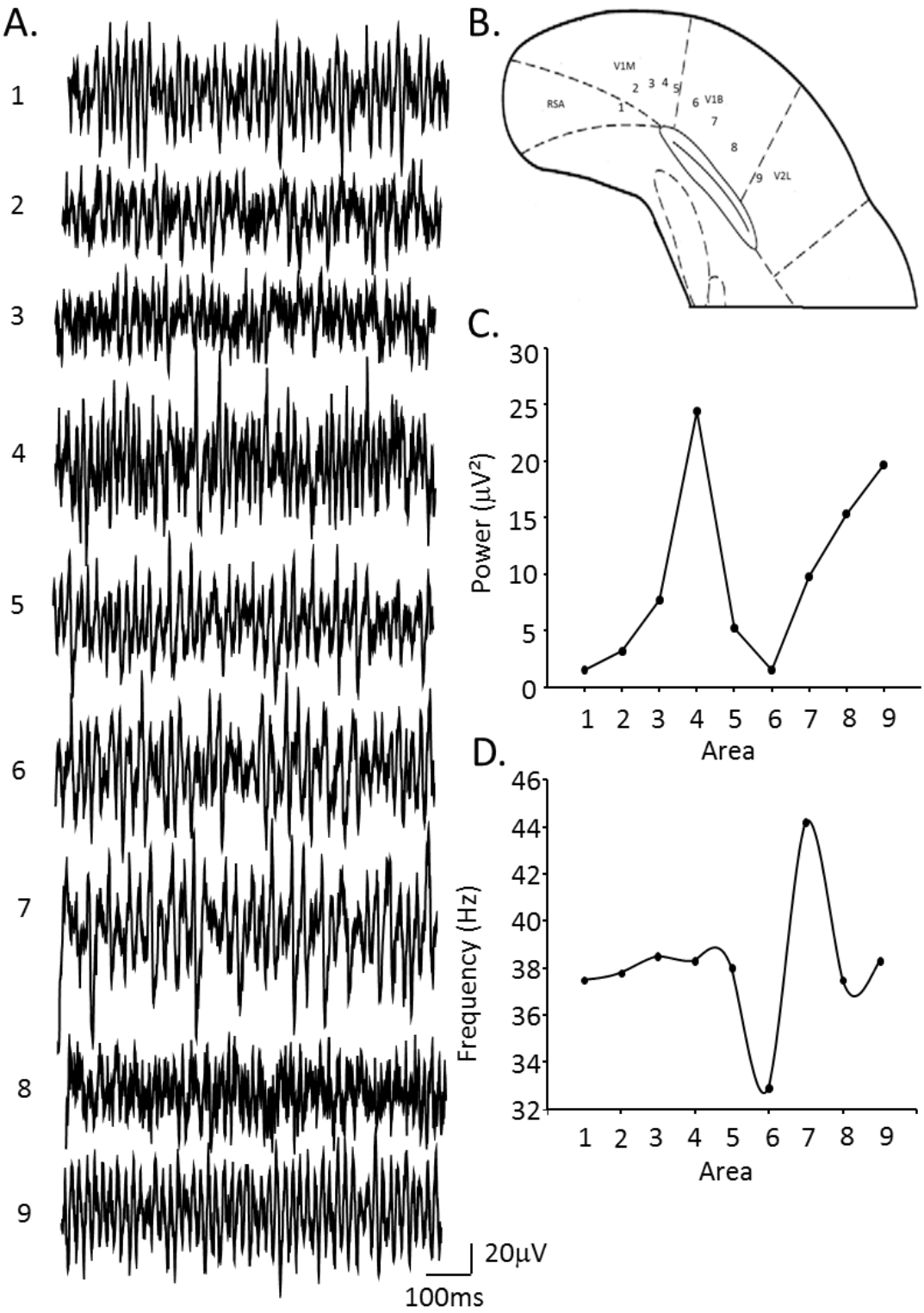

Figure 3.19 Horizontal profiles of gamma activity in visual and adjacent areas. A. 1 second example traces of extracellular activity recorded across the visual cortex. **B.** Illustration of the brain slice and position of the electrodes from which extracellular field recordings were obtained from layer IV or equivalent distance from pial surface across different areas of the visual cortex**. C and D.** Mean amplitude and frequency of gamma activity recorded from layer IV across the visual cortex from pooled 60 epochs of extracellular data (n=1).

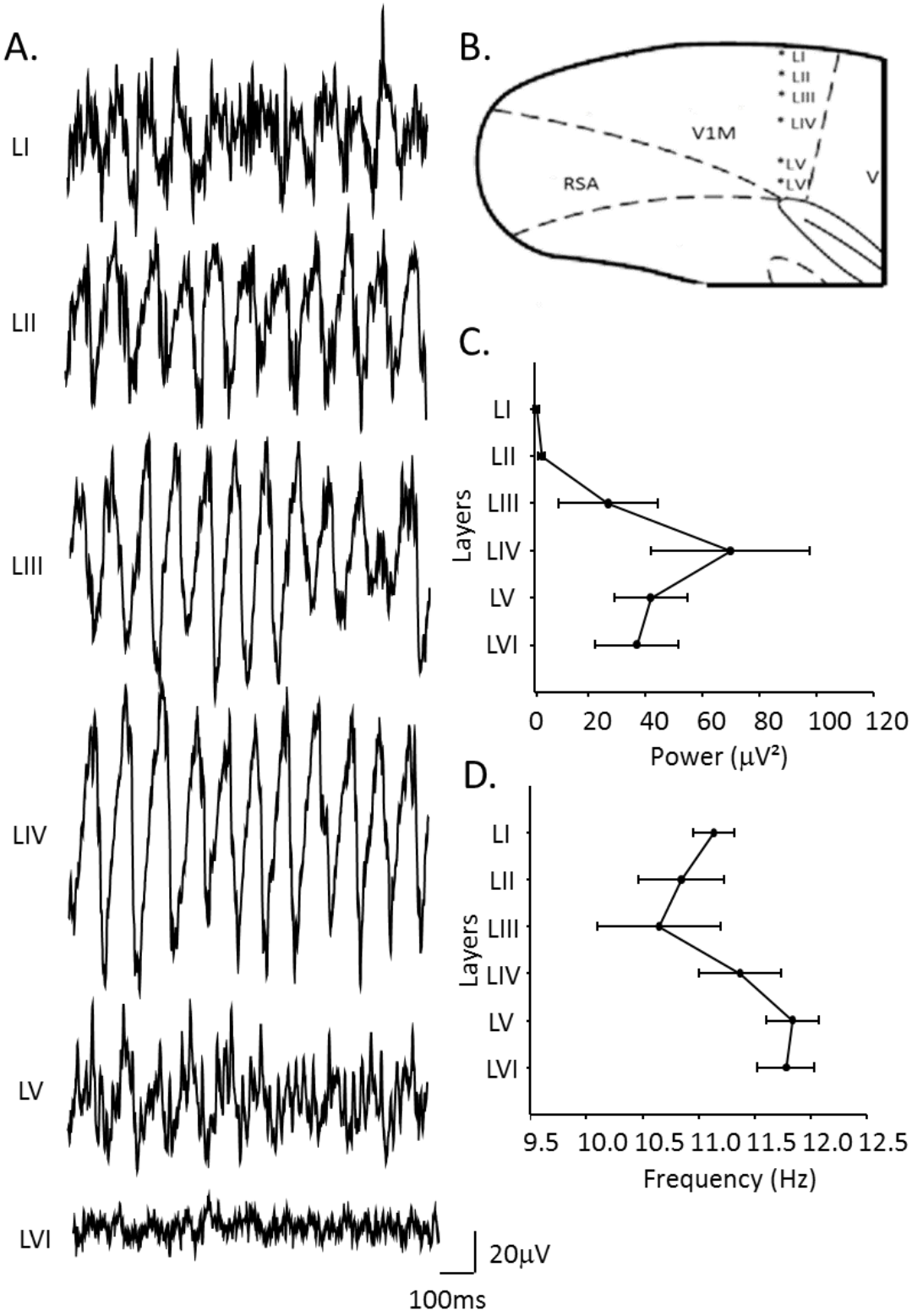

Figure 3.20 Laminar profiles of alpha activity in the primary visual cortex. A. 1 second example traces of extracellular activity recorded from layers I to VI of a single cortical column. **B.** Illustration of the brain slice and position of the electrodes from which extracellular field recordings were obtained across the different layers**. C and D.** Mean amplitude and frequency of alpha activity from layers I to VI from pooled 60 epochs of extracellular data (n=9).

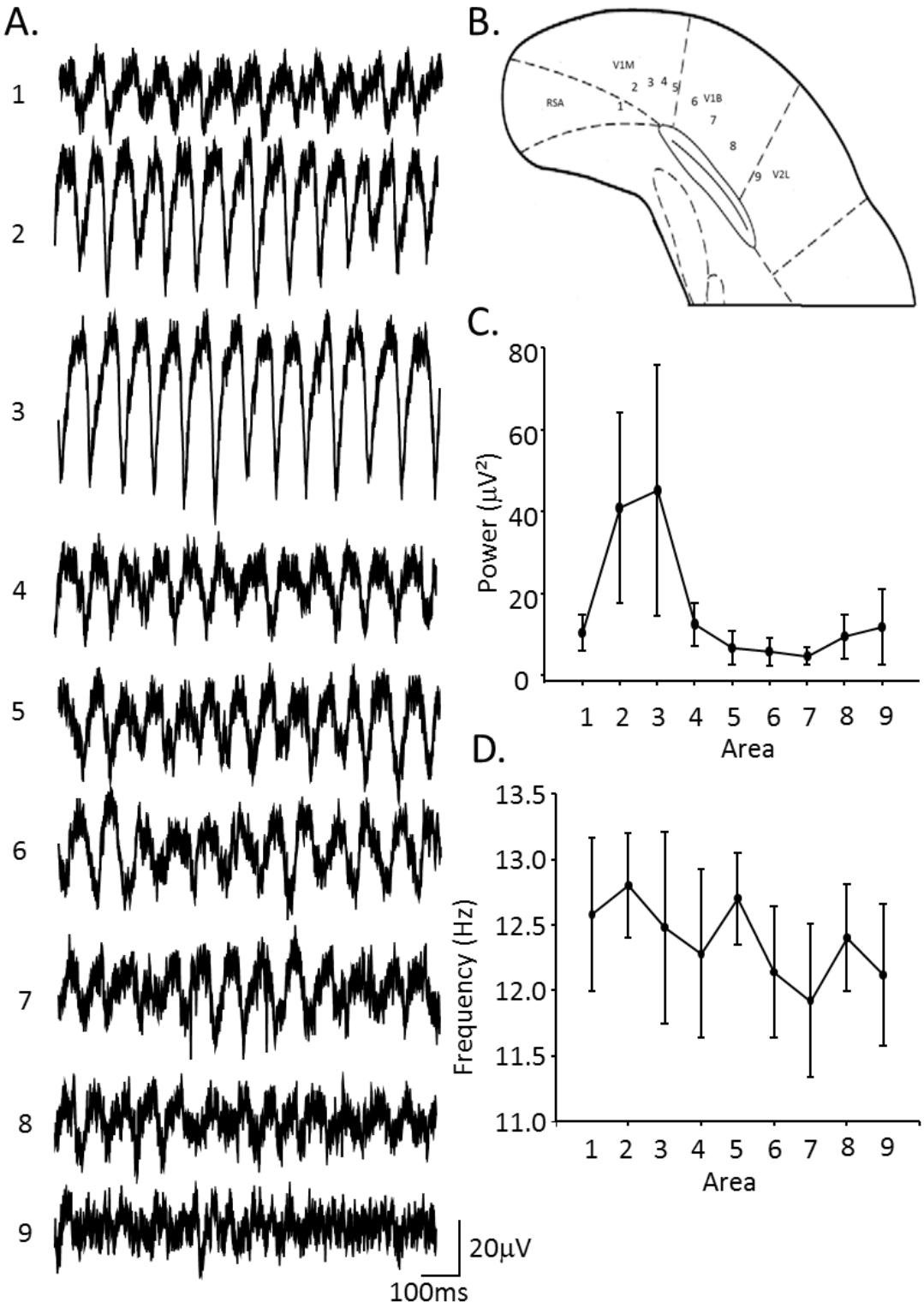

Figure 3.21 Horizontal profiles of alpha activity in visual and adjacent areas. A. 1 second example traces of extracellular activity recorded across the visual cortex. **B.** Illustration of the brain slice and position of the electrodes from which extracellular field recordings were obtained from layer IV or equivalent distance from pial surface across different areas of the visual cortex. **C** and **D.** Mean amplitude and frequency of alpha activity recorded from layer IV across the visual cortex from pooled 60 epochs of extracellular data (n=5).

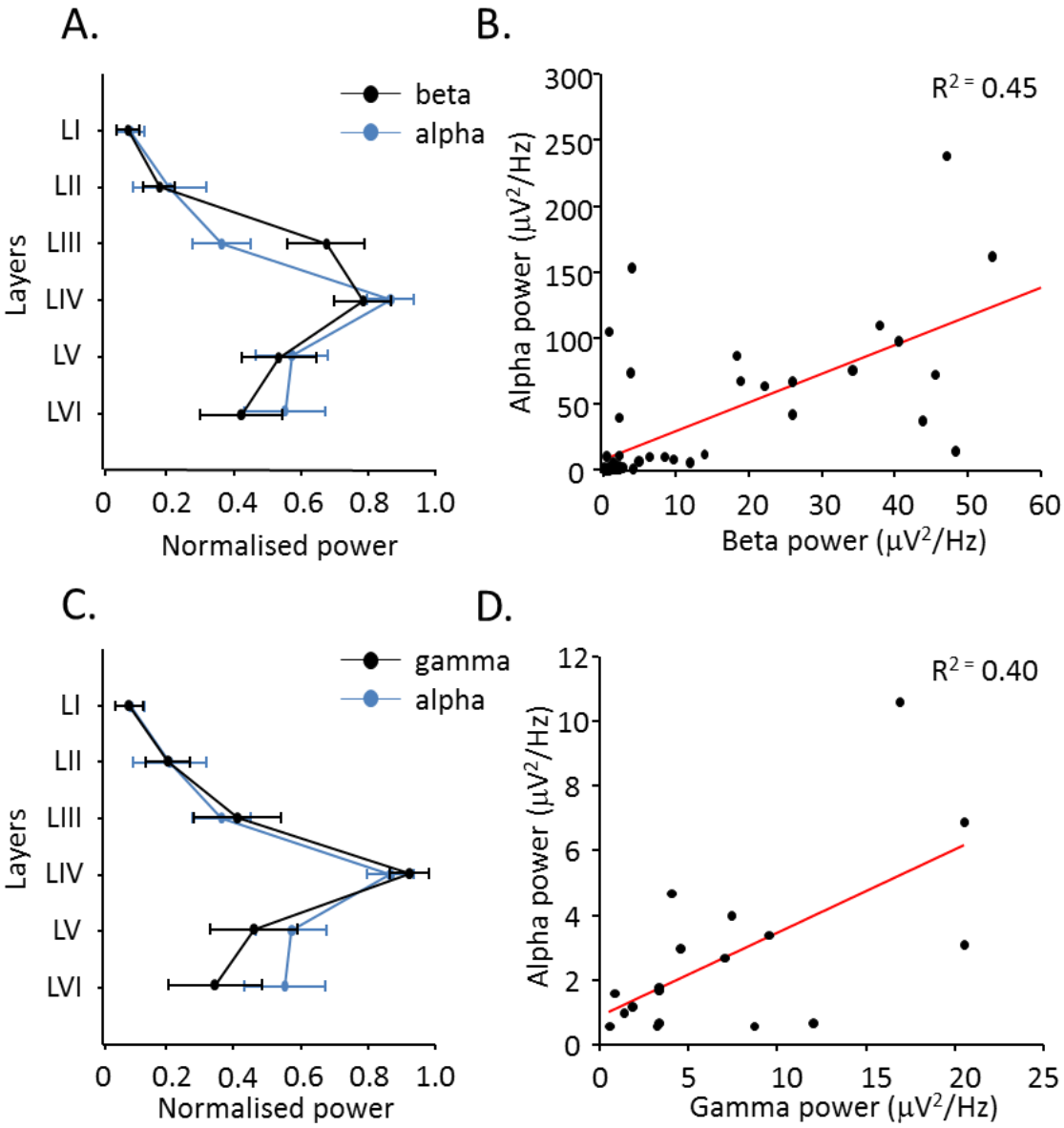

Figure 3.22 Alpha oscillation power was not proportional to prior beta oscillation power across layers I-VI of the visual cortex. A. Mean amplitude of alpha (in blue) and beta (in black) activity recorded across layers I-VI of the primary visual cortex produced from pooled epochs of extracellular data (n=9). **B.** Diagram with regression line showing the relationship between alpha power and the preceding beta power produced from laminar profiles shown in A**. C.** Mean amplitude of alpha (in blue) and gamma (in black) activity recorded across layers I-VI of the primary visual cortex produced from pooled epochs of extracellular data (n=9 for alpha, n=6 for gamma). **D.** Diagram with regression line showing the relationship between alpha power and the preceding gamma power produced from laminar profiles shown in C (note axis between B and D differ).

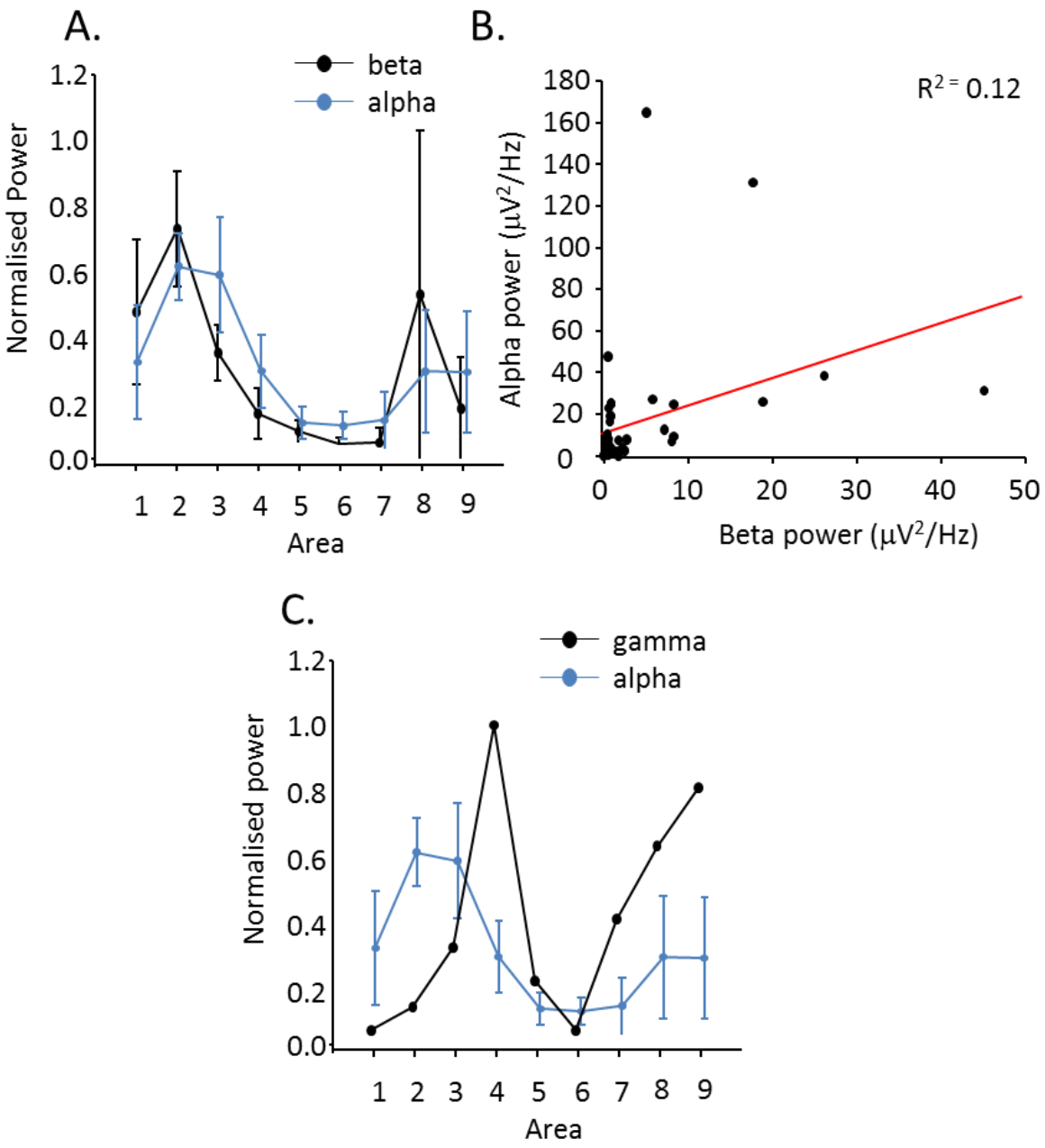

Figure 3.23 Alpha oscillation power spatially corresponded to prior beta, but not gamma, oscillation power across visual cortex. A. Mean amplitude of alpha (in black) and beta (in blue) activity recorded across the visual cortex produced from pooled epochs of extracellular data (n=5). **B.** Diagram with regression line showing the relationship between alpha power and the preceding beta power produced from horizontal profiles show in A**. C.** Mean amplitude of alpha (in black) and gamma (in red) activity recorded across the visual cortex produced from pooled epochs of extracellular data (n=5 for alpha, n=1 for gamma).

power and subsequent alpha rhythm power was weak with an R squared value of 0.40 (n=18, P=0.094).

In view of these findings, for the purpose of all pharmacological and intracellular studies in further chapters, all recordings were carried out in layer IV of the V1M.

3.4 Discussion

3.4.1 Mimicking the pattern of excitation and suppression characteristic of post-stimulus alpha *in vivo* induces alpha frequency oscillations *in vitro*

The results in this chapter show that a visual cortical alpha rhythm can be generated in isolated brain slice preparations, independent of connections to the thalamus, and using stimuli of physiological relevance. The alpha rhythm produced had frequency and amplitude (relative to frequencies seen in activated cortex) characteristic of those seen from *in vivo* EEG recordings after closing of the eyes or removal of visual stimulus.

The main findings from these experiments were:

1) All the rhythms seen in the KA model were confined to (or maximal in) layer IV of the V1M.

2) Generation of the alpha rhythm on reduction of excitation was critically dependent on the prior presence of a beta frequency oscillation and not a gamma frequency oscillation.

3) Whatever plastic changes were associated with the beta rhythm depended on the activity of the intrinsic conductance I_h.

4) In contrast to 3), manifestation of the alpha rhythm required the reduction in I_h conductance.

Each of these findings appeared to suggest clues to the origin of the occipital alpha rhythm seen so readily in humans. The following sections deal with each in turn.

3.4.2 Why is alpha power greatest in layer IV of the medial primary visual cortex?

Following all of these pharmacological manipulations, the alpha rhythm emerged as the predominant frequency component of all oscillatory activity throughout the brain slice upon analysis of laminar and horizontal profiles. Alpha, beta and gamma power were all found to be strongest in V1M. V1M corresponds to the primary visual area, and V1B to the lateral visual area or V2 (Swanson, 2004). Neurons in the V1 project out to extrastriate areas involved in movement (see chapter 6.4). As alpha oscillations were found to be strongest in the primary visual cortex rather than the V2; these findings could indicate a possible role for alpha oscillations in the processing of movement during an eyes closed state.

Alpha activity was seen in all 6 cortical laminae with power being highest in layer IV. Previous *in vitro* studies have suggested alpha power is highest in layer V (Silva et al., 1991), however, this work used slice conditions that were epileptogenic in nature (see 3.1.1). *In vivo* animal studies suggest a different laminar origin for the alpha rhythm. A recent study conducted by (Haegens et al., 2015) analysed laminar profiles of LFP and multiunit activity (MUA) from the primary visual cortex, primary auditory cortex and primary somatosensory cortex of macaques. In this study current source density (CSD) analysis showed alpha generators were strongest in supragranular layers (I-III); these findings were consistent with van Kerkoerle et al. (2014a) who also suggest alpha is generated in the superficial layers. However, these authors noted that LFP alpha power was strongest in infragranular layers (V-VI). This apparent separation in CSD and raw oscillation power has been seen before for delta rhythms (Carracedo et al., 2013) and was argued to occur owing to the long apical dendrites of layer V pyramidal cells: The LFP is a combination of synaptic inputs and active conductances (bursting) in perisomatic compartments. The CSD signal quantified predominantly synaptic inputs only and, in this cell type, most of these are on the apical dendritic tufts located in superficial layers. Other studies have also shown alpha power to be greatest in infragranular layers in the V1 (Maier et al., 2010; Buffalo et al., 2011; Spaak et al., 2012).

An additional complicating factor is that *in vivo* studies like those cited above deal with activity in the whole brain. There is a strong alpha rhythm generator in visual thalamus (see Introduction) and ascending thalamic inputs to neocortex can innervate supragranular layers (Broicher et al., 2010; Viaene et al., 2011b), layer IV (Ferster et al., 1996) and increasing recent evidence suggests a strong, direct excitation of layer V too (Viaene et al., 2011a). A careful study using dense linear arrays of electrodes, CSD and Granger causality estimates, showed that the laminar profile of the alpha rhythm varied across different visual subregions (Bollimunta et al., 2008). Unfortunately this study did not include the V1 – the region the experiments in this thesis showed was the main alpha-generating region (Figure 3.21).

The laminar profiles conducted in this thesis are taken from extracellular field recordings and do not take (CSD) into account. However, the high signal:noise inherent in slice experiments – with their absence of thalamic and long range cortical inputs – makes the data presented here highly compelling in its suggestion that a purely neocortical alpha rhythm generator may exist in layer IV. Nevertheless, more detailed experiments about the cells involved in the generation of alpha rhythms and their activity in layer IV compared to other layers are required. Some of these will be presented and discussed in chapter 5.

3.4.3 Why does the V1 alpha rhythm require prior beta frequency activity patterns?

Alpha oscillations were generated from a preceding beta rhythm. When present, this beta rhythm had power that was also highest in layer IV of the V1M. The present experiments did not find a strong linear positive correlation between beta power and subsequent alpha power but the evidence for beta rhythms as an absolute prerequisite was quite strong. This apparent dichotomy may suggest a non-linear relationship between beta and alpha powers. For example, when compensating for laminar recording location, plotting pairwise beta and subsequent alpha powers suggested an abrupt increase in alpha power when comparing prior beta powers greater or less than ca. 10-20 μV^2 (Figure 3.22B). Using this value as a

threshold and dividing the whole dataset accordingly showed 10-fold greater alpha power arising from the higher beta powers than the lower (Figure 3.12C). This relationship suggested that it may not have been the presence of a prior beta rhythm that was *directly* responsible for changing network configuration in favour of the alpha rhythm. Instead it may be that the dynamics of the beta rhythm that mediated network plasticity.

There are many forms of plasticity in a neuronal network: Changes in the intrinsic excitability of individual neurons can enhance their output probability for a given input (Springer et al., 2015), altered electrical connectivity via gap junctions can increase cooperativity in neurons for up to 1 hour after stimulation (Park et al., 2011), patterned excitatory synaptic input can increase the strength of subsequent excitatory synaptic events (Bliss and Collingridge, 1993). It is this last form of plasticity that appears to be the most sensitive to the temporal arrangement of activity in a network. The temporal order of activity in presynaptic structures (axons, boutons) compared with postsynaptic structures (the dendritic compartment of the target cell) strongly determines whether subsequent synaptic events are strengthened or weakened (Bi and Poo, 1998). The majority of these synaptic plastic changes occur over the time course of one beta rhythm period (40-50ms).

Most mechanistic studies on synaptic plasticity involve a focus on the N-methyl-D-aspartate (NMDA) subtype of glutamate receptor. Strong depolarisation of a post-synaptic cell causes the opening of NMDA channels; this increases post-synaptic, intracellular Ca^{2+} concentration and facilitates the incorporation of more excitatory ion channels/glutamate receptors into the postsynaptic membrane (Lynch, 2004). In contrast, weak depolarisation of the post-synaptic cell does the opposite, there is a reduction in Ca^{2+} concentration which is thought to induce long term depression (LTD) (Malenka and Nicoll, 1993).

AMPA receptors also play a critical role in synaptic plasticity. Increases or decreases in AMPA receptors at the post-synaptic membrane are another important factor in determining subsequent synaptic strength (Shepherd and Huganir, 2007). KA

receptors have also been shown to exhibit synaptic plasticity in response to activity. It is thought that the activation of pre-synaptic KA receptors results in increased levels of glutamate which results in increased levels of synaptic transmission therefore increased activation of pre-synaptic KA receptors (Lauri et al., 2001). Which form(s) of glutamate receptor may be involved in the network changes seen during beta rhythms are investigated in the next chapter of this thesis.

In general, plasticity as a consequence of beta rhythms has been shown in a number of neocortical systems. In association cortex a similar experimental protocol to that used here (a period of kainate-mediated excitation followed by reducing drive with a low-concentration of NBQX) also causes abrupt frequency changes. In this case, dual gamma and beta2 rhythms transformed into a beta1 rhythm upon reduction of excitation. Experiments showed that plasticity at NMDA receptor-mediated synaptic transmission sites was vital for this (Roopun et al., 2008), and subsequent computational modelling predicted the key locus of plasticity to be recurrent excitatory connections between layer 5 intrinsically bursting cells (Kramer et al., 2008). However, the beta rhythm seen in the above studies was faster than that seen in this thesis (ca. 25-28 Hz, vs. ca. 19-22 Hz) and at no point did the rhythm slow to alpha frequencies. It is therefore not prudent to suggest that a similar locus of plasticity is at work in alpha generation.

The above, plasticity-dependent, gamma/beta2 to beta1 frequency shift was also critically dependent on prior gamma rhythm generation. The present data strongly suggested that this was not the case in the V1 for alpha generation (see Figure 3.10). This, in itself, is confusing as gamma rhythms have been associated with plasticity in a number of systems. For example, in hippocampus a brief period of intense gamma rhythm generation switches to a beta rhythm in a manner dependent on potentiation of recurrent excitatory synapses (Whittington et al., 1997). In addition, a detailed modelling study showed that gamma rhythms could generate strong synaptic potentiation, via NMDA receptors, when pre- and postsynaptic frequencies were the same or at specific ratios (Lee et al., 2009). However, in this study no changes in frequency were associated with such potentiation.

From all these precedents above it appears that whatever plasticity is associated with alpha rhythm generation in the V1, it takes a different form from those previously described. A reason for this may be the local circuitry involved: In each cortical example above, it was layer 5 that was critical for the beta-rhythm plasticity, and layers 2/3 for the gamma rhythm plasticity. Neither of these frequencies were strongest in these layers in the current experiments, suggesting that a process internal to layer IV (where both rhythms were maximal) may underlie the generation of the alpha rhythm. Other than a recognition of the existence of very strong recurrent NMDA receptor-mediated synaptic connections between layer IV neurons (Binshtok et al., 2006), very little is known about rhythm-driven synaptic plasticity in layer IV. This will therefore be investigated further in the next chapter. One thing that was clear about potential plasticity mechanisms was that they required the presence of the hyperpolarising conductance I_h (Figures 3.7 & 3.8).

3.4.4 A role for I_h in alpha rhythm generation?

The frequency of oscillations seen in this thesis was reduced by approximately 10Hz upon addition of NBQX [5μM] giving a beta I frequency. To reduce the frequency further to that in the alpha range it was necessary to also reduce intrinsic excitability of neurons. This was done through blockade of hyperpolarisation activated current (I_h). This conductance is an inward current activated by hyperpolarisation from resting membrane potential, it modulates action potential firing frequency in excitable cells (Momin et al., 2008). I_h channels allow the influx of calcium ions upon hyperpolarisation and I_h channels blockers inhibit this calcium influx (Yu et al. 2004).

By blocking I_h channels using ZD7288 or DK-AH269, at the same time – or after – reducing network drive with NBQX, the firing frequency of neurons was reduced (see chapter 5), and the frequency of oscillations was reduced from beta I to alpha. The time that I_h blockers were introduced into the bathing medium was critical. If I_h was blocked during the excitatory phase (kainate alone) no change in beta rhythm power or frequency was seen, but alpha rhythms could not be generated following

subsequent reduction in excitation (Figure 3.15). From this it appeared that I_h was performing two different roles in the model system described in this chapter: First, it seemed to constitute an absolute requirement for whatever plastic mechanisms were active during the beta rhythm. Secondly, and perhaps conversely, the overt manifestation of an alpha rhythm required the reduction in I_h.

I will consider the possible role in synaptic plasticity first. The precedents for a role of I_h in synaptic plasticity are equivocal and confusing in places. Most of this confusion seems to stem from the lack of 100% selectivity of drugs used as blockers (Chevaleyre and Castillo, 2002). In addition, functional expression of I_h in multiple neuronal compartments (dendrite, soma, presynaptic terminal) also confuses matters. In general, I_h is considered to be vital for certain types of rhythm generation in the cortex (Alonso and Llinas, 1989). It can also induce plasticity in rhythm generation, particularly at theta frequencies (Li et al., 2014). Using knock-out animals it has been shown that HCN1 (protein ionophore responsible for ca. 50-80% of I_h in neurons) plays a vital role in synaptic plasticity recorded as long term potentiation (LTP): Loss of HCN1 hugely increased LTP and subsequent visuospatial memory performance (Nolan et al., 2004). However, these authors noted that only LTP at synapses on distal dendrites were affected. In contrast, reducing I_h in somatic compartments actually reduced neuronal responsivity (van Welie et al., 2004) Similarly, reduced I_h in presynaptic terminals also reduced LTP (Mellor et al., 2002).

The situation is further confused if we consider the timecourse of synaptic plasticity. Reduced I_h causes a large increase in short term depression at excitatory synapses (a brief (a few seconds) decrease in synaptic efficacy with repeated stimulation) (Dietrich et al., 1997). However, stimuli that generate longer-term synaptic potentiation also increase the I_h current (Brager et al., 2013). From this evidence it is hard to predict why I_h was essential, during the beta rhythm, for the subsequent generation of alpha in this thesis. We would need to know the mechanism underlying this visual layer IV beta generator to make any prediction as to which of the above phenomena may be playing a role in 'setting up' the network for alpha rhythm generation.

The second effect of I_h was seemingly in contrast to its effect during the excitation phase of the protocol. Reducing network drive alone could reduce LFP frequency down to the low-teens of Hz but this was always accompanied by a reduction in power. Concurrent reduction in I_h pushed the frequency down to the alpha band and generated very large (5+ fold) increases in LFP power. In other words, while I_h was essential to set the network up to generate alpha rhythms when drive was reduced, it had to be reduced itself for successful generation of the alpha rhythm. Activity-dependent modulation of I_h has been well documented (Honnuraiah and Narayanan, 2013), and a subtle interplay between intracellular calcium levels and cAMP levels seems to powerfully modulate the conductance (Beaumont and Zucker, 2000; Narayanan and Johnston, 2010). In general, increased intracellular calcium ion concentration shifts the activation curve for I_h to more depolarised levels and reduces deactivation (Luthi and McCormick, 1998).

For a low level of network drive, following a period of intense excitation (the KA-induced beta rhythm), it may be the case that high intracellular calcium levels coincide with quite hyperpolarised membrane potentials. The net effect of this combination would be to reduce the dynamic nature of I_h. To reinforce rhythm generation, I_h must have rapid activation and inactivation kinetics. This allows it to interact with depolarisation-activated conductances like I_{NaP} (the persistent sodium current) to boost neuronal resonant properties (Alonso and Llinas, 1989). Interestingly, the I_h blockers used here have a far greater effect in slowing I_h kinetics than they do in actually reducing maximal conductance (Harris and Constanti, 1995).

However, none of these effects would be expected to lead to the large increase in power at alpha frequencies seen in the present experiments. Instead, we need to consider the effects of I_h on burst generation in neurons. High levels of I_h conductance interact strongly with low threshold calcium conductances (so called T-current) to generate slow, delta-frequency oscillations (1-4 Hz) (Hughes et al., 1998). At the same time, high levels of I_h also constrain more rapid, sodium channel-mediated dendritic bursts (Lorincz et al., 2002). Shifting the activation curve to more depolarised levels, and making I_h more persistent (see above)

antagonises the interaction with T-current-induced bursting but would be expected to potentiate dendritic sodium channel-mediated bursts. If this suggestion holds true then the prediction would be that T-current blockade should have little effect on the V1 layer IV alpha rhythm seen here. This is in contrast to the core role for T-current in existing computational models of alpha rhythm (Jones et al., 2000a; Ching et al., 2010). This will be tested in the next chapter.

3.4.5 Summary

This chapter has described the processes involved in the generation and optimisation of an *in vitro* visual cortical alpha rhythm. A robust model of the cortical alpha rhythm has been established by the activation of KA receptors using KA [800nM] followed by a reduction in synaptic and intrinsic neuronal excitability using NBQX [5μM] and DK-AH269 [10μM] to 450μM sections of the primary visual cortex cut in the coronal plane. Alpha activity was found to be highest in layer IV of the V1M and for the purpose of all further experiments, activity will be recorded from this area unless stated otherwise.

The development of this *in vitro* cortical alpha model provides an introduction to a novel area of research providing opportunities for investigation. The next chapters will look into the cortical alpha rhythm in more depth, to study the properties of the rhythm and the mechanisms behind its generation. The next chapter will look into the basic pharmacological properties of the alpha rhythm to identify the key synaptic and intrinsic cellular conductance's implication in the alpha rhythm.

Chapter 4: Results – Pharmacological Studies

4.1 Introduction

The previous chapter detailed the generation of a robust model of the visual cortical alpha rhythm including its spatial characteristics and basic electrophysiological properties at the LFP level. The results showed this rhythm seemed to dominate in layer IV of the primary visual cortex. The generation and maintenance of alpha oscillations required the contribution of many synaptic receptors and ion channels. This chapter will focus on the key synaptic connections and potential intrinsic conductances involved in the alpha rhythm.

4.1.1 NMDA receptors

As mentioned in the previous chapter, alpha rhythm generation appeared to require a form of synaptic plasticity during the preceding beta oscillation. NMDA receptors have been extensively studied in relation to synaptic plasticity and are thought to play a major role in this phenomenon.

NMDA receptors are glutamatergic receptors characterised by their response to N-methyl-D-aspartate (NMDA). NMDARs are ligand-gated ion channels and require co-activation by binding of glutamate and glycine (Kleckner and Dingledine, 1988). Most NMDA receptors exhibit strong, non-linear voltage dependence. At resting membrane potential (RMP) magnesium ions (Mg^{2+}) sit inside the ion channel. Upon depolarisation, the Mg^{2+} is released allowing the influx of Ca^{2+}, K^{+} and Na^{2+} ions (Collingridge et al., 1992). Calcium influx through NMDARs is thought to be critical in synaptic plasticity, providing the stimulus for activation of a number of kinases which, in turn, control postsynaptic structure and receptor complement (Lynch et al., 1990)

NMDARs form a heterotetramer, requiring the contribution of two NR1 and NR2 subunits. The NR2 subunits have 4 different isoforms: NR2A, NR2B, NR2C and NR2D. These subunits are differentially expressed across various cell types and fine-tune the electrophysiological functions of the NMDAR complex (Schoepfer R, 1994). For example, during early childhood there is an activity-dependent switch from expression of the NR2B subunit to the NR2A subunit (Matta et al., 2011). As a

consequence the kinetics of the NMDA receptor heteromer become faster, promoting higher frequency cortical rhythms and enhancing temporal precision at central synapses (Williams et al., 1993). In addition, only NR2A and NR2B subunits confer an open-channel Mg^{2+} block to the ionophore. Thus, in areas of the brain where NR2C/D subunits dominate, a different voltage dependence is seen allowing NMDA receptors to be active at synapses at much more hyperpolarised membrane potentials (Binshtok et al., 2006). Interestingly, these NMDA receptors are strongly expressed in layer IV of neocortex, suggesting they may play a role in the layer IV alpha rhythm defined in the previous chapter.

Results from the previous chapter strongly suggested some form of plasticity needed to occur, via beta rhythms, during the excitation preceding alpha rhythm generation. Most of the work on excitatory synaptic plasticity has focussed on a mechanism whereby activation of NMDA receptors is critical (Bliss and Collingridge, 1993). This synaptic event results in an increase in the number of AMPA receptors incorporated into postsynaptic membranes, thus enhancing the postsynaptic membrane conductance change for a given amount of glutamate released (Malinow and Malenka, 2002). However, the model of alpha rhythms used here required a reduction in AMPA receptor function to work, suggesting that plastic changes in AMPA receptor-mediated synaptic excitation were not involved in alpha rhythm generation.

Independently of any plastic changes in AMPA receptor number brought about by NMDA receptor activity, the NMDA receptors themselves may be subject to plastic changes (Rebola et al., 2010). The subject is controversial, with some researchers demonstrating LTP of purely NMDA receptor-mediated synaptic transmission (Berretta et al., 1991), while others do not (Muller and Lynch, 1988). More recent work appears to suggest that such NMDA-specific plasticity can indeed occur. Co-activation of NMDA receptors and type 1 metabotropic glutamate receptors, coupled with an increase in calcium release from intracellular stores, reliably induces enhanced NMDA currents in central synapses (Rebola et al., 2008; Harnett et al., 2009). Interestingly, the resultant NMDA currents are not only enhanced in magnitude, but have different kinetics and open-channel block characteristics:

Increased expression of NR2A, NR2B and NR2D-containing receptors has been seen (Harney et al., 2008; Peng et al., 2010).

There is a little evidence to suggest a role for NMDA receptors in alpha rhythm generation: Blocking NMDA receptors in monkey visual cortex has been shown to suppress alpha rhythms (van Kerkoerle et al., 2014b) suggesting NMDARs play a role in their generation. The nootropic drug piracetam boosts alpha and beta1 frequency rhythms in rats in an NMDA receptor-dependent manner (Vorobyov et al., 2011). The alpha rhythm is very much implicated in selective attention and working memory (see chapter 1) and NMDA receptors have been implicated in attention related disorders. Impaired NMDA receptor function in the pre-frontal cortex in rats has been shown to impair cognition and lowers the ability to sustain attention (Lehohla et al., 2004). Similarly, selective cognitive deficits in attention and working memory appear to be a common feature of NMDA receptor antagonists (Smith et al., 2011). While this is far from conclusive evidence for a role for NMDA receptors in alpha rhythm generation, the above connection to plasticity suggests a possible mechanistic contribution to the model developed in the previous chapter.

4.1.2 GABA receptors

GABA receptors are a group of receptors which are responsive to gamma-aminobutyric acid (GABA) the main inhibitory neurotransmitter in the brain. There are two distinct classes of GABA receptors in the CNS: $GABA_A$ which are ligand gated ion channels, their opening allows the influx of Cl^- ions into the cell causing hyperpolarisation and decreased membrane resistance (Schwartz, 1988), and $GABA_B$ which are G-protein coupled receptors and modulate neuronal excitability via enhanced K^+ or reduced Ca^{2+} channel-mediated activity (Bowery, 1989; Tatebayashi and Ogata, 1992). $GABA_A$ receptors are characterised by their sensitivity to the antagonists bicuculline and picrotoxin (Takeuchi and Takeuchi, 1969; Takeuchi and Onodera, 1972).

GABAergic interneurons have been shown to play a crucial role in the generation and synchronization of many neuronal oscillations: fast postsynaptic inhibition is a critical component of gamma rhythms in the CNS (Whittington et al., 2011), slower $GABA_A$ receptor mediated events on dendrites underlie theta rhythm generation in hippocampus (White et al., 2000), dendritic GABAergic inhibition is also fundamental to acetylcholine-mediated beta2 rhythms in auditory cortex (Roopun et al., 2010) and a combination of fast and slow $GABA_A$ receptor-mediated inhibition underlies beta1 rhythm generation in association cortex (Roopun et al., 2008). They are also thought to be involved in the generation of alpha activity in thalamus (Lorincz et al., 2009). Whether this is involved in the alpha rhythm in humans is contentious though. Enhancement of $GABA_A$ receptor-mediated inhibition with lorazepam has been shown to reduce the power of alpha oscillations in visual cortex in human MEG studies (Ahveninen et al., 2007; Lozano-Soldevilla et al., 2014). The concentration of GABA has shown to be reduced in children with attention related disorders (Edden et al., 2012) – a pathology associated with modified alpha rhythms in patients (see chapter 1). In addition, $GABA_B$ receptors have been shown to be involved in the generation of delta (Carracedo et al., 2013) and slow wave oscillations (Mann et al., 2009) in rodent models.

This strong connection between GABAergic inhibition and rhythm generation is perhaps not surprising when considering the powerful effect synaptic inhibition has on timing the outputs of neurons (Pouille and Scanziani, 2004). Sharing inhibition from a small population of interneurons with divergent connections is a robust way to generate synchronous outputs from neurons despite long conduction delays between them (Traub et al., 1996). Given the connection between the alpha rhythm and cortical 'inhibition' (see chapter 1) it seems likely that the underlying alpha rhythm mechanism may also involve synaptic inhibition. However, in addition to the negative effects of boosting GABAergic activity with benzodiazepines (above) studies on a range of different GABA potentiating drugs fail to provide any evidence for a common effect on alpha rhythms (Nutt et al., 2015).

4.1.3 Gap junctional coupling

In addition to GABAergic chemical synaptic inhibition, direct electrical connections between neurons are also a common feature in rhythm generating mechanisms. All of the rhythms described in the previous section display sensitivity to drugs that block gap junction-mediated interneuronal communication. Gap junctions are a non-chemical synaptic mechanism for cellular communication (Dermietzel, 1998). Many excitatory neurons in the brain communicate via gap junctions, particularly during early development (Kandler and Katz, 1998). Gap junctions allow the passage of small molecules between cells as well as the passage of electrical charge. As such, dye-coupling between gap-junctionally connected neurons is common. Such coupling is seen in visual cortex in rodents up until ca. postnatal day (PND) 15 (Kasper et al., 1994). After this time the dye coupling decreases as the neurons develop their mature phenotype. Similar developmental patterns of dye coupling were also seen in layer 2/3 neurons (Rörig and Sutor, 1996). Even a small, residual level of gap junctional communication between principal cells can have a profound effect on network function (Traub et al., 2002).

Unlike principal cells, interneurons maintain a strong profile of gap junctional connectivity throughout adulthood. Principal cells appear to be connected such that one cell contacts, on average, between only one and two others (Traub et al., 2002). In contrast, interneurons are connected via gap junctions to between twenty and fifty post-junctional partners (Amitai et al., 2002). In visual cortex, coupling between interneurons is particularly strong in layer IV (Fortier, 2011) where they have been linked to the formation of contrast-invariant orientation columns, perhaps via the formation of functional intercolumnar networks (Fukuda et al., 2006).

As with GABAergic signalling, gap junctional coupling is often strong enough to mediate synchronization of spiking activity amongst close clusters of neurons (Connors and Long, 2004). Interestingly, the dynamics of such synchrony, at least in some cortical interneuron subtypes, leads to alpha rhythm generation (Gibson et al., 1999; Beierlein et al., 2000).

Hughes et al. (2004) showed that *in vitro* alpha oscillations can be observed in the LGN of cats; these oscillations do not require chemical synapses as they can be sustained solely by gap junctional coupling between thalamocortical neurons. This group then went on to show that in behaving cats, administration of carbenoxolone (CBX) a gap junction inhibitor, suppressed both LGN and EEG alpha oscillations whilst also decreasing neuronal synchrony (Hughes et al., 2011).

Gap junctional coupling, like the alpha rhythm, has also been linked to attention (Aston-Jones et al., 1999). These authors came up with a computational model for the results they observed in a visual discrimination task requiring attention in monkeys. They found neurons exhibit phasic or tonic modes of activity that correspond to good or poor performance in this task. Their model predicts electrical coupling is needed to produce the different modes of activity and therefore gap junctions are required in attention related tasks.

4.1.4 Neuromodulators and the alpha rhythm.

Preliminary investigations into the model for cortical alpha rhythms, as shown in the previous chapter, demonstrated that in the presence of nicotine, alpha oscillations can be observed in the primary visual cortex after spritzing with glutamate. Many studies have demonstrated oscillatory changes in the alpha band due to acute nicotine administration. These changes include increased EEG alpha power and increases in frequency of alpha rhythms (Foulds et al., 1994; Harkrider and Champlin, 2001). A study by Bowers et al. (2015) has shown that nicotine increases the power of EEG alpha oscillations in both frontocentral and parietal/occipital regions, along with a faster peak frequency of alpha oscillations.

Nicotine has been implicated in the improvement of cognitive function in smokers (Wesnes and Warburton, 1983; Bell et al., 1999). It has also been shown to treat the attentional symptoms of ADHD (Levin et al., 1996; Potter and Newhouse, 2004) and can improve attention in healthy non-smokers (Levin et al., 1998; Poltavski and Petros, 2006). It is well documented that alpha rhythms are involved in attention

(see section 1.5.3); an increased EEG alpha power could lead to the improved attention observed upon nicotine administration.

As described in the previous chapter, I_h current is important in the generation of alpha rhythms. By blocking I_h channels, intrinsic neuronal excitability is reduced and this was accompanied by a reduction of oscillation frequency into the alpha band. This, in turn was accompanied by a large increase in oscillation power which may involve an I_h-mediated change in the pattern and origin of burst generation in dendrites (see 3.4.4). Nicotine has also been shown to be involved in controlling I_h conductance. Griguoli et al. (2010) showed that nicotine blocks I_h by directly interfering with the channel protein responsible for this current in a concentration dependent manner in oriens-lacunosum moleculare (O-LM) interneurons in mice. Application of nicotine to beta I oscillations may therefore be a more physiological way to block I_h and induce alpha oscillations in our model.

While the cholinergic system appears to play a strong role in alpha rhythm generation, other neuromodulatory systems appear not to have much of an effect, or even antagonise this frequency band. Polymorphisms in a key enzyme controlling dopamine levels in the brain – catechol-o-methyl transferase (COMT) result in only subtle (ca. 1 Hz) differences in peak alpha rhythm frequency in otherwise healthy male subjects (Bodenmann et al., 2009). The D2 receptor antagonist sulpiride had no significant effect on the alpha rhythm in normal subjects (Chavanon et al., 2007). Similarly, neither apomorphine (D1/2 agonist) or quinpirole (D2/3 agonist) had any significant effect on alpha rhythms (Sebban et al., 1999).

In contrast, alpha rhythm generation in visual cortex is antagonised by noradrenergic receptor activation (Rougeul-Buser and Buser, 1997). Similarly, elevated cerebrospinal fluid noradrenaline levels have been shown to be negatively correlated with alpha rhythm power (Kemali et al., 1985). No mechanism has been proposed for this effect. However, while nicotinic receptor activation can reduce I_h activity, stimulation of alpha1 adrenergic receptors has been shown to potentiate I_h via elevation of cyclic adenosine monophosphate (cAMP) levels (He et al., 2014).

4.1.5 Aims and objectives

The previous chapter described a robust, *in vitro* model for visual cortical alpha rhythms. The properties and mechanisms behind its generation needed to be studied; therefore the main aim was to investigate the underlying pharmacological properties in terms of the key synaptic and intrinsic cellular conductances involved in the alpha rhythm. To attempt to address this aim the following objectives were set:

1) To carry out pharmacological manipulations of the NMDA receptor complex to identify which, if any, subunits of the NMDAR were responsible for the plastic process required for the generation of alpha oscillations.

2) To investigate the effects of $GABA_A$ mediated inhibition to determine if alpha rhythms require recurrent excitation and inhibition.

3) To assess the need for gap junctional coupling in the generation of the alpha rhythm.

4) To determine the key neuromodulators required in the cortical alpha rhythm.

4.2 Methods

All experiments described in this chapter were carried out using *in vitro* brain slice preparations (450 μM slice thickness) from adult male Wistar rats (150-200g). Visual cortex containing slices were cut coronally and were prepared and maintained as described in chapter 2.1-2.4. All data obtained from experiments from this chapter was via extracellular field recordings outlined in chapter 2.7 and all data acquisition and analysis are described in chapter 2.8-2.9. Beta activity was induced by application of KA [800nM] and alpha activity was induced prior, with co-application of NBQX [5μM] and DK-AH269 [10μM]. All pharmacological agents were bath applied to slices and their activity was monitored for approximately 30 minutes, unless no effects were observed in which case their activity would be observed for 1-2 hours. The power of the activity of the alpha rhythm was taken as

the indicator of strength of oscillations and was taken between 8-12Hz unless otherwise stated.

4.3 Results

4.3.1 Involvement of NMDA receptors in the generation and maintenance of alpha oscillations in the V1

Given the pre-eminent role of NMDA receptors in synaptic plasticity we looked for a role for these receptors in the apparent plastic processes involved in generating the alpha rhythm from a prior beta rhythm. The first step was to investigate the contribution of NMDA receptors as a whole to the alpha rhythm once generated. This effect was studied using (RS)-3-(2-Carboxypiperazin-4-yl)-propyl-1-phosphonic acid (CPP), a non-subunit-selective, non-competitive NMDA receptor antagonist. Upon application of CPP [10μM] to the alpha rhythm, the power of the rhythm was almost completely abolished with no detectable spectral peak observed. Control values of $32.0\mu V^2 \pm 20.5\mu V^2$ were reduced to $0.3\mu V^2 \pm 0.1\mu V^2$ in the presence of drug ($P<0.01$, n=5, Mann-Whitney Rank Sum Test, figure 4.1). There was little change in the frequency of the rhythm when it was possible to detect one. The control frequency in this set of experiments was 11.0Hz ± 0.5Hz and this was marginally but not significantly reduced to 9.3Hz ± 0.7Hz ($P=0.088$, n=5, Two-Tailed T-Test). Auto-correlation analysis was carried out to assess the rhythmicity of the rhythm. Prior to the addition of CPP the graph showed a sinusoidal form indicating a high degree of rhythmicity within the alpha band, however after application of CPP the graph was no longer sinusoidal in shape suggesting any activity that was left was not very rhythmic (Figure 4.1C) 0.800 ± 0.200 vs. 0.010 ± 0.002 ($P<0.005$, n=5, Two-Tailed T-Test).

These data showed that antagonising NMDA receptors during the alpha oscillation almost completely abolished all power and rhythmicity. The next experiment was to investigate the contribution of NMDA receptors to the beta rhythm and any plastic processes that may be functionally reshaping the network leading to the alpha rhythm on reducing network and cellular drive. The addition of CPP [10μM] to the

initial beta rhythm did not significantly affect the frequency 28.7Hz ± 2.3Hz vs. 28.1Hz ± 2.5Hz (P=0.873, n=5, Two-Tailed T-Test, figure 4.2), or rhythmicity 0.6 ± 0.2 vs. 0.9 ± 0.4 (P=0.548, n=5, Mann-Whitney Rank Sum Test) of the rhythm. The power of the rhythm increased slightly ($7.8\mu V^2 \pm 3.1\mu V^2$ vs. $27.0\mu V^2 \pm 12.6\mu V^2$, P=0.222, n=5, Mann-Whitney Rank Sum Test), however this effect was non-significant. Thus, the beta rhythm could occur independently of NMDA receptors; however, the alpha rhythm could not.

After antagonising NMDA receptors during beta rhythms, subsequent application of NBQX [5μM] and DK-AH269 [10μM] did not result in production of a strong alpha rhythm. Instead, almost all rhythmicity 0.900 ± 0.400 vs. 0.020 ± 0.004 (P<0.01, n=5, Mann-Whitney Rank Sum Test, figure 4.2) and power $27.0\mu V^2 \pm 12.6\mu V^2$ vs. $1.2\mu V^2 \pm 0.4\mu V^2$ (P<0.05, n=5, Mann-Whitney Rank Sum Test) of the beta rhythm was abolished. However, a very weak frequency peak was seen in the alpha rhythm range 28.1Hz ± 2.5Hz vs. 8.7Hz ± 0.6Hz (P<0.001, n=5, Two-Tailed T-Test). These results were also significant when comparing to the original control beta rhythms (Figure 4.2D). The frequency of the rhythm dropped significantly from 28.7Hz ± 2.3Hz to 8.7Hz ± 0.6Hz (KA alone vs. KA + CPP + NBQX + DK-AH269, P<0.01, n=5, Mann-Whitney Rank Sum Test). The power of the rhythm was also significantly reduced from $7.8\mu V^2 \pm 3.1\mu V^2$ to $1.2\mu V^2 \pm 0.4\mu V^2$ (P<0.05, n=5, Mann-Whitney Rank Sum Test), as was the rhythmicity 0.600 ± 0.200 to 0.020 ± 0.004 (P<0.01, n=5, Mann-Whitney Rank Sum Test), showing that the antagonism of NMDA receptors prevented the subsequent generation and maintenance of alpha oscillations in the primary visual cortex.

4.3.1.1 The effect of specific NMDA receptor subunit antagonism on the generation and maintenance of alpha oscillations in the V1

Given that NMDA receptors were needed for the generation and maintenance of alpha oscillations, specific subunit antagonism of the NMDA receptor subunits were carried out to investigate which particular subunits of the NMDA receptor were

required for alpha rhythms. NR1 receptors are an absolute requirement for formation of functional heterotetramers with all other subunits (Monyer et al., 1992) so selective antagonists of the NR2A, NR2B and NR2C/D subunits were examined during alpha oscillations.

Alpha oscillations were first generated in the V1. Upon addition of the drug (2S*,3R*)-1-(Phenanthren-2-carbonyl)piperazine-2,3-dicarboxylic acid (PPDA) [10μM] to preferentially block NR2C/D subunits (Feng et al., 2004), there was no detectable spectral peak observed. The frequency of oscillations was not significantly altered from control values of 11.8Hz ± 0.2Hz to 10.7Hz ± 1.3Hz (P=0.444, n=5, Two-Tailed T-Test, figure 4.3). However, blocking NR2C/D subunits almost completely abolished power in the alpha band. Control values of 52.70μV^2 ± 26.80μV^2 were reduced to 0.20μV^2 ± 0.04μV^2 (P<0.01, n=5, Two-Tailed T-Test). Rhythmicity in the LFP was also almost completely abolished in the presence of this drug. Very strong control values in this dataset (1.000 ± 0.100) were reduced to almost zero (0.020 ± 0.004, P<0.01, n=5, Mann-Whitney Rank Sum Test).

As alpha oscillations were abolished upon antagonism of the NR2C/D subunit, PPDA was added to the preceding beta oscillation to determine what effect, if any, NR2C/D subunit antagonism has on the prior beta rhythm. Again, application of PPDA [10μM] to the KA induced beta rhythm caused no significant change in the frequency: 27.8Hz ± 2.5Hz vs. 27.0Hz ± 3.2Hz (P=0.989, n=5, Two-Tailed T-Test, figure 4.4) or rhythmicity (0.30 ± 0.04 vs. 0.30 ± 0.16, P=0.809, n=5, Two-Tailed T-Test). However, a near 2-fold increase in mean power was seen, with values changing from 6.6μV^2 ± 1.2μV^2 to 16.9μV^2 ± 11.0μV^2 but this did not reach significance (P=0.841, n=5, Mann-Whitney Rank Sum Test).

As with blockade of all NMDA receptors with CPP, antagonising the NR2C/D subunit during the prior beta rhythm had no effect on beta rhythms but almost abolished the subsequent alpha rhythms on reduction in network and cellular drive. After antagonism of NR2C/D subunits during beta, further application of NBQX and DK-AH269 did not result in a strong alpha rhythm. A significant decrease in the frequency from the beta band (27.0Hz ± 3.2Hz) to the alpha band (11.7Hz ± 1.3Hz)

was seen (P<0.01, n=5, Mann-Whitney Rank Sum Test, figure 4.4). However, this was accompanied by a reduction in the mean power 16.9$\mu V^2 \pm$ 11.0μV^2 vs. 0.8$\mu V^2 \pm$ 0.2μV^2 (P=0.056, n=5, Mann-Whitney Rank Sum Test) and rhythmicity 0.300 $\pm$ 0.160 vs. 0.006 $\pm$ 0.003 (P=0.193, n=5, Two-Tailed T-Test). These results were not significant when comparing data before and after application of NBQX and DK-AH269 to reduce excitation. However, when comparing to the original control beta rhythms each of the measurement were significantly changed (Figure 4.4D). The frequency of the rhythm dropped significantly from 27.8Hz $\pm$ 2.5Hz to 11.7Hz $\pm$ 1.3Hz (KA alone vs. KA + PPDA + NBQX + DK-AH269, P<0.001, n=5, Two-Tailed T-Test). The power of the rhythm was also significantly reduced from 6.6$\mu V^2 \pm$ 1.2μV^2 to 0.8$\mu V^2 \pm$ 0.2μV^2 (P<0.01, n=5, Two-Tailed T-Test), as was the rhythmicity 0.300 $\pm$ 0.040 vs. 0.006 $\pm$ 0.003 (P<0.01, n=5, Two-Tailed T-Test), showing that the antagonism of the NR2C/D subunit of NMDA receptors prevented the generation and maintenance of alpha oscillations in the primary visual cortex.

The next step was to test the contribution of the NR2A subunit of NMDA receptors to the alpha rhythm. The selective NR2A subunit antagonist 3-Chloro-4-fluoro-N-[4-[[2-(phenylcarbonyl)hydrazino]carbonyl]benzyl]benzenesulfonamide (TCN201) (Bettini et al., 2010) was applied at a concentration of [10μM] to alpha oscillations. This caused no significant change in the frequency of oscillations: 11.8Hz $\pm$ 1.0Hz vs. 10.2Hz $\pm$ 0.4Hz (P=0.173, n=5, Two-Tailed T-Test, figure 4.5). The mean power of oscillations slightly increased from 15.6$\mu V^2 \pm$ 3.4μV^2 to 23.6$\mu V^2 \pm$ 14.4μV^2 (P=0.690, n=5, Mann-Whitney Rank Sum Test), and the rhythmicity of oscillations decreased slightly from 0.50 $\pm$ 0.07 to 0.30 $\pm$ 0.13 (P=0.379, n=5, Two-Tailed T-Test), however these results were not significant. Therefore antagonising the NR2A subunit of NMDA receptors did not appear to have a significant effect on alpha oscillations in the model used in this thesis.

NMDA receptors are expressed both pre- and post-synaptically. The presynaptic receptor complement has been suggested to be more sensitive to blockade by the polyamine/NR2B-site selective drug ifenprodil (Cull-Candy and Leszkiewicz, 2004). To test whether the effects of general NMDA receptor blockade (above) had any

presynaptic component, (1R*,2S*)-erythro-2-(4-Benzylpiperidino)-1-(4-hydroxyphenyl)-1-propanol (Ifenprodil [10μM]) was applied to the alpha rhythm.. This caused no significant change in the frequency of the rhythm 11.7Hz ± 0.5Hz vs. 10.3Hz ± 0.8Hz (P=0.177, n=5, Two-Tailed T-Test, figure 4.6). There was a slight but non-significant increase in the power of the alpha oscillation upon application of Ifenprodil 14.7μV^2 ± 6.3μV^2 vs. 26.7μV^2 ± 17.3μV^2 (P=0.841, n=5, Mann-Whitney Rank Sum Test). The rhythmicity of the oscillation also remained unchanged 0.3 ± 0.1 vs. 0.3 ± 0.1 (P=0.923, n=5, Two-Tailed T-Test). These results show that selectively antagonising putative presynaptic NMDA receptors via the polyamine site does not affect the alpha rhythm.

Finally, a selective block of all NR2B receptors (both pre- and postsynaptic) was attempted. The drug 1-[2-(4-Hydroxyphenoxy)ethyl]-4-[(4-methylphenyl)methyl]-4-piperidinol (CO101244 [10μM]) is a highly selective NR2B antagonist (Zhou et al., 1999). Application of CO101244 during alpha rhythms almost completely abolished the rhythm, leaving no detectable spectral peak. There was a significant reduction in frequency of the rhythm from 11.5Hz ± 0.7Hz to 7.6Hz ± 1.0Hz (P<0.01, n=6, Mann-Whitney Rank Sum Test, figure 4.7), along with a marked attenuation in the power at the alpha frequency 10.8μV^2 ± 5.9μV^2 vs. 2.2μV^2 ± 1.0μV^2 (P<0.05, n=6, Mann-Whitney Rank Sum Test) and rhythmicity 0.6 ± 0.2 vs. 0.1 ± 0.1 (P<0.05, n=6, Two-Tailed T-Test) suggesting NR2B subunits may contribute to alpha oscillations.

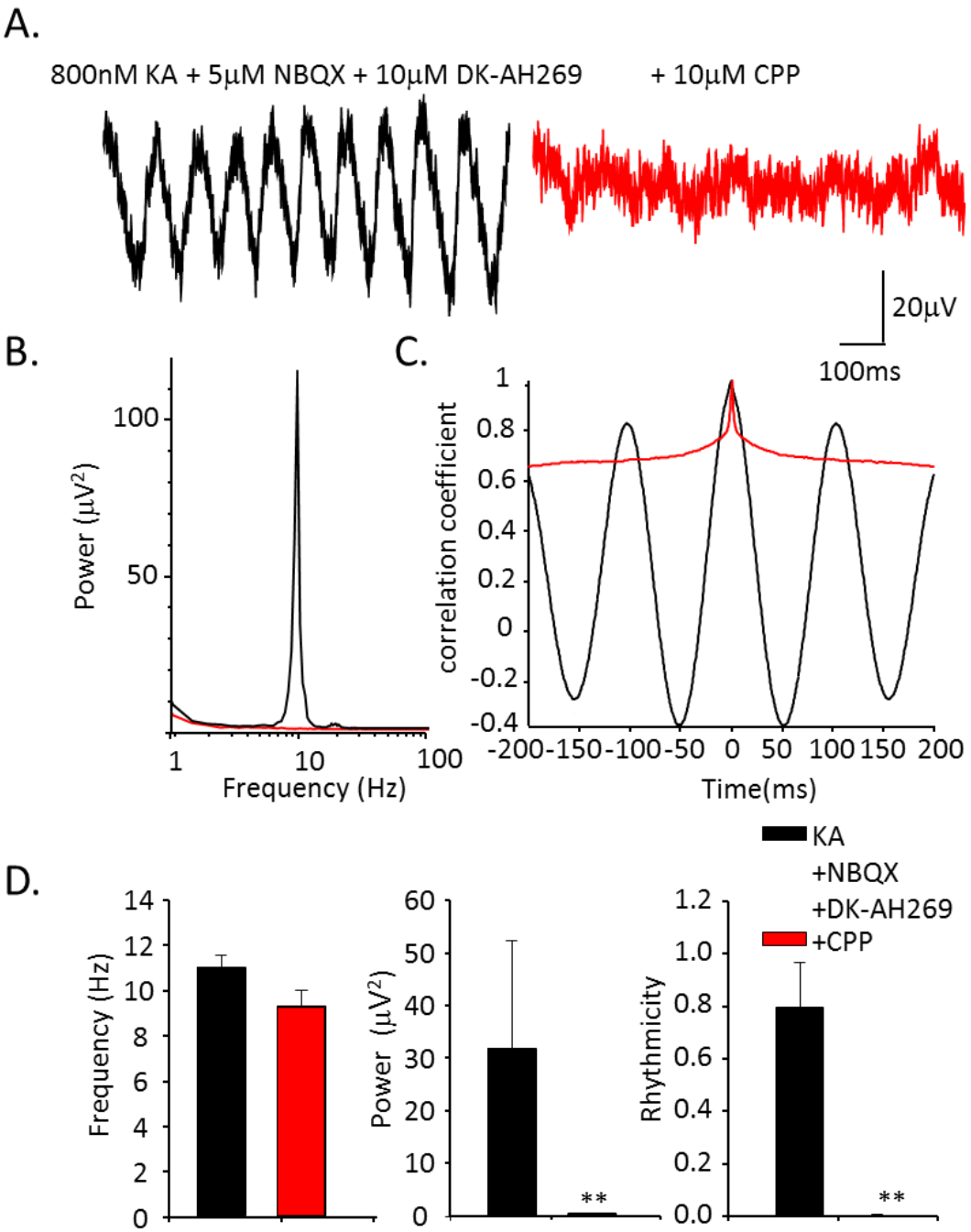

Figure 4.1 NMDA receptors were required for the generation of the alpha rhythm. A. 1 second example traces of extracellular activity induced by Kainate [800nM] and subsequent application of NBQX [5µM] and DK-AH [10µM] (black trace) and 30 minutes after addition of CPP [10µM] (red trace). **B.** Example power spectra produced from traces in A showing the effect of CPP on alpha oscillations. **C.** Example auto-correlations produced from 60 second epochs of extracellular data showing rhythmicity before (in black) and after (in red) application of CPP. **D.** Graphs showing the change in frequency, amplitude and rhythmicity of oscillations before and after application of CPP. (frequency $P>0.05$, Two-Tailed T-Test, amplitude $P<0.05$, Mann-Whitney Rank Sum Test, rhythmicity $P<0.01$, Two-Tailed T-Test, n=5)

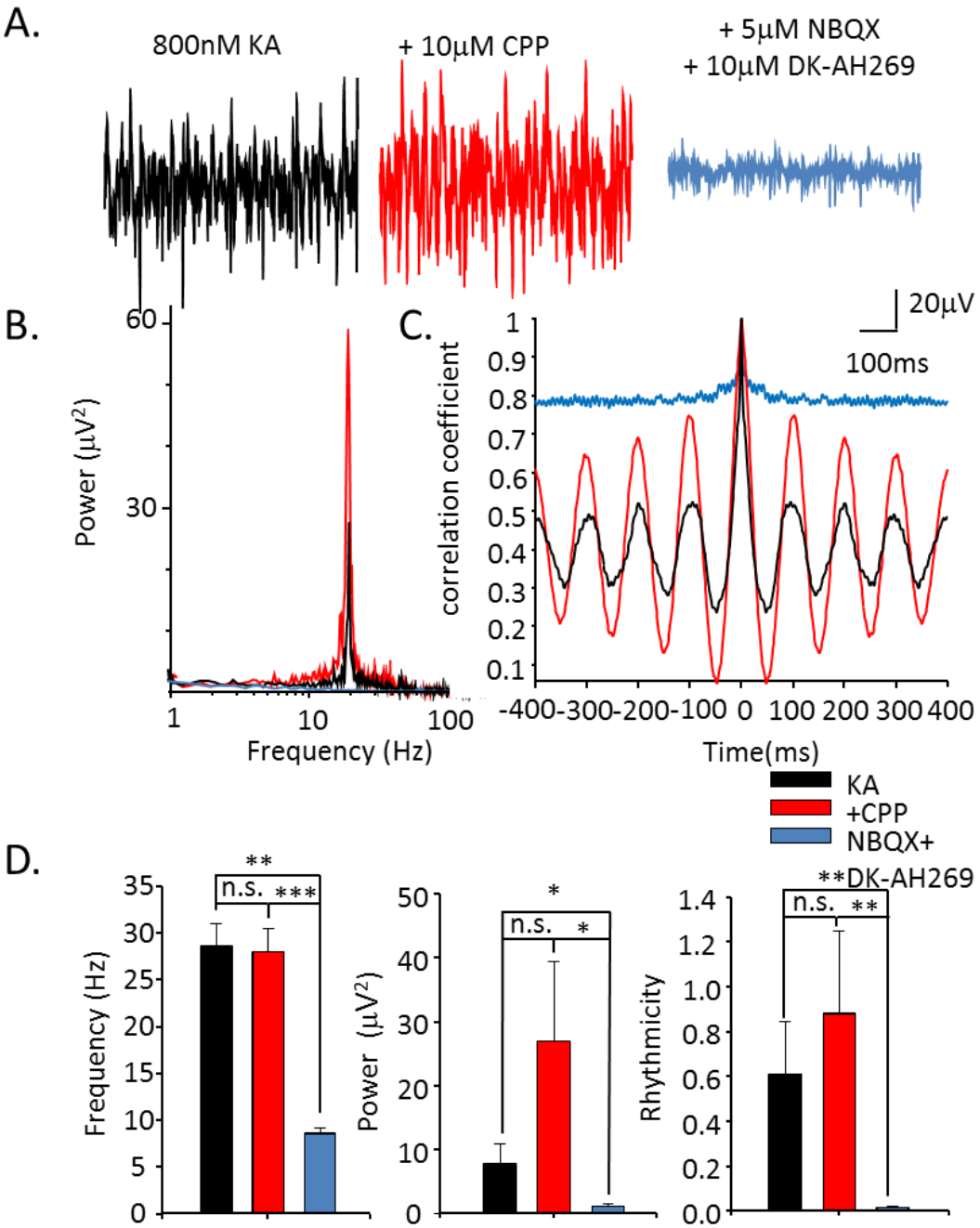

Figure 4.2 Blocking NMDA receptors prevented generation of the alpha rhythm. A. 1 second example traces of extracellular activity induced by Kainate [800nM] (black trace), 30 minutes after application of CPP [10µM] (red trace), and subsequent application of NBQX [5µM] and DK-AH269 [10µM] (blue trace). **B.** Example power spectra produced from traces in A. **C.** Example auto-correlations produced from 60 second epochs of extracellular data showing rhythmicity before (in black) and after (in red) application of CPP and with subsequent addition of NBQX and DK-AH269 (in blue). **D.** Graphs showing the change in frequency ($P>0.05$ for KA-CPP, $P<0.001$, for KA-DK-AH, $P<0.01$ for CPP-DK-AH, n=5), amplitude ($P>0.05$ for KA-CPP, $P<0.05$ for KA- DK-AH and CPP-DK-AH, n=5) and rhythmicity ($P>0.05$ for KA-CPP, $P<0.01$ for KA-DK-AH and CPP-DK-AH, n=5, all Two-Tailed T-Test or Mann-Whitney Rank Sum Test) of oscillations.

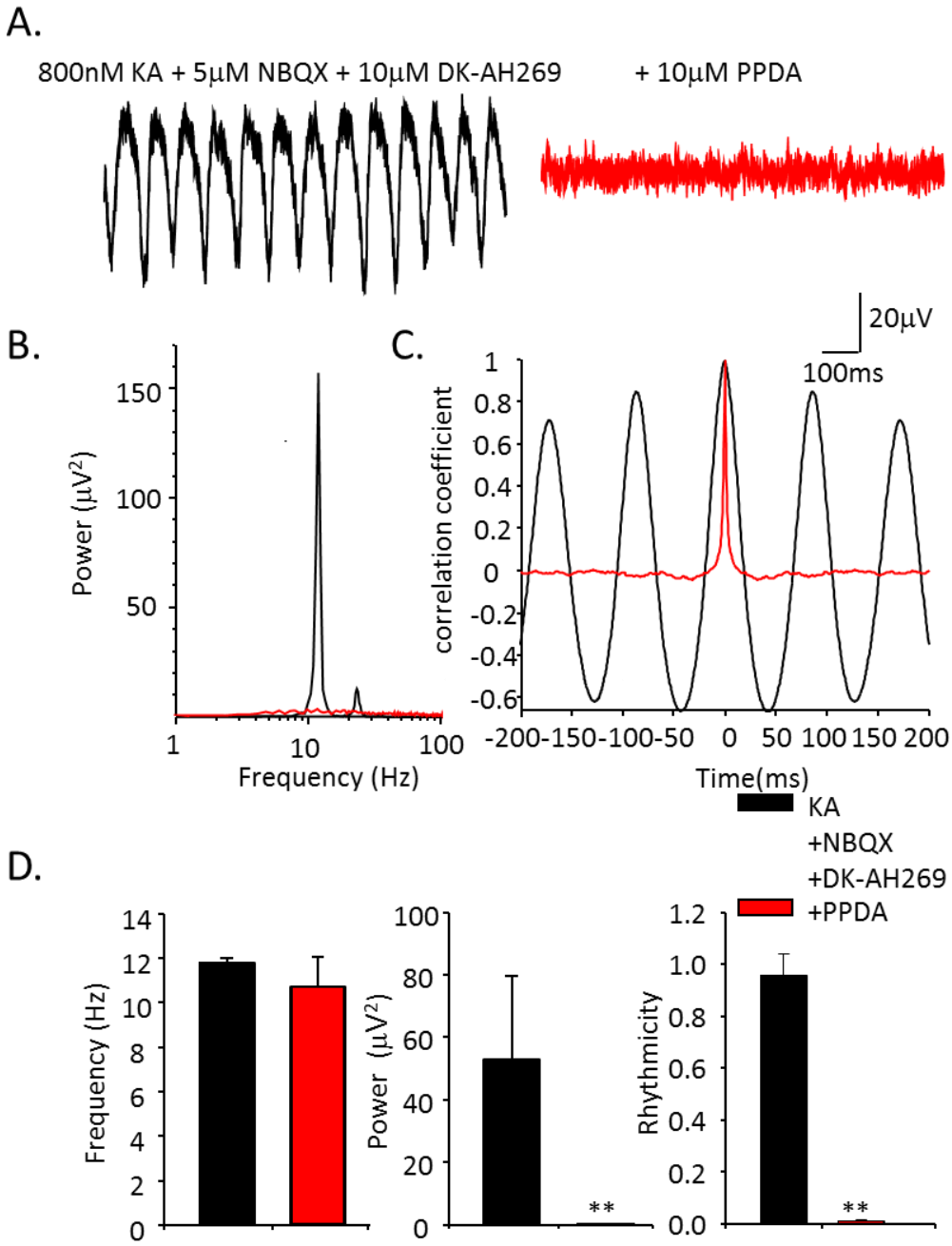

Figure 4.3 The NR2C/D subunit of NMDA receptors was required for the generation of the alpha rhythm. A. 1 second example traces of extracellular activity induced by Kainate [800nM] and subsequent application of NBQX [5µM] and DK-AH [10µM] (black trace) and 30 minutes after addition of PPDA [10µM] (red trace). **B.** Example power spectra produced from traces in A showing the effect of PPDA on alpha oscillations. **C.** Example auto-correlations produced from 60 second epochs of extracellular data showing rhythmicity before (in black) and after (in red) application of PPDA. **D.** Graphs showing the change in frequency ($P>0.05$, n=5, Two-Tailed T-Test), amplitude ($P<0.01$, n=5, Two-Tailed T-Test) and rhythmicity ($P<0.01$, n=3, Mann-Whitney Rank Sum Test) of oscillations before and after application of PPDA.

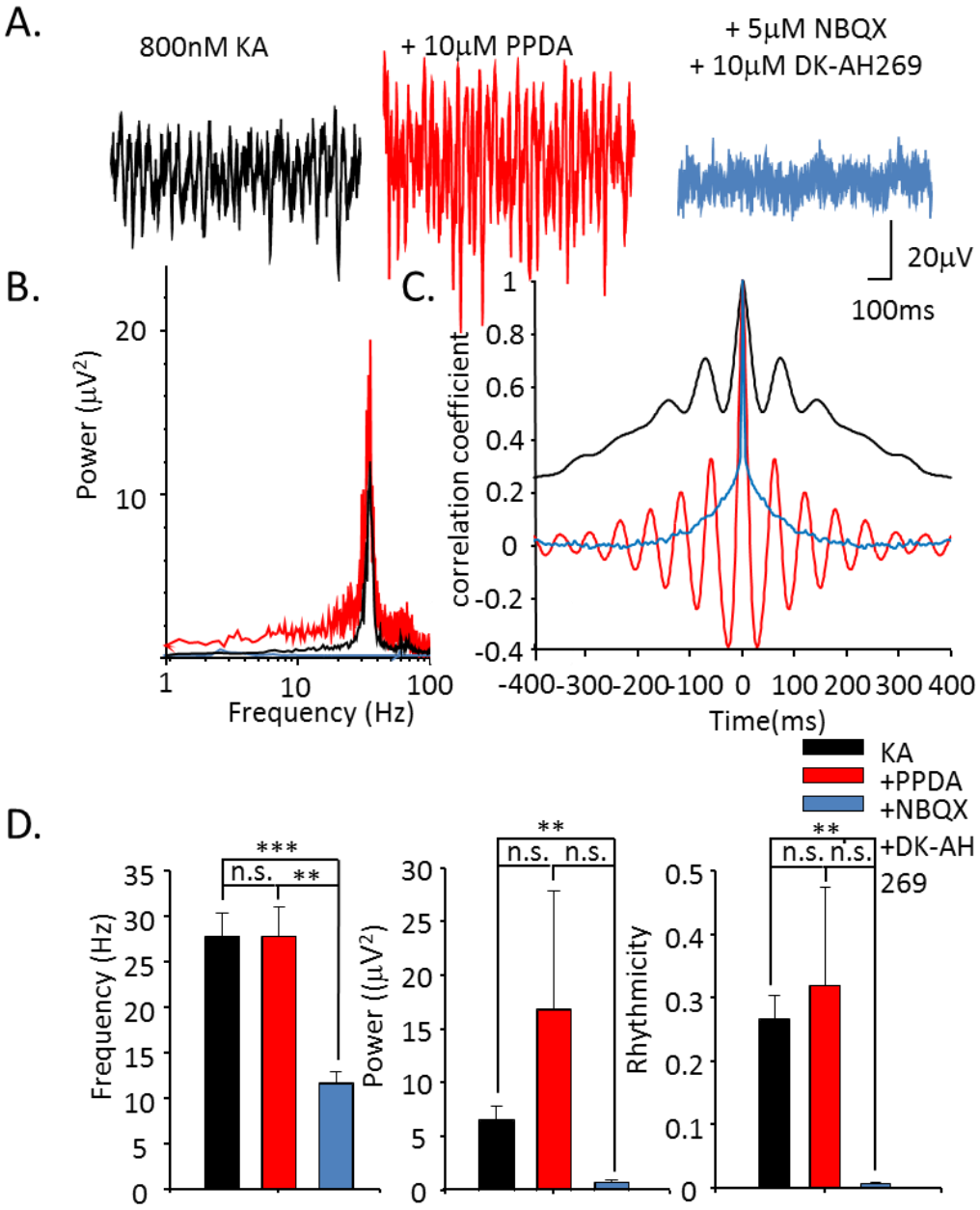

Figure 4.4 Blocking the NR2C/D subunit of NMDA receptors prevented generation of the alpha rhythm. A. 1 second example traces of extracellular activity induced by Kainate [800nM] (black trace), 30 minutes after application of PPDA [10µM] (red trace), and subsequent application of NBQX [5µM] and DK-AH269 [10µM] (blue trace). **B.** Example power spectra produced from traces in A. **C.** Example auto-correlations produced from 60 second epochs of extracellular data showing rhythmicity before (in black) and after (in red) application of PPDA and with subsequent addition of NBQX and DK-AH269 (in blue). **D.** Graphs showing the change in frequency ($P>0.05$ for KA-PPDA, $P<0.001$ for KA-DK-AH, $P<0.01$ for PPDA-DK-AH, n=5), amplitude ($P<0.01$ for KA-DK-AH, $P>0.05$ for KA-PPDA and PPDA-DK-AH, n=5) and rhythmicity ($P>0.01$ for KA-PPDA and PPDA-DK-AH, $P<0.05$ for KA-DK-AH, n=5, all Two-Tailed T-Test or Mann-Whitney Rank Sum Test) of oscillations.

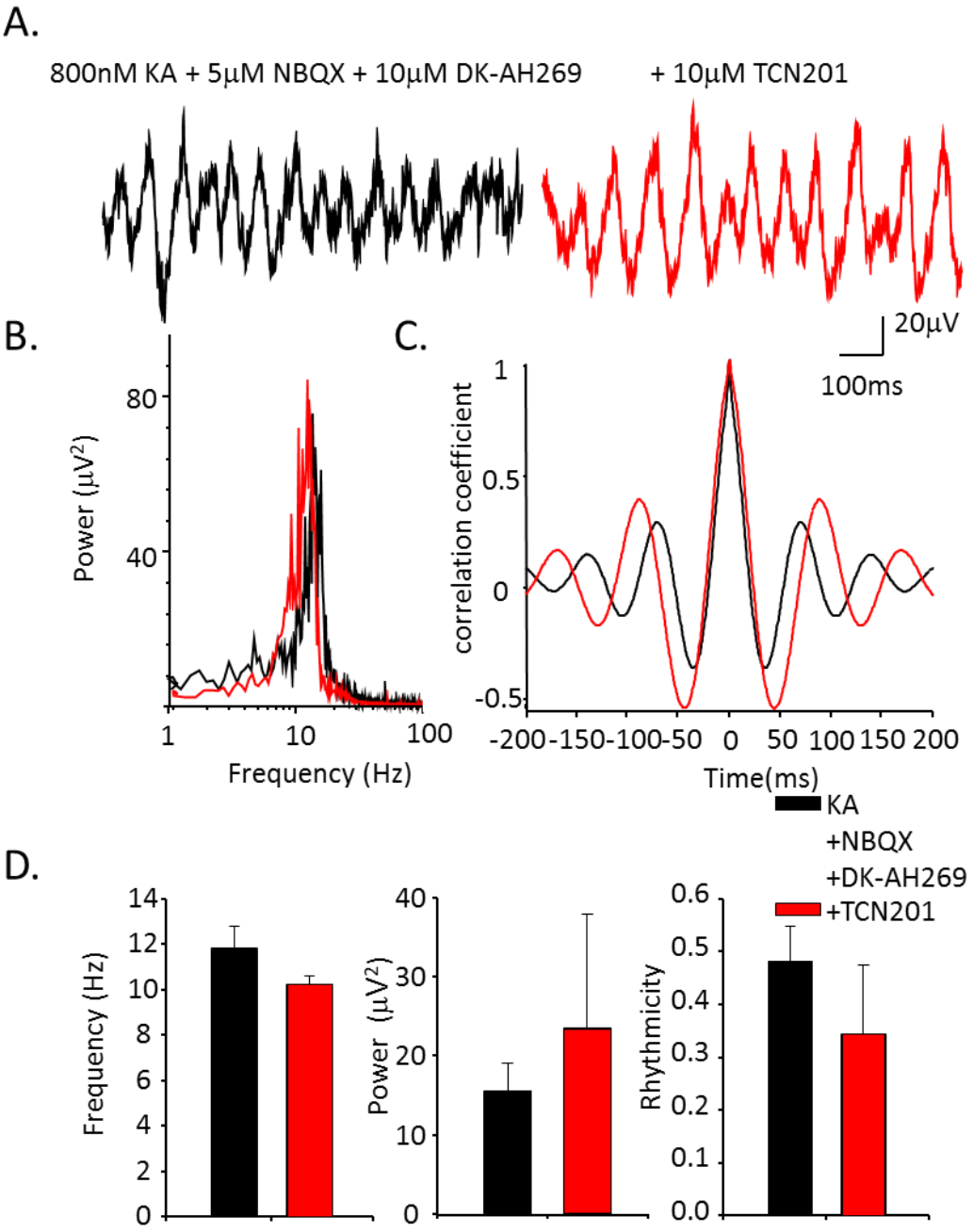

Figure 4.5 The NR2A subunit of NMDA receptors was not required for the generation of the alpha rhythm. A. 1 second example traces of extracellular activity induced by Kainate [800nM] and subsequent application of NBQX [5µM] and DK-AH [10µM] (black trace) and 30 minutes after addition of TCN [10µM] (red trace). **B.** Example power spectra produced from traces in A showing the effect of TCN on alpha oscillations. **C.** Example auto-correlations produced from 60 second epochs of extracellular data showing rhythmicity before (in black) and after (in red) application of TCN. **D.** Graphs showing the change in frequency (P>0.05, Two-Tailed T-Test, n=5), amplitude (P>0.05, Mann-Whitney Rank Sum Test, n=5) and rhythmicity (P>0.05, Two-Tailed T-Test, n=5) of oscillations before and after application of TCN.

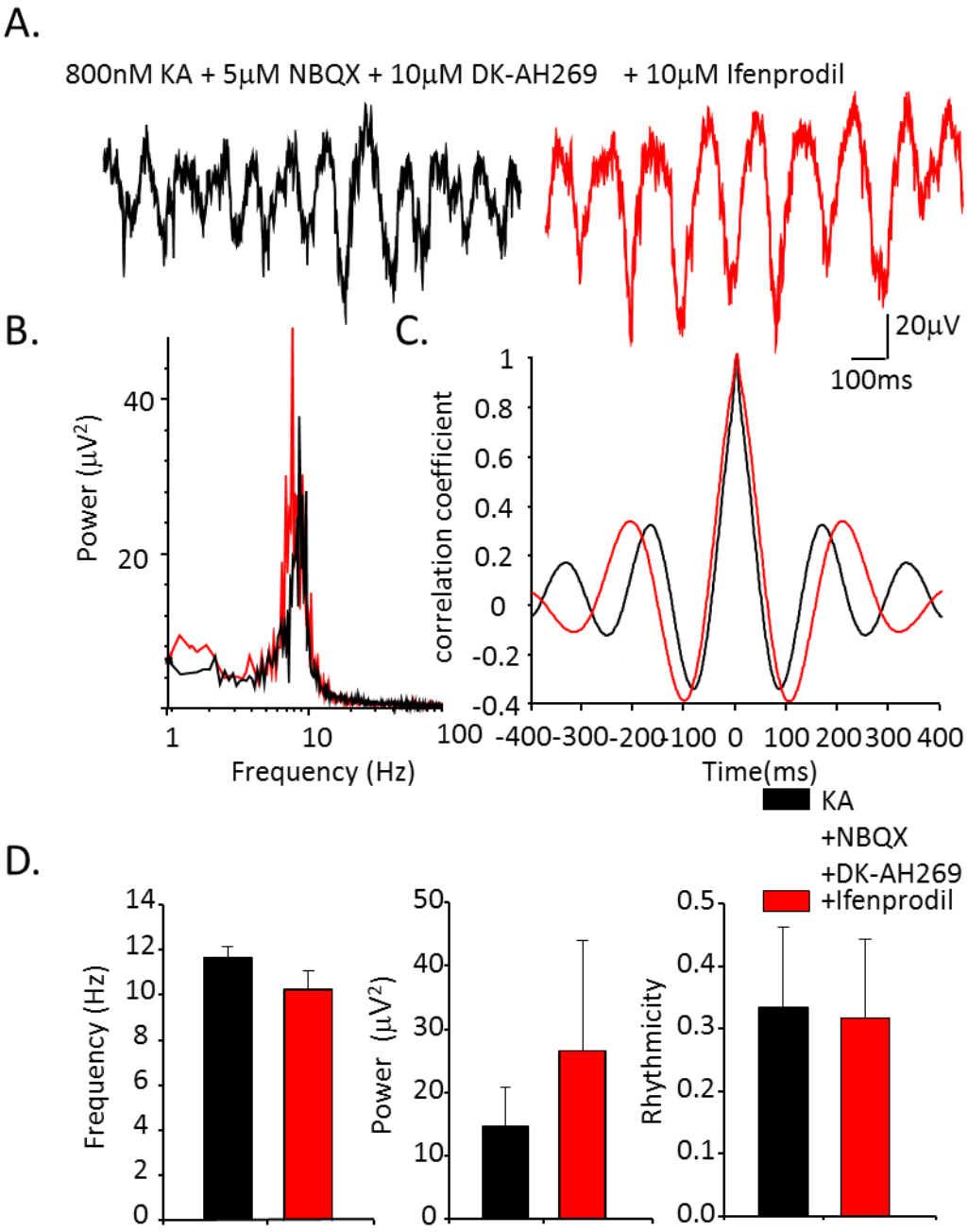

Figure 4.6 Blocking NMDA receptors via the polyamine site had no effect on the alpha rhythm. A. 1 second example traces of extracellular activity induced by Kainate [800nM] and subsequent application of NBQX [5µM] and DK-AH [10µM] (black trace) and 30 minutes after addition of Ifenprodil [10µM] (red trace). **B.** Example power spectra produced from traces in A showing the effect of Ifenprodil on alpha oscillations. **C.** Example auto-correlations produced from 60 second epochs of extracellular data showing rhythmicity before (in black) and after (in red) application of Ifenprodil. **D.** Graphs showing the change in frequency ($P>0.05$, Two-Tailed T-Test, n=5), amplitude ($P>0.05$, Mann-Whitney Rank Sum Test, n=5) and rhythmicity ($P>0.05$, Two-Tailed T-Test, n=5) of oscillations before and after application of Ifenprodil.

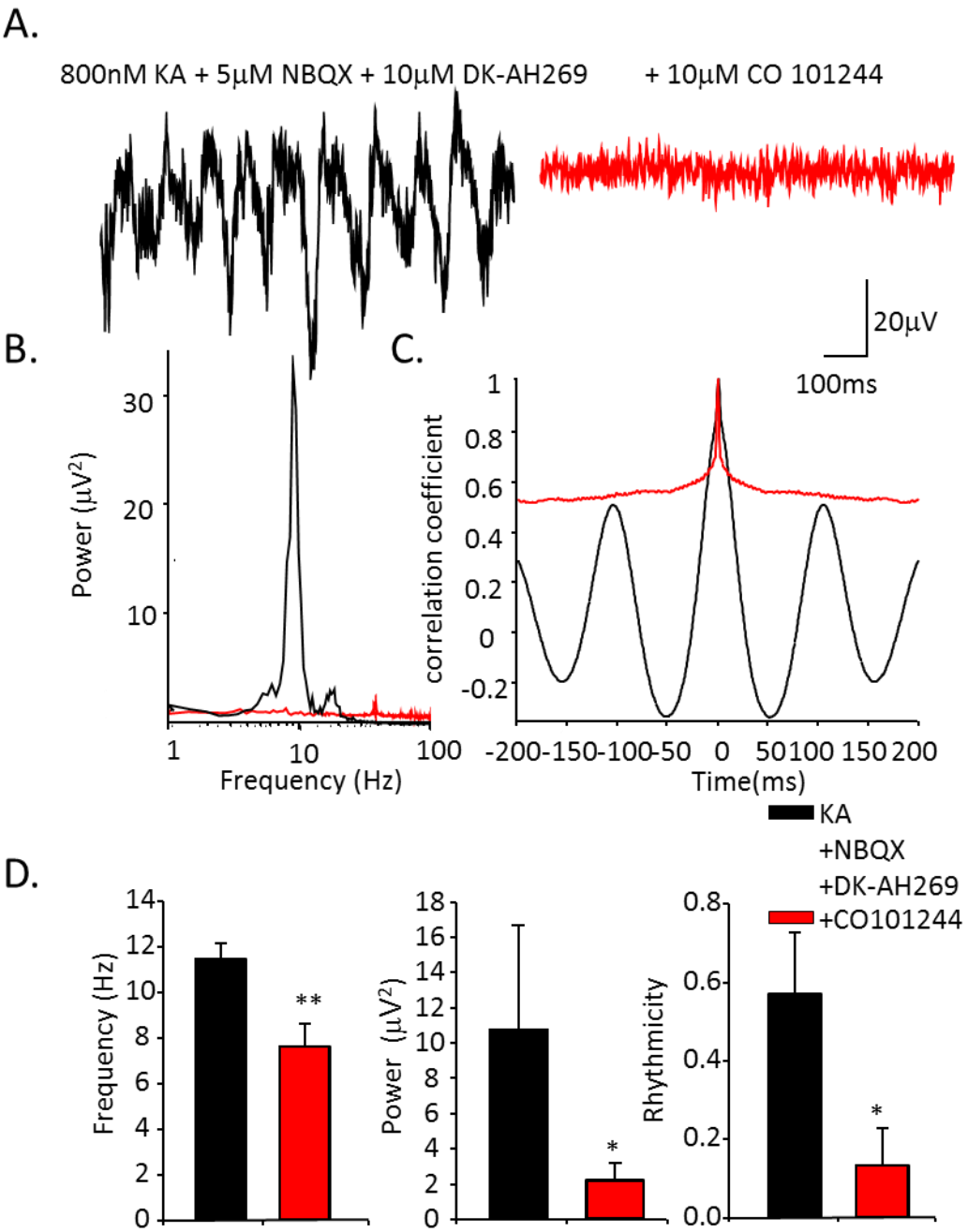

Figure 4.7 The NR2B subunit of NMDA receptors was required for the generation of the alpha rhythm. A. 1 second example traces of extracellular activity induced by Kainate [800nM] and subsequent application of NBQX [5µM] and DK-AH [10µM] (black trace) and 30 minutes after addition of CO101244 [10µM] (red trace). **B.** Example power spectra produced from traces in A showing the effect of CO on alpha oscillations. **C.** Example auto-correlations produced from 60 second epochs of extracellular data showing rhythmicity before (in black) and after (in red) application of CO101244. **D.** Graphs showing the change in frequency ($P<0.01$, n=6, Mann-Whitney Rank Sum Test), amplitude ($P<0.05$, n=6, Mann-Whitney Rank Sum Test) and rhythmicity ($P<0.05$, n=6, Two-Tailed T-test) of oscillations before and after application of CO101244.

These data demonstrated that the alpha rhythm is dependent upon excitatory NMDA receptors, in particular the NR2C/D and NR2B subunits. The role of inhibitory $GABA_A$ receptors was then studied to see if alpha rhythms also required fast synaptic inhibition.

4.3.2 Involvement of $GABA_A$ receptors in alpha oscillations

The highly-selective $GABA_A$ receptor antagonist 6-Imino-3-(4-methoxyphenyl)-1(6H)-pyridazinebutanoic acid (Gabazine [1μM]) (Heaulme et al., 1986) was applied to the alpha rhythm to determine the contribution of inhibitory $GABA_A$ receptors. Antagonising $GABA_A$ receptors in this manner almost completely abolished the alpha rhythm, leaving no detectable spectral peak. Analysis of the residual LFP rhythm revealed a significant reduction in the frequency from 12.2Hz $\pm$ 0.9Hz to 9.3Hz $\pm$ 0.6 ($P<0.05$, n=5, Two-Tailed T-Test, figure 4.8) in this dataset. Gabazine almost abolished all power in the alpha band: $21.2\mu V^2 \pm 5.6\mu V^2$ to $0.4\mu V^2 \pm 0.1\mu V^2$ ($P<0.01$, n=5, Mann-Whitney Rank Sum Test). Rhythmicity was also almost abolished: 1.00 ± 0.02 vs. 0.02 ± 0.01 ($P<0.001$, n=5, Two-Tailed T-Test). These data indicated that inhibitory $GABA_A$ receptors were required for maintenance of alpha oscillations in this experimental model.

The role of GABA receptors in rhythm generation is often accompanied by a role for gap junctional communication too (see section 4.1). The next set of experiments was therefore designed to determine whether non-chemical receptor mediated transmission (i.e. electrical coupling) was required in the alpha rhythm.

4.3.3 Involvement of gap junctional mediated coupling in alpha oscillations

The contribution of gap junctional coupling in the generation of alpha oscillations was studied using gap junction blocker (3β,20β)-3-(3-Carboxy-1-oxopropoxy)-11-oxoolean-12-en-29-oic acid (Carbenoxolone (CBX)). Application of 100μM CBX caused a statistically significant reduction in the frequency of the alpha rhythm

from 12.5Hz ± 0.5Hz to 9.0Hz ± 0.3Hz (P<0.001, n=5, Two-Tailed T-Test, figure 4.9). The power and rhythmicity of alpha oscillations however remained almost the same 45.6μV^2 ± 27.3μV^2 vs. 45.9μV^2 ± 15.7μV^2 (P=0.690, n=5, Mann-Whitney Rank Sum Test) and 1.1 ± 0.1 vs. 1.2 ± 0.1 (P=0.834, n=5, Two-Tailed T-Test). An increased concentration of 500μM CBX was next applied to the alpha rhythm. This again caused a significant reduction in the frequency of the rhythm 12.5Hz ± 0.5Hz to 7.5Hz ± 0.5Hz (P<0.001, n=5, Two-Tailed T-Test). This higher concentration of CBX significantly reduced the power from 45.6μV^2 ± 27.3μV^2 to 2.6μV^2 ± 1μV^2 (P<0.01, n=5, Mann-Whitney Rank Sum Test) and abolished all rhythmicity 1.1 ± 0.1 vs. 0.01 ± 0.006 (P<0.01, n=5, Mann-Whitney Rank Sum Test).

The findings indicate that alpha rhythms require interplay between excitatory NMDA receptor and inhibitory $GABA_A$ receptor mediated transmission along with a potential involvement for electrical coupling. The next section investigated the suggested role for dendritic T-channel-mediated burst discharges (Jones et al., 2000b) in alpha rhythm generation.

4.3.4 Decreasing T-type calcium channel function had no effect on the alpha rhythm

The next experiment was done to investigate what the effects of antagonism of low-voltage activated calcium channels would have on the alpha rhythm. Burst-like behaviour has been shown to be mediated, in part, by interaction between I_h current and T-type calcium channels (Foehring and Waters, 1991). This has been predicted to be a mechanism of cortical alpha rhythms by computational modelling studies (Jones et al., 2000b). We used the drug (1S,2S)-2-[2-[[3-(1H-Benzimidazol-2-yl)propyl]methylamino]ethyl]-6-fluoro-1,2,3,4-tetrahydro-1-(1-methylethyl)-2-naphthalenyl cyclopropanecarboxylate (NNC 55-0396) as a highly selective T-type calcium channel blocker (Huang et al., 2004). This was applied to the alpha rhythm at a concentration of [50μM]. Application of NNC 55-0396 caused no significant change in the frequency of the alpha rhythm: 10.9Hz ± 0.9Hz vs. 9.5Hz ± 1.0Hz (P=0.299, n=5, Two-Tailed T-Test, figure 4.10), nor did it change power (12.7μV^2 ± 9.9μV^2 vs. 7.7μV^2 ± 3.5μV^2, P=0.537, n=5, Mann-Whitney

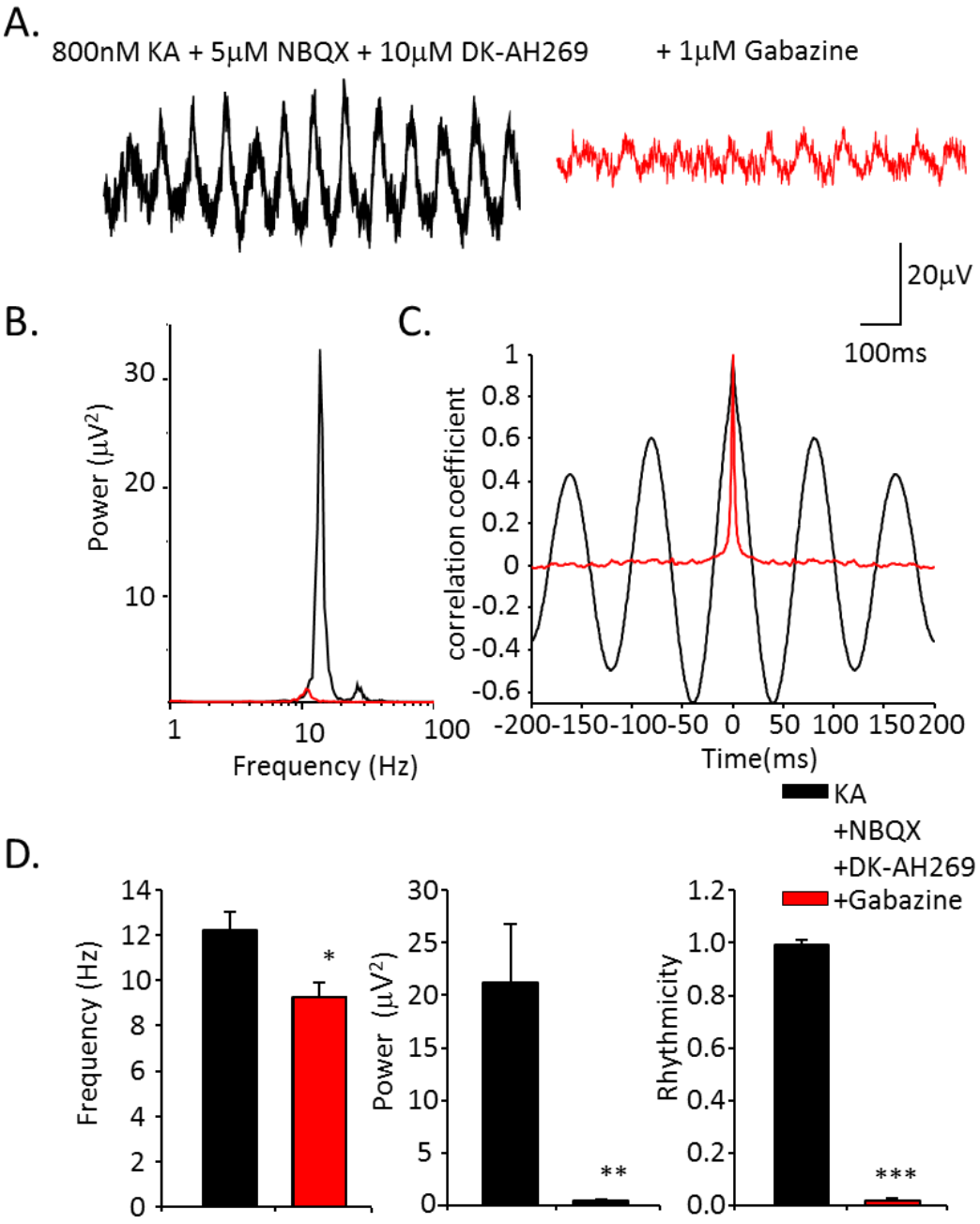

Figure 4.8 Reducing $GABA_A$ mediated inhibition reduced power and rhythmicity of the alpha rhythm. A. 1 second example traces of extracellular activity recorded from layer IV of the V1 following application of Kainate [800nM], and subsequent application of NBQX [5µM] and DK-AH [10µM] (black trace), and 30 minutes after addition of Gabazine [1µM] (red trace). **B.** Example power spectra produced from the traces in A showing the effect of Gabazine on alpha oscillations. **C.** Example auto-correlations produced from 60 second epochs of extracellular data showing rhythmicity before (in black) and after (in red) application of Gabazine. **D.** Graphs showing the change in frequency ($P<0.05$, n=5, Two-Tailed T-Test), amplitude ($P<0.05$, n=5, Mann-Whitney Rank Sum Test) and rhythmicity ($P<0.001$, n=5, Two-Tailed T-Test) of oscillations before and after application of Gabazine.

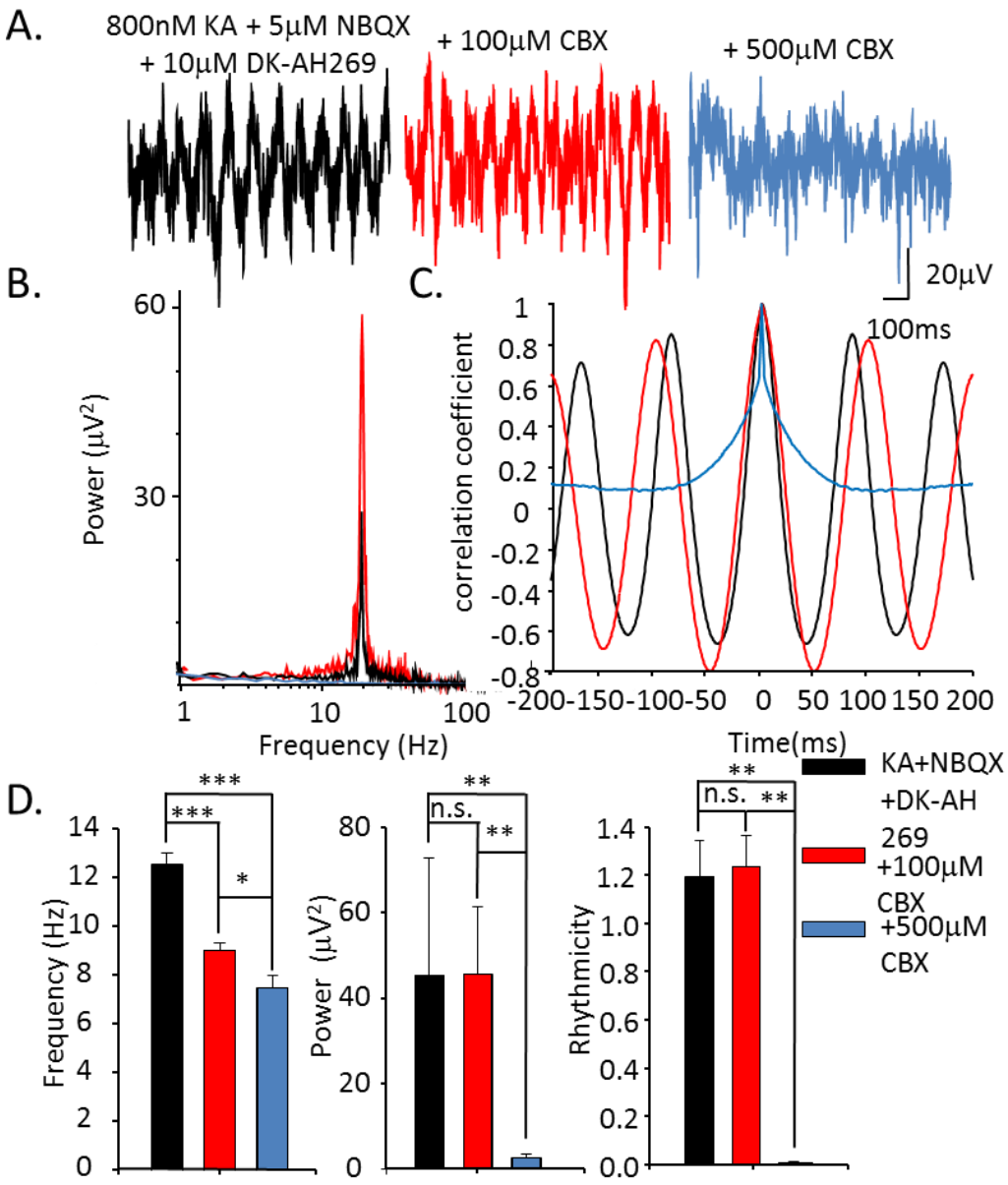

Figure 4.9 Gap-junctional mediated coupling was required for the generation of the alpha rhythm. A. 1 second example traces of extracellular activity recorded from layer IV of the V1 following application of Kainate [800nM] and subsequent application of NBQX [5µM] and DK-AH [10µM] (black trace), 30 minutes after addition of Carbenoxolone [100µM] (red trace) and [500µM] (blue trace). **B.** Example power spectra produced from the traces in A. **C.** Example auto-correlations produced from 60 second epochs of extracellular data showing rhythmicity before and after application of Carbenoxolone. **D.** Graphs showing the change in frequency ($P<0.001$ KA-100µM CBX and KA-500µM CBX, $P<0.05$ 100µM CBX-500µM CBX, n=5), amplitude ($P>0.05$ for KA-100µM CBX, $P<0.01$ for KA-500µM CBX, $P<0.05$ for 100µM CBX-500µM CBX, n=5) and rhythmicity ($P>0.05$ for KA-100µM CBX, $P<0.01$ for KA-500µM CBX and 100µM CBX-500µM CBX, n=5, all Two-Tailed T-Test or Mann-Whitney Rank Sum Test).of oscillations before and after application of Carbenoxolone.

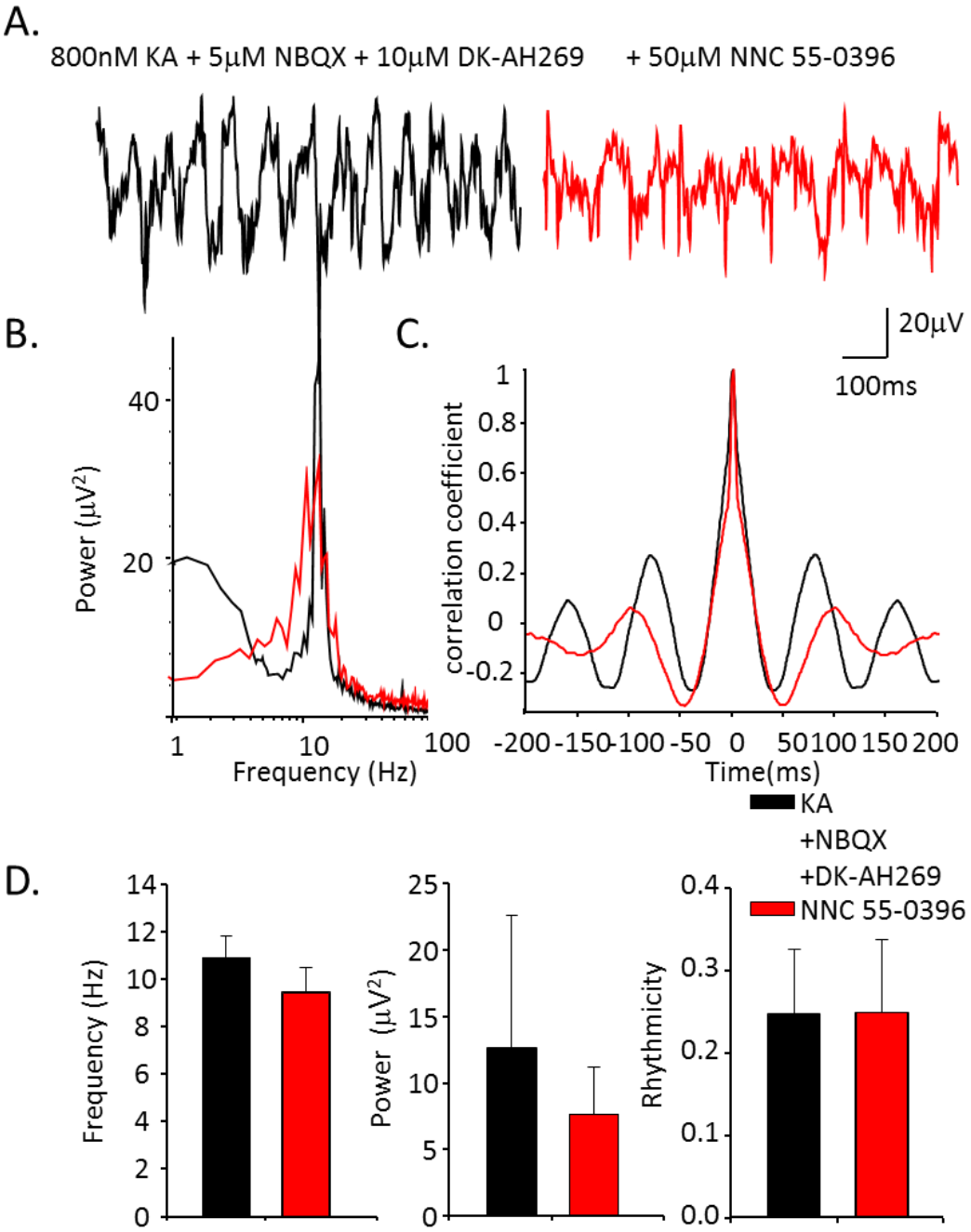

Figure 4.10 Decreasing T-type calcium channel function had no effect on the alpha rhythm. **A.** 1 second example traces of extracellular activity recorded from layer IV of the V1 following application of Kainate [800nM] and subsequent application of NBQX [5µM] and DK-AH [10µM] (black trace), and 30 minutes after addition of NNC 55-0396 [50µM] (red trace). **B.** Example power spectra produced from the traces in A showing the effect of NNC 55-0396 on alpha oscillations. **C.** Example auto-correlations produced from 60 second epochs of extracellular data showing rhythmicity before (in black) and after (in red) application of NNC 55-0396. **D.** Graphs showing the change in frequency (P>0.05, n=5, Two-Tailed T-Test), amplitude (P>0.05, n=5, Mann-Whitney Rank Sum Test) and rhythmicity (P>0.05, n=5, Two-Tailed T-Test) of oscillations before and after application of NNC 55-0396.

Rank Sum Test) or rhythmicity (0.20 ± 0.08 vs. 0.30 ± 0.09, P=0.987, n=5, Two-Tailed T-Test) of oscillations. T-type calcium channels therefore do not appear to affect the generation or maintenance of the alpha rhythm in this model.

4.3.5 Nicotine could partially generate alpha oscillations in the V1

Nicotine has been shown to enhance the alpha rhythm (Domino et al., 2009) and reduce I_h current (Griguoli et al., 2010), and nicotinic receptor activation is a key component of the cortical arousal system (Arroyo et al., 2014). Furthermore, nicotinic receptor activation plays a critical role in attentional task performance (Proulx et al., 2014) – a cognitive process where alpha rhythms are thought to be involved (see chapter 1). Also, as blocking of I_h current has been shown to be crucial in the generation of the alpha rhythm in the present model, we sought to reproduce the preliminary results illustrated in figure 3.1 in this more persistent mode of alpha rhythm generation. Nicotine [50μM] was added to the beta rhythm following the reduction in synaptic excitation with NBQX [5μM] but in the absence of the direct I_h modulator DK-AH269. This caused a significant reduction in frequency of the rhythm from 15.6Hz ± 0.5Hz to 13.9Hz ± 0.2Hz (P<0.05, n=5, Two-Tailed T-Test, figure 4.11) along with a non-significant increase in mean power (16.2μV^2 ± 5.9μV^2 vs. 42.3μV^2 ± 14.1μV^2 ,P=0.064, n=5, Two-Tailed T-Test) and rhythmicity 0.3 ± 0.1 vs. 0.6 ± 0.2, P=0.107, n=5, Two-Tailed T-Test).

These effects were qualitatively similar to those of DK-AH269 but of lower magnitude. We therefore sought to test whether these effects of nicotine could be additive to those of DK-AH269. DK-AH269 [10μM] was added to the rhythm following application of Nicotine [50μM]. This caused a further significant decrease of the frequency of the rhythm from 13.9Hz ± 0.2Hz to 12.0Hz ± 0.3Hz (P<0.001, n=5, Two-Tailed T-Test) and further increased the power from 42.3μV^2 ± 14.1μV^2 to 80.7μV^2 ± 25.7μV^2 (P=0.139, n=5, Two-Tailed T-Test) and rhythmicity from 0.6 ± 0.2 to 0.7 ± 0.2 (P=0.568, n=5, Two-Tailed T-Test). However, again these were non-significant changes.

These results were not significant when comparing data before and after application of Nicotine and DK-AH269. However, when comparing to the original control beta rhythms each of the measurement were significantly changed (Figure 4.11D). The frequency of the rhythm dropped significantly from 15.6Hz ± 0.5Hz to 12.0Hz ± 0.3Hz (KA + NBQX vs. KA +NBQX + Nicotine + DK-AH269, P<0.001, n=5, Two-Tailed T-Test). The power of the rhythm was also significantly reduced from 16.2μV^2 ± 5.9μV^2 to 80.7μV^2 ± 25.7μV^2 (P<0.05, n=5, Two-Tailed T-Test), as was the rhythmicity 0.3 ± 0.1 vs. 0.7 ± 0.2 (P<0.05, n=5, Two-Tailed T-Test).

4.3.6 Noradrenaline prevented the generation of alpha oscillations

While there is little evidence for effects of noradrenaline on alpha rhythms it has also been shown to block or enhance I_h current in *in vitro* preparations of rat brain slices in a manner dependent on the alpha1/alpha2 expression ratios for noradrenergic receptors (Arencibia-Albite et al., 2007). Noradrenaline [10μM] was applied to the beta rhythm, after reduction in drive with NBQX [5μM] to replace DK-AH269. Application of NA to the beta rhythm caused no effect on the frequency of the rhythm, with control frequencies of 19.1Hz ± 1.0Hz and 18.7Hz ± 0.8Hz in the presence of noradrenaline (P=0.805, n=6, Two-Tailed T-Test, figure 4.12). Noradrenaline did however cause an increase in beta rhythm power from 2.3μV^2 ± 0.3μV^2 to 14.2μV^2 ± 5.6μV^2 (P<0.01, n=6, Mann-Whitney Rank Sum Test). Rhythmicity at beta frequencies was also increased, with control values of 0.20 ± 0.05 changing to 0.50 ± 0.10 in the presence of noradrenaline (P<0.05, n=6, Two-Tailed T-Test). Subsequent addition of DK-AH269 [10μM] caused no reduction in frequency to the alpha band when noradrenaline was pre-applied as above. A control beta frequency of 18.7Hz ± 0.8Hz in the presence of noradrenaline was little changed at 18.0Hz ± 0.5Hz following further addition of DK-AH269 (P=0.269, n=6, Two-Tailed T-Test). Neither power (14.2μV^2 ± 5.6μV^2 vs. 20.2μV^2 ± 6.1μV^2, P=0.589, n=6, Mann-Whitney Rank Sum Test), nor rhythmicity (0.5 ± 0.1 vs. 0.6 ± 0.1, P=0.618, n=6, Two-Tailed T-Test) of oscillations were altered either. These data.

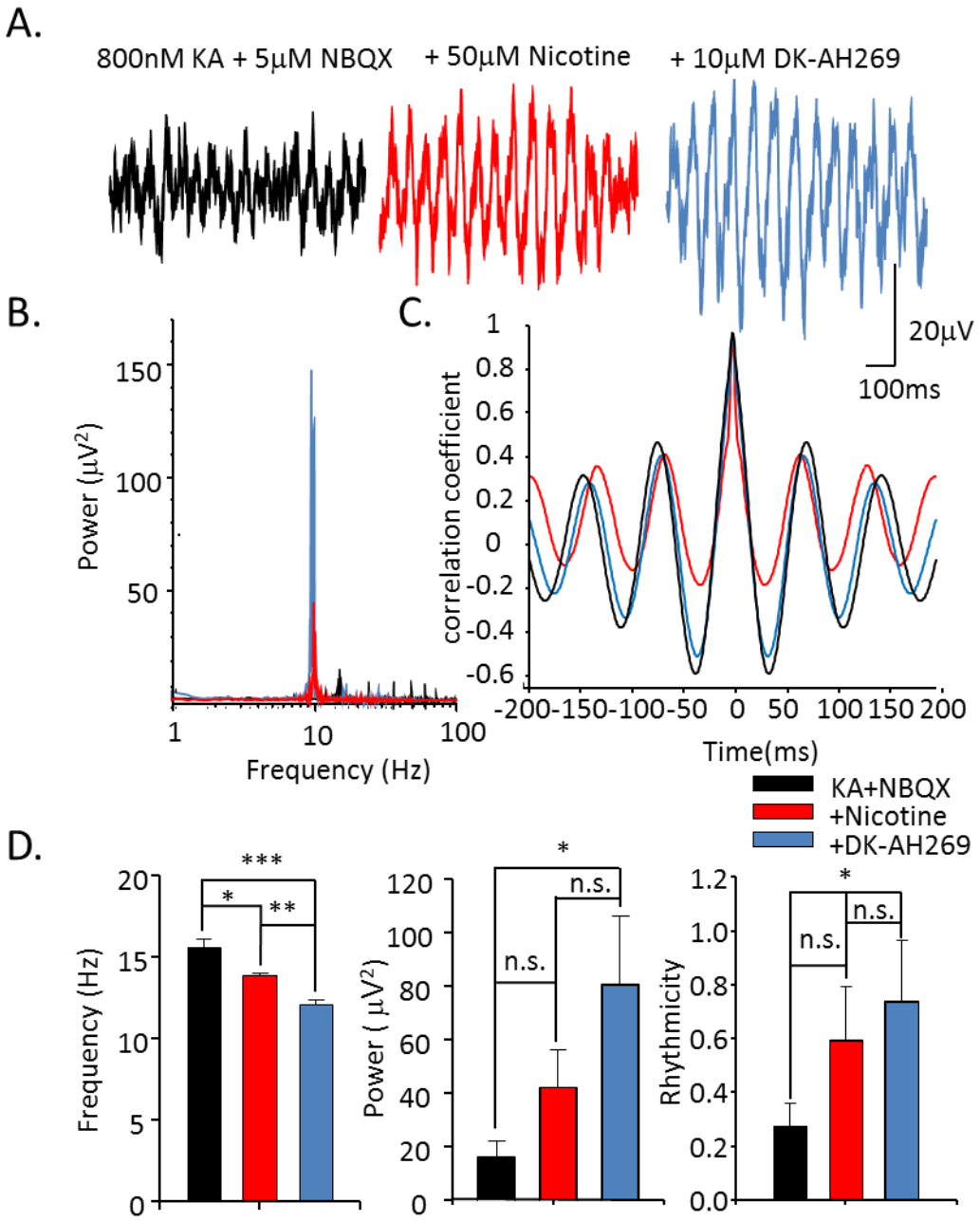

Figure 4.11 Nicotine could generate alpha frequency oscillations. A. 1 second example traces of extracellular activity induced by Kainate [800nM] and subsequent addition of NBQX [5µM] (black trace), 30 minutes after addition of Nicotine [50µM] (red trace), and 30 minutes after addition of DK-AH [10µM] (blue trace). **B.** power spectra produced from traces in A. **C.** Example auto-correlations produced from 60 second epochs of extracellular data showing rhythmicity before (in black) and after (in red) application of Nicotine, and after subsequent addition of DK-AH (in blue). **D.** Graphs showing the change in frequency (KA+NBQX-Nicotine $P<0.05$, KA+NBQX-DK-AH $P<0.001$, Nicotine-DK-AH $P<0.005$, n=5), amplitude (KA+NBQX-Nicotine and Nicotine-DK-AH $P>0.05$, for KA+NBQX-DK-AH $P<0.05$, n=5) and rhythmicity ($P>0.05$ KA+NBQX-Nicotine and Nicotine-DK-AH, $P<0.05$ for KA+NBQX-DK-AH, n=5, all Two-Tailed T-Test) of oscillations after application of KA and NBQX, Nicotine and DK-AH.

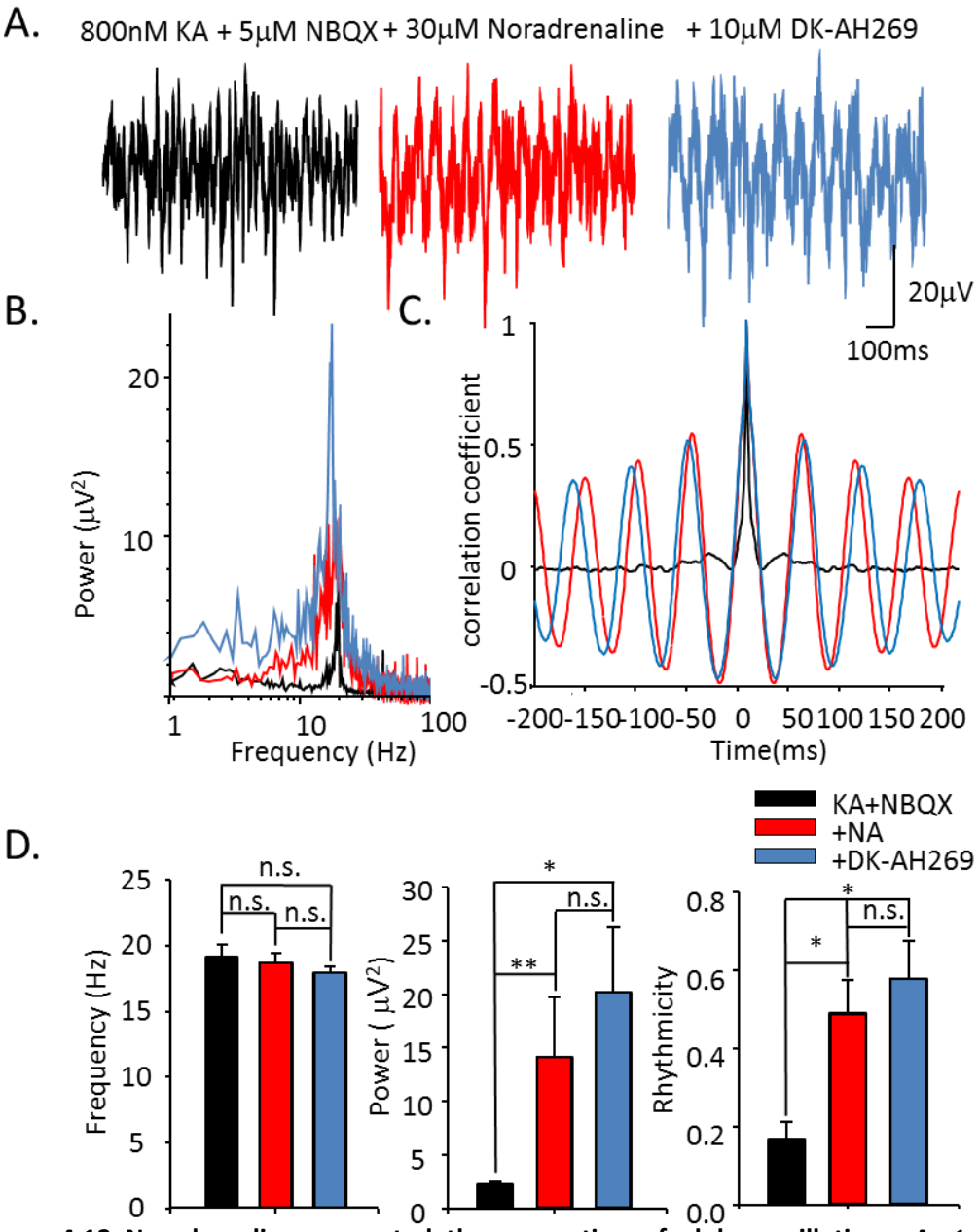

Figure 4.12 Noradrenaline prevented the generation of alpha oscillations. A. 1 second example traces of extracellular activity induced by Kainate [800nM] and NBQX [5µM] (black trace), 30 minutes after addition of Noradrenaline [30µM] (red trace), and 30 minutes after addition of DK-AH [10µM] (blue trace). **B.** power spectra produced from traces in A. **C.** Example auto-correlations produced from 60 second epochs of extracellular data showing rhythmicity before (in black) and after (in red) application of Noradrenaline, and after subsequent addition of DK-AH (in blue). **D.** Graphs showing the change in frequency ($P>0.05$, n=6), amplitude (KA+NBQX-NA $P<0.01$, KA+NBQX-DK-AH $P<0.05$, NA-DK-AH $P>0.05$, n=6) and rhythmicity (KA+NBQX-NA and KA+NBQX-DK-AH $P<0.05$, NA-DK-AH $P>0.05$, n=6, all Two-Tailed T-Test or Mann-Whitney Rank Sum Test) of oscillations after application of KA and NBQX , NA and DK-AH.

suggested that NA prevents the generation of alpha rhythms from a prior beta rhythm in the visual cortex

4.3.7 Increasing dopamine D1 receptor function did not affect the alpha rhythm

To determine the effects of increasing dopamine on alpha oscillations, the dopamine D1 receptor agonist (±)-6-Chloro-2,3,4,5-tetrahydro-1-phenyl-1H-3-benzazepine (SKF81297 [20μM]) was applied to the alpha rhythm. This caused no significant change in the frequency (11.0Hz ± 0.4Hz vs. 9.9Hz ± 0.2Hz, P=0.065, n=6, Mann-Whitney Rank Sum Test, figure 4.13), power (6.7μV^2 ± 2.7μV^2 vs. 11.8μV^2 ± 7.7μV^2, P=0.699, n=6, Mann-Whitney Rank Sum Test), or rhythmicity (0.30 ± 0.05 vs. 0.40 ± 0.09, P=0.589, n=6, Two-Tailed T-Test) of alpha oscillations.

4.3.8 Results from the effects of other pharmacological agents

Table 4.1 shows a list of pharmacological agents applied to the slice in an attempt to generate oscillatory activity in the visual cortex. Oke et al. (2010) showed that gamma rhythms could be induced *in vitro* in the V1 upon application of KA [400nM] and CCH [20μM]. 10μM carbachol (CCH) was applied to slices after 800nM KA. Application of CCH caused no significant change in the frequency of oscillations 29.9Hz ± 1.6Hz vs. 31.5Hz ± 1.1Hz (P=0.172, n=5, Two-Tailed T-Test), or the power 4.7μV^2 ± 1.5μV^2 vs. 9.0μV^2 ± 3.5μV^2 (P=0.253, n=5, Two-Tailed T-Test).

Hughes et al. (2004) showed alpha oscillations could be generated *in vitro* in slices of LGN upon application of the mGLUR1 receptor agonist *trans*-ACPD [100-150μM] (see section 3.1.1). Application of the mGLUR1 agonist DHPG [10μM] to slices containing V1 prior to the addition of any other pharmacological agents, produced no detectable spectral peak. Subsequent application of 800nM KA gave gamma frequency oscillations at 37.9Hz ± 9.0Hz. The power of oscillations in this frequency band after application of DHPG were 0.2μV^2 ± 0.1μV^2, which then increased to 13.3μV^2 ± 17.9μV^2 after application of 800nM KA (n=2). DHPG [5μM] was also added to slices

after excitation with KA [800nM]. There was no change in the frequency 31.3Hz ± 3.4Hz vs. 32.5Hz ± 1.3Hz or power 2.2μV^2 ± 1.3μV^2 vs. 1.5μV^2 ± 1.0μV^2 (n=4) of oscillations after application of DHPG.

Previous pilot studies have shown post-response alpha oscillations can be generated in the V1 after microdrop application of glutamate (1mM, 70nL) in the presence of nicotine [10μM] (see figure 3.1). Nicotine has also been shown to enhance alpha rhythms (see section 4.3.5). Application of nicotine [10μM] to slices containing primary visual cortex gave no detectable spectral peak. Subsequent application of KA [800nM] produced beta frequency oscillations (26.2Hz ± 1.0Hz). The power of oscillations in this frequency band after application of nicotine [10μM] was 0.1μV^2 ± 0.0μV^2, which then increased to 11.0μV^2 ± 8.1μV^2 after application of KA [800nM] (n=2).

CIQ is a potentiator of NMDA receptors containing the NR2C or D subunit which enhances NMDA receptor responses. Cortical alpha rhythms have been shown to depend on the NR2C/D subunit of NMDA receptors (see section 4.3.1.1). The NR2C subunit is found to be highly expressed in layer IV of the neocortex (Binshtok et al., 2006), the cortical lamina where alpha oscillations were found to have the greater power (figure 3.20). CIQ was added before application of any other pharmacological agents to see if potentiation of NR2C/D subunits could give rise to alpha oscillations without the need for other pharmacological agents. Application of CIQ (10μM) to slices containing V1 produced no detectable spectral peak. Subsequent application of KA [800nM] produced oscillations with a frequency of 34.3Hz ± 2.5Hz. The power of oscillations in this frequency after application of CIQ was 0.1μV^2 ± 0.0μV^2, which then increased to 22.6μV^2 ± 19.2μV^2 upon application of KA [800nM]. Further application of NBQX [5μM] and DK-AH [10μM] was required to produce oscillations in the alpha frequency (13.7Hz ± 0.4Hz, 67.9μV^2 ± 37.7μV^2, n=2). CIQ [50μM] was then applied to alpha oscillations, to investigate what effects if any, potentiating the NR2C/D subunit would have on the dynamics of the alpha rhythm. Application of CIQ caused no change in frequency of oscillations (9.9Hz ± 1.9Hz vs. 10.4Hz ± 1.9Hz), however, CIQ did reduce the power of oscillations (15.6μV^2 ± 18.4μV^2 vs. 5.7μV^2 ± 6.5μV^2, n=2).

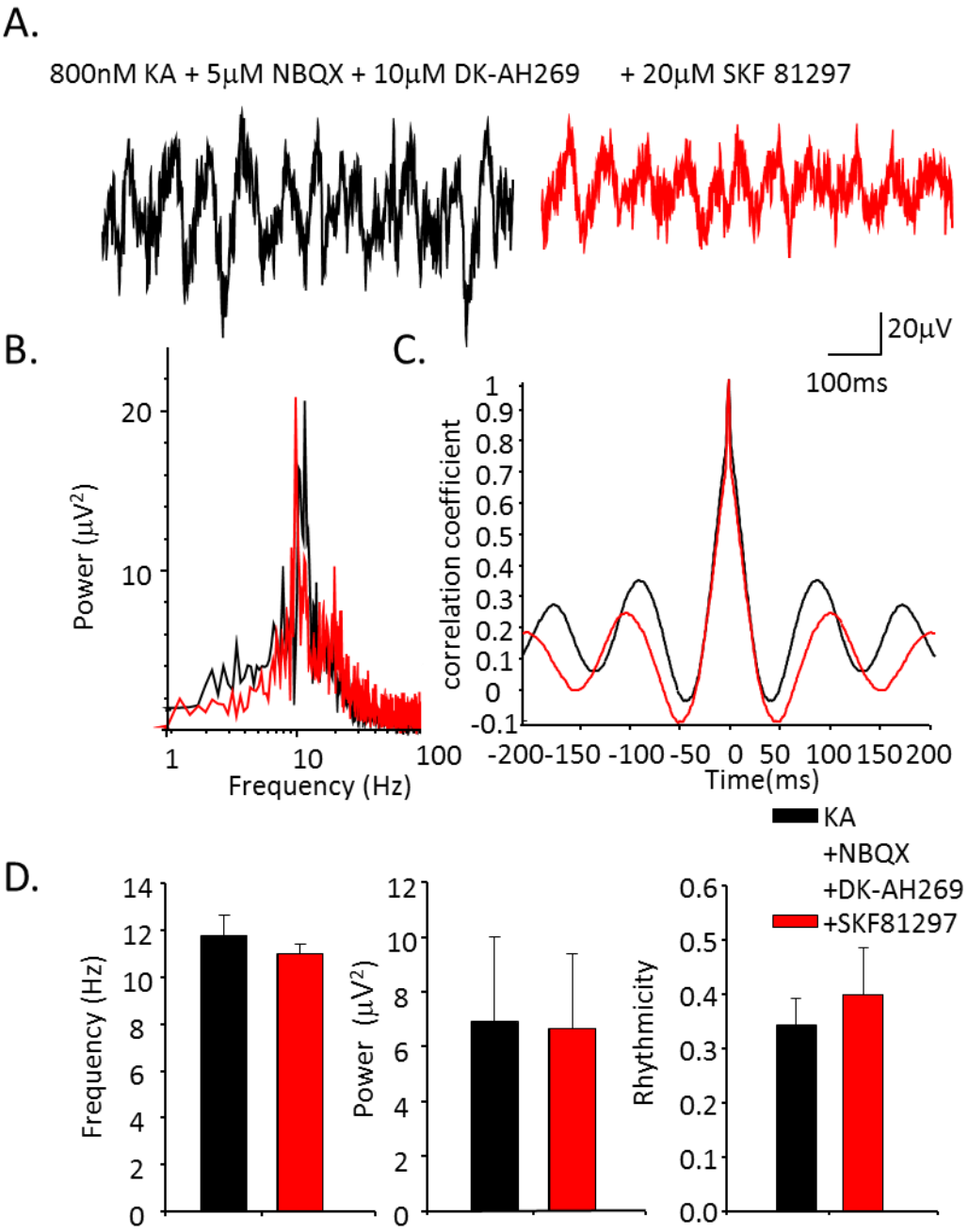

Figure 4.13 Increasing dopamine D1 receptor activity did not affect the alpha rhythm. A. 1 second example traces of extracellular activity recorded from layer IV for the V1 following application of Kainate [800nM], and subsequent application of NBQX [5µM] and DK-AH [10µM] (black trace), and 30 minutes after addition of SKF [20µM] (red trace). **B.** Example power spectra produced from the traces in A showing the effect of SKF on alpha oscillations. **C.** Example auto-correlations produced from 60 second epochs of extracellular data showing rhythmicity before (in black) and after (in red) application of SKF. **D.** Graphs showing the change in frequency ($P>0.05$, n=6, Mann-Whitney Rank Sum Test), amplitude ($P>0.05$, n=6, Mann-Whitney Rank Sum Test) and rhythmicity ($P>0.05$, n=6, Two-Tailed T-Test) of oscillations before and after application of SKF.

Drug	Added before 800nM KA		Added after 800nM KA		Added after 5μM NBQX and 10μM DK-AH	
	Frequency (Hz)	Power (μV)	Frequency (Hz)	Power (μV)	Frequency (Hz)	Power (μV)
10μM CCH	N/A	N/A	29.9 ± 1.6 vs. 31.5 ± 1.1	4.7 ± 1.5 vs. 8.9 ± 3.5	N/A	N/A
10μM DHPG	32.7 ± 6.5 vs. 37.9 ± 8.0	0.2 ± 0.1 vs. 13.3 ± 17.9	N/A	N/A	N/A	N/A
5μM DHPG	N/A	N/A	31.3 ± 3.4 vs. 32.5 ± 1.3	2.2 ± 1.3 vs. 1.5 ± 1.0	N/A	N/A
10μM Nicotine	31.5 ± 1.7 vs. 26.2 ± 1.1	0.1 ± 0.0 vs. 11.0 ± 8.1	N/A	N/A	N/A	N/A
10μM CIQ	31.5 ± 5.2 vs. 34.3 ± 2.5	0.1 ± 0.0 vs. 22.6 ± 19.2	N/A	N/A	11.7 ± 2.1 vs. 9.9 ± 1.9	11.4 ± 8.6 vs. 15.6 ± 18.4
50μM CIQ	N/A	N/A	N/A	N/A	11.7 ± 2.1 vs. 10.4 ± 1.4	11.4 ± 8.6 vs. 5.7 ± 6.5

Table 4.1 Summary of pharmacological agents applied to slices containing V1 in an attempt to generate alpha oscillations. Outline of the effect of specific pharmacological agents to the oscillations in V1. Pharmacological agents were either applied before KA, after KA (i.e. on beta oscillations) or after NBQX and DK-AH application (i.e. on alpha oscillations). Data relating to the pharmacological agents in question are highlighted.

4.4 Discussion

The results from this chapter outline the basic pharmacological properties of the cortical alpha rhythm. The results in chapter 3 indicated that the power of the alpha rhythm was greatest in layer IV of the primary visual cortex suggesting that this is where alpha rhythms are generated. The results in this chapter provide further evidence that the source of alpha rhythms come from this layer and are dependent upon excitatory NMDA receptors and are mediated by gap junctional coupling.

The main findings from these experiments were:

1) The alpha rhythm is dependent upon NMDA receptors, specifically the NR2C/D and NR2B subunits

2) There is a role for GABA and gap junctional coupling similar to other rhythms

3) T-type calcium channels are not involved in the generation of neocortical alpha oscillations

4) There are similarities between the occipital model of the alpha rhythm and the neuromodulator profile of human alpha

Each of these findings suggests clues to the properties of the alpha rhythm and are dealt with in the following sections.

4.4.1 Why are alpha rhythms particularly dependent upon the NR2C/D subunit of NMDA receptors?

The previous chapter described the need for a plastic process occurring during prior beta rhythms for the generation of the alpha rhythm. Pharmacological manipulations of the NMDA receptor complex revealed that alpha oscillations required NMDA receptors but beta rhythms did not. Inhibition of NMDA receptors during beta oscillations caused an increase in the power of beta oscillations, however this increase was non-significant. However, this inhibition prevented the generation of alpha rhythms. As mentioned in 3.4.2, NMDA receptors are involved

in synaptic plasticity (Malenka and Nicoll, 1993; Lynch, 2004) suggesting that the plasticity which occurred in the prior beta rhythm involved NMDA receptors.

Further manipulations into the specific subunits of the NMDA receptor revealed it was the NR2C/D subunit which was mainly involved in the NMDA mediated plasticity. Interestingly, the NR2C subunit is found to be highly expressed in layer IV of the neocortex (Munoz et al., 1999; Binshtok et al., 2006), which is the cortical lamina where alpha oscillations have greatest power, this finding could provide further evidence for layer IV being where alpha is generated.

The alpha rhythm was also shown to be dependent upon the NR2B subunit. This subunit is also involved in synaptic plasticity and there is a switch from NR2B to NR2A subunits during early development (see 4.1.2). Erisir and Harris (2003) showed that in layer IV of ferret visual cortex, NR2B levels remain high throughout the critical period (a period in which neuronal circuits undergo phases of plasticity (Levelt and Hubener, 2012)) and then become reduced towards the end demonstrating a role for NR2B subunits in regulating the ocular dominance plasticity. In adulthood the NR2B subunit is still present, but at a low level. However, it plays a disproportionately powerful role in cognitive function. Increasing NR2B receptor function in adult rats and humans has been shown to have powerful pro-cognitive effect (Wang et al., 2014).

The possible role for I_h in synaptic plasticity has already been discussed (see 3.4.4). I_h is required in the excitatory phase (KA alone) for the subsequent generation of alpha rhythms: If I_h is blocked during this phase, alpha rhythms cannot be generated. It must therefore be considered how I_h plasticity may fit in with the NMDA mediated plasticity. I_h allows the influx of calcium ions upon hyperpolarisation. As described above (see section 4.1.1) in NMDAR specific plasticity, both co-activation of NMDAR and mGLuR1 coupled with an increased calcium release from intracellular stores reliably induces enhanced NMDA currents in central synapses (Rebola et al., 2008; Harnett et al., 2009). This calcium release from intracellular stores could be dependent upon I_h. Interestingly the resultant NMDA currents have increased expression of NR2D subunits (Harney et al., 2008)

which are shown to be responsible for the NMDA mediated plasticity from the results in this chapter. If I_h is blocked during the period of excitation, the NMDA mediated plasticity may be reduced, which could prevent the generation of alpha rhythms upon reduction in synaptic excitation.

There has been limited research conducted into the role of AMPA receptors in alpha oscillations. AMPA receptors have been shown to be involved in alpha/theta frequency oscillations (4-9Hz) in *in vitro* slice preparations of the thalamus (Richardson et al., 2009). Blockade of AMPA receptors resulted in shortened oscillation epochs. Results from the previous chapter have demonstrated the requirement for a reduction in AMPA receptor function in the generation of alpha oscillations, suggesting that AMPA mediated synaptic excitation was not involved in alpha rhythm generation. Excitatory synaptic plasticity via NMDAR can result in an increased number of post-synaptic AMPA receptors. Due to the need for a reduction in synaptic excitation in the generation of the cortical alpha rhythm, an AMPA mediated increase in excitability may not be an important factor in alpha oscillations.

4.4.2 Is there a role for $GABA_A$ mediated inhibition and gap junctional coupling required in alpha oscillations

GABAergic inhibition has been shown to play a crucial role in the generation of many rhythms (see intro section 4.1.2). Results from the experiments in this chapter have demonstrated that reducing $GABA_A$ mediated synaptic inhibition almost completely abolished the alpha rhythm. However, whether GABA is involved in the alpha rhythm is debateable. As described above, increased $GABA_A$ receptor-mediated inhibition using lorazepam has been shown to lead to decreased occipital alpha oscillations (Ahveninen et al., 2007) parametrically with drug dosage (Lozano-Soldevilla et al., 2014). Propofol which increases GABA-mediated inhibition gives rise to frontal alpha oscillations which are spatially distinct from occipital alpha rhythms (Feshchenko et al., 2004; Buhry and Hutt, 2013). Ching et al. (2010) went on to suggest that propofol potentiates $GABA_A$ which enhances the strength of

projections from cortex to thalamus resulting in a thalamocortical alpha rhythm. Potentiation of $GABA_A$ causes a reduction in I_h which abolishes occipital alpha rhythms by silencing HTC cells and gives rise to a new hyperpolarised alpha rhythm in fronothalamic nuclei (Vijayan et al., 2013b; Vijayan et al., 2013a). The effect of GABA on occipital alpha oscillations remains unclear due to variations in results (Nutt et al., 2015). In addition, GABA receptors may in fact be excitatory if present on axons (Traub et al, 2003). If GABA is not contributing to the generation of cortical alpha rhythms, then these rhythms may come from a purely intrinsic neuronal rhythm generator.

Electrical coupling has been found to be critical for fast oscillations throughout the brain (Cunningham et al., 2004; Roopun et al., 2006; Traub et al., 2008). Gap junctions between principal neurons can lead to network oscillations (Traub et al., 2002). The axons of pyramidal cells are connected via gap junctions to form the axonal plexus which can generate network oscillations through population events (Traub et al., 1999a). Gap junctional coupling has also been shown to lead to the generation of alpha rhythms in specific interneuron populations (Gibson et al., 1999; Beierlein et al., 2000).

The results from experiments in this chapter have shown that the generation of the alpha rhythm requires gap junctions; gap junction blockers abolished all rhythmicity of the alpha rhythm. The initial concentration of carbenoxolone used was 100μM, however this concentration may not eliminate all electrical coupling in the brain (Connors, 2012), therefore the concentration was increased to 500μM to ensure all electrical coupling had been blocked. Gap junctions have been shown to be required for both *in vitro* alpha oscillations in the LGN of cats, these oscillations can be sustained solely by gap junctional coupling between TC neurons (Hughes et al., 2004; Lörincz et al., 2008; Lorincz et al., 2009) and *in vivo* EEG and LGN alpha in cats (Hughes et al., 2011). These studies provide evidence of the generation of alpha oscillations via gap junctions. Gap junction blockers such as CBX have a well-documented lack of selectivity at gap junctions (Rouach et al., 2003). CBX has also been shown to be an antagonist of NMDARs which have shown to be crucial in the

generation of alpha rhythms (see chapter 4.3.1) (Chepkova et al., 2008). Other non-specific effects of carbenoxolone, especially at such high concentrations [500μM] include its ability to reduce excitatory synaptic currents through a pre-synaptic effect, its interference of $GABA_A$ receptors therefore reducing inhibitory synaptic currents (Rouach et al., 2003; Tovar et al., 2009), its suppression of action potentials (Rekling et al., 2000) and blockade of calcium channels (Vessey et al., 2004). However, given the fact that gap-junctions have been shown to be critical in alpha oscillations, it is likely that abolition of alpha oscillations in the visual cortical model in the presence of CBX is indeed due to the blockade of gap junctions.

4.4.3 Is there a role for dendritic calcium channel-mediated electrogenesis?

As described in the last chapter, persistent I_h provides a tonic dendritic depolarisation which would antagonise I_T induced bursting; predicting I_T has no involvement in the neocortical model of alpha. Results from this chapter show that blockade of T-type calcium channels has no effect on the alpha rhythm, providing evidence that these calcium channels are not involved in the generation or maintenance of neocortical alpha rhythms. This is in contrast to the computational models of alpha rhythms which suggest that I_h and I_T produce and regulate alpha rhythms (Jones et al., 2000b).

The reduction in I_h is associated with a large increase in power in the neocortical model of alpha rhythms developed in this thesis. In rhythm generation, I_h interacts with depolarisation-activated conductances to boost neuronal resonant properties (Alonso and Llinas, 1989). The large increase in power could be attributed to the effects of I_h on burst generation in neurons. Bursting occurs upon distal dendritic excitation (Larkum et al., 1999). It is clear from the results in this chapter that this bursting is not T-channel mediated. At more depolarised levels, I_h will favour dendritic, sodium channel-mediated bursts. In the globus pallidus (GP) in rats, neuron dendrites express fast, voltage dependent sodium channels (NaF channels) (Hanson et al., 2004). Turner et al. (1994) found that dendritic sodium channels

elicited spikes which were followed by a depolarising afterpotential; this afterpotential could increase in amplitude to spike threshold and generate spike doublets which, upon repetition, gave rise to burst discharges. Bursting cells can serve as pacemakers for network oscillations. Edgerton et al. (2010) went on to show that in a model of GP neurons, high dendritic expression of NaF channels can result in synchronous excitatory events occurring close together on the dendrites. They then described how a high concentration of dendritic NaF channels can reduce the propagation of input oscillations from neurons to their targets, whereas a low concentration can increase phase locking with input oscillations (Edgerton and Jaeger, 2011). This implicates NaF channels in input phase-locking properties of neurons and oscillations. There is little evidence of NaF channels involvement in oscillations. The large increase in power at alpha frequencies could be attributed to burst discharges from neurons driving the rhythm. The ability of NaF channels to generate burst discharges in neurons may implicate an involvement of these channels in the alpha rhythm.

4.4.4 How do neuromodulators affect the alpha rhythm?

The results from this chapter provide evidence of similarities between the occipital alpha rhythm and the neuromodulator profile of human alpha. There is a lack of DA effect described in the human alpha rhythm (see 4.1.4). Antagonism of DA receptors in the brain has been shown to have no effect on the alpha rhythm (Sebban et al., 1999; Chavanon et al., 2007). Results from experiments conducted in this chapter demonstrated that application of the dopamine agonist SKF81297 produced no significant alterations in the occipital alpha rhythm.

Similarly, human alpha rhythms are antagonised by NA. In an *in vivo* study, administration of DSP4 (a drug which destroys noradrenergic endings in the CNS), gave rise to an increase in the amount of mu rhythms (14Hz) (Delagrange et al., 1989). Similarly, in cat visual cortex, blocking NA dramatically increased both alpha and mu rhythms (Rougeul-Buser and Buser, 1997). Kemali et al. (1985) reported increased levels of NA in the CNS antagonised the visual cortical alpha rhythm and gave rise to beta activity in human patients. The results from this chapter provide

evidence of an increased power of beta oscillations and a prevention of the generation of alpha oscillations upon application of NA. This provides further evidence of the neuromodulatory similarities between the neocortical model of alpha and human alpha. There is no proposed mechanism for the effects of NA on alpha oscillations, however, activations of adrenergic receptors has been shown to increase I_h levels (He et al., 2014) which could account for the prevention of alpha rhythms upon reduction in synaptic and intrinsic neuronal excitation.

The results from this chapter show that application of Nicotine to beta oscillations after reduction in synaptic excitation with NBQX can partly generate alpha frequencies in the visual cortex. Acetylcholine (ACh) has been shown to exhibit an inhibitory effect on I_h. *In vitro* studies have reported a reduced I_h current upon administration of nicotine (Chevallier et al., 2006; Dai and Jordan, 2010). Nicotine has been shown to block I_h in interneurons in the same way as ZD7288, by binding to the inner pore of the HCN channels. This resulted in interference with I_h causing a slowing down of the interspike depolarising slope and the firing rate in interneurons, resulting in disruption of oscillatory activity (Griguoli et al., 2010).

Nicotine only reduced the frequency of oscillations to 13.9Hz which is above the 8-12Hz frequency band in which alpha oscillations are typically categorised. Nicotine has however been shown to increase the frequency of alpha oscillations in occipital regions in human EEG studies (Bowers et al., 2015) which could account for the slightly higher peak frequency of alpha oscillations observed upon addition of nicotine as opposed to DK-AH269/ZD7288. It is however proposed that alpha rhythms operate in a wider frequency band than 8-12Hz (Haegens et al., 2014). Alpha and beta rhythms are often categorised together as a single entity and alpha activity has been observed between 6-16Hz (Buffalo et al., 2011; Killian and Buffalo, 2014), therefore, strictly limiting alpha frequencies into an 8-12Hz band may bias results.

The neuromodulatory effects from the data in this chapter show a similarity between the cortical model of the alpha rhythm and the human profile of alpha activity. If this model of alpha is such a close fit to the human profile of alpha, a

question as to the role of the thalamus in alpha is raised. What part is the thalamus playing in occipital alpha rhythms? Studies into the effects of neuromodulators during arousal in the thalamus have shown that ACh and NA depress low frequency responses *in vitro* (Castro-Alamancos and Calcagnotto, 2001), in contrast to the evidence for a role of ACh in alpha rhythm generation. Computational modelling studies have also shown the need for mAChR or mGluR1 in a thalamic model of awake alpha (Vijayan and Kopell, 2012).

4.4.5 Summary

The work carried out in this chapter has outlined the pharmacological properties of the alpha rhythm. The data reported from the previous two chapters suggests that the alpha rhythm is generated by layer IV neurons in the primary visual cortex. The findings from this chapter described the need for NMDA mediated plasticity and gap junctional coupling, along with neuromodulatory effects similar to the human profile of alpha for the generation of *in vitro* cortical alpha rhythms. The results from this chapter and chapter 3 suggest that the alpha rhythm is generated in layer IV of the primary visual cortex. It cannot be determined that layer IV is where alpha rhythms are generated purely from extracellular LFP recordings. Recording from individual neurons during alpha oscillations will give a better insight into which cells are involved and will help determine which layer alpha rhythms are being generated. The following chapter will be based on intracellular recordings from key cell types and will be able to provide a more detailed insight into the network activity underlying the alpha rhythm.

Chapter 5: Results – Intracellular Studies

5.1 Introduction

The results in the previous two chapters have described a model for cortical alpha rhythms and its basic pharmacological properties. The results indicate alpha rhythms can be generated in layer IV of the primary visual cortex. It is very difficult to understand both the mechanisms of a network rhythm and its putative function on the basis of field recordings only. Therefore, this chapter will investigate individual neuronal activity in terms of their inputs and outputs during alpha, beta and gamma oscillations in the primary visual cortex.

5.1.1 Cells in the Visual cortex

The primary visual cortex is a well understood area of the mammalian brain. Its local circuitry, anatomy, responses to thalamic input and downstream projections are well studied. Little known about the functional properties of neurons in the primary visual cortex of the rat (Girman et al., 1999). However, more recent findings indicate that rodent V1 is responsible for higher brain functions such as ocular dominance plasticity (Sawtell et al., 2003) image, motion and orientation discrimination (Petruno et al., 2013), reward-timing prediction and spatiotemporal sequence learning (Gavornik and Bear, 2014), suggesting it is a rich and dynamic cortical area with higher brain functions similar to human V1.

There are 3 main cell types in the primary visual cortex (see section 1.1): excitatory pyramidal and stellate cells and inhibitory interneurons. Layer IV or 'striate cortex' is densely packed with neurons and is the main target of axons from the LGN (Hubel and Weisel, 1972). Stellate cells which have a star shaped cell body are resident cells in the V1. They consist of spiny stellate cells with their cell bodies in layer IV which are the main thalamorecipient neurons for outputs from the LGN. Smooth stellate cells are inhibitory and are local circuit neurons which only contact cells locally within the V1. Pyramidal cells have pyramid shaped cell bodies and spiny, apical dendrites. They project information out of the visual cortex (see figure 5.4 for images of cell types).

Layer IV of the primary visual cortex has an abundance of excitatory, spiny stellate cells. The axons of spiny stellate cells project to all cortical layers but primarily establish synaptic connections with other layer IV spiny stellate cells and layer II/III pyramidal cells (Feldmeyer et al., 1999; Feldmeyer et al., 2002). These cells are thought to constitute the first processing units for the visual cortical response – the 'simple cells' (Hubel and Wiesel, 1962). However, layer IV is far from a 'simple' lamina. In higher, more visual, mammals it can be anatomically and functionally subdivided into at least 3 further layers (4A-C) with even further subdivisions in non-human primate and man (Yabuta and Callaway, 1998). In general the upper subdivision (4A) contains no pyramidal or stellate cells; layer 4B contains a sparse number of pyramidal cells (Meynert cells) with columnar local projections and also projections out to area middle temporal (MT) and superior colliculus (Fries and Distel, 1983). Layer 4C, where present, is the layer densely packed with spiny stellate cells which densely innervate both other layer IV neurons and supragranular layer neurons as well (Gilbert and Wiesel, 1983). While both pyramid and stellate cells are found in most, if not all, mammalian V1 layer IV, the above patterns of sublamination are far less obvious (Rowell et al., 2010).

In layer 4C of the visual cortex, spiny stellate cells receive input from the thalamus. However, thalamic input is not the sole determinant of spiny stellate cell activity in the cortical response. Microcircuitry between stellate cells allows the cortex to modulate its response according to the particular computation being performed (da Costa and Martin, 2011). Interplay between local stellate cell excitation and inhibition, and ascending inputs from LGN are thought to provide the basis for contrast-invariant simple cell behaviour (Lauritzen and Miller, 2003). It has been proposed, through mapping of spiny stellate and pyramidal neurons in rat somatosensory cortex, that spiny stellate cells act predominantly as signal processors in vision whereas pyramidal cells integrate top-down information within a functional column (Schubert et al., 2003). Stellate cells feed forward to pyramidal cells in layer II/III. Pyramidal cells in the visual cortex, located in layers II-VI, send axons out of the cortex. Information processing in the visual cortex is dependent upon its inputs and outputs, diverse classes of cells respond to different

depolarizing currents with action potentials that differ in both firing patterns and frequency (Connors and Gutnick, 1990). Regular spiking cells such as spiny stellate cells found in layer IV of the visual cortex are usually glutamatergic excitatory cells, whereas fast spiking cells are usually GABAergic inhibitory interneurons. Results from the previous chapter outlined the need for excitatory glutamatergic transmission in alpha oscillations. The alpha rhythm was dependent specifically upon NMDA subunits and required NMDA receptor mediated plasticity for its generation.

In rat primary visual cortex, GABAergic interneurons are organised into three different families including those which can be identified by the expression of PV (parvalbumin), SOM (somatostatin) and CB (calbindin) which account for ca. 85% of GABAergic neurons across all cortical layers (Gonchar and Burkhalter, 1997). In mouse neocortex, there have been 3 types of inhibitory interneuron subtypes described which account for almost 100% of neocortical interneurons: parvalbumin expressing (PV), somatostatin-expressing (SOM), and vasointestinal peptide-expressing (VIP) neurons (Rudy et al., 2011). In the supragranular and infragranular layers of mouse visual cortex, PV interneurons strongly inhibit each other but do not inhibit other populations. In contrast, SOM interneurons avoid inhibiting one another but strongly inhibit other subtypes, whereas VIP interneurons preferentially inhibit SOM interneurons (Pfeffer et al., 2013). The role of GABAergic interneurons in cortical circuits is to orchestrate synchronised activity by forming a network of inhibitory connections. This can be achieved by their interaction with excitatory neurons, or by interaction amongst themselves (Staiger et al., 1997; Gibson et al., 1999; Hu et al., 2011). Thalamocortical (TC) inputs can directly activate both excitatory and inhibitory neurons in LIV of the V1. Kloc and Maffei (2014) showed that LGN afferents make monosynaptic connections with both pyramidal cells and fast-spiking interneurons in mouse V1. Different mechanisms of activation of feedforward excitatory and inhibitory neurons in LIV of the V1 provide neurons with different response properties to incoming visual stimuli.

5.1.2 Cells involved with the generation of alpha oscillations

Initial studies indicated that pyramidal cells in layer V of the visual cortex display pacemaker characteristics which control alpha rhythms (Lopes da Silva, 1991). *In vitro* recordings of alpha activity in the neocortex described layer V pyramidal neurons to fire single spikes, or bursts of spikes rhythmically between 5-12Hz which required sodium and calcium-dependent conductances and the 4-10Hz synchronized activity was dependent upon NMDA receptors. Computational modelling studies of TC and reticular (RE) cells demonstrated alpha activity (8-10Hz) was brought about by calcium regulation of I_h channels, this model was also dependent upon GABA mediated inhibition (Destexhe et al., 1993).

More recent studies carried out from *in vitro* recordings from the thalamus described TC neurons which elicited repetitive high threshold bursts (HTBs) with intervals occurring at the alpha frequency, dependent upon gap junctional coupling, which drove the synchronised activity in the LGN slice (Hughes et al., 2011). Alpha activity has been observed in the thalamus in the presence of mGluR1 agonists (Hughes et al., 2004) or mAChR agonists (Lörincz et al., 2008), these agonists are thought to bring about bursting activity in HTB neurons by reducing potassium leak conductances (McCormick and Prince, 1986) and activation of an I_T channel which acts at more depolarised membrane potentials (Hughes et al., 2008). These neurons elicit bursting behaviour; similar to that of the fast rhythmic bursting (FRB) behaviour recorded from layer II/III pyramidal cells in the neocortex (Traub et al., 2003; Cunningham et al., 2004).

Gamma oscillations have been generated in the neocortex by intrinsic neuronal properties (Cunningham et al., 2004). These FRB cells were dependent upon gap junctional coupling. Intrinsic neuronal activity from principal cells in the neocortex has also been shown to generate 10-50Hz oscillations in layer IV of the mammalian cortex.

Other neurons which elicit bursting behaviour are regulated by dendritic voltage-gated ion channels. Action potential bursting was found to be inhibited by calcium

channel blockers in hippocampal CA1 pyramidal neurons (Magee and Carruth, 1999) and in supragranular cortical neurons, high frequency bursting was inhibited by blocking sodium channels (Brumberg et al., 2000). Little is known about the actions of cells in the neocortex during alpha oscillations. The results from studies conducted in thalamic slices implicate bursting cells in the generation of alpha oscillations. These neurons, along with bursting neurons involved in gamma oscillations require gap junctional mediated coupling. The previous chapter described the requirement for gap junctional coupling in the generation of alpha oscillations in this cortical model; therefore it is likely that bursting cells are involved. As described in the previous chapter, the need for a decrease in I_h could be attributed to dendritic sodium channel mediated bursts. NaF channels which give rise to burst discharges could be involved in alpha generation, driving high power alpha rhythms. High expression of NaF channels can result in synchronous excitatory evets (Edgerton et al., 2010). Cell types involved in the generation of alpha oscillations in the visual cortex will be described in section 5.3.

Aims and objectives

The previous two chapters described an *in vitro* model for cortical alpha rhythms, similar to the human profile of alpha, which dominates in layer IV of the V1M and is dependent upon NMDA receptor mediated plasticity and gap junctional coupling. The main aim of this chapter was to identify the key neuronal cell types that are involved in the generation of network activity during alpha oscillations; this was achieved by using intracellular recordings from individual neurons in layer IV of the V1M. To attempt to address this aim the following objectives were set:

1) To determine the firing properties of individual neurons, along with excitatory and inhibitory inputs they receive and their comparison to the local field potential

2) To characterise and investigate the properties of different cells and carry out immunohistochemistry to determine the cell type

Once the cellular nature of the layer IV alpha generator was established we set the further aim of understanding the supposed functional 'inhibitory' nature of visual alpha rhythms (see chapter 1). To address this we set a further objective:

3) To carry out intracellular recordings in different layers of the V1 to investigate the interactions that occur across local networks in layer IV, layer V and layers II/III.

These objectives helped to determine which cells are involved in the generation of the alpha rhythm and in the confirmation of the location of the alpha generator within the cortical column.

5.2 Methods

All experiments described in this chapter were carried out using *in vitro* brain slice preparations (450 μM slice thickness) from adult male Wistar rats (150-200g). Visual cortex containing slices were cut coronally and were prepared and maintained as described in chapter 2.1-2.4. All data obtained from experiments in this chapter was via intracellular and extracellular field recordings outlined in chapter 2.7. Acquisition of intracellular data and subsequent analysis techniques are described in chapter 2.8-2.9. Beta activity was induced by application of KA [800nM] and subsequent alpha activity was induced with co-application of NBQX [5μM] and DK-AH269 [10μM]. The occurrence of alpha oscillations was confirmed prior to intracellular recordings with an extracellular field electrode. This electrode was kept in the slice during intracellular recordings so activity between individual neurons and the LFP could be compared.

5.2.1 Intracellular recordings

Intracellular recordings were obtained using sharp borosilicate glass microelectrodes filled with potassium acetate solution [2M] containing dissolved Biocytin hydrochloride [4-6%] as described in chapter 2.6. The characterisation of individual neurons was achieved using a 0.2nA depolarising step from a hyperpolarised level i.e. -70mV. Depending on the cells response, they were classified into either regular spiking (R.S.) or bursting cells. The EPSPs and IPSPs

received by a cell were exposed by tonically hyperpolarising or depolarising the cell to -70mV or -20mV respectively. Analysis of individual neurons was carried out by measuring the cells resistance, RMP, spike rate, post step AHP, AHP, ADP, width of action potential at half height and rise time, decay time and amplitude of both EPSPs and IPSPs as described in chapter 2.9.2. For analysis of each of these properties of individual neurons, ≥20 measurements of each property were taken from each cell and then averaged to produce an n of 1, where N=number of cells and n=number of measurements taken.

5.2.2 Immunohistochemistry techniques

Once recordings had been taken from cells, Biocytin was injected into cells for over 30 minutes. Fixation and staining of cells was carried out as described in chapter 2.10.

5.3 Results

Intracellular recording revealed four cell types in the primary visual cortex: regular spiking (R.S.) cells, bursting cells, fast adapting (FAD) cells and fast-spiking interneurons. This chapter will focus on the first 2 cell subtypes, regular spiking and bursting cells, found in layer IV, and their contribution to the beta, alpha and gamma rhythms. The electrophysiological identity of cells was confirmed by the injection of square pulses of current (see figure 5.1C and 5.2C). The action potentials that were generated by positive current injection produced regular spikes for the regular spiking cells (figure 5.1C) and an initial burst discharge followed by single spikes (figure 5.2C) for the bursting cells.

5.3.1 Properties of regular spiking cells in the V1

The identity of R.S. cells was characterised by injection of square pulses of current (0.2nA). The action potentials generated by positive current injection produced regular spikes, with the spike train terminated by a small, post step AHP (see figure 5.1Ci for beta, 5.1Cii for alpha and 5.7C for gamma). The mean of this post step AHP produced from 0.2nA of current injection during beta was 1.8mV ± 0.5mV, 0.6mV ±

0.2mV during alpha and 0.7mV ± 0.4mV during gamma oscillations. There was a statistically significant difference in the mean of the post-depolarising current injection AHP amplitude between R.S. cells during beta and alpha ($P<0.05$, N=9, n=60 for alpha, N=5, n=40 for beta, Two-Tailed T-Test) and during beta and gamma ($P<0.05$, N=5, n=40 for beta, N=8, n=31 for gamma, Mann Whitney Rank Sum Test), however no difference in AHP amplitude was seen between alpha and gamma oscillations ($P=0.806$, N=9, n=60 for alpha, N=8, n=31 for gamma, Mann Whitney Rank Sum Test). The input resistance of R.S. cells was found to be 34.8MΩ ± 2.1MΩ during alpha oscillations, 27.7MΩ ± 9.1MΩ during beta oscillations and 40.9MΩ ± 10.8MΩ during gamma oscillations. There were slight but non-significant differences in mean R.S. cell resistances between alpha and beta oscillations ($P=0.905$, N=5, n=100, Mann Whitney Rank Sum Test), alpha and gamma oscillations ($P=0.599$, N=5, n=100, Two-Tailed T-Test) and beta and gamma oscillations ($P=0.599$, N=5, n=100, Two-Tailed T-Test).

The post-spike AHP, ADP (if present) and width at half height of individual action potentials was next calculated (see methods section 2.9.2, see figure 5.3Ai for LIV R.S. cell spike, including AHP and ADP during beta and 5.3Aii during alpha). The mean width at half height was 1.1ms ± 0.2ms during alpha, 1.3ms ± 0.2ms during beta and 1.1ms ± 0.2ms during gamma. There were no statistically significant differences in the width at half height between alpha and beta oscillations ($P=0.650$, N=5, n=100, Two-Tailed T-Test), alpha and gamma oscillations ($P=0.834$, N=5, n=100, Two-Tailed T-Test) or beta and gamma oscillations ($P=0.560$, N=5, n=100, Two-Tailed T-Test). The AHP of R.S. cells was also very similar in all 3 conditions: 2.0mV ± 0.8mV during alpha, 2.0mV ± 0.3mV during beta and 2.3mV ± 0.5mV during gamma oscillations. There were no statistically significant differences in the mean AHP in alpha and beta oscillations ($P=0.642$, N=5, n=100, Two-Tailed T-Test), alpha and gamma ($P=0.767$, N=5, n=100, Two-Tailed T-Test) or beta and gamma ($P=0.291$, N=5, n=100, Two-Tailed T-Test). The mean duration of the ADP of R.S. cells was found to be 3.2ms ± 0.3ms during alpha oscillations, 4.5ms ± 1.7ms during beta oscillations and 6.0ms ± 2.0ms during gamma oscillations. Again there were no statistically significant differences in the mean ADP in alpha and beta

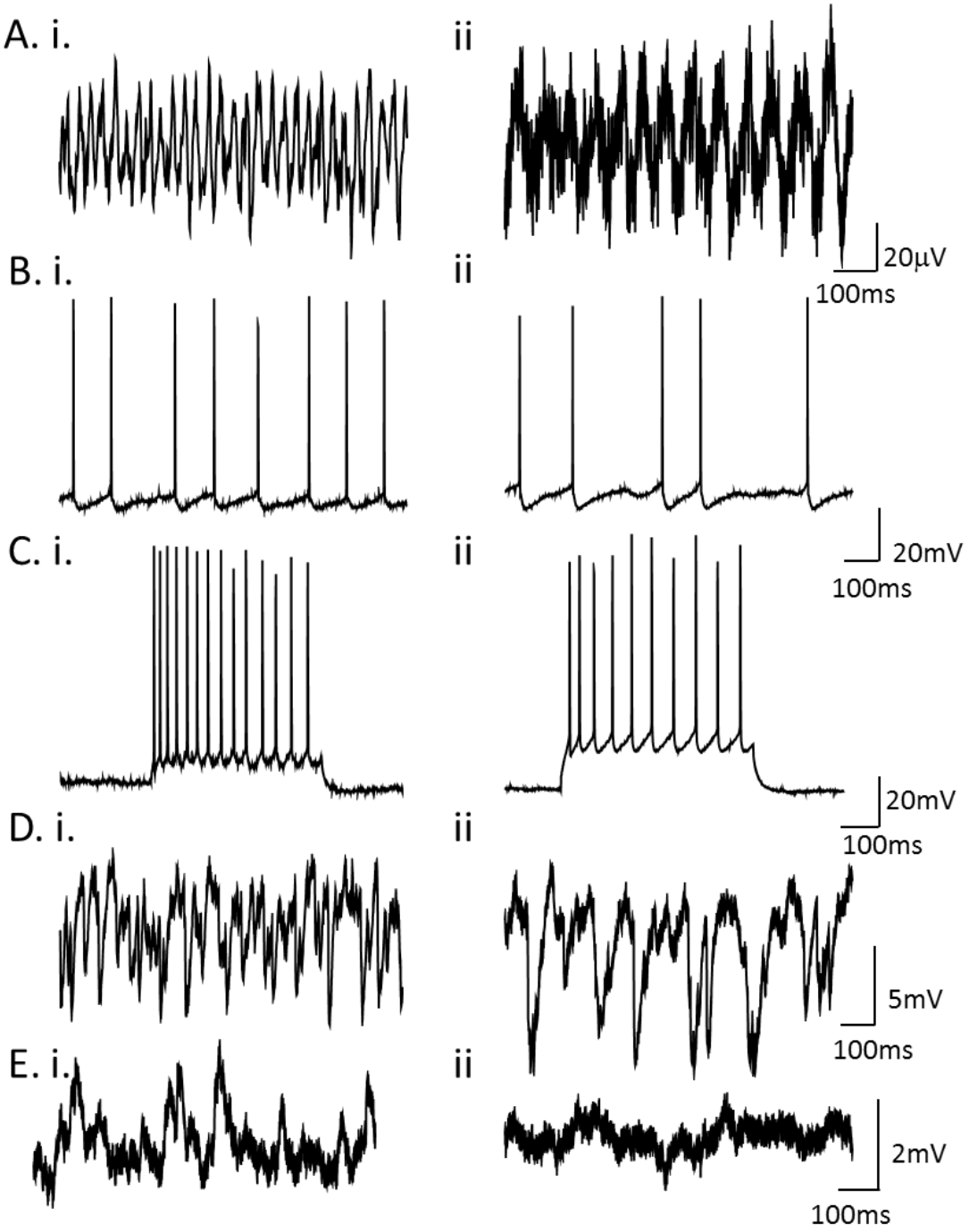

Figure 5.1 Activity of regular spiking cells in Layer IV of the primary visual cortex during beta and alpha activity. A. 1 second example extracellular field recording during **i.** beta oscillations and **ii.** alpha oscillations. **B.** Intracellular recording of stellate cell firing at resting membrane potential taken concurrently with the trace shown in during A **i.** beta oscillations and **ii.** alpha oscillations. **C.** Response to 0.2nA depolarising current steps, tonic hyperpolarising current was injected to stop spontaneous spikes during **i.** beta oscillations and **ii.** alpha oscillations. **D.** Intracellular recording of IPSP's when held at -20mV during **i.** beta oscillations and **ii.** alpha oscillations. **E.** Intracellular recording of EPSPs whilst the cell was held at -80mV during **i.** beta oscillations and **ii.** alpha oscillations.

oscillations (P=0.172, N=5, n=100, Two-Tailed T-Test), alpha and gamma oscillations (P=0.310, N=5, n=100, Mann-Whitney Rank Sum Test), or beta and gamma oscillations (P=0.651, N=5, n=100 Two-Tailed T-Test).

5.3.2 Properties of bursting cells in the V1

Bursting cells were found during both beta and alpha oscillations. The identity of bursting cells were characterised by injection of square pulses of current (0.2nA), as with R.S. cells (above), from a hyperpolarised membrane potential (-70mV). The action potentials generated by positive current injection produced an initial burst followed by regular spikes and was terminated by a very small AHP (see figure 5.2Ci for beta and 5.2Cii for alpha). The mean of this post step AHP produced from 0.2nA of current injection during beta was lower than that during alpha (0.36mV $\pm$ 0.15mV vs. 1.46mV $\pm$ 0.3mV), however statistical tests were carried out between bursting cells during alpha and beta oscillations due to the low sample size (n=2 for beta, n=4 for alpha). The input resistance of bursting cells was found to be higher during beta oscillations than during alpha oscillations (44.6MΩ $\pm$ 18.7MΩ vs. 27.5MΩ $\pm$ 1.4MΩ).

The AHP, ADP and width at half height of individual action potentials from bursting neurons was calculated (see methods section 2.9.2 and figure 5.3 for visual examples and measurements). There was not much difference in the mean width at half height of action potential in bursting cells during alpha (1.20ms $\pm$ 0.03ms) and beta oscillations (1.00ms $\pm$ 0.10ms). The AHP of bursting cells was approximately doubled during alpha oscillations compared to beta oscillations (1.9mV $\pm$ 0.3mV vs. 0.8mV $\pm$ 0.2mV). There was also a 6-fold difference in the mean duration of the ADP during alpha oscillations compared with beta oscillations (18.1ms $\pm$ 3.1ms vs. 3.1ms $\pm$ 0.1ms).

The properties of R.S. cells did not differ much during alpha, beta and gamma rhythms. Table 5.1 gives a summary of cells properties. There were statistically significant differences between the post step AHP of R.S. cells during alpha and gamma oscillations and alpha and beta oscillations. The resistance, resting

membrane potential, width of action potential, spike rate, AHP and ADP values did not have a significant difference between the 3 conditions. The properties of bursting cells differed during beta or alpha oscillations. Table 5.1 shows there were differences particularly in the post step AHP, AHP, ADP of individual bursting cells. There were also differences in the resistance, resting membrane potential and spike rate of the bursting cells during the 2 conditions, however, it cannot be determined if these differences are significant.

Figure 5.3 shows the characteristics of action potentials from R.S. and bursting cells. The width at half height of action potentials is similar in both R.S. and bursting cells in both conditions. R.S. cells have a larger AHP than the bursting cells; however the bursting cells have a much larger ADP during alpha oscillations than during beta oscillations, the ADP is also much larger than the small ADP observed in R.S. cells. Figure 5.4 shows an example of a regular spiking and bursting cell biocytin fill used to aid in characterisation. The regular spiking layer IV cells had cell shapes that resembled stellate cells. The cell body was star shaped as opposed to the characteristic triangular shape of pyramidal cells (see figure 5.4A) and there was no dominant apical dendrite. The GAD67 staining showed this cell to be likely excitatory as there was no GAD present in the cell body, there was however GAD around the cell body indicating that the cell may have received strong perisomatic inhibitory inputs (figure 5.4A). Using biocytin fill and reconstruction the bursting cell subtype was identified as a pyramidal cell; this was due to its triangular cell body. It also had a prominent apical dendrite which projected up to layer 1 (not shown) and distal dendritic arbours, typical of pyramidal cells (see figure 5.4C). The GAD67 staining also showed there to be no GAD in the cell body, but again there was GAD perisomatically indicating that this cell was excitatory but may have received inhibitory inputs (figure 5.4D). Now the properties of the cell types in the V1 had been characterised, we needed to investigate the actions of the cells during alpha, beta and gamma rhythms including their inputs in order to determine which cells may have been responsible for the generation of alpha rhythms.

	Beta bursting cell	Alpha bursting cell	Beta R.S. cell	Alpha R.S. cell	Gamma R.S. cell
RMP (mV)	-66.5 ± 33.2	-58.3 ± 5.3	-63.9 ± 1.9	-62.3 ± 3.5	-60.5 ± 4.0
Post step AHP (mV)	1.5 ± 0.4	0.4 ± 0.3	1.8 ± 0.5 *	0.57 ± 0.2 * *	0.7 ± 0.4 *
Width AP (ms)	1.0 ± 0.1	1.2 ± 0.1	1.3 ± 0.2	1.1 ± 0.2	1.1 ± 0.2
AHP (mV)	0.8 ± 0.3	1.9 ± 0.5	2.0 ± 0.3	2.0 ± 0.8	2.3 ± 0.5
ADP (ms)	3.1 ± 0.2	18.8 ± 6.2	4.5 ± 1.0	3.2 ± 0.3	6.0 ± 2.0
Spike rate	15.9 ± 11.2	9.6 ± 5.1	5.9 ± 1.2	6.0 ± 1.6	3.4 ± 1.2
Resistance (Ω)	27.5 ± 1.9	44.6 ± 37.4	27.7 ± 9.1	34.8 ± 2.1	40.9 ± 10.8

Table 5.1 Summary of properties of cells in the V1. Outline of the properties of both regular spiking and bursting cells during alpha beta and gamma rhythms in layer IV of the V1 for the experiments detailed in chapter 5.3. * indicates a significant difference of $P<0.05$, properties that are statistically significant are shown in red.

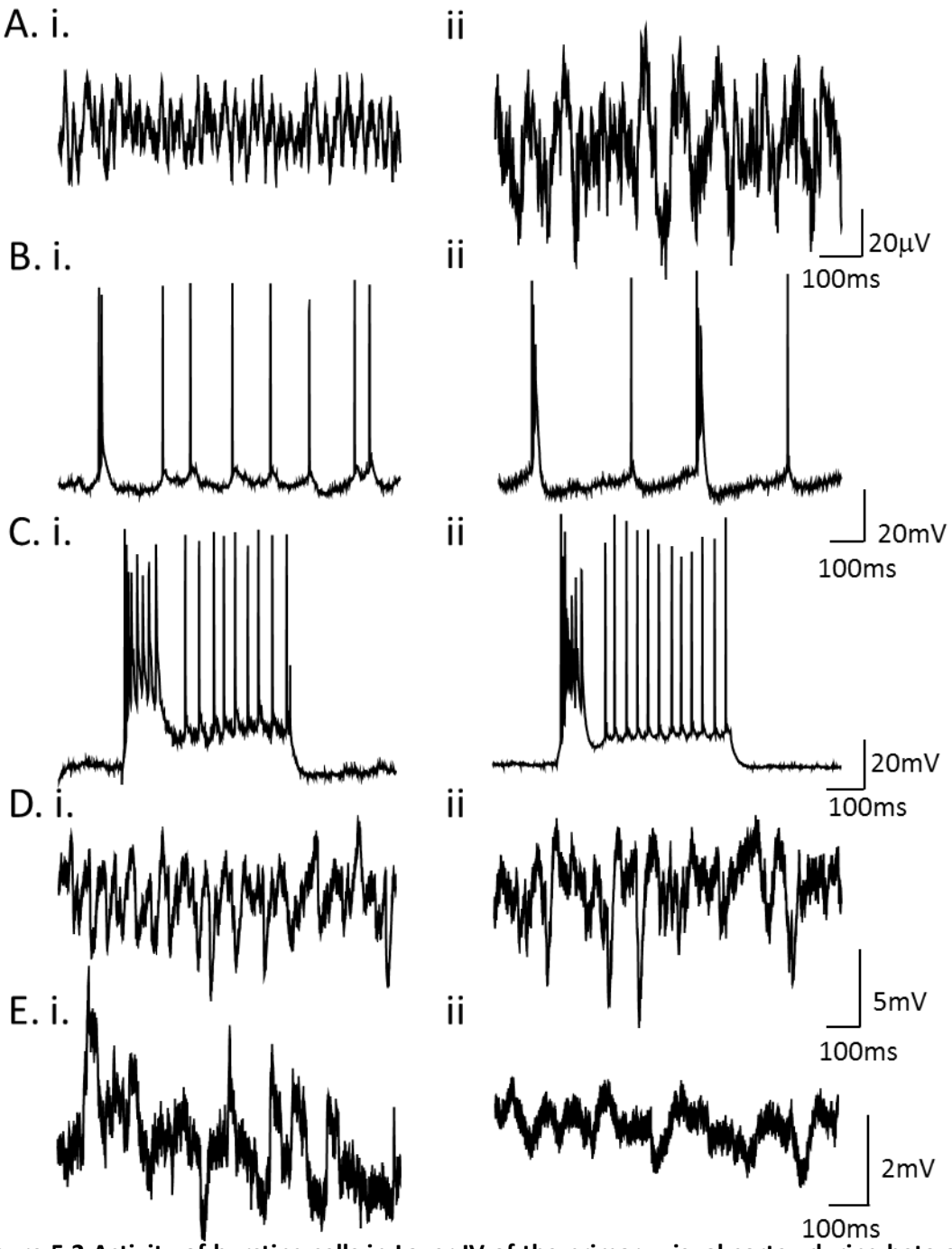

Figure 5.2 Activity of bursting cells in Layer IV of the primary visual cortex during beta and alpha activity. A. 1 second example extracellular field recording during **i.** beta oscillations and **ii.** alpha oscillations. **B.** Intracellular recording of stellate cell firing at resting membrane potential taken concurrently with the trace shown in A during **i.** beta oscillations and **ii.** alpha oscillations. **C.** Response to 0.2nA depolarising current steps from hyperpolarised membrane potential (-70mV) during **i.** beta oscillations and **ii.** alpha oscillations. **D.** Intracellular recording of IPSP's when held at -20mV during **i.** beta oscillations and **ii.** alpha oscillations. **E.** Intracellular recording of EPSPs whilst the cell was held at -80mV during **i.** beta oscillations and **ii.** alpha oscillations.

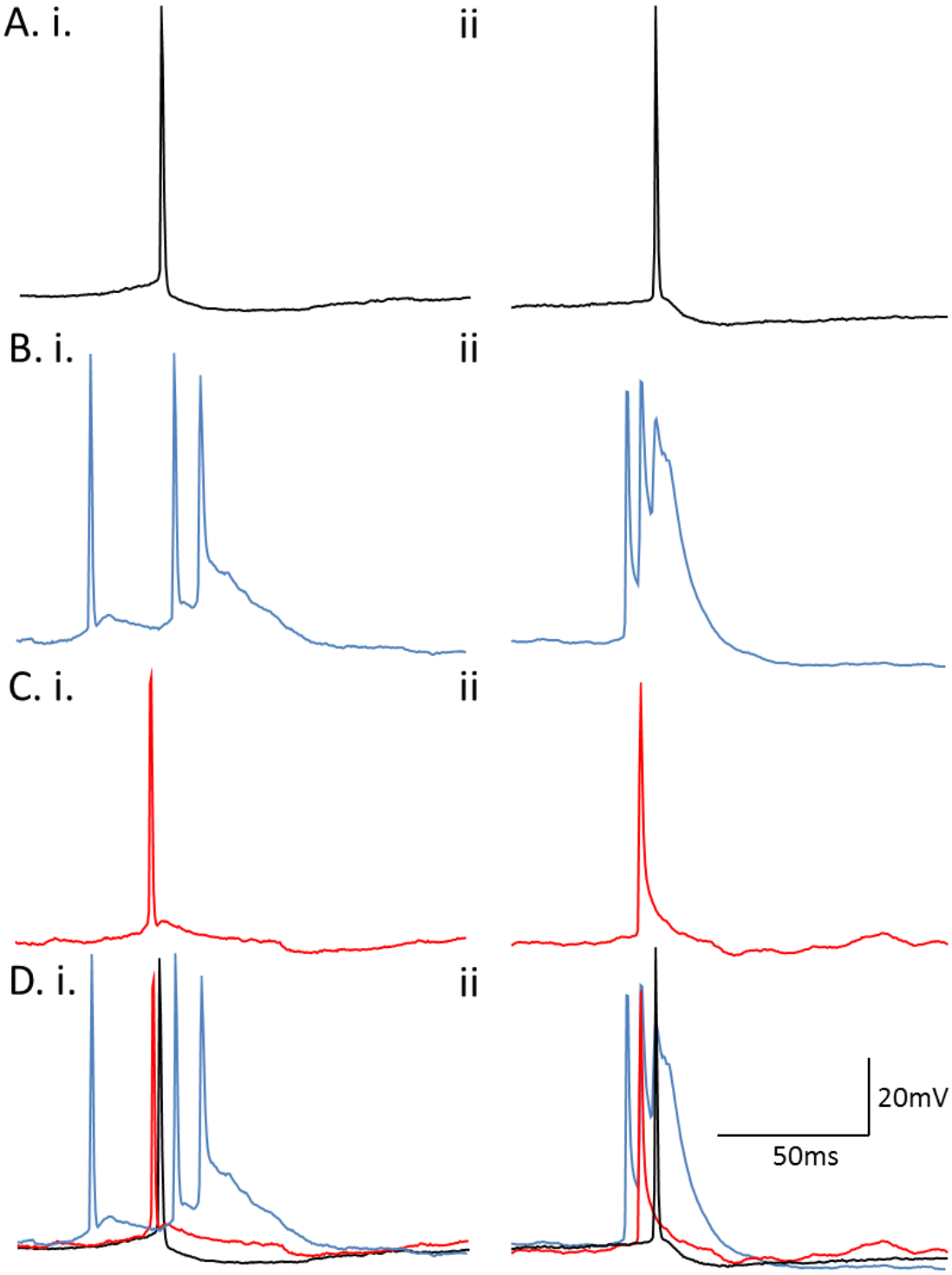

Figure 5.3 Characteristics of action potentials from R.S. and bursting cells in Layer IV of the primary visual cortex during beta and alpha oscillations. A. Example spike taken from LIV R.S. cell during **i.** beta oscillations **ii.** alpha oscillations. **B.** Example burst from LIV bursting cell during **i.** beta oscillations **ii.** alpha oscillations. **C.** Example single spike taken from LIV bursting cells during **i.** beta oscillations **ii.** alpha oscillations. **D.** Spikes from A (in black), B (in blue) and C (in red) superimposed to show differences in spikes, AHPs and ADPs during **i.** beta oscillations **ii.** alpha oscillations.

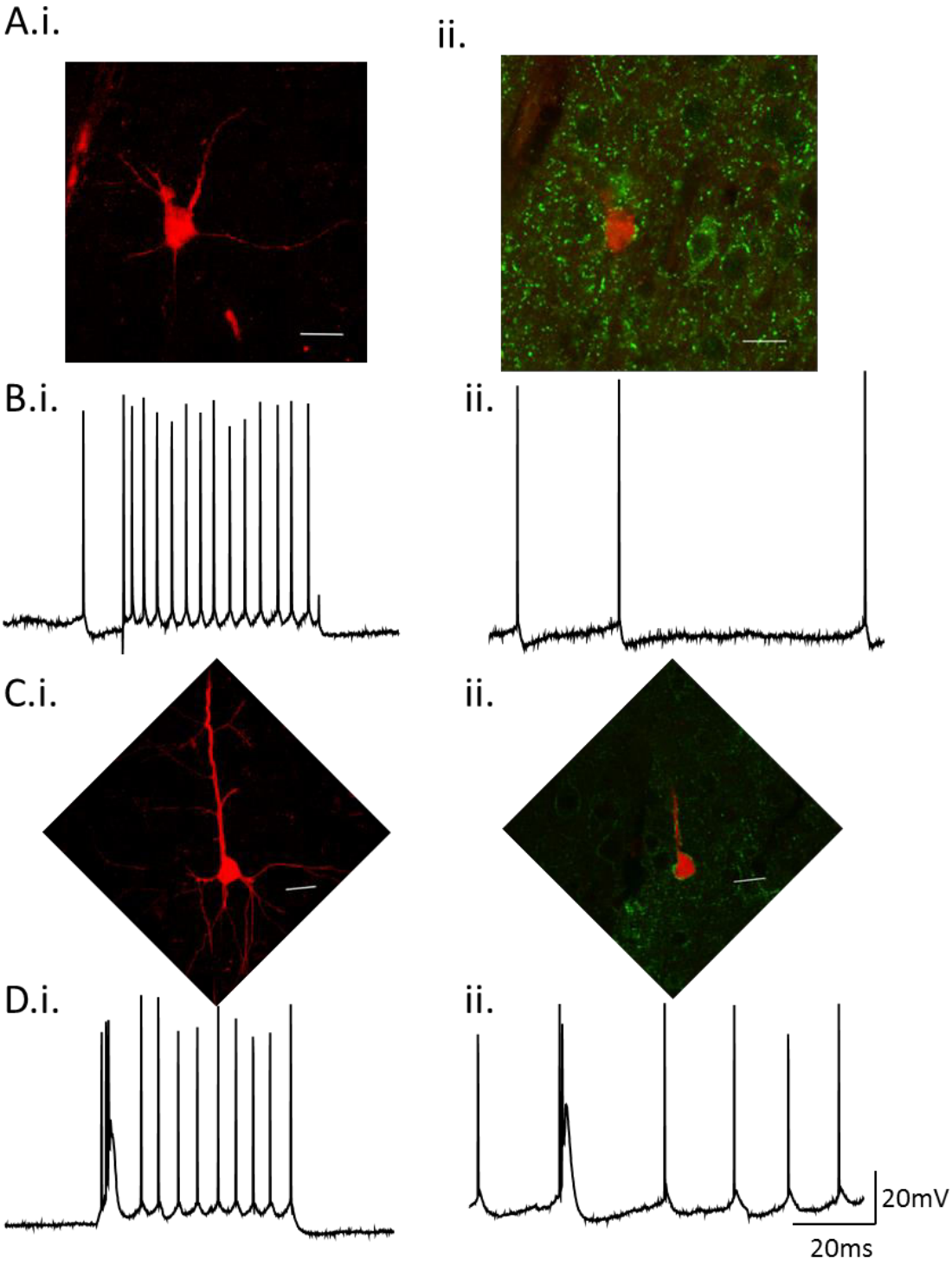

Figure 5.4 Cell types in layer IV the V1. A.i. Picture of Biocytin filled stellate cell. **ii.** GAD67 staining of stellate cell shown in i (magnification x63, scale bar 20μm). **B.** Action of stellate cell **i.** in response to 0.2nA depolarising step **ii.** at resting membrane potential during alpha oscillations. **C.i.** Picture of Biocytin filled bursting cell **ii.**.GAD67 staining of bursting cell shown in i (magnifiction x20, scale bar 20μm) **D.** Action of bursting cell **i.** in response to 0.2nA depolarising step **ii.** at resting membrane potential during alpha oscillations.

5.3.3 Contribution of layer IV R.S. cells to the alpha and other rhythms

The resting membrane potential of R.S cells (presumed stellate cells) during beta oscillations was -63.9mV ± 1.9mV, -62.3mV ± 3.5mV during alpha oscillations and -60.5mV ± 4.0mV during gamma oscillations. There were no statistically significant differences in the RMP between alpha and beta oscillations (P=0.185, n=15, n=18, Mann Whitney Rank Sum Test), alpha and gamma oscillations (P=0.567, n=15, n=11, Mann Whitney Rank Sum Test) or beta and gamma oscillations (P=0.125, n=18, n=11, Mann Whitney Rank Sum Test).

Intracellular recordings obtained from R.S. cells in layer IV revealed that the mean firing rate of these cells was at a lower frequency than that of the field. Analysis of the firing patterns of R.S. cells revealed that they fired at an average of 5.9Hz ± 1.2Hz during beta oscillations (see figure 5.1Bi for example), 6.0Hz ± 1.6Hz during alpha oscillations (see figure 5.1Bii for example) and 3.4Hz ± 1.2Hz during gamma oscillations (see 5.7B for example). There was no statistically significant differences in the firing rate between alpha and beta oscillations (P=1.000, n=15, n=19, Mann Whitney Rank Sum Test), alpha and gamma oscillations (P=0.458, n=15, n=11, Mann Whitney Rank Sum Test) or beta and gamma oscillations (P=0.324, n=19, n=11, Mann Whitney Rank Sum Test). Further analysis into the spike-field coherences revealed that R.S. cells were at least partially phase locked to the field beta rhythm (figure 5.5E and F) and gamma field (figure 5.7H and I) but there was almost no phase locking between the spiking pattern of R.S. cells and the alpha field (figure 5.6E and F).

It was clear that there was a relationship between the firing of action potentials by R.S. cells and the local field potential during beta and gamma rhythms; however there was no clear relationship between R.S. cell outputs and alpha rhythms thus far. The next step was to investigate the inputs received by these cells in the 3 conditions to determine any further relationships between these cells and the local field potential.

5.3.3.1 Synaptic inputs received by layer IV R.S. cells

The EPSPs received by R.S. cells can be visualised in figure 5.1Ei and 5.5C during beta oscillations, figure 5.1Eii and 5.6C during alpha oscillations and 5.7E for gamma oscillations. The mean peak amplitude of EPSPs during alpha oscillations was calculated to be 2.1mV $\pm$ 0.4mV, 2.1mV $\pm$ 0.1mV during beta oscillations and 2.3mV $\pm$ 0.3mV during gamma oscillations. There were no statistically significant differences between the mean of the peak amplitude of EPSPs during alpha or beta oscillations (P=0.890, N=5, n=100, Two-Tailed T-Test), alpha or gamma oscillations (P=0.763, N=5, n=100, Two-Tailed T-Test) or beta and gamma oscillations (P=0.621, N=5, n=100, Two-Tailed T-Test).

The rise time was calculated as the time it took for the EPSP to reach its peak amplitude and the decay time was calculated from the time it took for the EPSP to decay to 63.2% of its peak amplitude. The rise time for R.S. cell EPSPs during alpha oscillations was calculated to be 56.1ms $\pm$ 7.7ms, 33.2ms $\pm$ 6.9ms during beta oscillations and 25.4ms $\pm$ 5.7ms during gamma oscillations. There were no statistically significant differences in the rise time of EPSPs during alpha and beta oscillations (P=0.075, N=5, n=100, Two-Tailed T-Test) or during beta and gamma oscillations (P=0.488, N=5, n=100, Two-Tailed T-Test). There was however a significant difference in EPSP rise time between alpha and gamma oscillations (P<0.05, N=5, n=100, Two-Tailed T-Test). Similarly there were no statistically significant differences between the decay times of EPSPs during alpha and beta oscillations 80.0ms $\pm$ 10.7ms vs. 48.5ms $\pm$ 8.0ms (P=0.077, N=5, n=100, Two-Tailed T-Test) or beta and gamma oscillations 48.5ms $\pm$ 8.0ms vs. 31.8ms $\pm$ 8.7ms (P=0.486, N=5, n=100, Two-Tailed T-Test). There was again, a statistically significant difference between the decay time of EPSPs during alpha and gamma oscillations 80.0ms $\pm$ 10.7ms vs. 31.8ms $\pm$ 8.7ms (P<0.05, N=5, n=100, Two-Tailed T-Test). The excitatory inputs that were received by layer IV R.S. cells during beta rhythms were phase locked to the oscillation (figure 5.5D) as they were during alpha (figure 5.6D) and gamma oscillations (5.7G) (note blue line represents the mean and the red and pink lines the SEM for all remaining figures).

The IPSPs received by R.S. cells can be visualised in figure 5.1Di and 5.5A during beta oscillations, figure 5.1Dii and 5.6A during alpha oscillations and 5.7D for gamma oscillations. The mean peak amplitude of R.S. cell IPSPs during alpha oscillations was calculated to be 8.8mV $\pm$ 0.6mV, 4.1mV $\pm$ 0.4mV during beta oscillations and 5.2mV $\pm$ 0.8mV during gamma oscillations. There were statistically significant differences in the mean of the peak amplitude of IPSPs during alpha and beta oscillations ($P<0.01$, N=5, n=100, Two-Tailed T-Test) and alpha and gamma oscillations ($P<0.05$, N=5, n=100, Two-Tailed T-Test), however no significant differences in IPSP peak amplitude was observed between beta and gamma oscillations ($P=0.492$, N=5, n=100, Two-Tailed T-Test).

The IPSP rise time was calculated as the time it took for the IPSP to reach its peak amplitude and the decay time was calculated from the time it took for the IPSP to decay to 63.2% of its peak amplitude. The rise time for R.S. cell IPSPs during alpha oscillations was calculated to be 16.1ms $\pm$ 2.1ms. This was approximately 3-fold longer than the values recorded during beta and gamma rhythms: 4.6ms $\pm$ 0.3ms during beta oscillations and 5.0ms $\pm$ 0.5ms during gamma oscillations. Again there were significant differences in the rise time of IPSPs during alpha and beta oscillations ($P<0.05$, N=5, n=100, Two-Tailed T-Test), and alpha and gamma oscillations ($P<0.05$, N=5, n=100, Two-Tailed T-Test), however, no significant differences between the IPSPs rise time during beta and gamma oscillations ($P=0.719$, N=5, n=100, Two-Tailed T-Test). Similarly there were statistically significant differences in the decay time of IPSPs during alpha and beta oscillations ($P<0.05$, n=5, Two-Tailed T-Test), and alpha and gamma oscillations ($P<0.05$, N=5, n=100, Two-Tailed T-Test). Again, no significant differences were observed between the decay time of IPSPs during beta or gamma oscillations ($P=1.000$, N=5, n=100, Mann Whitney Rank Sum Test). The inhibitory inputs that were received by layer IV R.S. cells during beta rhythms were phase locked to the oscillation (figure 5.5B) as they were during alpha (figure 5.6B) and there was strong phase locking between IPSPs during gamma oscillations and the local field potential (5.7F). The differences in excitatory inputs between R.S. cells during the 3 conditions were minimal. Table 5.2 gives a summary of the synaptic properties of the cells. All EPSPs were phase

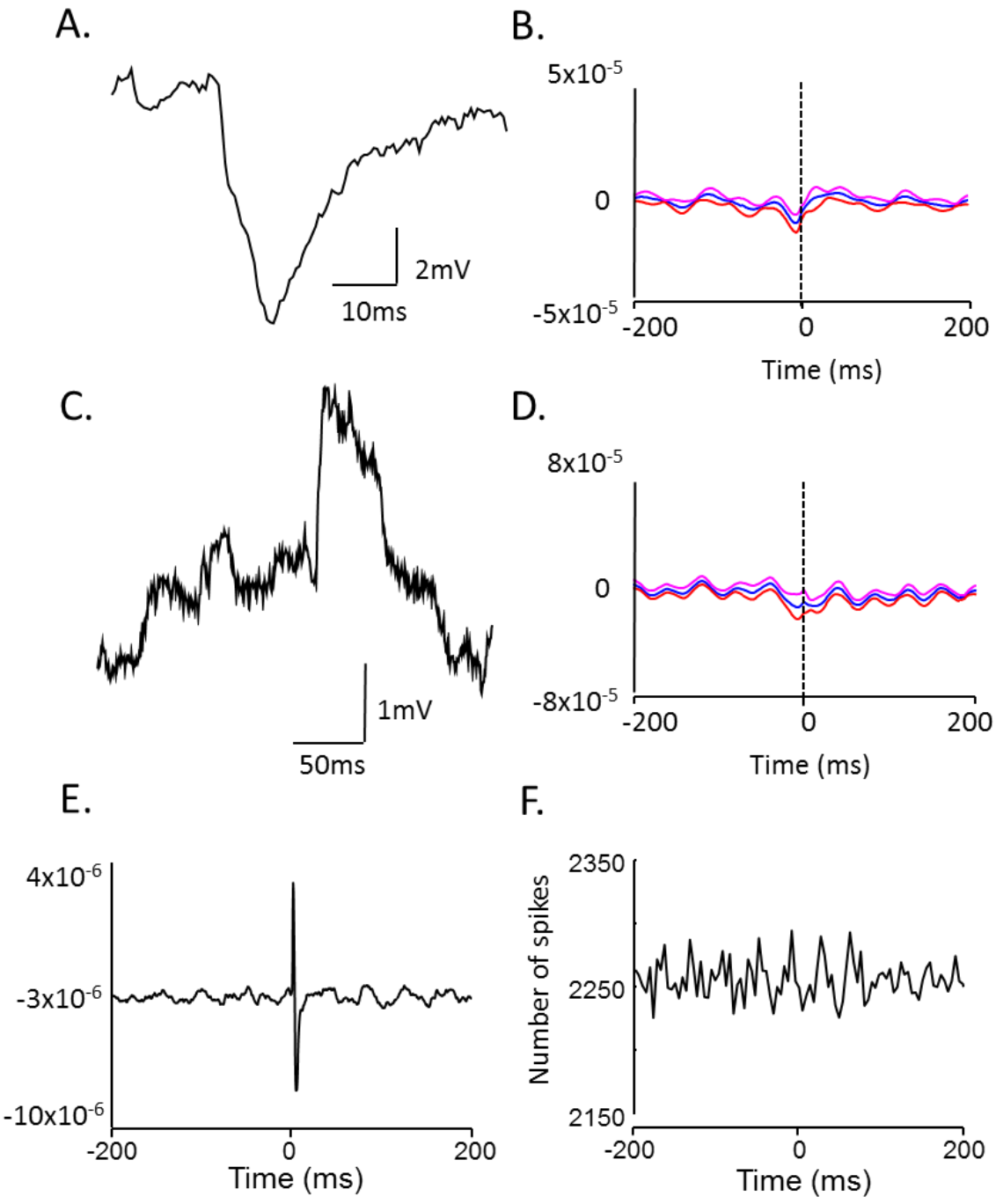

Figure 5.5 Activity of R.S. cells in Layer IV of the primary visual cortex during beta oscillations. A. Example IPSP from LIV R.S. cell taken during beta oscillations. **B.** Mean cross-covariance showing the phase relationship between the beta field and IPSPs (n=17, the mean is represented by the blue line and SEM by the red and pink lines). **C.** Example EPSP from LIV R.S. cell taken during beta oscillations. **D.** Mean cross-covariance showing the phase relationship between the beta field and EPSPs (n=16). **E.** Mean spike triggered average of the field and **F.** Mean field triggered average of the spikes (n=7) showing the relationship between cell firing and the beta field.

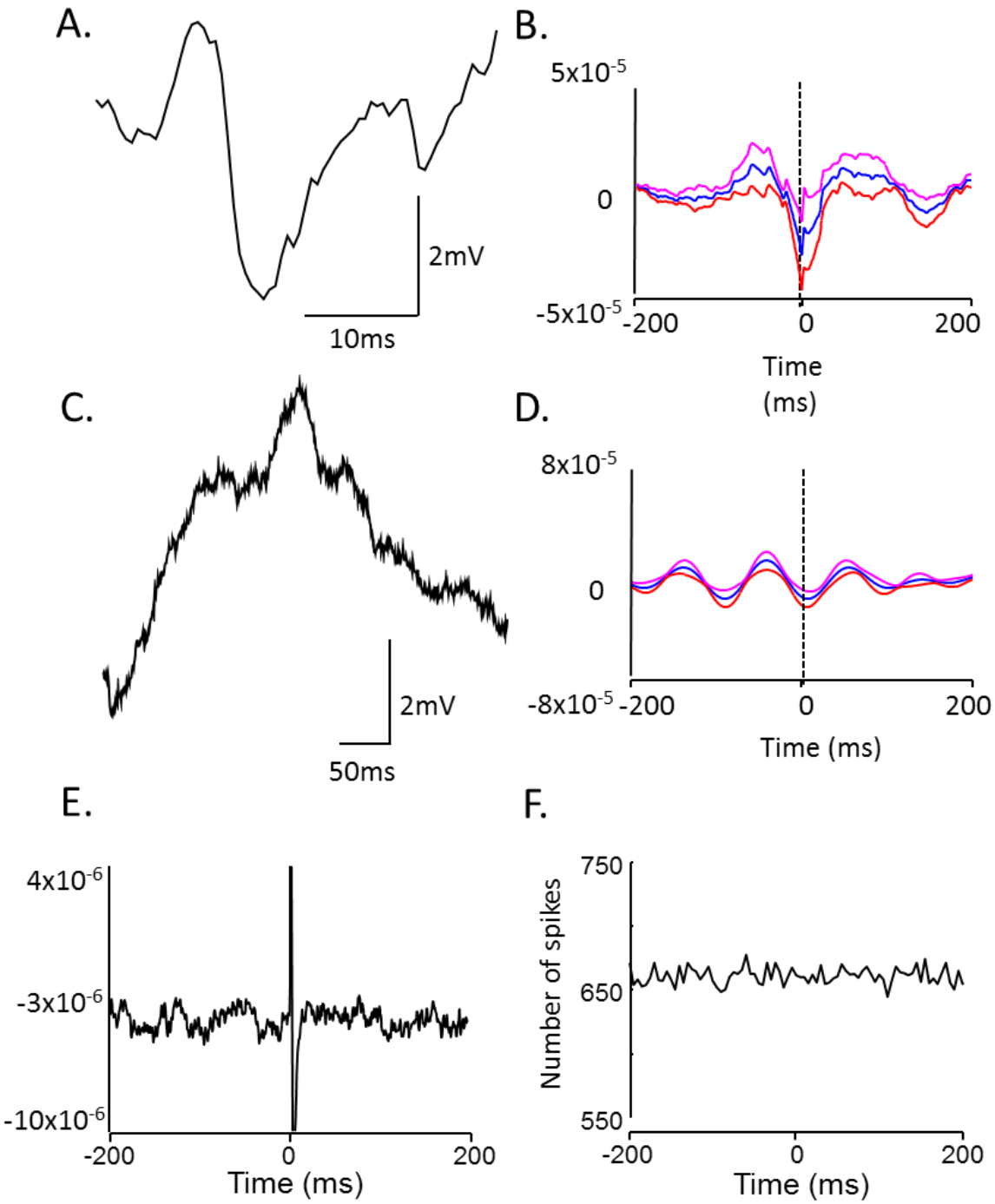

Figure 5.6 Activity of R.S. cells in Layer IV of the primary visual cortex during alpha oscillations. A. Example IPSP from LIV R.S. cell taken during alpha oscillations. **B.** Mean cross-covariance showing the phase relationship between the alpha field and IPSPs (n=13). **C.** Example EPSP from LIV R.S. cell taken during alpha oscillations. **D.** Mean cross-covariance showing the phase relationship between the beta field and EPSPs (n=15). **E.** Mean spike triggered average of the field and **F.** Mean field triggered average of the spikes (n=7) showing the relationship between cell firing and the alpha field.

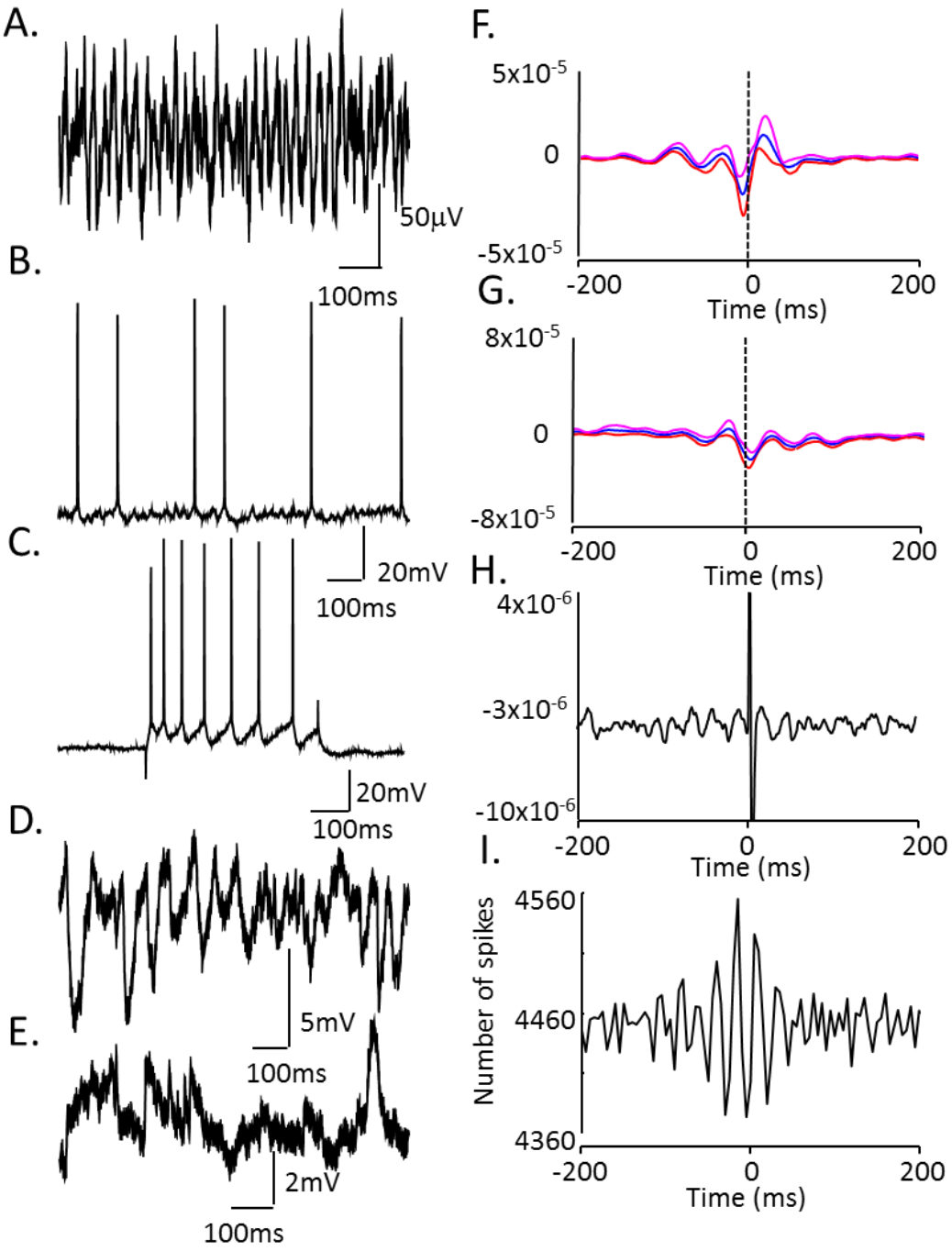

Figure 5.7 Activity of R.S. cells in Layer IV of the primary visual cortex during gamma oscillations. A. 1 second example extracellular field recording taken during gamma oscillations. **B.** Intracellular recording of R.S. cell firing at resting membrane potential taken concurrently with the trace shown in A. **C.** Response to 0.2nA depolarising current steps. **D.** Intracellular recording of IPSP's when held at -20mV. **E.** Intracellular recording of EPSPs whilst the cell was held at -80mV. **F** and **G.** Mean cross-covariance and showing the phase relationship between the gamma field and IPSPs (n=11) and EPSPs (n=10) respectively. **H.** Mean spike triggered average of the field and **I.** Mean field triggered average of the spikes (n=7) showing the relationship between cell firing and the gamma field.

locked to the beta, gamma and alpha field and there were no significant differences between the amplitude of EPSPs between the 3 oscillations. There were statistically significant differences in the rise and decay times of EPSPs during alpha and gamma oscillations with EPSPs during alpha taking over twice the time to reach peak amplitude and decay. All IPSPs were also phase locked to the beta, alpha and very strongly to the gamma field. There were differences in the amplitude, rise time and decay time of IPSPs between alpha and beta rhythms and alpha and gamma rhythms.

We have now looked at the properties of individual R.S. cells during alpha, beta and gamma oscillations in layer IV of the primary visual cortex. These regular spiking cells did not seem to contribute to the generation of alpha oscillations as there was no phase locking between the cell firing and local field potential. This suggests that there must be other cells playing a role in the generation of alpha oscillations. In the next section, the actions of the second cell type found in layer IV of the V1 - bursting cells is detailed.

5.3.4 Contribution of layer IV bursting cells to the alpha and other rhythms

The resting membrane potential of bursting cells during beta oscillations was -67.4mV ± 23.5mV and -58.3mV ± 2.7mV during alpha oscillations. These differences were not significant (P=1.000, n=2, n=4, Two-Tailed T-Test).

Intracellular recordings obtained from bursting cells in layer IV revealed that the firing of these cells occurred at a frequency similar to that of the field. Analysis of the firing patterns of bursting cells revealed that they fired at an average of 15.8Hz ± 8.0Hz during beta oscillations (see figure 5.2Bi for example), and 9.6Hz ± 2.5Hz during alpha oscillations (see figure 5.2Bii for example). However, there was no statistically significant difference in the firing rate (P=0.369, n=2, n=4, Two-Tailed T-Test) between the two rhythms. Further analysis into the spike-field coherences

revealed that bursting cells were strongly phase locked to the alpha (figure 5.9E and F) but only weakly correlated with the beta field (figure 5.8E and F).

It was clear that there was a relationship between the firing of bursting cells and the local field potential during alpha rhythms. This indicated a possible involvement of the bursting cells in the generation of the alpha rhythm. The next step was to investigate the inputs received by these cells during beta and alpha oscillations to determine any further relationships between these cells and the local field potential.

5.3.4.1 Synaptic inputs received by layer IV bursting cells

The EPSPs received by bursting cells can be visualised in figure 5.2Ei and 5.8C during beta oscillations and figure 5.2Eii and 5.9C during alpha oscillations. The mean peak amplitude of EPSPs was calculated to be 1.5mV ± 0.1mV during alpha oscillations vs. 4.0mV ± 0.2mV during beta oscillations. The peak amplitude of EPSPs of bursting cells during alpha was significantly smaller than that during beta ($P<0.01$, N=3, n=60 for alpha, N=2, n=40 for beta, Two-Tailed T-Test). The mean rise time for bursting cell EPSPs during alpha oscillations was smaller than that during beta (57.8ms ± 7.8ms vs. 64.3ms ± 10.9ms) however this difference was not significant ($P=0.689$, N=3, n=60 for alpha, N=2, n=40 for beta, Two-Tailed T-Test). Similarly there were no statistically significant differences between the decay times of EPSPs during alpha and beta oscillations 83.8ms ± 7ms vs. 93.8ms ± 13.2ms ($P=0.622$, N=3, n=60 for alpha, N=2, n=40 for beta, Two-Tailed T-Test). The excitatory inputs that were received by layer IV bursting cells during alpha rhythms were phase locked to the oscillation (figure 5.9D) but not during beta (figure 5.8D).

The IPSPs received by bursting cells can be visualised in figure 5.2Di and 5.8A during beta oscillations and figure 5.2Dii and 5.9A during alpha oscillations. The mean peak amplitude of bursting cell IPSPs during alpha oscillations was calculated to be 7mV ± 0.3mV and 8.5mV ± 3.5mV during beta oscillations, this was not statistically different ($P=1.000$, N=4, n=60 for alpha, N=2, n=40 for beta, Mann Whitney Rank Sum Test). There were no significant differences in the rise time 16.1ms ± 2.1ms vs. 7.3ms ± 0.4ms ($P=0.133$, N=4, n=60 for alpha, N=2, n=40 for beta, Mann Whitney Rank Sum Test) or decay time 31.2ms ± 4.8ms vs. 16ms ± 2.1ms ($P=0.758$, N=4,

n=60 for alpha, N=2, n=40 for beta, Two-Tailed T-Test) for bursting cell IPSPs during alpha and beta oscillations. The inhibitory inputs that were received by these cells during the alpha rhythm were phase locked to the oscillation during both beta (figure 5.8B) and alpha (figure 5.9B).

The differences in excitatory inputs between bursting cells during the alpha and beta oscillations were minimal. Table 5.2 gives a summary of the synaptic properties of the cells. EPSPs were phase locked to the alpha field but not the beta and there was a statistically significant difference in the amplitude of EPSPs between alpha and beta oscillations with beta EPSPs being over twice the amplitude of alpha EPSPs. There were no statistically significant differences in the rise and decay times of EPSPs. All IPSPs were phase locked to the beta and alpha rhythms. But there were no significant differences in the amplitude, rise time and decay time of IPSPs between alpha and beta rhythms.

We have now looked at the properties of both LIV R.S. cells and bursting cells during alpha, beta and gamma oscillations in the primary visual cortex. The regular spiking cells did not seem to contribute to the generation of alpha oscillations as there was no phase locking between the cell firing and local field potential. The bursting cells had a high degree of phase locking between the cell firing and the local field potential suggesting that these cells may drive the alpha rhythm. The next section looks into other cortical layers to investigate the actions of cells in regards to the layer IV rhythms.

5.3.5 Contribution of layer II/III regular spiking cells to the alpha and beta rhythms

Regular spiking cells were also found in layers II/III of the V1 during alpha beta and gamma oscillations. The resting membrane potential of R.S. cells during alpha oscillations was -73.8mV $\pm$ 6.2mV, -70.4mV $\pm$ 3.0mV during beta oscillations and -78.0mV $\pm$ 3.3mV during gamma oscillations. There were no statistically significant differences in the RMP between alpha and beta oscillations (P=0.603, n=7, n=5,

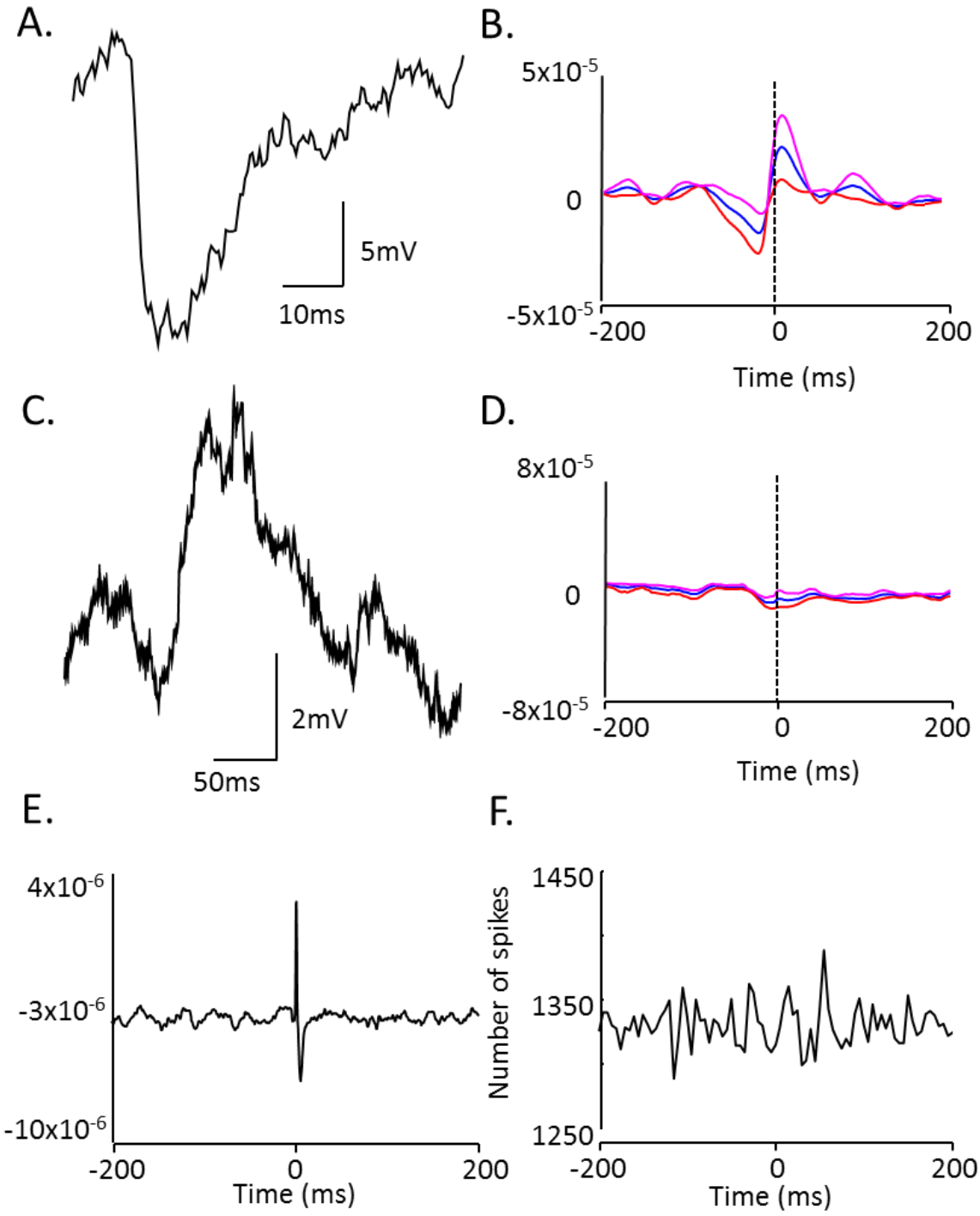

Figure 5.8 Activity of bursting cells in Layer IV of the primary visual cortex during beta oscillations. A. Example IPSP from LIV bursting cell taken during beta oscillations. **B.** Mean cross-covariance showing the phase relationship between the beta field and IPSPs (n=2). **C.** Example EPSP from LIV bursting cell taken during beta oscillations. **D.** Mean cross-covariance showing the phase relationship between the beta field and EPSPs (n=3). **E.** Mean spike triggered average of the field and **F.** Mean field triggered average of the spikes (n=4) showing the relationship between cell firing and the beta field.

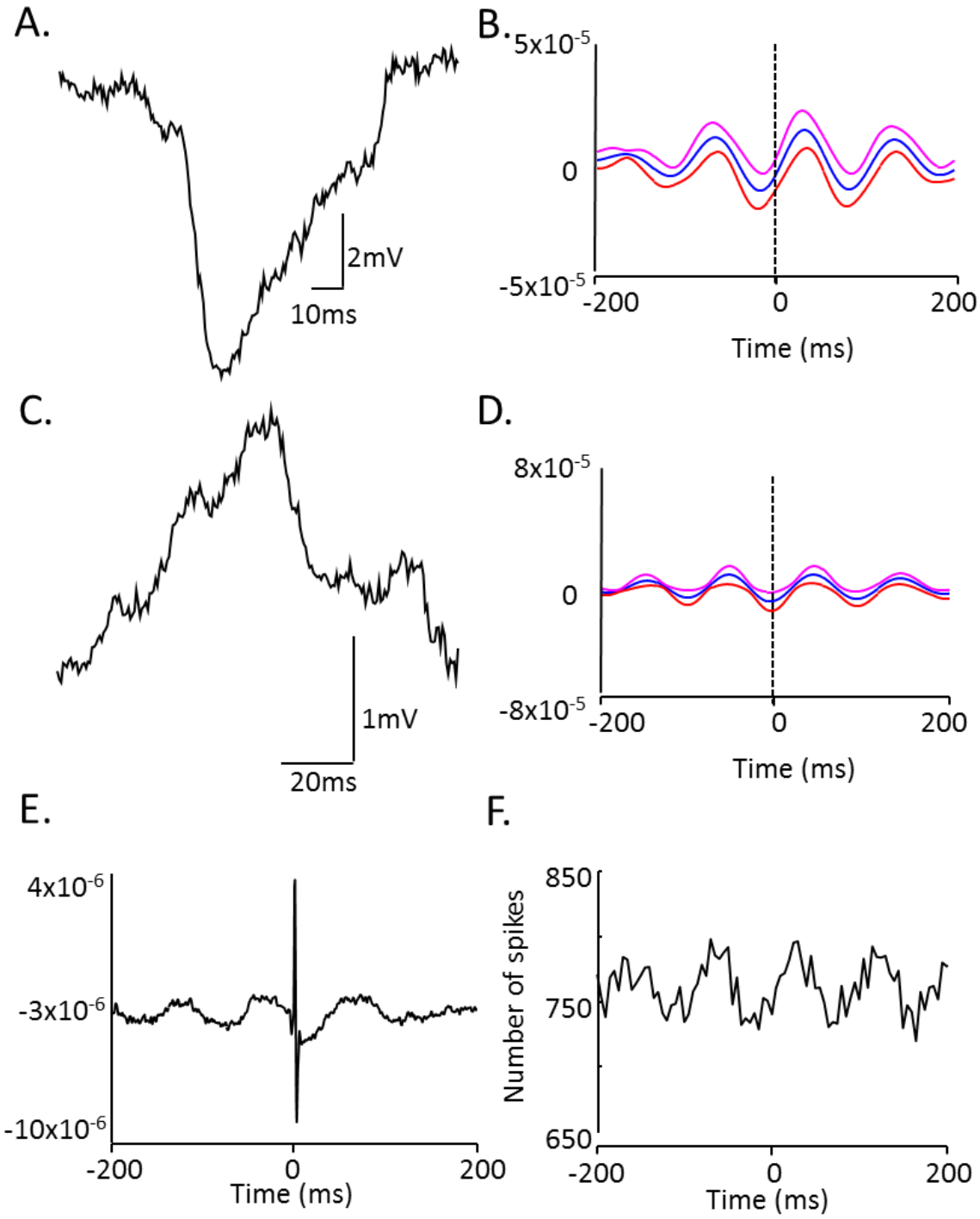

Figure 5.9 Activity of bursting cells in Layer IV of the primary visual cortex during alpha oscillations. A. Example IPSP from LIV bursting cell taken during alpha oscillations. **B.** Mean cross-covariance showing the phase relationship between the alpha field and IPSPs (n=8). **C.** Example EPSP from LIV bursting cell taken during alpha oscillations. **D.** Mean cross-covariance showing the phase relationship between the alpha field and EPSPs (n=7). **E.** Mean spike triggered average of the field and **F.** Mean field triggered average of the spikes (n=3) showing the relationship between cell firing and the alpha field.

	Beta bursting cell	Alpha bursting cell	Beta R.S. cell	Alpha R.S. cell	Gamma R.S. cell
IPSP amplitude (mV)	8.5 ± 4.9	7.0 ± 0.7	4.1 ± 0.4 **	8.8 ± 0.6	5.2 ± 0.8 *
IPSP decay (τ) (ms)	16 ± 2.1	31.2 ± 9.5	9.4 ± 0.7 *	17.8 ± 2.4	9.5 ± 0.5 *
IPSP rise time (ms)	7.3 ± 0.5	16.1 ± 4.1	4.6 ± 0.3 *	8.6 ± 1.3	5 ± 0.5 *
EPSP amplitude (mV)	4.0 ± 0.2	1.5 ± 0.1	2.1 ± 0.1	2.1 ± 0.4	2.3 ± 0.3
EPSP decay (τ) (ms)	93.8 ± 18.7	83.8 ± 12.1	48.5 ± 8	80 ± 10.7	31.8 ± 8.7 *
EPSP rise time (ms)	64.3 ± 15.5	57.8 ± 13.4	33.2 ± 6.9	56.1 ± 7. 7	25.4 ± 5.7 *

Table 5.2 Summary of synaptic properties of cells in the V1. Outline of the synaptic properties of both R.S. and bursting cells during alpha beta and gamma rhythms in layer IV of the V1 for the experiments detailed in chapter 5.3. * indicates a significant difference of P<0.05, ** indicates a significant difference of P<0.01. No statistical tests carried out between bursting cell properties during beta and alpha oscillations as low sample size (n=2 beta, n=4 alpha).

Two-Tailed T-Test), alpha and gamma oscillations (P=0.144, n=7, n=4, Two-Tailed T-Test) or beta and gamma oscillations (P=0.599, n=5, n=4, Two-Tailed T-Test). The firing rate of these cells occurred less frequently than that of R.S. cells (presumed stellates) located in layer IV. During gamma oscillations these cells did not fire at all (n=4), during beta they fired at a rate of 2.4Hz $\pm$ 1.5Hz (n=7) and during alpha at a rate of 2.7Hz $\pm$ 1.6Hz (n=5). There was no statistically significant differences in the firing rate between alpha and beta oscillations (P=1.000, n=7, n=5, Mann Whitney Rank Sum Test), alpha and gamma oscillations (P=0.527, n=7, n=4, Mann Whitney Rank Sum Test) or beta and gamma oscillations (P=0.413, n=5, n=4, Mann Whitney Rank Sum Test). Further analysis into the spike-field coherences revealed that layer II/III R.S. cell firing was phase locked to the beta (figure 5.10E and F), there was also a degree of phase locking to the alpha field (figure 5.11E and F).

The EPSPs received by R.S. cells can be visualised in figure 5.10C during beta oscillations, figure 5.11C during alpha oscillations and 5.12C for gamma oscillations. The excitatory inputs that were received by layer II/III R.S. cells during beta and gamma rhythms were loosely phase locked to the oscillation (figure 5.10D and 5.12D) during alpha oscillations there was a higher degree of phase locking of EPSPs to the field (5.11D).

The IPSPs received by R.S. cells can be visualised in figure 5.10A during beta oscillations, figure 5.11A during alpha oscillations and 5.12A for gamma oscillations. The inhibitory inputs that were received by layer II/III cells during beta rhythms were loosely phase locked to the oscillation (figure 5.10B) as they were during alpha (figure 5.11B) and there was strong phase locking between IPSPs during gamma oscillations and the local field potential (5.12B).

We have now looked into LII/III R.S. cell involvement during alpha, beta and gamma oscillations in layer IV of the primary visual cortex. These regular spiking cells may contribute to the beta rhythm however, there is not much phase locking observed between the alpha field and cell spiking. In the next section, the actions of layer V R.S. cells are detailed.

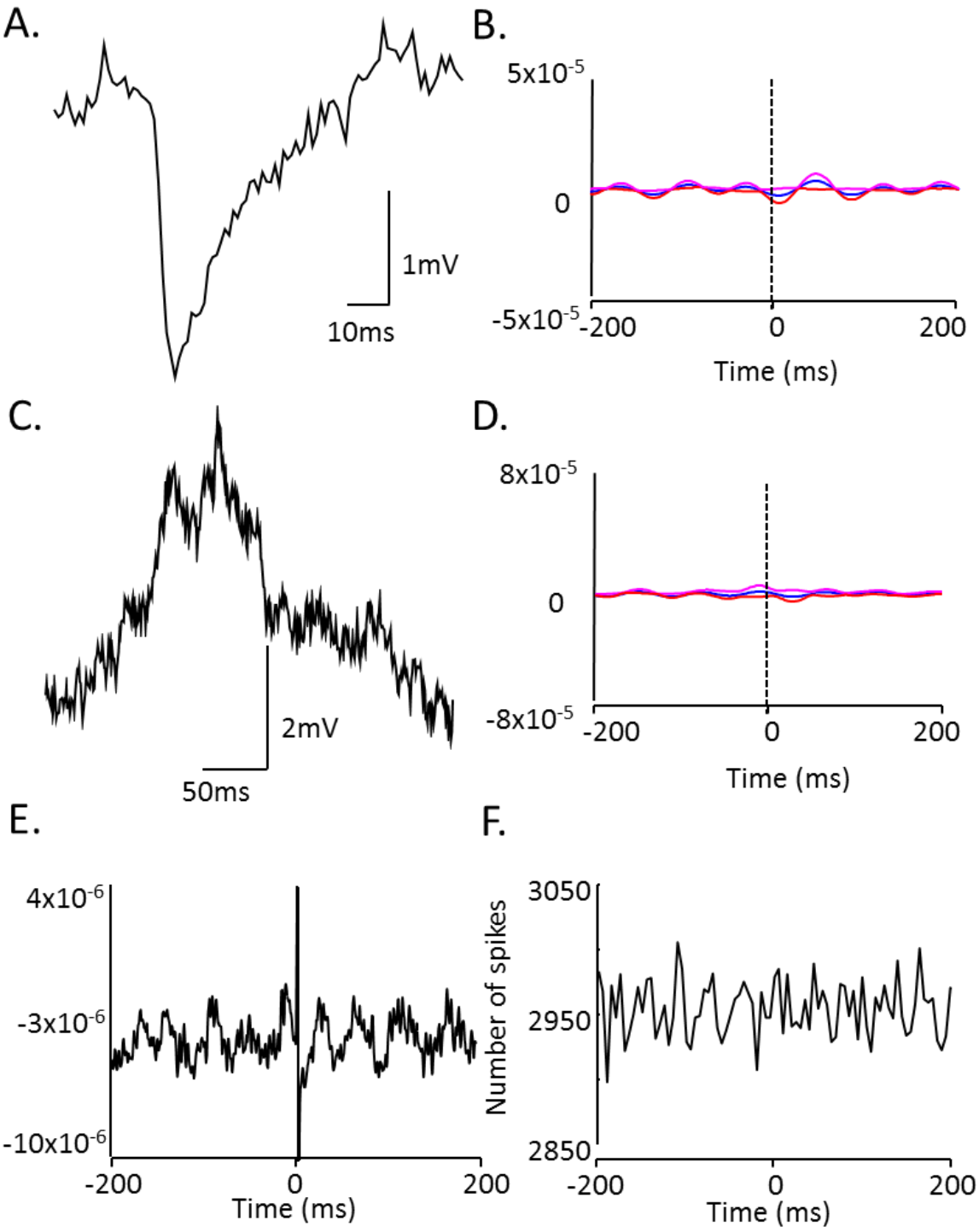

Figure 5.10 Activity of regular spiking cells in Layer II/III of the primary visual cortex during beta oscillations. A. Example IPSP from LII/III regular spiking cell taken during beta oscillations. **B.** Mean cross-covariance showing the phase relationship between the beta field and IPSPs (n=5). **C.** Example EPSP from LIV bursting cell taken during beta oscillations. **D.** Mean cross-covariance showing the phase relationship between the beta field and EPSPs (n=7). **E.** Mean spike triggered average of the field and **F.** Mean field triggered average of the spikes (n=2) showing the relationship between cell firing and the beta field.

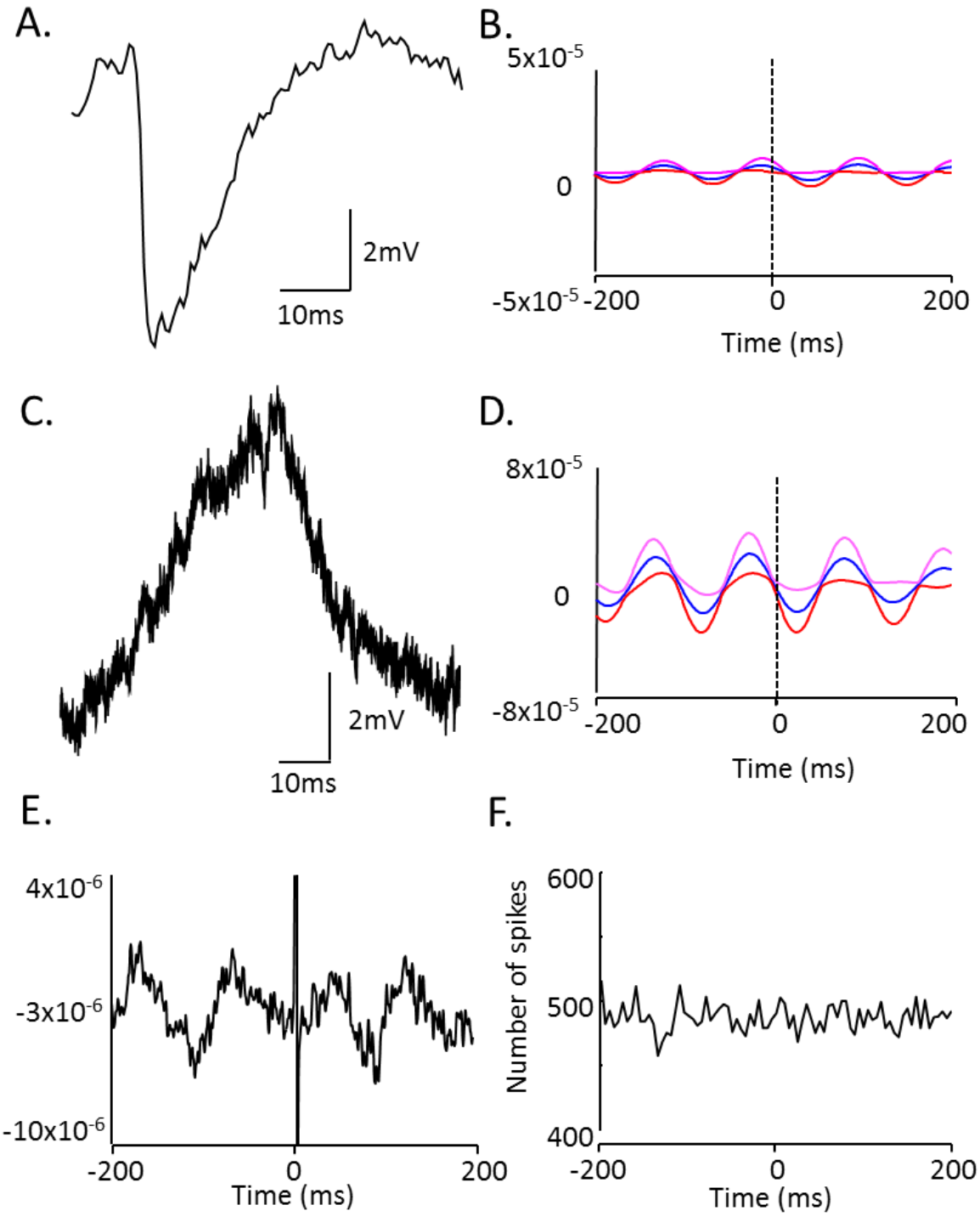

Figure 5.11 Activity of regular spiking cells in Layer II/III of the primary visual cortex during alpha oscillations. A. Example IPSP from LII/III regular spiking cell taken during alpha oscillations. **B.** Mean cross-covariance showing the phase relationship between the alpha field and IPSPs (n=4). **C.** Example EPSP from LIV bursting cell taken during alpha oscillations. **D.** Mean cross-covariance showing the phase relationship between the alpha field and EPSPs (n=5). **E.** Mean spike triggered average of the field and F. Mean field triggered average of the spikes (n=2) showing the relationship between cell firing and the alpha field.

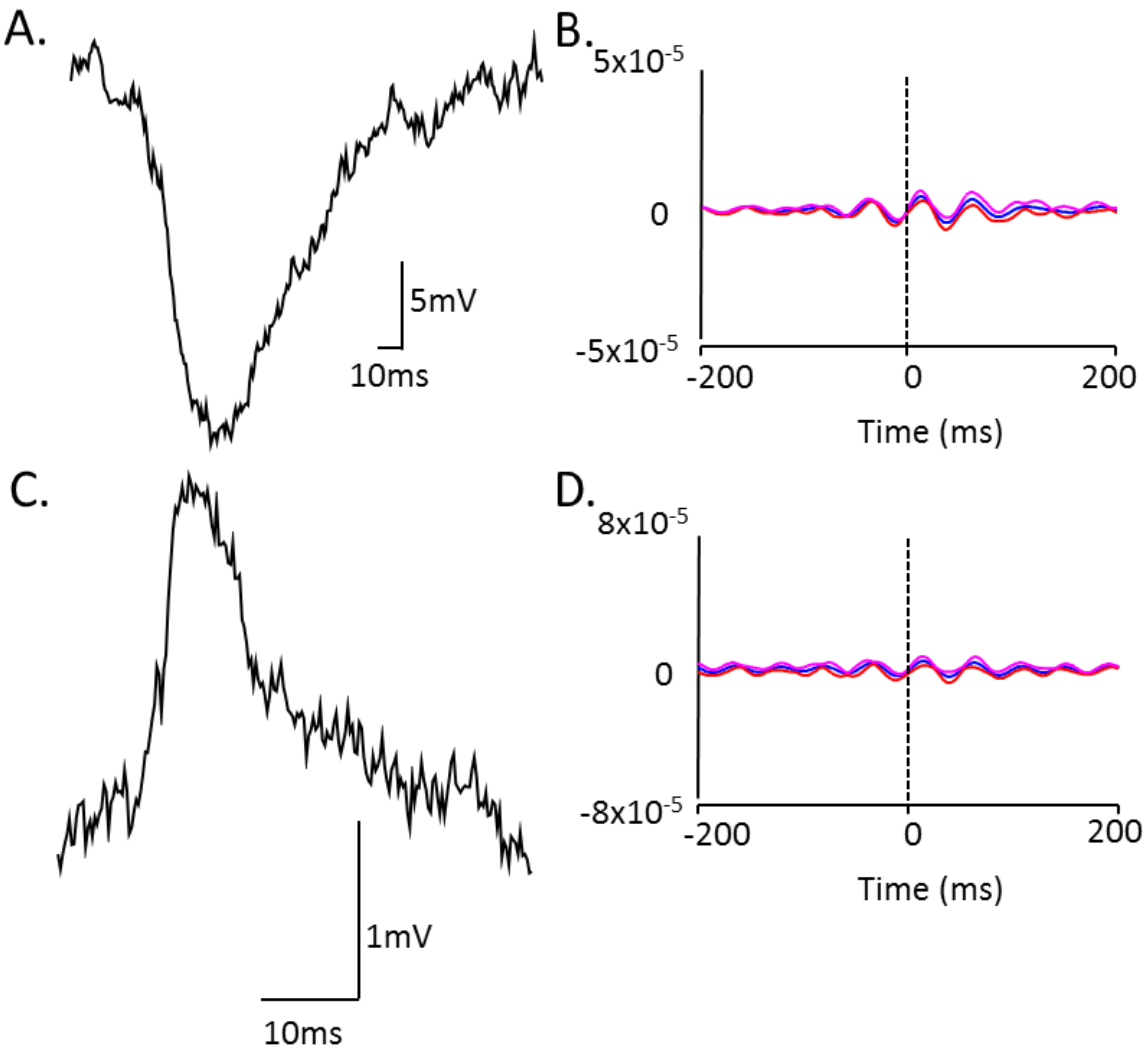

Figure 5.12 Activity of regular spiking cells in Layer II/III of the primary visual cortex during gamma oscillations. A. Example IPSP from LII/III R.S. cell taken during gamma oscillations. **B.** Mean cross-covariance showing the phase relationship between the gamma field and IPSPs (n=3). **C.** Example EPSP from LIV bursting cell taken during gamma oscillations. **D.** Mean cross-covariance showing the phase relationship between the gamma field and EPSPs (n=4).

5.3.6 Contribution of layer V regular spiking cells to rhythms in the V1

Regular spiking cells were also found in layers V of the V1 during alpha and beta oscillations. The resting membrane potential of R.S. cells during alpha oscillations was -63.6mV ± 4.1mV and 57.4mV ± 1.5mV during beta oscillations. There were no statistically significant differences in the RMP between alpha and beta oscillations (P=0.470, n=5, Two-Tailed T-Test). The firing rate of these cells occurred at a similar rate to the R.S. cells located in layer IV. During beta oscillations they fired at a rate of 3.6Hz ± 1.9Hz and during alpha at a rate of 5.5Hz ± 1.7Hz. There was no statistically significant differences in the firing rate between alpha and beta oscillations (P=0.190, n=5, Two-Tailed T-Test). Further analysis into the spike-field coherences revealed that R.S. cell firing was phase locked to the beta (figure 5.13E and F) and alpha field (figure 5.14E and F).

The EPSPs received by R.S. cells can be visualised in figure 5.13C during beta oscillations and figure 5.14C during alpha oscillations. The excitatory inputs that were received by layer V R.S. cells during beta and alpha rhythms were phase locked to the oscillation (figure 5.13D and 5.14D).

The IPSPs received by R.S. cells can be visualised in figure 5.13A during beta oscillations and figure 5.14A during alpha oscillations. The inhibitory inputs that were received by layer V R.S. cells during beta rhythms had a strong degree of phase locking to the oscillation (figure 5.13B) however the inhibitory inputs received during alpha oscillations had only loose phase locking to the field (figure 5.14B).

We have now looked into LV R.S. cell involvement during alpha and beta oscillations in LIV of the primary visual cortex. Bursting cells were also found in LV of the V1 during alpha and beta oscillations. In the next section, the actions of layer V bursting cells are detailed.

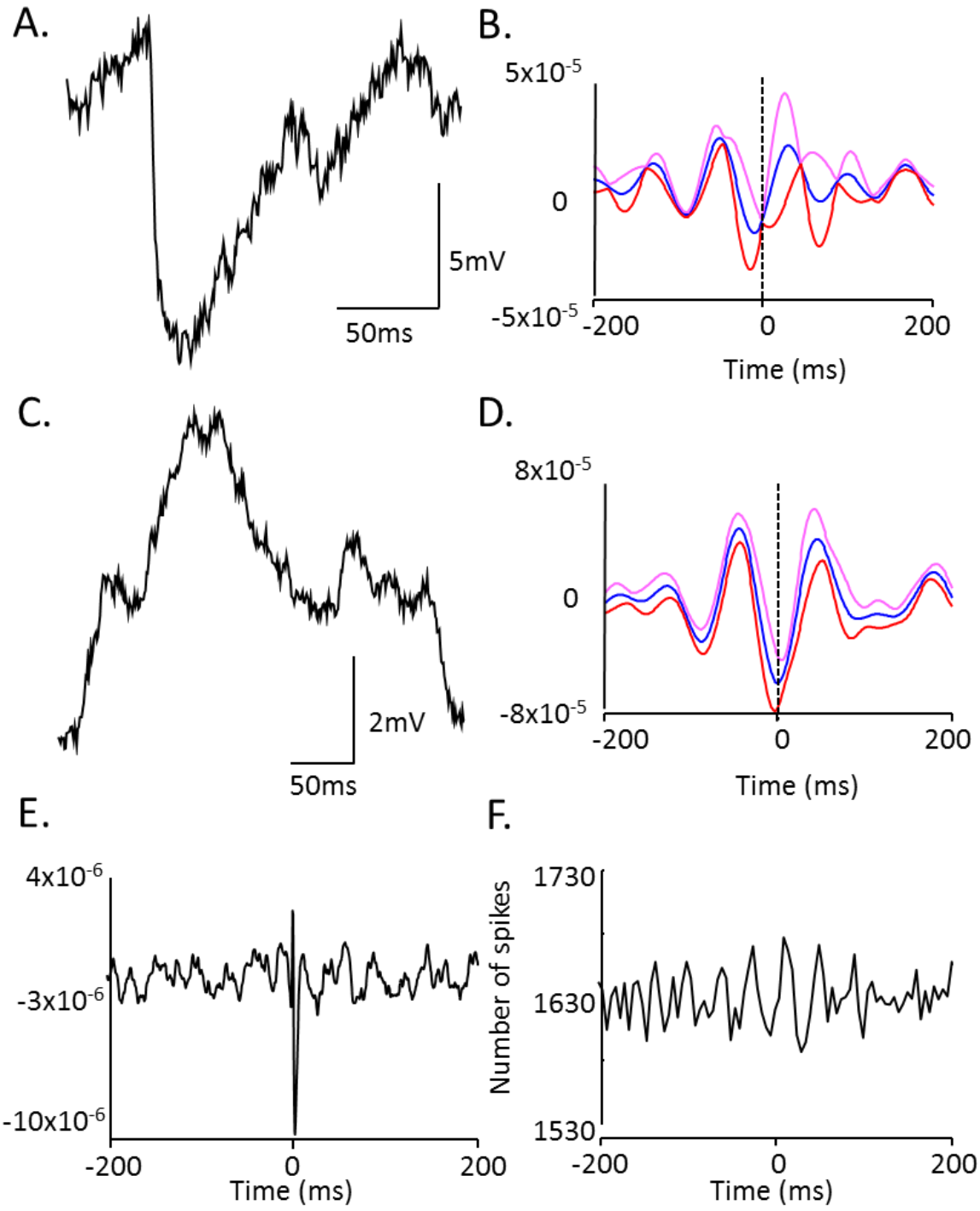

Figure 5.13 Activity of regular spiking cells in Layer V of the primary visual cortex during beta oscillations. A. Example IPSP from LV regular spiking cell taken during beta oscillations. **B.** Mean cross-covariance showing the phase relationship between the beta field and IPSPs (n=3). **C.** Example EPSP from LIV bursting cell taken during beta oscillations. **D.** Mean cross-covariance showing the phase relationship between the beta field and EPSPs (n=5). **E.** Mean spike triggered average of the field and **F.** Mean field triggered average of the spikes (n=3) showing the relationship between cell firing and the beta field.

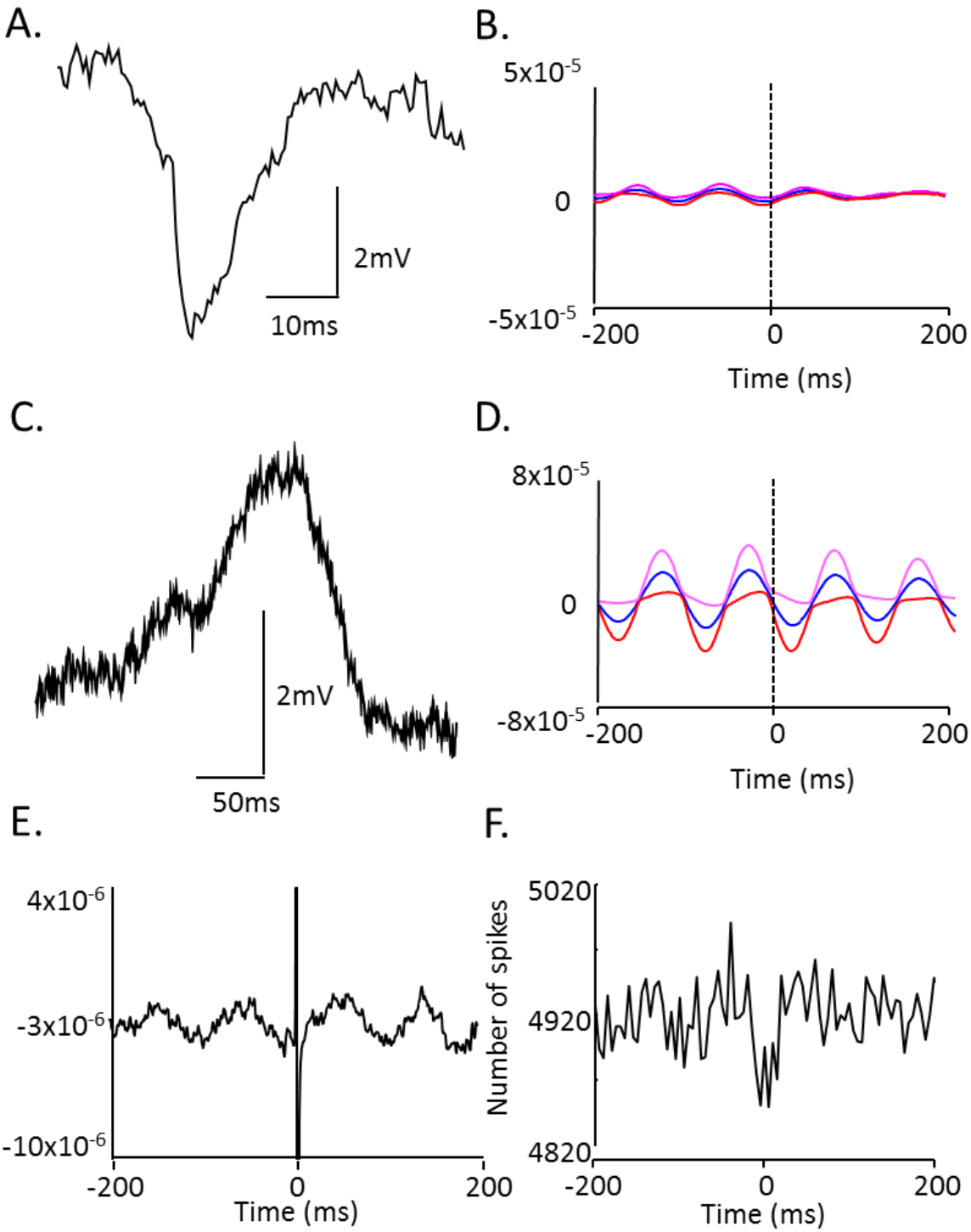

Figure 5.14 Activity of regular spiking cells in Layer V of the primary visual cortex during alpha oscillations. A. Example IPSP from LV regular spiking cell taken during alpha oscillations. **B.** Mean cross-covariance showing the phase relationship between the alpha field and IPSPs (n=3). **C.** Example EPSP from LIV bursting cell taken during alpha oscillations. **D.** Mean cross-covariance showing the phase relationship between the alpha field and EPSPs (n=5). **E.** Mean spike triggered average of the field and **F.** Mean field triggered average of the spikes (n=4) showing the relationship between cell firing and the alpha field.

5.3.7 Contribution of layer V bursting cells to rhythms in the V1

The resting membrane potential of bursting cells during alpha oscillations was -83.0mV ± 4.0mV and -76.0mV during beta oscillations. The firing rate of these cells was similar to the rate of firing of bursting cells located in layer IV. During beta oscillations the cell fired at a rate of 11.2Hz (n=1) and during alpha at a rate of 13.9Hz ± 0.9Hz (n=3). Further analysis into the spike-field coherences revealed that bursting cell firing had a strong degree of phase locking to the beta (figure 5.15E and F) and alpha field (figure 5.16E and F).

The EPSPs received by bursting cells can be visualised in figure 5.15A during beta oscillations and figure 5.16C during alpha oscillations. The excitatory inputs that were received by layer V bursting cells during beta and alpha rhythms were phase locked to the oscillation (figure 5.15C and 5.16D).

The IPSPs received by bursting cells can be visualised in figure 5.16A during alpha oscillations. The inhibitory inputs that were received were phase locked to the oscillation (figure 5.16B). No IPSPs were recorded from LV bursting cells during beta oscillations.

5.3.8 Alpha rhythms dynamically uncoupled layer IV R.S. cell activity from other layers

It was clear from the results described above that the bursting cells were involved in the generation of the alpha rhythm and both R.S. and bursting cells were involved in the generation of the beta rhythm. Figure 5.17 provides a summary of cross-correlational analysis of the field-triggered average of the spikes from LIV R.S. and bursting cells, with layers II/III and V R.S. cells and bursting cells during both beta and alpha oscillations. The cross-correlations from the field triggered average of the spikes showed a high degree of correlation between layer IV R.S. cells and layer II/III R.S. cells, layer V R.S. cells and layer V bursting cells during beta oscillations. There was an even higher degree of correlation between layer IV bursting cells and layer II/III R.S., layer V R.S., and layer V bursting cells during beta

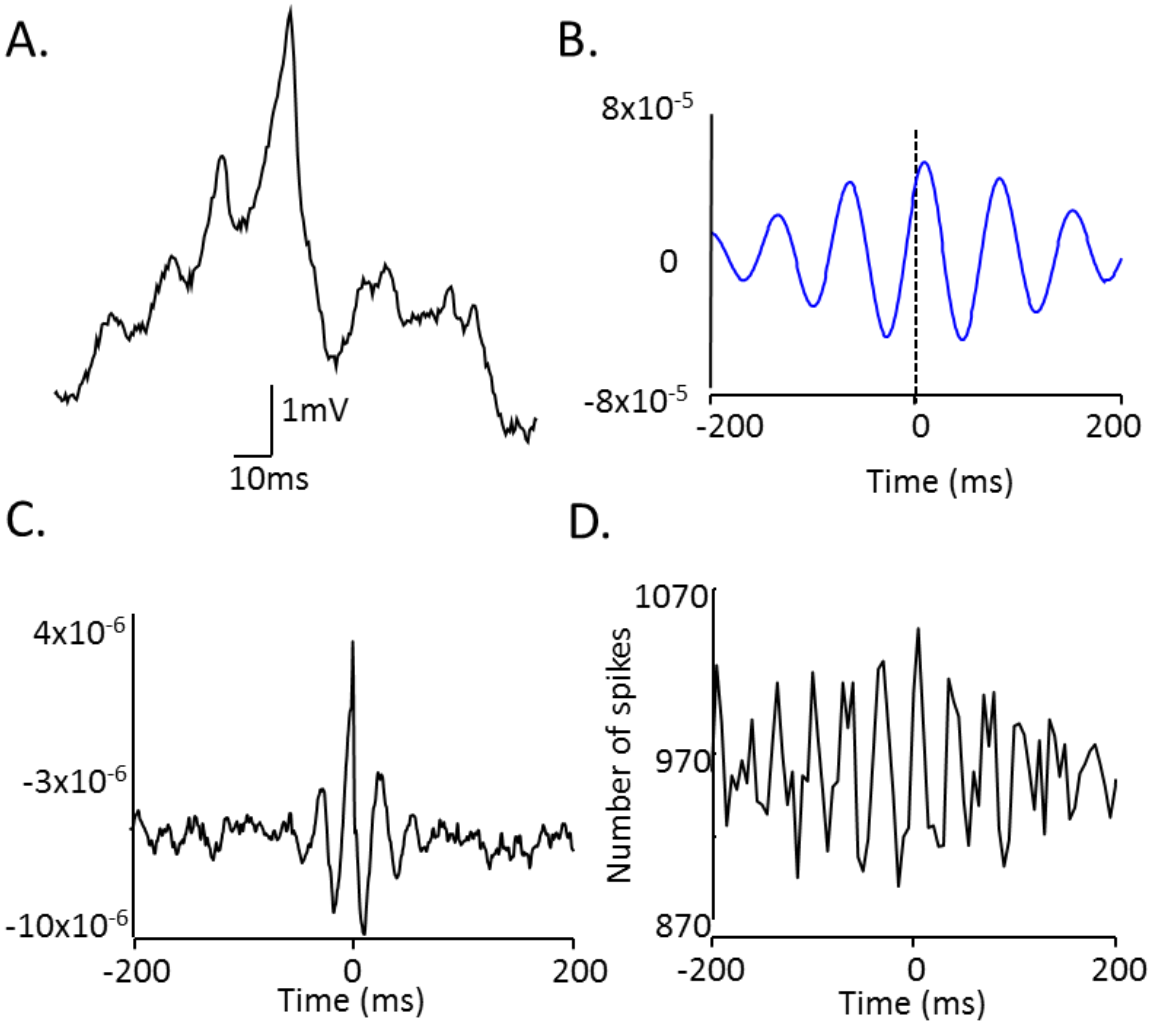

Figure 5.15 Activity of bursting cells in Layer V of the primary visual cortex during beta oscillations. A. Example EPSP from LIV bursting cell taken during beta oscillations. **B.** Mean cross-covariance showing the phase relationship between the beta field and EPSPs (n=1). **C.** Mean spike triggered average of the field and **D.** Mean field triggered average of the spikes (n=1) showing the relationship between cell firing and the beta field.

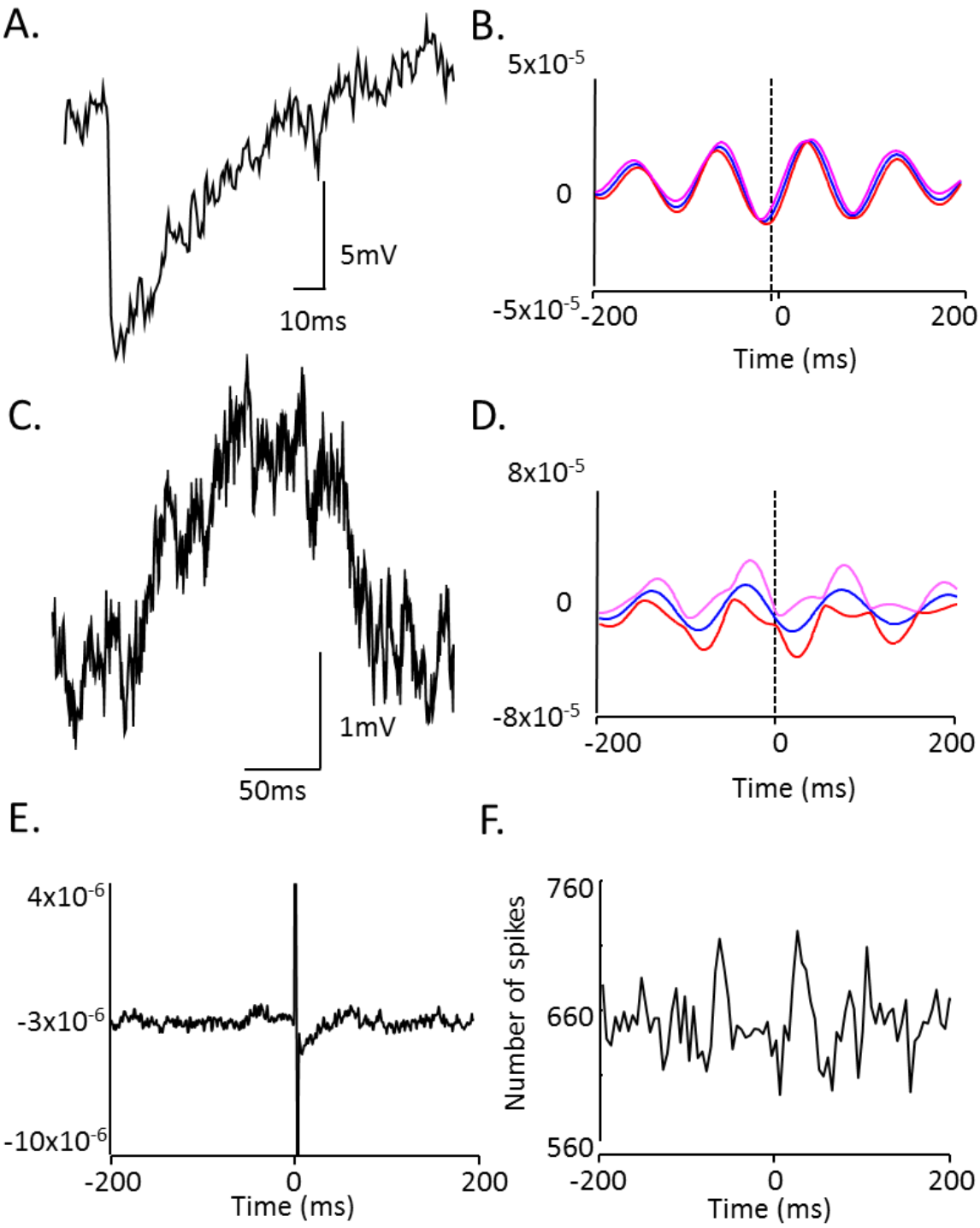

Figure 5.16 Activity of bursting cells in Layer V of the primary visual cortex during alpha oscillations. A. Example IPSP from LV bursting cell taken during alpha oscillations. **B.** Mean cross-covariance showing the phase relationship between the alpha field and IPSPs (n=3). **C.** Example EPSP from LIV bursting cell taken during alpha oscillations. **D.** Mean cross-covariance showing the phase relationship between the alpha field and EPSPs (n=5). **E.** Mean spike triggered average of the field and **F.** Mean field triggered average of the spikes (n=2) showing the relationship between cell firing and the alpha field.

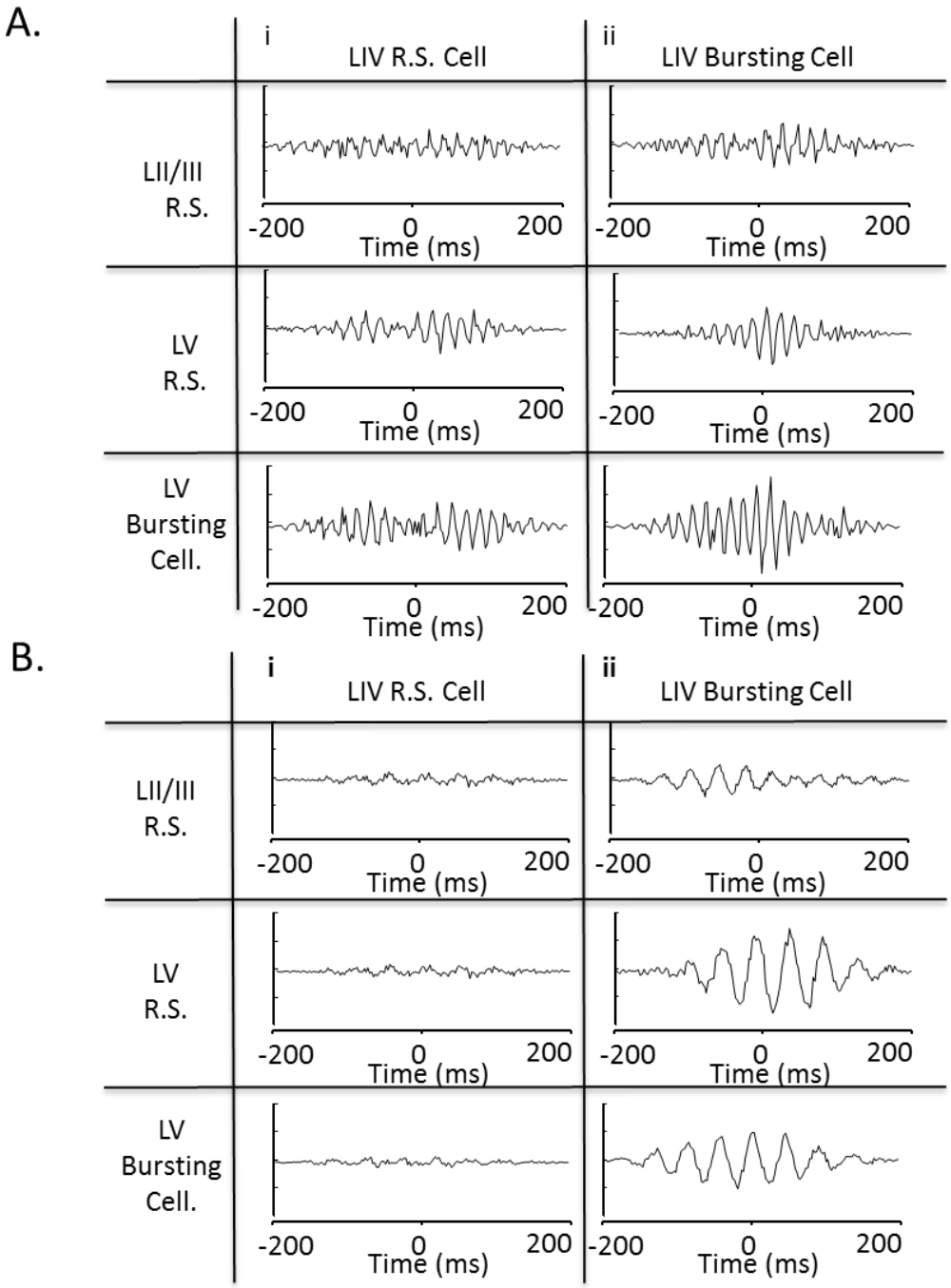

Figure 5.17 Alpha rhythms may uncouple regular spiking cell activity from layers II/III and V in the primary visual cortex. A. Cross correlations of the mean field triggered average between **i.** layer IV regular spiking (R.S.) cells and layers II/III R.S. cells, LV R.S. cells and LV bursting cells and **ii.** layer IV bursting cells and layer II/III R.S. cells, LV R.S cells and LV bursting cells during beta oscillations. **B.** Cross correlations of the mean of the field triggered average between **i.** layer IV R.S. cells and LII/III R.S. cells, LV R.S. cells and LV bursting cells and **ii.** Cross correlations of the mean of the field triggered average between layer IV bursting cells and LII/III R.S. cells, LV R.S. cells and LV bursting cells during alpha oscillations (all axes on same scale of $1.5x10^{-4}$ to $-1.5x10^{-4}$).

oscillations. There was an obvious change in the correlations during alpha rhythms however. The layer IV bursting cells continued to show a high degree of correlation with layer II/III R.S., layer V R.S. and layer V bursting cells. However, the correlation was visibly diminished between layer IV R.S. cells and layer II/III R.S., layer V R.S., and layer V bursting cells during alpha. This provided evidence to suggest that alpha rhythms may dynamically uncouple R.S. cell activity from layers II/III and V.

5.4 Discussion

There were four cell types in total found in the primary visual cortex from the intracellular experiments described in this chapter. These were bursting cells, regular spiking cells, fast adapting (FAD) cells and fast spiking interneurons. The FAD cells were found throughout beta and alpha oscillations however these cells did not fire during either rhythm implying they were not involved in the generation of these rhythms, therefore no analysis of these cells types was shown in this chapter. There were 2 fast spiking interneurons recorded from during alpha and beta oscillations, however preliminary analysis did not implicate these in the rhythms and due to the small number found, these results were also not shown in this chapter. This chapter focused on the 2 layer IV excitatory subtypes found to be involved in beta or alpha rhythms: R.S. cells and bursting cells. They have provided further evidence to suggest that generators of the cortical alpha rhythm are located in layer IV.

The main findings from these experiments were:

1) Bursting cells fired phase locked to the alpha field and these seem to be involved in the generation of alpha rhythms

2) Regular spiking cells were involved in the beta rhythm and not alpha rhythms

3) Alpha rhythms may uncouple R.S. cell activity from other layers in terms of relative spike timings

Each of these findings gives us clues into the generation of the alpha rhythm and are dealt with in the following sections.

5.4.1 Why are bursting cells involved in alpha rhythm generation?

The results from this chapter indicate that bursting cells are involved in the generation of alpha rhythms. Previous studies have found bursting cells to be involved in the generation of alpha oscillations in the thalamus (see introduction section 5.1.2 (Hughes et al., 2004; Hughes et al., 2011; Vijayan and Kopell, 2012)). These cells fire burst discharges at hyperpolarised membrane potentials and sustained tonic firing in response to depolarisation. The results indicated that bursting cells were present in layer 4C of the V1. This layer is also known to contain an abundance of spiny stellate cells (Gilbert and Wiesel, 1983). Neurones in layer 4C of the visual cortex project up to layer 4B and layers II/III. They also project out of the V1 to extrastriate areas including the MT and back to superior colliculus. These areas are known to be involved with perception of movement and the guidance of some eye movements, together they function to allow eye tracking and fixation on a moving object. The V1 is thought to provide a very important input to MT. As alpha oscillations have been found to be involved with functional inhibition (see section 1.5.3) outputs from these cells during alpha oscillations may silence the processing of motion, maintaining sensory information upon removal of visual stimulus or an eyes closed state, acting in a short-term memory role.

During the preceding beta oscillations, the bursting cells fired more single action potentials, like the tonic firing in response to depolarisation described in the Hughes et al. (2004) study. Upon blocking of I_h, the firing frequency of these neurons was reduced, which also resulted in increased bursting and doublet firing from these neurons. This would account for the decrease in frequency of the oscillations and increase in power. However, the results indicate that there was no significant change in membrane potential from the transition from beta to alpha oscillations. This raises a question as to what is causing this change in activity of the bursting cells. This could be attributed to the involvement of K^+ channels. The Kv10.2 channel (which is encoded by the KCNH5 gene) corresponds to the EAG2 gene (Saganich et al., 1999; Ludwig et al., 2000). Rowell et al. (2010) found the EAG2 specific gene expression to be enriched in layer IV of ferret visual cortex.

EAG2 gives rise to voltage-gated, non-inactivating potassium current which could play a role in neuronal membrane conductance and is sensitive to intracellular calcium and levels of activity (Ludwig et al., 2000). These channels are open at more negative membrane potentials and do not inactivate, therefore they contribute to sustained outward currents and more hyperpolarised membrane potentials. Due to their abundance in layer IV of the neocortex (the main recipient of thalamocortical input), EAG2 channels may play a role in the gating of sensory information to the neocortex. During the change from beta to alpha oscillations in the cortical model of alpha, and the change in activity of the bursting cells; Kv10.2 channels may become activated and contribute to the bursting properties of the neurons thought to be involved in alpha oscillations.

As mentioned in the previous chapter (section 4.4.3) I_h provides a tonic dendritic depolarisation, depolarisation has been shown to give rise to tonic firing (Hughes et al., 2004). The reduction in I_h required for alpha oscillations could therefore counter this depolarisation and give rise to burst discharges. The previous chapter indicated that the burst-discharges in this cortical model of alpha rhythms are not mediated by T-type calcium channels (section 4.4.3). Calcium has been shown to be critical in bursting type cells in the hippocampus (Magee and Carruth, 1999). I_h allows the influx of calcium ions upon hyperpolarisation. Inhibiting calcium could therefore also affect the role that I_h plays on bursting neurons. The results from this chapter however, indicate that due to the absence of a post-current step AHP, these burst discharges are unlikely to be due to L-type calcium channels (Lima and Marrion, 2007). The large increase in power could be due to the possible effects of I_h on sodium channel-mediated bursts. Sodium has been found to be critical for bursting neurons in *in vitro* slices from ferret visual cortex (Brumberg et al., 2000). Persistent sodium currents (I_{NaP}) have also been shown to play a role in burst generation in mesencephalic V neurons by amplification of a K^+ dependent membrane resonance (Wu et al., 2001; Wu et al., 2005). Therefore the effect I_h has on sodium channels could be responsible for the bursting behaviours of neurons. This provides further evidence of the synaptic and intrinsic cellular conductances thought to be crucial to alpha rhythm generation.

There was also evidence of bursting cells playing a role during beta oscillations. Results showed a phase relationship between bursting cell firing and the LFP during beta in both layers IV and layer V. There was however no bursting cells found during gamma oscillations. There was strong phase locking between the gamma rhythm and layer IV R.S. cell firing. This implicates R.S. cell involvement in the generation of gamma rhythms. If there is no contribution of bursting cells to the gamma rhythm, this would mean the gamma and beta rhythms generated in the V1 could be mechanistically different, which has been shown in hippocampus (Kopell et al., 2000) and olfactory bulb (David et al., 2015). In this area, gamma is associated with synchronisation of the visual response, whereas beta has been implicated in long-distance coherence between parietal and temporal cortices during multimodal processing (von Stein et al., 1999). Mechanistic differences in gamma and beta rhythms could account for why alpha oscillations cannot be generated from a prior gamma oscillation.

5.4.2 Why are R.S. cells involved with beta rhythms but not alpha?

In layer IV of the primary visual cortex, stellate cells have been shown to receive inputs from the thalamus, whilst also modulating their response via circuitry between themselves (see 5.1.2 (da Costa and Martin, 2011)). They process feed-forward excitation to layer II/III pyramidal cells which then send axons out of the cortex. Results from this chapter implicate regular spiking cells which are presumed to be of the stellate subtype (see figure 5.4) in the beta rhythm. Beta oscillations have been shown to be involved with an attentive state in the visual system (see chapter 1 (Wrobel et al., 1994; Hanslmayr et al., 2007; Güntekin et al., 2013)). Upon visual stimulation, beta oscillations are observed in the visual cortex; upon removal of visual stimulus or an eyes closed state, alpha rhythms dominate. These excitatory cells may be involved with the attentive state in the V1 during beta oscillations, which may then become quiescent upon the removal of stimulus. Results from these experiments have shown that R.S. cells are not involved with the generation of the alpha rhythm in the V1. However, these cells are still receiving inputs which

are phased locked to the alpha rhythm. Upon the transition into alpha frequency oscillations, I_h is reduced; this could be making the cells more hyperpolarised and therefore less likely to fire. Stellate cells have been shown to be involved in maintaining the local circuitry in the visual cortex (see above); these cells may therefore be maintained at a minimum during alpha rhythms due to the role alpha oscillations play in functional inhibition – silencing the local circuitry and therefore directing attention to task relevant areas.

5.4.3 Why do alpha rhythms uncouple R.S. cell activity from other layers?

Results from these experiments also indicate the possible involvement of alpha rhythms in uncoupling R.S. (stellate) cell activity from other layers. Figure 5.17 shows cross correlations of the mean of the field triggered average of the spikes between layer IV R.S. cells and layer II/III and V regular spiking cells during both beta and alpha oscillations. It is clear from these cross correlations that layer IV R.S. cells show a phase relationship to layer II/III and layer V R.S. cells during beta oscillations. However upon the transition into alpha rhythms, this phase relationship is almost completely abolished. The IPSPs from both cell types have a longer decay time, rise time and higher amplitude during alpha oscillations than the beta oscillations. These cell types could be receiving stronger inhibition during alpha oscillations, however it is very hard to measure the inputs received as they are compound. The dynamic uncoupling observed could be attributed to the role alpha rhythms play in inhibition of task irrelevant areas (see introduction (Pfurtscheller et al., 1994; Pfurtscheller et al., 1996; Klimesch, 2012)), directing attention to task relevant areas giving an optimal brain state for task execution (Cooper et al., 2003; Jensen and Mazaheri, 2010; Mathewson et al., 2011). This functional inhibition of alpha rhythms may be attributed to the dynamic uncoupling of R.S. cell activity from other layers. This could provide a mechanism of attentional selection, to silence the network during alpha frequency oscillations; by uncoupling R.S. cells from supragranular layers, alpha oscillations could prevent the information flow up through the visual cortical hierarchy. The role of alpha rhythms

in uncoupling cortical layers has not been seen before during other brain rhythms which suggest that the dynamic uncoupling seen during alpha rhythms is a novel mechanism.

5.4.4 Summary

The work carried out in this chapter has outlined the cell types involved in the generation of rhythms in the visual cortex. Both excitatory R.S. cells and pyramidal bursting cells have been shown to be involved in the beta rhythm. Upon the transition into alpha oscillations, these R.S. cells are silenced and the alpha rhythm is driven by bursting cells. The results have also implicated alpha oscillations in the uncoupling of R.S. cell activity from other layers which compliments the functional inhibition theory of alpha oscillations. The bursting cells involved in alpha generation have been found in layer IV of the V1. This finding, combined with the findings from the previous two chapters, provides further evidence that layer IV is the location of the alpha generator in visual cortex.

Chapter 6: General Discussion

6.1 Summary of findings

The results in this thesis document an attempt to generate and characterise an *in vitro* model of the occipital alpha rhythm. The rhythm has been known since the pioneering work of Hans Berger published in 1929. However, almost nothing is known about the cellular origins of this rhythm in neocortex. This may, in large part, be due to the 'reactive' nature of alpha oscillations. Unlike their spontaneous counterpart, with origins in frontal cortices and the thalamus, occipital alpha rhythms have to be 'induced' by a prior period of visual sensory activity (Ben-Simon et al., 2008). Therefore, any attempt to model the rhythm experimentally by simply activating visual areas tonically (as with most *in vitro* brain rhythm models used to date) was bound to fail.

By mimicking a period of visual cortical activation by application of a glutamatergic receptor agonist, and then subsequently reducing that activation with a general antagonist (simply 'washing-out' the activator being far too slow), we succeeded in generating robust alpha rhythms in visual cortical slices. These rhythms were almost entirely confined to area V1, with little or no alpha power in adjacent retrosplenial (posterior cingulate) or higher-order visual areas (V2). Further attempts at anatomical localisation showed that it was layer IV of the V1 that appeared to be the locus of this oscillation. These two observations complemented each other. Area V1 has a highly specialised layer IV (Gennari, 1782) which clearly delineates it from neighbouring regions, even under light microscopy. The degree of specialisation of this layer increases phylogenetically, but in most mammals, very specialised neuronal subtypes can be found there (see chapter 5.1 and 5.4). The present studies indicated that one particular neuronal subtype – pyramidal cells with transient bursting characteristics – may constitute the primary feature of local networks generating the alpha rhythm.

Pharmacological studies showed that this alpha rhythm was critically dependent on NMDA receptor-mediated connections between neurons. These connections appeared to require the need to be potentiated – in this case by a period of prior excitation leading to beta frequency network rhythms (see Chapter 3.3 and 4.3) – and were mediated by a particular NMDA receptor subunit that conferred strong

activation even at hyperpolarised membrane potentials. This observation may be critical as alpha rhythms in visual areas are most often seen during periods of low activation ('eyes-closed'). They also required the 'blockade' of the normal, membrane potential-reactive form of I_h, though this may not be, strictly speaking, a 'blockade' on transmembrane conductance (see below).

Finally, an investigation into the local dynamic consequences of the layer IV alpha rhythm revealed that it was not dominated by synaptic inhibition despite the 'functional inhibition' role it is thought to play. Instead, the presence of the alpha rhythm appeared to dynamically disconnect (de-correlate) activity in the primary thalamorecipient neurons – the layer IV R.S. (stellate) cells – from down-stream activity in both supragranular and infragranular layers. In this manner the alpha rhythm appears to be ideally constructed to prevent ascending visual information from both passing onto higher order visual areas and also being influenced by top-down signal from these areas (see sections 6.3, 6.4).

6.2 Cellular properties relevant to the alpha generator

All the data collected in this thesis pointed to a fundamental change in the output behaviour of layer IV pyramidal cells being vital for alpha generation. Depolarising current injection suggested two distinct modes of output – a transient burst when activity was elicited from hyperpolarised membrane potentials and regular, single spiking when activity was elicited from more depolarised potentials (see chapter 5.3). However, even during alpha rhythms somatic recordings rarely revealed the generation of full burst discharges. Instead, doublet or triplet spikes per alpha period were common. This suggested a more dendritic origin for the change in output behaviour. During these studies two recordings from presumed layer IV pyramidal cell dendrites were taken: not enough to constitute inclusion in the results section but mentioned here because they reveal a number of possible clues to the behaviour change predicted by a detailed computational model under construction in collaboration with R. D. Traub at IBM Watson Research Center in the USA (Figure 6.1).

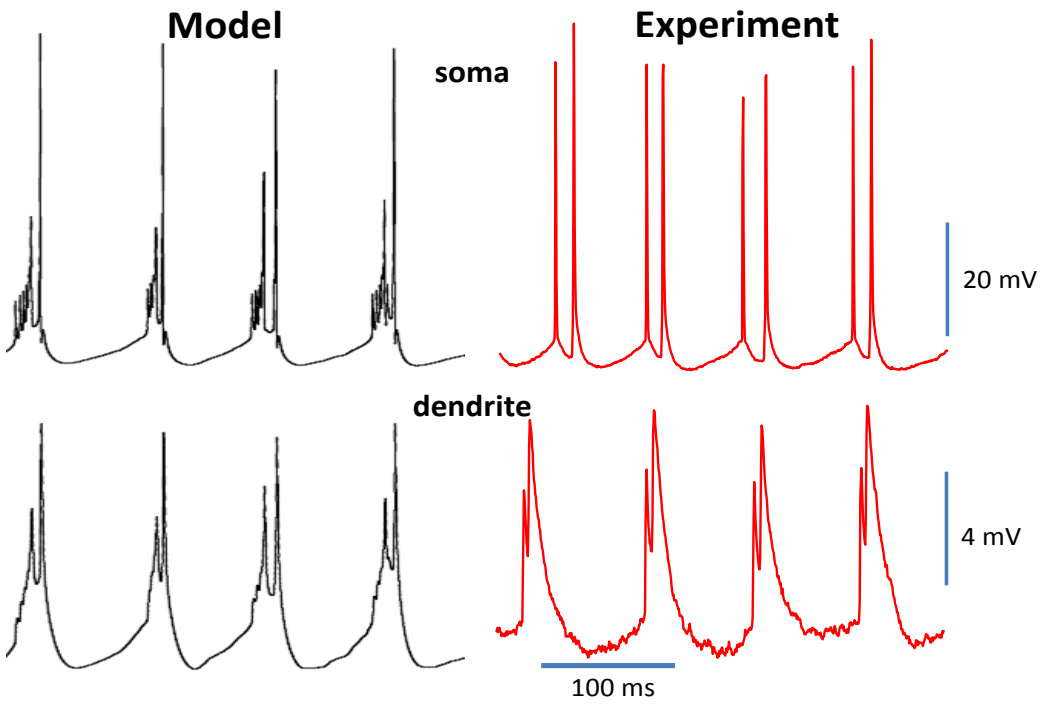

Figure 6.1. Model and preliminary experiments suggest a dendritic locus for multiple spike generation in layer IV pyramids during the alpha rhythm.

A dendritic origin for the change from single to multiple spikes per alpha period fits superficially with the strong relationship between alpha generation and reduced intrinsic excitation with I_h blockers. I_h is up to 30-fold more prevalent on distal dendrites than it is in somatic compartments (Lorincz et al., 2002; Kole et al., 2006). However, whether blockade of I_h was necessary, or a transition to more tonic inward current, is far from straightforward. I_h, in the unmodulated, low intracellular calcium state, is activated on hyperpolarisations from membrane potentials above ca. -70 mV down to below -80 mV. Preliminary dendritic recordings reveal a tonic depolarisation of dendrites at ca. -60 mV with no fluctuations beyond ca. -65 mV. This would be insufficient to activate I_h in these normal conditions. However, with neuromodulator influences and particularly elevated calcium levels intracellularly the activation voltage shifts to more depolarised levels and inactivation slows dramatically (McCormick and Pape, 1990) – providing a tonic depolarising current. While the 'blockers' ZD7288 and DK-AH269 do reduce overall channel conductance they also shift activation to more depolarised voltages and slow inactivation in a similar manner (see chapter 4.4 and chapter 5).

The peculiar dendritic spike profiles predicted by the model, and seen in preliminary recordings, required calcium currents with fast onset/offset kinetics. However, this was shown not to be T-current (chapter 4) as would have perhaps been obvious from the more depolarised dendritic membrane potentials: T-current requires depolarisations from ca. -80 mV (Halliwell and Adams, 1982). Another alternative is the N-current. This is also seen predominantly on dendrites (Westenbroek et al., 1992) and can have extremely fast kinetics (Delcour et al., 1993). It would also perhaps explain the role of NMDA receptors in generating the alpha rhythm. Dual dendritic spikes, as seen above and predicted by the model, have been seen to be generated by the interplay between NMDA-receptor-mediated synaptic input to dendrites and a fast dendritic calcium conductance such as the N-type (Larkum et al., 2007). *In vivo* experiments have shown that such dendritic; NMDA receptor-dependent spiking has a strong influence on primary sensory processing (Palmer et al., 2014).

6.3 Is the alpha rhythm really an inhibitory rhythm?

Evidence for the alpha rhythm being a source of 'functional inhibition' during visual cognitive tasks is strong (see chapter 1). Data from the present model do not support this functionality as coming from actual synaptic inhibition though. IPSPs were the same or weaker during alpha compared to prior beta rhythms and the computational model predicts no necessary involvement in synaptic inhibition at all for alpha generation. A transition from single to multiple spike outputs, as seen in this thesis, also point to a local circuit disinhibitory phenomenon. This may be reflected in non-invasive human studies.

Excellent work has been done recently trying to relate the blood oxygen level (BOLD) fMRI signal to different EEG rhythms (Sclocco et al., 2014). In general it is thought that the faster the frequency of EEG signal recorded the larger the BOLD response (Jann et al., 2010). However, the alpha rhythm does not fit this scheme. Alpha rhythms in general have an inverse relationship with BOLD: The larger the power of the alpha signal, the more negative the BOLD signal (Moosmann et al., 2003). This relationship holds for both the reactive, occipital alpha rhythm as

modelled here and the more frontal, spontaneous alpha rhythms (Ben-Simon et al., 2008). Some researchers have related this to cortical 'deactivation' caused by the functional inhibition related to alpha rhythms (DiFrancesco et al., 2008). However, it is more likely that the converse is true. Careful optogenetic experiments revealed that it is activity of inhibitory, GABAergic interneurons that generate the BOLD signal (Lee et al., 2010). The argument being that the cortex continually attempts to balance excitation and inhibition – thus more intense (faster) rhythms recruit more interneurons. However, as this thesis at least partially shows, the alpha rhythm does not correspond to elevated levels of synaptic inhibition.

6.4 Clues to the function of the alpha rhythm from long-range V1 connectivity

Layer IV neurons in the V1 project mainly locally, with ascending projections to supragranular layers both within column and to adjacent columns dominant (see introduction to this chapter). In contrast, these supragranular targets project to higher order neocortical visual areas (Maunsell and van Essen, 1983). These projections can be strong, particularly to V2 (Burkhalter and Bernardo, 1989). It is interesting that almost no alpha rhythms were seen in V2 in the present experiments, despite the region being directly adjacent to the V1 in the orientation of slice used (chapter 3.3). This supports the idea that the alpha rhythm is a phenomenon local to the V1 and also that the dynamic un-coupling of stellate cells from supragranular layers seen here is highly efficient at preventing information passing up through the visual cortical hierarchy.

In contrast, the infragranular layers appear to be predominantly recipient in that they mainly receive information from higher order visual areas (top-down information). They then tend to project out of cortex, back to the LGN and to other up-stream regions like superior colliculus (Rockland and Pandya, 1979; Fries, 1985; Batardiere et al., 2002). Interestingly there is a small set of pyramidal-like neurons in the lower sublaminations of layer IV at the layer V border that do project out of the V1. These appear to provide input directly to area MT (V5) (Anderson et al., 1998). These lower layer IV/infragranular projections are interesting from the point

of view of the alpha rhythm during the eyes closed state. Area MT is responsible for coding movement in the visual field and superior colliculus can control eye movement. Together they function to allow eye tracking and fixation on moving objects. Given the short-term memory role proposed for the alpha rhythm (see chapter 1) it may be that the strong alpha rhythm in layer IV, coherent with that in layer 5 (see chapter 5.3) acts concurrently with these visual movement areas to prevent confusion when eyes are momentarily closed and the visual field changes owing to on-going movement.

Much is still to do with the model presented here. A more detailed quantification of the roles played by each of the layer IV pyramidal cell conductances is required, as is a thorough understanding of the dynamic state afforded by the transition from single to multiple spiking. A more analytical modelling approach is also needed in order to understand exactly how R.S. cell outputs are filtered out from supra- and infragranular layers. Only then can we begin to understand the selective attentional and short-term memory roles of this rhythm more fully.

References

Adrian ED, Matthews BH (1934) The interpretation of potential waves in the cortex. The Journal of physiology 81:440-471.

Aghajanian GK, Rasmussen K (1989) Intracellular studies in the facial nucleus illustrating a simple new method for obtaining viable motoneurons in adult rat brain slices. Synapse 3:331-338.

Ahveninen J, Lin FH, Kivisaari R, Autti T, Hämäläinen M, Stufflebeam S, Belliveau JW, Kähkönen S (2007) MRI-constrained spectral imaging of benzodiazepine modulation of spontaneous neuromagnetic activity in human cortex. NeuroImage 35:577-582.

Ahveninen J, Jääskeläinen IP, Belliveau JW, Hämäläinen M, Lin F-H, Raij T (2012) Dissociable Influences of Auditory Object <italic>vs.</italic> Spatial Attention on Visual System Oscillatory Activity. PLoS ONE 7:e38511.

Ainsworth M, Lee S, Cunningham MO, Roopun AK, Traub RD, Kopell NJ, Whittington MA (2011) Dual Gamma Rhythm Generators Control Interlaminar Synchrony in Auditory Cortex. The Journal of neuroscience : the official journal of the Society for Neuroscience 31:10.1523/JNEUROSCI.2209-1511.2011.

Ainsworth M, Lee S, Cunningham MO, Traub RD, Kopell NJ, Whittington MA (2012) Rates and rhythms: a synergistic view of frequency and temporal coding in neuronal networks. Neuron 75:572-583.

Alonso A, Llinas RR (1989) Subthreshold Na+-dependent theta-like rhythmicity in stellate cells of entorhinal cortex layer II. Nature 342:175-177.

Amitai Y, Gibson JR, Beierlein M, Patrick SL, Ho AM, Connors BW, Golomb D (2002) The Spatial Dimensions of Electrically Coupled Networks of Interneurons in the Neocortex. The Journal of Neuroscience 22:4142-4152.

Anderson JC, Binzegger T, Martin KAC, Rockland KS (1998) The Connection from Cortical Area V1 to V5: A Light and Electron Microscopic Study. The Journal of Neuroscience 18:10525-10540.

Arencibia-Albite F, Paladini C, Williams JT, Jimenez-Rivera CA (2007) Noradrenergic modulation of the hyperpolarization-activated cation current (Ih) in dopamine neurons of the ventral tegmental area. Neuroscience 149:303-314.

Arroyo S, Bennett C, Hestrin S (2014) Nicotinic modulation of cortical circuits. Frontiers in Neural Circuits 8:30.

Aston-Jones G, Rajkowski J, Cohen J (1999) Role of locus coeruleus in attention and behavioral flexibility. Biol Psychiatry 46:1309-1320.

Baker SN, Kilner JM, Pinches EM, Lemon RN (1999) The role of synchrony and oscillations in the motor output. Experimental brain research 128:109-117.

Banks MI, White JA, Pearce RA (2000) Interactions between distinct GABA(A) circuits in hippocampus. Neuron 25:449-457.

Batardiere A, Barone P, Knoblauch K, Giroud P, Berland M, Dumas AM, Kennedy H (2002) Early specification of the hierarchical organization of visual cortical areas in the macaque monkey. Cerebral cortex (New York, NY : 1991) 12:453-465.

Beaumont V, Zucker RS (2000) Enhancement of synaptic transmission by cyclic AMP modulation of presynaptic Ih channels. Nat Neurosci 3:133-141.

Beierlein M, Gibson JR, Connors BW (2000) A network of electrically coupled interneurons drives synchronized inhibition in neocortex. Nat Neurosci 3:904-910.

Bell SL, Taylor RC, Singleton EG, Henningfield JE, Heishman SJ (1999) Smoking after nicotine deprivation enhances cognitive performance and decreases tobacco craving in drug abusers. Nicotine Tob Res 1:45-52.

Belov DR, Getmanenko OV, Kolodyazhanyi SF, Kanunikov IE (2009) Lateral inhibition in neural networks and the shape of EEG alpha rhythm waves. Neurosci Behav Physiol 39:261-268.

Ben-Simon E, Podlipsky I, Arieli A, Zhdanov A, Hendler T (2008) <italic>Never Resting Brain:</italic> Simultaneous Representation of Two Alpha Related Processes in Humans. PLoS ONE 3:e3984.

Berger H (1929) Über das Elektrenkephalogramm des Menschen. Archiv für Psychiatrie und Nervenkrankheiten 87:527-570.

Berretta N, Berton F, Bianchi R, Brunelli M, Capogna M, Francesconi W (1991) Long-term Potentiation of NMDA Receptor-mediated EPSP in Guinea-pig Hippocampal Slices. The European journal of neuroscience 3:850-854.

Bettini E, Sava A, Griffante C, Carignani C, Buson A, Capelli AM, Negri M, Andreetta F, Senar-Sancho SA, Guiral L, Cardullo F (2010) Identification and characterization of novel NMDA receptor antagonists selective for NR2A- over NR2B-containing receptors. J Pharmacol Exp Ther 335:636-644.

Bi GQ, Poo MM (1998) Synaptic modifications in cultured hippocampal neurons: dependence on spike timing, synaptic strength, and postsynaptic cell type. The Journal of neuroscience : the official journal of the Society for Neuroscience 18:10464-10472.

Binshtok AM, Fleidervish IA, Sprengel R, Gutnick MJ (2006) NMDA receptors in layer 4 spiny stellate cells of the mouse barrel cortex contain the NR2C subunit. The Journal of neuroscience : the official journal of the Society for Neuroscience 26:708-715.

Blasdel GG, Lund, J. S. (1983) Termination of afferent axons in macaque striate cortex. J Neurosci:1389-1413.

Bliss TVP, Collingridge GL (1993) A synaptic model of memory: long-term potentiation in the hippocampus. Nature 361:31-39.

Bodenmann S, Rusterholz T, Durr R, Stoll C, Bachmann V, Geissler E, Jaggi-Schwarz K, Landolt HP (2009) The functional Val158Met polymorphism of COMT predicts interindividual differences in brain alpha oscillations in young men. The Journal of neuroscience : the official journal of the Society for Neuroscience 29:10855-10862.

Bollimunta A, Chen Y, Schroeder CE, Ding M (2008) Neuronal mechanisms of cortical alpha oscillations in awake-behaving macaques. The Journal of neuroscience : the official journal of the Society for Neuroscience 28:9976-9988.

Bowers H, Smith D, de la Salle S, Choueiry J, Impey D, Philippe T, Dort H, Millar A, Daigle M, Albert PR, Beaudoin A, Knott V (2015) COMT polymorphism modulates the resting-state EEG alpha oscillatory response to acute nicotine in male non-smokers. Genes Brain Behav 14:466-476.

Bowery N (1989) GABAB receptors and their significance in mammalian pharmacology. Trends Pharmacol Sci 10:401-407.

Brager DH, Lewis AS, Chetkovich DM, Johnston D (2013) Short- and long-term plasticity in CA1 neurons from mice lacking h-channel auxiliary subunit TRIP8b. J Neurophysiol 110:2350-2357.

Bragin A, Jando G, Nadasdy Z, Hetke J, Wise K, Buzsaki G (1995) Gamma (40-100 Hz) oscillation in the hippocampus of the behaving rat. The Journal of neuroscience : the official journal of the Society for Neuroscience 15:47-60.

Broicher T, Bidmon HJ, Kamuf B, Coulon P, Gorji A, Pape HC, Speckmann EJ, Budde T (2010) Thalamic afferent activation of supragranular layers in auditory cortex in vitro: a voltage sensitive dye study. Neuroscience 165:371-385.

Brumberg JC, Nowak LG, McCormick DA (2000) Ionic mechanisms underlying repetitive high-frequency burst firing in supragranular cortical neurons. Journal of Neuroscience 20:4829-4843.

Buchholz VN, Jensen O, Medendorp WP (2014) Different roles of alpha and beta band oscillations in anticipatory sensorimotor gating. Frontiers in human neuroscience 8:446.

Buffalo EA, Fries P, Landman R, Buschman TJ, Desimone R (2011) Laminar differences in gamma and alpha coherence in the ventral stream. Proceedings of the National Academy of Sciences.

Buhry L, Hutt A (2013) Propofol-induced GABAergic Tonic Inhibition Diminishes α-rhythms and Induces δ-rhythms in neuronal populations. In.

Bunzeck N, Guitart-Masip M, Dolan RJ, Duzel E (2011) Contextual novelty modulates the neural dynamics of reward anticipation. The Journal of neuroscience : the official journal of the Society for Neuroscience 31:12816-12822.

Burkhalter A, Bernardo KL (1989) Organization of corticocortical connections in human visual cortex. Proc Natl Acad Sci U S A 86:1071-1075.

Buschman TJ, Miller EK (2007) Top-Down Versus Bottom-Up Control of Attention in the Prefrontal and Posterior Parietal Cortices. Science 315:1860-1862.

Calautti C, Baron JC (2003) Functional neuroimaging studies of motor recovery after stroke in adults: a review. Stroke 34:1553-1566.

Canolty RT, Edwards E, Dalal SS, Soltani M, Nagarajan SS, Kirsch HE, Berger MS, Barbaro NM, Knight RT (2006) High gamma power is phase-locked to theta oscillations in human neocortex. Science 313:1626-1628.

Carracedo LM, Kjeldsen H, Cunnington L, Jenkins A, Schofield I, Cunningham MO, Davies CH, Traub RD, Whittington MA (2013) A neocortical delta rhythm facilitates reciprocal interlaminar interactions via nested theta rhythms. The Journal of neuroscience : the official journal of the Society for Neuroscience 33:10750-10761.

Carta M, Fievre S, Gorlewicz A, Mulle C (2014) Kainate receptors in the hippocampus. The European journal of neuroscience 39:1835-1844.

Castro-Alamancos MA, Connors BW (1996) Cellular mechanisms of the augmenting response: short-term plasticity in a thalamocortical pathway. The Journal of neuroscience : the official journal of the Society for Neuroscience 16:7742-7756.

Castro-Alamancos MA, Calcagnotto ME (2001) High-pass filtering of corticothalamic activity by neuromodulators released in the thalamus during arousal: in vitro and in vivo. J Neurophysiol 85:1489-1497.

Chatila M, Milleret C, Buser P, Rougeul A (1992) A 10 Hz "alpha-like" rhythm in the visual cortex of the waking cat. Electroencephalogr Clin Neurophysiol 83:217-222.

Chatila M, Milleret C, Rougeul A, Buser P (1993) Alpha rhythm in the cat thalamus. C R Acad Sci III 316:51-58.

Chaumon M, Schwartz D, Tallon-Baudry C (2009) Unconscious learning versus visual perception: dissociable roles for gamma oscillations revealed in MEG. J Cogn Neurosci 21:2287-2299.

Chavanon ML, Wacker J, Leue A, Stemmler G (2007) Evidence for a dopaminergic link between working memory and agentic extraversion: an analysis of load-related changes in EEG alpha 1 activity. Biol Psychol 74:46-59.

Chepkova AN, Sergeeva OA, Haas HL (2008) Carbenoxolone impairs LTP and blocks NMDA receptors in murine hippocampus. Neuropharmacology 55:139-147.

Chevaleyre V, Castillo PE (2002) Assessing the role of Ih channels in synaptic transmission and mossy fiber LTP. Proceedings of the National Academy of Sciences 99:9538-9543.

Chevallier S, Nagy F, Cabelguen J-M (2006) Cholinergic control of excitability of spinal motoneurones in the salamander. The Journal of physiology 570:525-540.

Ching S, Cimenser A, Purdon PL, Brown EN, Kopell NJ (2010) Thalamocortical model for a propofol-induced α-rhythm associated with loss of consciousness. Proceedings of the National Academy of Sciences 107:22665-22670.

Classen J, Gerloff C, Honda M, Hallett M (1998) Integrative visuomotor behavior is associated with interregionally coherent oscillations in the human brain. J Neurophysiol 79:1567-1573.

Collingridge GL, Randall AD, Davies CH, Alford S (1992) The synaptic activation of NMDA receptors and Ca2+ signalling in neurons. Ciba Found Symp 164:162-171; discussion 172-165.

Connors BW, Gutnick MJ (1990) Intrinsic firing patterns of diverse neocortical neurons. Trends in neurosciences 13:99-104.

Connors BW, Amitai Y (1997) Making waves in the neocortex. Neuron 18:347-349.

Connors BW, Long MA (2004) Electrical synapses in the mammalian brain. Annual review of neuroscience 27:393-418.

Connors BW (2012) Tales of a Dirty Drug: Carbenoxolone, Gap Junctions, and Seizures. Epilepsy Currents 12:66-68.

Contractor A, Mulle C, Swanson GT (2011) Kainate receptors coming of age: milestones of two decades of research. Trends in neurosciences 34:154-163.

Cooper NR, Croft RJ, Dominey SJ, Burgess AP, Gruzelier JH (2003) Paradox lost? Exploring the role of alpha oscillations during externally vs. internally directed attention and the implications for idling and inhibition hypotheses. Int J Psychophysiol 47:65-74.

Crunelli V, Cope DW, Hughes SW (2006) Thalamic T-type Ca2+ channels and NREM sleep. Cell Calcium 40:175-190.

Csicsvari J, Hirase H, Czurko A, Mamiya A, Buzsaki G (1999) Fast network oscillations in the hippocampal CA1 region of the behaving rat. The Journal of neuroscience : the official journal of the Society for Neuroscience 19:RC20.

Cull-Candy SG, Leszkiewicz DN (2004) Role of distinct NMDA receptor subtypes at central synapses. Sci STKE 2004:re16.

Cunningham MO, Davies CH, Buhl EH, Kopell N, Whittington MA (2003) Gamma oscillations induced by kainate receptor activation in the entorhinal cortex in vitro. The Journal of neuroscience : the official journal of the Society for Neuroscience 23:9761-9769.

Cunningham MO, Whittington MA, Bibbig A, Roopun A, LeBeau FEN, Vogt A, Monyer H, Buhl EH, Traub RD (2004) A role for fast rhythmic bursting neurons in cortical gamma oscillations in vitro. Proceedings of the National Academy of Sciences of the United States of America 101:7152-7157.

da Costa NM, Martin KAC (2011) How Thalamus Connects to Spiny Stellate Cells in the Cat's Visual Cortex. The Journal of Neuroscience 31:2925-2937.

da Silva FH, van Lierop TH, Schrijer CF, van Leeuwen WS (1973a) Organization of thalamic and cortical alpha rhythms: spectra and coherences. Electroencephalogr Clin Neurophysiol 35:627-639.

da Silva FH, van Lierop TH, Schrijer CF, van Leeuwen WS (1973b) Essential differences between alpha rhythms and barbiturate spindles: spectra and thalamo-cortical coherences. Electroencephalogr Clin Neurophysiol 35:641-645.

Dai Y, Jordan LM (2010) Multiple Effects of Serotonin and Acetylcholine on Hyperpolarization-Activated Inward Current in Locomotor Activity-Related Neurons in Cfos-EGFP Mice. Journal of Neurophysiology 104:366-381.

Daria O, Dora H, Ole J (2008) Gamma Power Is Phase-Locked to Posterior Alpha Activity. PLoS ONE 3.

David F, Courtiol E, Buonviso N, Fourcaud-Trocmé N (2015) Competing mechanisms of gamma and beta oscillations in the olfactory bulb based on multimodal inhibition of mitral cells over a respiratory cycle. eneuro.

Delagrange P, Tadjer D, Bouyer JJ, Rougeul A, Conrath M (1989) Effect of DSP4, a neurotoxic agent, on attentive behaviour and related electrocortical activity in cat. Behav Brain Res 33:33-43.

Delcour AH, Lipscombe D, Tsien RW (1993) Multiple modes of N-type calcium channel activity distinguished by differences in gating kinetics. The Journal of neuroscience : the official journal of the Society for Neuroscience 13:181-194.

Dermietzel R (1998) Gap junction wiring: a 'new' principle in cell-to-cell communication in the nervous system? Brain Res Brain Res Rev 26:176-183.

Desimone R, Duncan J (1995) Neural mechanisms of selective visual attention. Annual review of neuroscience 18:193-222.

Destexhe A, McCormick DA, Sejnowski TJ (1993) A model for 8-10 Hz spindling in interconnected thalamic relay and reticularis neurons. Biophysical Journal 65:2473-2477.

Destexhe A, Bal T, McCormick DA, Sejnowski TJ (1996) Ionic mechanisms underlying synchronized oscillations and propagating waves in a model of ferret thalamic slices. J Neurophysiol 76:2049-2070.

Dietrich D, Beck H, Kral T, Clusmann H, Elger CE, Schramm J (1997) Metabotropic glutamate receptors modulate synaptic transmission in the perforant path: pharmacology and localization of two distinct receptors. Brain Res 767:220-227.

DiFrancesco MW, Holland SK, Szaflarski JP (2008) Simultaneous EEG/Functional Magnetic Resonance Imaging at 4 Tesla: Correlates of Brain Activity to Spontaneous Alpha Rhythm During Relaxation. Journal of clinical neurophysiology : official publication of the American Electroencephalographic Society 25:255-264.

Doesburg SM, Green JJ, McDonald JJ, Ward LM (2009) From local inhibition to long-range integration: a functional dissociation of alpha-band synchronization across cortical scales in visuospatial attention. Brain Res 1303:97-110.

Domino EF, Ni L, Thompson M, Zhang H, Shikata H, Fukai H, Sakaki T, Ohya I (2009) Tobacco Smoking Produces Widespread Dominant Brain Wave Alpha Frequency Increases. International journal of psychophysiology : official journal of the International Organization of Psychophysiology 74:192-198.

Edden RA, Crocetti D, Zhu H, Gilbert DL, Mostofsky SH (2012) Reduced GABA concentration in attention-deficit/hyperactivity disorder. Arch Gen Psychiatry 69:750-753.

Edgerton JR, Hanson JE, Günay C, Jaeger D (2010) Dendritic Sodium Channels Regulate Network Integration in Globus Pallidus Neurons: A Modeling Study. The Journal of Neuroscience 30:15146-15159.

Edgerton JR, Jaeger D (2011) Dendritic sodium channels promote active decorrelation and reduce phase locking to parkinsonian input oscillations in model globus pallidus neurons. The Journal of neuroscience : the official journal of the Society for Neuroscience 31:10919-10936.

Ergenoglu T, Demiralp T, Bayraktaroglu Z, Ergen M, Beydagi H, Uresin Y (2004) Alpha rhythm of the EEG modulates visual detection performance in humans. Brain Res Cogn Brain Res 20:376-383.

Erisir A, Harris JL (2003) Decline of the critical period of visual plasticity is concurrent with the reduction of NR2B subunit of the synaptic NMDA receptor in layer 4. The Journal of neuroscience : the official journal of the Society for Neuroscience 23:5208-5218.

Evans RH (1980) Evidence supporting the indirect depolarization of primary afferent terminals in the frog by excitatory amino acids. The Journal of physiology 298:25-35.

Feige B, Scheffler K, Esposito F, Di Salle F, Hennig J, Seifritz E (2005) Cortical and subcortical correlates of electroencephalographic alpha rhythm modulation. J Neurophysiol 93:2864-2872.

Feldman ML, Peters A (1978) The forms of non-pyramidal neurons in the visual cortex of the rat. The Journal of comparative neurology 179:761-793.

Feldmeyer D, Egger V, Lubke J, Sakmann B (1999) Reliable synaptic connections between pairs of excitatory layer 4 neurones within a single 'barrel' of developing rat somatosensory cortex. J Physiol-London 521:169-190.

Feldmeyer D, Lubke J, Silver RA, Sakmann B (2002) Synaptic connections between layer 4 spiny neurone-layer 2/3 pyramidal cell pairs in juvenile rat barrel cortex: physiology and anatomy of interlaminar signalling within a cortical column. J Physiol-London 538:803-822.

Fell J, Elfadil H, Roschke J, Burr W, Klaver P, Elger CE, Fernandez G (2002) Human scalp recorded sigma activity is modulated by slow EEG oscillations during deep sleep. Int J Neurosci 112:893-900.

Feng B, Tse HW, Skifter DA, Morley R, Jane DE, Monaghan DT (2004) Structure-activity analysis of a novel NR2C/NR2D-preferring NMDA receptor antagonist: 1-

(phenanthrene-2-carbonyl) piperazine-2,3-dicarboxylic acid. Br J Pharmacol 141:508-516.

Ferster D, Chung S, Wheat H (1996) Orientation selectivity of thalamic input to simple cells of cat visual cortex. Nature 380:249-252.

Feshchenko VA, Veselis RA, Reinsel RA (2004) Propofol-induced alpha rhythm. Neuropsychobiology 50:257-266.

Fingelkurts AA, Fingelkurts AA (2011) Persistent operational synchrony within brain default-mode network and self-processing operations in healthy subjects. Brain and Cognition 75:79-90.

Fingelkurts AA, Fingelkurts AA, Bagnato S, Boccagni C, Galardi G (2012) DMN Operational Synchrony Relates to Self-Consciousness: Evidence from Patients in Vegetative and Minimally Conscious States. Open Neuroimag J 6:55-68.

Fisahn A, Pike FG, Buhl EH, Paulsen O (1998) Cholinergic induction of network oscillations at 40 Hz in the hippocampus in vitro. Nature 394:186-189.

Fisahn A, Contractor A, Traub RD, Buhl EH, Heinemann SF, McBain CJ (2004) Distinct roles for the kainate receptor subunits GluR5 and GluR6 in kainate-induced hippocampal gamma oscillations. The Journal of neuroscience : the official journal of the Society for Neuroscience 24:9658-9668.

Fitzpatrick D, Itoh K, Diamond IT (1983) The laminar organization of the lateral geniculate body and the striate cortex in the squirrel monkey (Saimiri sciureus). The Journal of neuroscience : the official journal of the Society for Neuroscience 3:673-702.

Foehring RC, Waters RS (1991) Contributions of low-threshold calcium current and anomalous rectifier (Ih) to slow depolarizations underlying burst firing in human neocortical neurons in vitro. Neurosci Lett 124:17-21.

Fortier PA (2011) Effects of electrical coupling among layer 4 inhibitory interneurons on contrast-invariant orientation tuning. Experimental brain research 208:127-138.

Foulds J, McSorley K, Sneddon J, Feyerabend C, Jarvis M, Russell MH (1994) Effect of subcutaneous nicotine injections on EEG alpha frequency in non-smokers: a placebo-controlled pilot study. Psychopharmacology 115:163-166.

Foxe JJ, Simpson GV, Ahlfors SP (1998) Parieto-occipital approximately 10 Hz activity reflects anticipatory state of visual attention mechanisms. Neuroreport 9:3929-3933.

Foxe JJ, Snyder AC (2011) The Role of Alpha-Band Brain Oscillations as a Sensory Suppression Mechanism during Selective Attention. Frontiers in Psychology 2:154.

Freeman WJ (1978) Spatial properties of an EEG event in the olfactory bulb and cortex. Electroencephalography and Clinical Neurophysiology 44:586-605.

Freunberger R, Klimesch W, Griesmayr B, Sauseng P, Gruber W (2008) Alpha phase coupling reflects object recognition. NeuroImage 42:928-935.

Freyer F, Roberts JA, Becker R, Robinson PA, Ritter P, Breakspear M (2011) Biophysical mechanisms of multistability in resting-state cortical rhythms. The Journal of neuroscience : the official journal of the Society for Neuroscience 31:6353-6361.

Fries W, Distel H (1983) Large layer VI neurons of monkey striate cortex (Meynert cells) project to the superior colliculus. Proc R Soc Lond B Biol Sci 219:53-59.

Fries W (1985) Inputs from motor and premotor cortex to the superior colliculus of the macaque monkey. Behav Brain Res 18:95-105.

Fries P, Roelfsema PR, Engel AK, Konig P, Singer W (1997) Synchronization of oscillatory responses in visual cortex correlates with perception in interocular rivalry. Proc Natl Acad Sci U S A 94:12699-12704.

Fries P, Reynolds JH, Rorie AE, Desimone R (2001) Modulation of Oscillatory Neuronal Synchronization by Selective Visual Attention. Science 291:1560-1563.

Fries P (2005) A mechanism for cognitive dynamics: neuronal communication through neuronal coherence. Trends Cogn Sci 9:474-480.

Fries P, Womelsdorf T, Oostenveld R, Desimone R (2008) The Effects of Visual Stimulation and Selective Visual Attention on Rhythmic Neuronal Synchronization in Macaque Area V4. The Journal of Neuroscience 28:4823-4835.

Fukuda T, Kosaka T, Singer W, Galuske RAW (2006) Gap Junctions among Dendrites of Cortical GABAergic Neurons Establish a Dense and Widespread Intercolumnar Network. The Journal of Neuroscience 26:3434-3443.

Funkhouser EB (1915) THE VISUAL CORTEX, ITS LOCALIZATION, HISTOLOGICAL STRUCTURE, AND PHYSIOLOGICAL FUNCTION. J Exp Med 21:617-628.

Gastaut H (1974) Vom Berger-Rhythmus zum Alpha-Kult und zur Alpha-kultur. . Z EEG-EMG 5:189-199.

Gavornik JP, Bear MF (2014) Higher brain functions served by the lowly rodent primary visual cortex. Learning & memory (Cold Spring Harbor, NY) 21:527-533.

Gelety TJ, Burgess RJ, Drake ME, Jr., Ford CE, Brown ME (1985) Computerized spectral analysis of the interictal EEG in epilepsy. Clin Electroencephalogr 16:94-97.

Gennari F (1782) De Peculiari Structura Cerebri Parma Ex Regio Typographeo.

Gerrard JL, Burke SN, McNaughton BL, Barnes CA (2008) Sequence reactivation in the hippocampus is impaired in aged rats. The Journal of neuroscience : the official journal of the Society for Neuroscience 28:7883-7890.

Gibson JR, Beierlein M, Connors BW (1999) Two networks of electrically coupled inhibitory neurons in neocortex. Nature 402:75-79.

Gilbert CD, Wiesel TN (1983) Clustered intrinsic connections in cat visual cortex. The Journal of neuroscience : the official journal of the Society for Neuroscience 3:1116-1133.

Girman SV, Sauvé Y, Lund RD (1999) Receptive Field Properties of Single Neurons in Rat Primary Visual Cortex. Journal of Neurophysiology 82:301-311.

Gloveli T, Dugladze T, Rotstein HG, Traub RD, Monyer H, Heinemann U, Whittington MA, Kopell NJ (2005) Orthogonal arrangement of rhythm-generating microcircuits in the hippocampus. Proc Natl Acad Sci U S A 102:13295-13300.

Glykos V, Whittington MA, LeBeau FE (2015) Subregional differences in the generation of fast network oscillations in the rat medial prefrontal cortex (mPFC) in vitro. The Journal of physiology 593:3597-3615.

Goldman RI, Stern JM, Engel J, Jr., Cohen MS (2002) Simultaneous EEG and fMRI of the alpha rhythm. Neuroreport 13:2487-2492.

Gonchar Y, Burkhalter A (1997) Three distinct families of GABAergic neurons in rat visual cortex. Cerebral Cortex 7:347-358.

Gray CM, Singer W (1989) Stimulus-specific neuronal oscillations in orientation columns of cat visual cortex. Proc Natl Acad Sci U S A 86:1698-1702.

Griguoli M, Maul A, Nguyen C, Giorgetti A, Carloni P, Cherubini E (2010) Nicotine blocks the hyperpolarization-activated current Ih and severely impairs the oscillatory behavior of oriens-lacunosum moleculare interneurons. The Journal of neuroscience : the official journal of the Society for Neuroscience 30:10773-10783.

Gulyas AI, Miles R, Sik A, Toth K, Tamamaki N, Freund TF (1993) Hippocampal pyramidal cells excite inhibitory neurons through a single release site. Nature 366:683-687.

Güntekin B, Emek-Savaş DD, Kurt P, Yener GG, Başar E (2013) Beta oscillatory responses in healthy subjects and subjects with mild cognitive impairment. NeuroImage: Clinical 3:39-46.

Haegens S, Osipova D, Oostenveld R, Jensen O (2010) Somatosensory working memory performance in humans depends on both engagement and disengagement of regions in a distributed network. Hum Brain Mapp 31:26-35.

Haegens S, Handel BF, Jensen O (2011) Top-down controlled alpha band activity in somatosensory areas determines behavioral performance in a discrimination task. The Journal of neuroscience : the official journal of the Society for Neuroscience 31:5197-5204.

Haegens S, Cousijn H, Wallis G, Harrison PJ, Nobre AC (2014) Inter- and intra-individual variability in alpha peak frequency. NeuroImage 92:46-55.

Haegens S, Barczak A, Musacchia G, Lipton ML, Mehta AD, Lakatos P, Schroeder CE (2015) Laminar Profile and Physiology of the alpha Rhythm in Primary Visual, Auditory, and Somatosensory Regions of Neocortex. The Journal of neuroscience : the official journal of the Society for Neuroscience 35:14341-14352.

Haenschel C, Baldeweg T, Croft RJ, Whittington M, Gruzelier J (2000) Gamma and beta frequency oscillations in response to novel auditory stimuli: A comparison of human electroencephalogram (EEG) data with in vitro models. Proc Natl Acad Sci U S A 97:7645-7650.

Halliwell JV, Adams PR (1982) Voltage-clamp analysis of muscarinic excitation in hippocampal neurons. Brain Res 250:71-92.

Hanslmayr S, Aslan A, Staudigl T, Klimesch W, Herrmann CS, Bauml KH (2007) Prestimulus oscillations predict visual perception performance between and within subjects. NeuroImage 37:1465-1473.

Hanson JE, Smith Y, Jaeger D (2004) Sodium Channels and Dendritic Spike Initiation at Excitatory Synapses in Globus Pallidus Neurons. The Journal of Neuroscience 24:329-340.

Harkrider AW, Champlin CA (2001) Acute effect of nicotine on non-smokers: III. LLRs and EEGs. Hearing Research 160:99-110.

Harnett MT, Bernier BE, Ahn K-C, Morikawa H (2009) Burst Timing-Dependent Plasticity of NMDA Receptor-Mediated Transmission in Midbrain Dopamine Neurons. Neuron 62:826-838.

Harney SC, Jane DE, Anwyl R (2008) Extrasynaptic NR2D-Containing NMDARs Are Recruited to the Synapse during LTP of NMDAR-EPSCs. The Journal of Neuroscience 28:11685-11694.

Harris NC, Constanti A (1995) Mechanism of block by ZD 7288 of the hyperpolarization-activated inward rectifying current in guinea pig substantia nigra neurons in vitro. J Neurophysiol 74:2366-2378.

Hasselmo ME, Eichenbaum H (2005) Hippocampal mechanisms for the context-dependent retrieval of episodes. Neural Netw 18:1172-1190.

He C, Chen F, Li B, Hu Z (2014) Neurophysiology of HCN channels: from cellular functions to multiple regulations. Prog Neurobiol 112:1-23.

Heaulme M, Chambon JP, Leyris R, Molimard JC, Wermuth CG, Biziere K (1986) Biochemical characterization of the interaction of three pyridazinyl-GABA derivatives with the GABAA receptor site. Brain Res 384:224-231.

Hermens DF, Soei EXC, Clarke SD, Kohn MR, Gordon E, Williams LM (2005) Resting EEG theta activity predicts cognitive performance in attention-deficit hyperactivity disorder. Pediatric Neurology 32:248-256.

Honnuraiah S, Narayanan R (2013) A Calcium-Dependent Plasticity Rule for HCN Channels Maintains Activity Homeostasis and Stable Synaptic Learning. PLoS ONE 8:e55590.

Hu H, Ma Y, Agmon A (2011) Submillisecond Firing Synchrony between Different Subtypes of Cortical Interneurons Connected Chemically But Not Electrically. The Journal of Neuroscience 31:3351-3361.

Huang L, Keyser BM, Tagmose TM, Hansen JB, Taylor JT, Zhuang H, Zhang M, Ragsdale DS, Li M (2004) NNC 55-0396 [(1S,2S)-2-(2-(N-[(3-benzimidazol-2-yl)propyl]-N-methylamino)ethyl)-6-fluoro-1,2, 3,4-tetrahydro-1-isopropyl-2-naphtyl cyclopropanecarboxylate dihydrochloride]: a new selective inhibitor of T-type calcium channels. J Pharmacol Exp Ther 309:193-199.

Hubel DH, Wiesel TN (1962) Receptive fields, binocular interaction and functional architecture in the cat's visual cortex. The Journal of physiology 160:106-154.102.

Hubel DH, Weisel TN (1972) Laminar and columnar distribution of geniculo-cortical fibres in the macaque monkey. Journal of Computational Neurology 146:421-450.

Huber R, Ghilardi MF, Massimini M, Tononi G (2004) Local sleep and learning. Nature 430:78-81.

Huettel SA SAaMG (2014) Functional Magnetic Resonance Imaging, 3rd Edition. Sunderland, Massachusetts: Sinauer Associates.

Hughes SW, Cope DW, Crunelli V (1998) Dynamic clamp study of Ih modulation of burst firing and delta oscillations in thalamocortical neurons in vitro. Neuroscience 87:541-550.

Hughes SW, Lörincz M, Cope DW, Blethyn KL, Kékesi KA, Parri HR, Juhász G, Crunelli V (2004) Synchronized Oscillations at α and θ Frequencies in the Lateral Geniculate Nucleus. Neuron 42:253-268.

Hughes SW, Crunelli V (2005) Thalamic mechanisms of EEG alpha rhythms and their pathological implications. Neuroscientist 11:357-372.

Hughes SW, Errington A, Lőrincz ML, Kékesi KA, Juhász G, Orbán G, Cope DW, Crunelli V (2008) Novel modes of rhythmic burst firing at cognitively-relevant frequencies in thalamocortical neurons. Brain Research 1235:12-20.

Hughes SW, Lorincz ML, Blethyn K, Kekesi KA, Juhasz G, Turmaine M, Parnavelas JG, Crunelli V (2011) Thalamic Gap Junctions Control Local Neuronal Synchrony and Influence Macroscopic Oscillation Amplitude during EEG Alpha Rhythms. Front Psychol 2:193.

Hunt MJ, Raynaud B, Garcia R (2006) Ketamine dose-dependently induces high-frequency oscillations in the nucleus accumbens in freely moving rats. Biol Psychiatry 60:1206-1214.

İlhan B, VanRullen R (2012) No Counterpart of Visual Perceptual Echoes in the Auditory System. PLoS ONE 7:e49287.

Iragui VJ, McCutchen CB (1983) Physiologic and prognostic significance of "alpha coma". J Neurol Neurosurg Psychiatry 46:632-638.

Isaichev SA, Derevyankin VT, Koptelov Yu M, Sokolov EN (2001) Rhythmic alpha-activity generators in the human EEG. Neurosci Behav Physiol 31:49-53.

Isaichev SA, Osipova DS, Koptelov Iu M (2003) [Dipole models of alpha-rhythm generators]. Zh Vyssh Nerv Deiat Im I P Pavlova 53:577-586.

Iversen JR, Repp BH, Patel AD (2009) Top-down control of rhythm perception modulates early auditory responses. Ann N Y Acad Sci 1169:58-73.

Jacobs J (2014) Hippocampal theta oscillations are slower in humans than in rodents: implications for models of spatial navigation and memory. Philosophical Transactions of the Royal Society B: Biological Sciences 369:20130304.

Jahr CE, Stevens CF (1990) Voltage dependence of NMDA-activated macroscopic conductances predicted by single-channel kinetics. The Journal of neuroscience : the official journal of the Society for Neuroscience 10:3178-3182.

Jang HJ, Cho KH, Park SW, Kim MJ, Yoon SH, Rhie DJ (2012) Layer-specific serotonergic facilitation of IPSC in layer 2/3 pyramidal neurons of the visual cortex. J Neurophysiol 107:407-416.

Jann K, Kottlow M, Dierks T, Boesch C, Koenig T (2010) Topographic Electrophysiological Signatures of fMRI Resting State Networks. PLoS ONE 5:e12945.

Jensen O, Gelfand J, Kounios J, Lisman JE (2002) Oscillations in the Alpha Band (9–12 Hz) Increase with Memory Load during Retention in a Short-term Memory Task. Cerebral Cortex 12:877-882.

Jensen O, Kaiser J, Lachaux JP (2007) Human gamma-frequency oscillations associated with attention and memory. Trends in neurosciences 30:317-324.

Jensen O, Mazaheri A (2010) Shaping functional architecture by oscillatory alpha activity: gating by inhibition. Frontiers in human neuroscience 4.

Jensen O, Bonnefond M, VanRullen R (2012) An oscillatory mechanism for prioritizing salient unattended stimuli. Trends in Cognitive Sciences 16:200-206.

Jensen O, Bonnefond M, Marshall TR, Tiesinga P (2015) Oscillatory mechanisms of feedforward and feedback visual processing. Trends in neurosciences 38:192-194.

Jokeit H, Makeig S (1994) Different event-related patterns of gamma-band power in brain waves of fast- and slow-reacting subjects. Proceedings of the National Academy of Sciences of the United States of America 91:6339-6343.

Jones S, Pinto D, Kaper T, Kopell N (2000a) Alpha-Frequency Rhythms Desynchronize over Long Cortical Distances: A Modeling Study. Journal of computational neuroscience 9:271-291.

Jones SR, Pinto DJ, Kaper TJ, Kopell N (2000b) Alpha-frequency rhythms desynchronize over long cortical distances: a modeling study. Journal of computational neuroscience 9:271-291.

Jouvet M (1969) Biogenic amines and the states of sleep. Science 163:32-41.

Kaas JH, Huerta MF, Weber JT, Harting JK (1978) Patterns of retinal terminations and laminar organization of the lateral geniculate nucleus of primates. The Journal of comparative neurology 182:517-553.

Kanamori N (1993) Rhythmic slow waves of lateral geniculate nucleus in the cat: Relation to vigilance. International Journal of Neuroscience 68:117-122.

Kandel ER SJ, Jessell TM (2000) Principles of Neural Science,, 4th Edition. New York: McGraw-Hill,.

Kandler K, Katz LC (1998) Coordination of Neuronal Activity in Developing Visual Cortex by Gap Junction-Mediated Biochemical Communication. The Journal of Neuroscience 18:1419-1427.

Kasper EM, Lubke J, Larkman AU, Blakemore C (1994) Pyramidal neurons in layer 5 of the rat visual cortex. III. Differential maturation of axon targeting, dendritic

morphology, and electrophysiological properties. The Journal of comparative neurology 339:495-518.

Kelly SP, Gomez-Ramirez M, Foxe JJ (2009) The strength of anticipatory spatial biasing predicts target discrimination at attended locations: a high-density EEG study. The European journal of neuroscience 30:2224-2234.

Kemali D, Maj M, Iorio G, Marciano F, Nolfe G, Galderisi S, Salvati A (1985) Relationship between CSF noradrenaline levels, C-EEG indicators of activation and psychosis ratings in drug-free schizophrenic patients. Acta Psychiatr Scand 71:19-24.

Kidd FL, Isaac JTR (1999) Developmental and activity-dependent regulation of kainate receptors at thalamocortical synapses. Nature 400:569-573.

Kidd FL, Coumis U, Collingridge GL, Crabtree JW, Isaac JTR (2002) A presynaptic kainate receptor is involved in regulating the dynamic properties of thalamocortical synapses during development. Neuron 34:635-646.

Killian NJ, Buffalo EA (2014) Distinct frequencies mark the direction of cortical communication. Proceedings of the National Academy of Sciences 111:14316-14317.

Kleckner N, Dingledine R (1988) Requirement for glycine in activation of NMDA-receptors expressed in Xenopus oocytes. Science 241:835-837.

Klemm WR (1976) Physiological and behavioral significance of hippocampal rhythmic, slow activity ("theta rhythm"). Progress in Neurobiology 6, Part 1:23-47.

Klimesch W, Sauseng P, Hanslmayr S (2007) EEG alpha oscillations: the inhibition-timing hypothesis. Brain Res Rev 53:63-88.

Klimesch W, Fellinger R, Freunberger R (2011) Alpha oscillations and early stages of visual encoding. Front Psychol 2:118.

Klimesch W (2012) Alpha-band oscillations, attention, and controlled access to stored information. Trends in Cognitive Sciences 16:606-617.

Kloc M, Maffei A (2014) Target-specific properties of thalamocortical synapses onto layer 4 of mouse primary visual cortex. The Journal of neuroscience : the official journal of the Society for Neuroscience 34:15455-15465.

Kole MH, Hallermann S, Stuart GJ (2006) Single Ih channels in pyramidal neuron dendrites: properties, distribution, and impact on action potential output. The Journal of neuroscience : the official journal of the Society for Neuroscience 26:1677-1687.

Kopell N, Ermentrout GB, Whittington MA, Traub RD (2000) Gamma rhythms and beta rhythms have different synchronization properties. Proceedings of the National Academy of Sciences 97:1867-1872.

Kopell N, Kramer MA, Malerba P, Whittington MA (2010) Are different rhythms good for different functions? Frontiers in human neuroscience 4:187.

Kopell N, Whittington MA, Kramer MA (2011) Neuronal assembly dynamics in the beta1 frequency range permits short-term memory. Proceedings of the National Academy of Sciences 108:3779-3784.

Koshino Y, Niedermeyer E (1975) Enhancement of Rolandic mu-rhythm by pattern vision. Electroencephalography and Clinical Neurophysiology 38:535-538.

Kramer MA, Roopun AK, Carracedo LM, Traub RD, Whittington MA, Kopell NJ (2008) Rhythm generation through period concatenation in rat somatosensory cortex. PLoS Comput Biol 4:e1000169.

Krause CM, Pesonen M, Hamalainen H (2010) Brain oscillatory 4-30 Hz electroencephalogram responses in adolescents during a visual memory task. Neuroreport 21:767-771.

Lansbergen MM, Arns M, van Dongen-Boomsma M, Spronk D, Buitelaar JK (2011) The increase in theta/beta ratio on resting-state EEG in boys with attention-deficit/hyperactivity disorder is mediated by slow alpha peak frequency. Prog Neuropsychopharmacol Biol Psychiatry 35:47-52.

Larkum ME, Zhu JJ, Sakmann B (1999) A new cellular mechanism for coupling inputs arriving at different cortical layers. Nature 398:338-341.

Larkum ME, Waters J, Sakmann B, Helmchen F (2007) Dendritic spikes in apical dendrites of neocortical layer 2/3 pyramidal neurons. The Journal of neuroscience : the official journal of the Society for Neuroscience 27:8999-9008.

Lauri SE, Delany C, VR JC, Bortolotto ZA, Ornstein PL, J TRI, Collingridge GL (2001) Synaptic activation of a presynaptic kainate receptor facilitates AMPA receptor-mediated synaptic transmission at hippocampal mossy fibre synapses. Neuropharmacology 41:907-915.

Lauritzen TZ, Miller KD (2003) Different roles for simple-cell and complex-cell inhibition in V1. The Journal of neuroscience : the official journal of the Society for Neuroscience 23:10201-10213.

Lee JH, Durand R, Gradinaru V, Zhang F, Goshen I, Kim D-S, Fenno LE, Ramakrishnan C, Deisseroth K (2010) Global and local fMRI signals driven by neurons defined optogenetically by type and wiring. Nature 465:788-792.

Lee S, Sen K, Kopell N (2009) Cortical gamma rhythms modulate NMDAR-mediated spike timing dependent plasticity in a biophysical model. PLoS Comput Biol 5:e1000602.

Lee S, Kruglikov I, Huang ZJ, Fishell G, Rudy B (2013) A disinhibitory circuit mediates motor integration in the somatosensory cortex. Nat Neurosci 16:1662-1670.

Lehohla M, Kellaway L, Russell VA (2004) NMDA receptor function in the prefrontal cortex of a rat model for attention-deficit hyperactivity disorder. Metab Brain Dis 19:35-42.

Levelt CN, Hubener M (2012) Critical-period plasticity in the visual cortex. Annual review of neuroscience 35:309-330.

Levin ED, Conners CK, Sparrow E, Hinton SC, Erhardt D, Meck WH, Rose JE, March J (1996) Nicotine effects on adults with attention-deficit/hyperactivity disorder. Psychopharmacology (Berl) 123:55-63.

Levin ED, Conners CK, Silva D, Hinton SC, Meck WH, March J, Rose JE (1998) Transdermal nicotine effects on attention. Psychopharmacology (Berl) 140:135-141.

Li C, Guo Z, Wang Y, Li X, Henderson Z, Lu CB (2014) A model of synaptic plasticity: activation of mGluR I induced long-term theta oscillations in medial septal diagonal band of rat brain slice. Neurol Sci 35:551-557.

Liang H, Bressler SL, Buffalo EA, Desimone R, Fries P (2005) Empirical mode decomposition of field potentials from macaque V4 in visual spatial attention. Biological Cybernetics 92:380-392.

Lima PA, Marrion NV (2007) Mechanisms underlying activation of the slow AHP in rat hippocampal neurons. Brain Res 1150:74-82.

Livingstone MS HD (1988) Segregation of Form, Color, Movement, and Depth: Anatomy, Physiology, and Perception. Science 240:740-749.

Lopes Da Silva FH, Storm Van Leeuwen W (1977) The cortical source of the alpha rhythm. Neuroscience Letters 6:237-241.

Lopes da Silva FH, Vos JE, Mooibroek J, van Rotterdam A (1980) Relative contributions of intracortical and thalamo-cortical processes in the generation of alpha rhythms, revealed by partial coherence analysis. Electroencephalography and Clinical Neurophysiology 50:449-456.

Lopes da Silva F (1991) Neural mechanisms underlying brain waves: from neural membranes to networks. Electroencephalogr Clin Neurophysiol 79:81-93.

Lorincz A, Notomi T, Tamas G, Shigemoto R, Nusser Z (2002) Polarized and compartment-dependent distribution of HCN1 in pyramidal cell dendrites. Nat Neurosci 5:1185-1193.

Lörincz ML, Crunelli V, Hughes SW (2008) Cellular Dynamics of Cholinergically Induced α (8–13 Hz) Rhythms in Sensory Thalamic Nuclei In Vitro. The Journal of Neuroscience 28:660-671.

Lorincz ML, Kekesi KA, Juhasz G, Crunelli V, Hughes SW (2009) Temporal framing of thalamic relay-mode firing by phasic inhibition during the alpha rhythm. Neuron 63:683-696.

Lozano-Soldevilla D, ter Huurne N, Cools R, Jensen O (2014) GABAergic Modulation of Visual Gamma and Alpha Oscillations and Its Consequences for Working Memory Performance. Current Biology 24:2878-2887.

Ludwig J, Weseloh R, Karschin C, Liu Q, Netzer R, Engeland B, Stansfeld C, Pongs O (2000) Cloning and functional expression of rat eag2, a new member of the ether-a-go-go family of potassium channels and comparison of its distribution with that of eag1. Mol Cell Neurosci 16:59-70.

Lukashevich IP, Sazonova OB (1996) [The effect of lesions of different parts of the optic thalamus on the nature of the bioelectrical activity of the human brain]. Zh Vyssh Nerv Deiat Im I P Pavlova 46:866-874.

Lund JS (1973) Organization of neurons in the visual cortex, area 17, of

the monkey. J Comp Neurol I47:455-496.

Lund JS, Yoshioka T (1991) Local circuit neurons of macaque monkey striate cortex: III. Neurons of laminae 4B, 4A, and 3B. The Journal of comparative neurology 311:234-258.

Luthi A, McCormick DA (1998) H-current: properties of a neuronal and network pacemaker. Neuron 21:9-12.

Lynch G, Kessler M, Arai A, Larson J (1990) The nature and causes of hippocampal long-term potentiation. Prog Brain Res 83:233-250.

Lynch MA (2004) Long-term potentiation and memory. Physiol Rev 84:87-136.

MacKay WA, Mendonca AJ (1995) Field potential oscillatory bursts in parietal cortex before and during reach. Brain Res 704:167-174.

MacLean JN, Fenstermaker V, Watson BO, Yuste R (2006) A visual thalamocortical slice. Nat Meth 3:129-134.

MacLean MH, Arnell KM, Cote KA (2012) Resting EEG in alpha and beta bands predicts individual differences in attentional blink magnitude. Brain Cogn 78:218-229.

Magee JC, Carruth M (1999) Dendritic voltage-gated ion channels regulate the action potential firing mode of hippocampal CA1 pyramidal neurons. Journal of Neurophysiology 82:1895-1901.

Maier A, Adams GK, Aura C, Leopold DA (2010) Distinct superficial and deep laminar domains of activity in the visual cortex during rest and stimulation. Front Syst Neurosci 4.

Malenka RC, Nicoll RA (1993) NMDA-receptor-dependent synaptic plasticity: multiple forms and mechanisms. Trends in neurosciences 16:521-527.

Malinow R, Malenka RC (2002) AMPA receptor trafficking and synaptic plasticity. Annual review of neuroscience 25:103-126.

Mann EO, Kohl MM, Paulsen O (2009) Distinct roles of GABA(A) and GABA(B) receptors in balancing and terminating persistent cortical activity. The Journal of neuroscience : the official journal of the Society for Neuroscience 29:7513-7518.

Mathewson KE, Gratton G, Fabiani M, Beck DM, Ro T (2009) To see or not to see: prestimulus alpha phase predicts visual awareness. The Journal of neuroscience : the official journal of the Society for Neuroscience 29:2725-2732.

Mathewson KE, Lleras A, Beck DM, Fabiani M, Ro T, Gratton G (2011) Pulsed Out of Awareness: EEG Alpha oscillations represent a pulsed inhibition of ongoing cortical processing. Frontiers in Psychology 2.

Mathewson KJ, Jetha MK, Drmic IE, Bryson SE, Goldberg JO, Schmidt LA (2012) Regional EEG alpha power, coherence, and behavioral symptomatology in autism spectrum disorder. Clin Neurophysiol 123:1798-1809.

Matta JA, Ashby MC, Sanz-Clemente A, Roche KW, Isaac JTR (2011) mGluR5 and NMDA Receptors Drive the Experience- and Activity-Dependent NMDA Receptor NR2B to NR2A Subunit Switch. Neuron 70:339-351.

Maunsell JH, van Essen DC (1983) The connections of the middle temporal visual area (MT) and their relationship to a cortical hierarchy in the macaque monkey. The Journal of neuroscience : the official journal of the Society for Neuroscience 3:2563-2586.

Mazaheri A, Coffey-Corina S, Mangun GR, Bekker EM, Berry AS, Corbett BA (2010) Functional Disconnection of Frontal Cortex and Visual Cortex in Attention-Deficit/Hyperactivity Disorder. Biological Psychiatry 67:617-623.

Mazaheri A, Fassbender C, Coffey-Corina S, Hartanto TA, Schweitzer JB, Mangun GR (2014) Differential oscillatory electroencephalogram between attention-deficit/hyperactivity disorder subtypes and typically developing adolescents. Biol Psychiatry 76:422-429.

McCormick DA, Prince DA (1986) Acetylcholine induces burst firing in thalamic reticular neurones by activating a potassium conductance. Nature 319:402-405.

McCormick DA, Pape HC (1990) Noradrenergic and serotonergic modulation of a hyperpolarization-activated cation current in thalamic relay neurones. The Journal of physiology 431:319-342.

Meeuwissen EB, Takashima A, Fernandez G, Jensen O (2011) Increase in posterior alpha activity during rehearsal predicts successful long-term memory formation of word sequences. Hum Brain Mapp 32:2045-2053.

Melloni L, Molina C, Pena M, Torres D, Singer W, Rodriguez E (2007) Synchronization of neural activity across cortical areas correlates with conscious perception. The Journal of neuroscience : the official journal of the Society for Neuroscience 27:2858-2865.

Mellor J, Nicoll RA, Schmitz D (2002) Mediation of Hippocampal Mossy Fiber Long-Term Potentiation by Presynaptic Ih Channels. Science 295:143-147.

Melyan Z, Wheal HV, Lancaster B (2002) Metabotropic-mediated kainate receptor regulation of IsAHP and excitability in pyramidal cells. Neuron 34:107-114.

Middleton SJ, Racca C, Cunningham MO, Traub RD, Monyer H, Knopfel T, Schofield IS, Jenkins A, Whittington MA (2008) High-frequency network oscillations in cerebellar cortex. Neuron 58:763-774.

Momin A, Cadiou H, Mason A, McNaughton PA (2008) Role of the hyperpolarization-activated current Ih in somatosensory neurons. The Journal of physiology 586:5911-5929.

Monyer H, Sprengel R, Schoepfer R, Herb A, Higuchi M, Lomeli H, Burnashev N, Sakmann B, Seeburg PH (1992) Heteromeric NMDA receptors: molecular and functional distinction of subtypes. Science 256:1217-1221.

Moosmann M, Ritter P, Krastel I, Brink A, Thees S, Blankenburg F, Taskin B, Obrig H, Villringer A (2003) Correlates of alpha rhythm in functional magnetic resonance imaging and near infrared spectroscopy. NeuroImage 20:145-158.

More JC, Troop HM, Dolman NP, Jane DE (2003) Structural requirements for novel willardiine derivatives acting as AMPA and kainate receptor antagonists. Br J Pharmacol 138:1093-1100.

Muller D, Lynch G (1988) Long-term potentiation differentially affects two components of synaptic responses in hippocampus. Proceedings of the National Academy of Sciences of the United States of America 85:9346-9350.

Munoz A, Woods TM, Jones EG (1999) Laminar and cellular distribution of AMPA, kainate, and NMDA receptor subunits in monkey sensory-motor cortex. The Journal of comparative neurology 407:472-490.

Murthy VN, Fetz EE (1996) Oscillatory activity in sensorimotor cortex of awake monkeys: synchronization of local field potentials and relation to behavior. Journal of Neurophysiology 76:3949-3967.

Narayanan R, Johnston D (2010) The h Current Is a Candidate Mechanism for Regulating the Sliding Modification Threshold in a BCM-Like Synaptic Learning Rule. Journal of Neurophysiology 104:1020-1033.

Naruse Y, Matani A, Miyawaki Y, Okada M (2010) Influence of coherence between multiple cortical columns on alpha rhythm: a computational modeling study. Hum Brain Mapp 31:703-715.

Nauta WJH (1954) Terminal distribution of some afferent fiber systems in the cerebral cortex. Anat Rec 118,:333.

Nieldermeyer E (1993) Sleep and EEG. Electroencephalography: Basic Principles, 3rd Edition. Baltimore: Williams and Wilkins.

Nolan MF, Malleret G, Dudman JT, Buhl DL, Santoro B, Gibbs E, Vronskaya S, Buzsaki G, Siegelbaum SA, Kandel ER, Morozov A (2004) A behavioral role for dendritic integration: HCN1 channels constrain spatial memory and plasticity at inputs to distal dendrites of CA1 pyramidal neurons. Cell 119:719-732.

Nutt D, Wilson S, Lingford-Hughes A, Myers J, Papadopoulos A, Muthukumaraswamy S (2015) Differences between magnetoencephalographic (MEG) spectral profiles of drugs acting on GABA at synaptic and extrasynaptic sites: A study in healthy volunteers. Neuropharmacology 88:155-163.

Nyhus E, Curran T (2010) Functional Role of Gamma and Theta Oscillations in Episodic Memory. Neuroscience and biobehavioral reviews 34:1023-1035.

O'Keefe J, Recce ML (1993) Phase relationship between hippocampal place units and the EEG theta rhythm. Hippocampus 3:317-330.

Oberman LM, Hubbard EM, McCleery JP, Altschuler EL, Ramachandran VS, Pineda JA (2005) EEG evidence for mirror neuron dysfunction in autism spectrum disorders. Brain Res Cogn Brain Res 24:190-198.

Ohmoto T, Mimura Y, Baba Y, Miyamoto T, Matsumoto Y, Nishimoto A, Matsumoto K (1978) Thalamic Control of Spontaneous Alpha-Rhythm and Evoked Responses. Stereotactic and Functional Neurosurgery 41:188-192.

Oke OO, Magony A, Anver H, Ward PD, Jiruska P, Jefferys JG, Vreugdenhil M (2010) High-frequency gamma oscillations coexist with low-frequency gamma oscillations in the rat visual cortex in vitro. The European journal of neuroscience 31:1435-1445.

Olufsen MS, Whittington MA, Camperi M, Kopell N (2003) New roles for the gamma rhythm: population tuning and preprocessing for the Beta rhythm. Journal of computational neuroscience 14:33-54.

Onton J, Delorme A, Makeig S (2005) Frontal midline EEG dynamics during working memory. NeuroImage 27:341-356.

Palmer LM, Shai AS, Reeve JE, Anderson HL, Paulsen O, Larkum ME (2014) NMDA spikes enhance action potential generation during sensory input. Nat Neurosci 17:383-390.

Palva S, Palva JM (2007) New vistas for alpha-frequency band oscillations. Trends in neurosciences 30:150-158.

Palva S, Palva JM (2011) The functional roles of alpha-band phase synchronization in local and large-scale cortical networks. Frontiers in Psychology 2.

Pantev C, Makeig S, Hoke M, Galambos R, Hampson S, Gallen C (1991) Human auditory evoked gamma-band magnetic fields. Proc Natl Acad Sci U S A 88:8996-9000.

Park H, Rugg MD (2010) Prestimulus hippocampal activity predicts later recollection. Hippocampus 20:24-28.

Park W-M, Wang Y, Park S, Denisova JV, Fontes JD, Belousov AB (2011) Interplay of Chemical Neurotransmitters Regulates Developmental Increase in Electrical Synapses. The Journal of neuroscience : the official journal of the Society for Neuroscience 31:5909-5920.

Peng Y, Zhao J, Gu QH, Chen RQ, Xu Z, Yan JZ, Wang SH, Liu SY, Chen Z, Lu W (2010) Distinct trafficking and expression mechanisms underlie LTP and LTD of NMDA receptor-mediated synaptic responses. Hippocampus 20:646-658.

Peters A, Sethares C (1991) Organization of pyramidal neurons in area 17 of monkey visual cortex. The Journal of comparative neurology 306:1-23.

Petruno SK, Clark RE, Reinagel P (2013) Evidence That Primary Visual Cortex Is Required for Image, Orientation, and Motion Discrimination by Rats. PLoS ONE 8:e56543.

Pfeffer CK, Xue M, He M, Huang ZJ, Scanziani M (2013) Inhibition of inhibition in visual cortex: the logic of connections between molecularly distinct interneurons. Nat Neurosci 16:1068-1076.

Pfurtscheller G (1992) Event-related synchronization (ERS): an electrophysiological correlate of cortical areas at rest. Electroencephalogr Clin Neurophysiol 83:62-69.

Pfurtscheller G, Neuper C (1992) Simultaneous EEG 10 Hz desynchronization and 40 Hz synchronization during finger movements. Neuroreport 3:1057-1060.

Pfurtscheller G, Neuper C, Mohl W (1994) Event-related desynchronization (ERD) during visual processing. Int J Psychophysiol 16:147-153.

Pfurtscheller G, Stancák Jr A, Neuper C (1996) Event-related synchronization (ERS) in the alpha band — an electrophysiological correlate of cortical idling: A review. International Journal of Psychophysiology 24:39-46.

Pfurtscheller G, Neuper C, Andrew C, Edlinger G (1997) Foot and hand area mu rhythms. Int J Psychophysiol 26:121-135.

Piantoni G, Kline KA, Eagleman DM (2010) Beta oscillations correlate with the probability of perceiving rivalrous visual stimuli. Journal of Vision 10.

Pineda JA, Allison BZ, Vankov A (2000) The effects of self-movement, observation, and imagination on mu rhythms and readiness potentials (RP's): toward a brain-computer interface (BCI). IEEE Trans Rehabil Eng 8:219-222.

Poltavski DV, Petros T (2006) Effects of transdermal nicotine on attention in adult non-smokers with and without attentional deficits. Physiol Behav 87:614-624.

Potter AS, Newhouse PA (2004) Effects of acute nicotine administration on behavioral inhibition in adolescents with attention-deficit/hyperactivity disorder. Psychopharmacology (Berl) 176:182-194.

Pouille F, Scanziani M (2004) Routing of spike series by dynamic circuits in the hippocampus. Nature 429:717-723.

Proulx E, Piva M, Tian MK, Bailey CDC, Lambe EK (2014) Nicotinic acetylcholine receptors in attention circuitry: the role of layer VI neurons of prefrontal cortex. Cellular and Molecular Life Sciences 71:1225-1244.

Quentin R, Chanes L, Vernet M, Valero-Cabre A (2014) Fronto-Parietal Anatomical Connections Influence the Modulation of Conscious Visual Perception by High-Beta Frontal Oscillatory Activity. Cerebral cortex (New York, NY : 1991).

Raichle ME, MacLeod AM, Snyder AZ, Powers WJ, Gusnard DA, Shulman GL (2001) A default mode of brain function. Proceedings of the National Academy of Sciences 98:676-682.

Rebola N, Lujan R, Cunha RA, Mulle C (2008) Adenosine A2A receptors are essential for long-term potentiation of NMDA-EPSCs at hippocampal mossy fiber synapses. Neuron 57:121-134.

Rebola N, Srikumar BN, Mulle C (2010) Activity-dependent synaptic plasticity of NMDA receptors. The Journal of physiology 588:93-99.

Rekling JC, Shao XM, Feldman JL (2000) Electrical Coupling and Excitatory Synaptic Transmission between Rhythmogenic Respiratory Neurons in the PreBötzinger Complex. The Journal of neuroscience : the official journal of the Society for Neuroscience 20:RC113-RC113.

Reynolds JH, Chelazzi L, Desimone R (1999) Competitive mechanisms subserve attention in macaque areas V2 and V4. The Journal of neuroscience : the official journal of the Society for Neuroscience 19:1736-1753.

Richardson RJ, Blundon JA, Bayazitov IT, Zakharenko SS (2009) Connectivity patterns revealed by mapping of active inputs on dendrites of thalamorecipient neurons in the auditory cortex. The Journal of neuroscience : the official journal of the Society for Neuroscience 29:6406-6417.

Rockland KS, Pandya DN (1979) Laminar origins and terminations of cortical connections of the occipital lobe in the rhesus monkey. Brain Res 179:3-20.

Roelfsema PR, Engel AK, Konig P, Singer W (1997) Visuomotor integration is associated with zero time-lag synchronization among cortical areas. Nature 385:157-161.

Roopun AK, Middleton SJ, Cunningham MO, LeBeau FE, Bibbig A, Whittington MA, Traub RD (2006) A beta2-frequency (20-30 Hz) oscillation in nonsynaptic networks of somatosensory cortex. Proc Natl Acad Sci U S A 103:15646-15650.

Roopun AK, Kramer MA, Carracedo LM, Kaiser M, Davies CH, Traub RD, Kopell NJ, Whittington MA (2008) Period concatenation underlies interactions between gamma and beta rhythms in neocortex. Front Cell Neurosci 2:1.

Roopun AK, Lebeau FE, Rammell J, Cunningham MO, Traub RD, Whittington MA (2010) Cholinergic neuromodulation controls directed temporal communication in neocortex in vitro. Front Neural Circuits 4:8.

Rörig B, Sutor B (1996) Serotonin Regulates Gap Junction Coupling in the Developing Rat Somatosensory Cortex. European Journal of Neuroscience 8:1685-1695.

Rotstein HG, Pervouchine DD, Acker CD, Gillies MJ, White JA, Buhl EH, Whittington MA, Kopell N (2005) Slow and fast inhibition and an H-current interact to create a theta rhythm in a model of CA1 interneuron network. J Neurophysiol 94:1509-1518.

Rouach N, Segal M, Koulakoff A, Giaume C, Avignone E (2003) Carbenoxolone blockade of neuronal network activity in culture is not mediated by an action on gap junctions. The Journal of physiology 553:729-745.

Rougeul-Buser A, Buser P (1997) Rhythms in the alpha band in cats and their behavioural correlates. Int J Psychophysiol 26:191-203.

Rouhinen S, Panula J, Palva JM, Palva S (2013) Load dependence of beta and gamma oscillations predicts individual capacity of visual attention. The Journal of neuroscience : the official journal of the Society for Neuroscience 33:19023-19033.

Rowell JJ, Mallik AK, Dugas-Ford J, Ragsdale CW (2010) Molecular analysis of neocortical layer structure in the ferret. The Journal of comparative neurology 518:3272-3289.

Rudy B, Fishell G, Lee S, Hjerling-Leffler J (2011) Three groups of interneurons account for nearly 100% of neocortical GABAergic neurons. Developmental Neurobiology 71:45-61.

Saalmann YB, Pinsk MA, Wang L, Li X, Kastner S (2012) The pulvinar regulates information transmission between cortical areas based on attention demands. Science 337:753-756.

Saganich MJ, Vega-Saenz de Miera E, Nadal MS, Baker H, Coetzee WA, Rudy B (1999) Cloning of components of a novel subthreshold-activating K(+) channel with a unique pattern of expression in the cerebral cortex. The Journal of neuroscience : the official journal of the Society for Neuroscience 19:10789-10802.

Salmelin R, Hari R (1994) Characterization of spontaneous MEG rhythms in healthy adults. Electroencephalography and Clinical Neurophysiology 91:237-248.

Sanchez-Vives MV, McCormick DA (2000) Cellular and network mechanisms of rhythmic recurrent activity in neocortex. Nat Neurosci 3:1027-1034.

Sauseng P, Klimesch W, Heise KF, Gruber WR, Holz E, Karim AA, Glennon M, Gerloff C, Birbaumer N, Hummel FC (2009) Brain oscillatory substrates of visual short-term memory capacity. Curr Biol 19:1846-1852.

Sawtell NB, Frenkel MY, Philpot BD, Nakazawa K, Tonegawa S, Bear MF (2003) NMDA Receptor-Dependent Ocular Dominance Plasticity in Adult Visual Cortex. Neuron 38:977-985.

Schmiedt JT, Maier A, Fries P, Saunders RC, Leopold DA, Schmid MC (2014) Beta oscillation dynamics in extrastriate cortex after removal of primary visual cortex. The Journal of neuroscience : the official journal of the Society for Neuroscience 34:11857-11864.

Schoepfer R KT, Behe P, Colquhoun D, Stern P (1994) Single channel properties of recombinant NMDA receptors expressed in Xenopus oocytes. Soc Neurosci Abstr 20:309.302.

Schreckenberger M, Lange-Asschenfeldt C, Lochmann M, Mann K, Siessmeier T, Buchholz HG, Bartenstein P, Grunder G (2004) The thalamus as the generator and modulator of EEG alpha rhythm: a combined PET/EEG study with lorazepam challenge in humans. NeuroImage 22:637-644.

Schubert D, Kotter R, Zilles K, Luhmann HJ, Staiger JF (2003) Cell type-specific circuits of cortical layer IV spiny neurons. The Journal of neuroscience : the official journal of the Society for Neuroscience 23:2961-2970.

Schürmann M, Başar E (2001) Functional aspects of alpha oscillations in the EEG. International Journal of Psychophysiology 39:151-158.

Schwartz RD (1988) The GABAA receptor-gated ion channel: biochemical and pharmacological studies of structure and function. Biochem Pharmacol 37:3369-3375.

Sclocco R, Tana MG, Visani E, Gilioli I, Panzica F, Franceschetti S, Cerutti S, Bianchi AM (2014) EEG-informed fMRI analysis during a hand grip task: estimating the relationship between EEG rhythms and the BOLD signal. Frontiers in human neuroscience 8:186.

Sebban C, Tesolin-Decros B, Millan MJ, Spedding M (1999) Contrasting EEG profiles elicited by antipsychotic agents in the prefrontal cortex of the conscious rat: antagonism of

the effects of clozapine by modafinil. British Journal of Pharmacology 128:1055-1063.

Shadlen MN, Movshon JA (1999) Synchrony unbound: a critical evaluation of the temporal binding hypothesis. Neuron 24:67-77, 111-125.

Shaw JC (2003) Brain's Alpha Rhythms and the Mind. Amsterdam: Elsevier.

Shepherd JD, Huganir RL (2007) The cell biology of synaptic plasticity: AMPA receptor trafficking. Annu Rev Cell Dev Biol 23:613-643.

Silva L, Amitai Y, Connors B (1991) Intrinsic oscillations of neocortex generated by layer 5 pyramidal neurons. Science 251:432-435.

Singer W (1999) Neuronal synchrony: a versatile code for the definition of relations? Neuron 24:49-65, 111-125.

Sirota A, Buzsaki G (2005) Interaction between neocortical and hippocampal networks via slow oscillations. Thalamus & related systems 3:245-259.

Smith JW, Gastambide F, Gilmour G, Dix S, Foss J, Lloyd K, Malik N, Tricklebank M (2011) A comparison of the effects of ketamine and phencyclidine with other antagonists of the NMDA receptor in rodent assays of attention and working memory. Psychopharmacology (Berl) 217:255-269.

Sokoliuk R, VanRullen R (2013) The flickering wheel illusion: when alpha rhythms make a static wheel flicker. The Journal of neuroscience : the official journal of the Society for Neuroscience 33:13498-13504.

Spaak E, Bonnefond M, Maier A, Leopold David A, Jensen O (2012) Layer-Specific Entrainment of Gamma-Band Neural Activity by the Alpha Rhythm in Monkey Visual Cortex. Current Biology 22:2313-2318.

Springer S, Burkett B, Schrader L (2015) Modulation of BK channels contributes to activity-dependent increase of excitability through MTORC1 activity in CA1 pyramidal cells of mouse hippocampus. Frontiers in Cellular Neuroscience 8.

Staiger JF, Freund TF, Zilles K (1997) Interneurons Immunoreactive for Vasoactive Intestinal Polypeptide (VIP) are Extensively Innervated by Parvalbumin-Containing Boutons in Rat Primary Somatosensory Cortex. European Journal of Neuroscience 9:2259-2268.

Steriade M, Nunez A, Amzica F (1993a) A novel slow (< 1 Hz) oscillation of neocortical neurons in vivo: depolarizing and hyperpolarizing components. The Journal of neuroscience : the official journal of the Society for Neuroscience 13:3252-3265.

Steriade M, Nunez A, Amzica F (1993b) Intracellular analysis of relations between the slow (< 1 Hz) neocortical oscillation and other sleep rhythms of the electroencephalogram. The Journal of neuroscience : the official journal of the Society for Neuroscience 13:3266-3283.

Steriade M, Amzica F, Contreras D (1996) Synchronization of fast (30-40 Hz) spontaneous cortical rhythms during brain activation. The Journal of neuroscience : the official journal of the Society for Neuroscience 16:392-417.

Straub H, Lücke A, Köhling R, Moskopp D, Pohl M, Wassmann H, Speckmann EJ (1992) Low-magnesium-induced epileptiform activity in the human neocortex maintained in vitro: Suppression by the organic calcium antagonist verapamil. Journal of Epilepsy 5:166-170.

Supp GG, Siegel M, Hipp JF, Engel AK (2011) Cortical hypersynchrony predicts breakdown of sensory processing during loss of consciousness. Curr Biol 21:1988-1993.

Swanson LW (2004) Brain Maps: Structure of the Rat Brain, 3rd Edition: Elsevier.

Szurhaj W, Bourriez J-L, Kahane P, Chauvel P, Mauguière F, Derambure P (2005) Intracerebral study of gamma rhythm reactivity in the sensorimotor cortex. European Journal of Neuroscience 21:1223-1235.

Takeuchi A, Takeuchi N (1969) A study of the action of picrotoxin on the inhibitory neuromuscular junction of the crayfish. The Journal of physiology 205:377-391.

Takeuchi A, Onodera K (1972) Effect of bicuculline on the GABA receptor of the crayfish neuromuscular junction. Nat New Biol 236:55-56.

Tallon-Baudry C, Bertrand O, Peronnet F, Pernier J (1998) Induced gamma-band activity during the delay of a visual short-term memory task in humans. The Journal of neuroscience : the official journal of the Society for Neuroscience 18:4244-4254.

Tallon-Baudry C, Kreiter A, Bertrand O (1999) Sustained and transient oscillatory responses in the gamma and beta bands in a visual short-term memory task in humans. Vis Neurosci 16:449-459.

Tallon-Baudry C, Bertrand O, Fischer C (2001) Oscillatory synchrony between human extrastriate areas during visual short-term memory maintenance. The Journal of neuroscience : the official journal of the Society for Neuroscience 21:Rc177.

Tallon-Baudry C, Mandon S, Freiwald WA, Kreiter AK (2004) Oscillatory synchrony in the monkey temporal lobe correlates with performance in a visual short-term memory task. Cerebral cortex (New York, NY : 1991) 14:713-720.

Tallon-Baudry C, Bertrand O, Henaff MA, Isnard J, Fischer C (2005) Attention modulates gamma-band oscillations differently in the human lateral occipital cortex and fusiform gyrus. Cerebral cortex (New York, NY : 1991) 15:654-662.

Tatebayashi H, Ogata N (1992) Kinetic analysis of the GABAB-mediated inhibition of the high-threshold Ca2+ current in cultured rat sensory neurones. The Journal of physiology 447:391-407.

Taylor K, Mandon S, Freiwald WA, Kreiter AK (2005) Coherent oscillatory activity in monkey area v4 predicts successful allocation of attention. Cerebral cortex (New York, NY : 1991) 15:1424-1437.

ter Huurne N, Onnink M, Kan C, Franke B, Buitelaar J, Jensen O (2013) Behavioral consequences of aberrant alpha lateralization in attention-deficit/hyperactivity disorder. Biol Psychiatry 74:227-233.

Thilo W, Pascal F, Partha PM, Robert D (2006) Gamma-band synchronization in visual cortex predicts speed of change detection. Nature 439:733-736.

Tiitinen HT, Sinkkonen J, Reinikainen K, Alho K, Lavikainen J, Naatanen R (1993) Selective attention enhances the auditory 40-Hz transient response in humans. Nature 364:59-60.

Tovar KR, Maher BJ, Westbrook GL (2009) Direct Actions of Carbenoxolone on Synaptic Transmission and Neuronal Membrane Properties. Journal of Neurophysiology 102:974-978.

Traub RD, Whittington MA, Stanford IM, Jefferys JG (1996) A mechanism for generation of long-range synchronous fast oscillations in the cortex. Nature 383:621-624.

Traub RD, Schmitz D, Jefferys JG, Draguhn A (1999a) High-frequency population oscillations are predicted to occur in hippocampal pyramidal neuronal networks interconnected by axoaxonal gap junctions. Neuroscience 92:407-426.

Traub RD, Whittington MA, Buhl EH, Jefferys JG, Faulkner HJ (1999b) On the mechanism of the gamma --> beta frequency shift in neuronal oscillations induced in rat hippocampal slices by tetanic stimulation. The Journal of neuroscience : the official journal of the Society for Neuroscience 19:1088-1105.

Traub RD, Bibbig A, Fisahn A, LeBeau FE, Whittington MA, Buhl EH (2000) A model of gamma-frequency network oscillations induced in the rat CA3 region by carbachol in vitro. The European journal of neuroscience 12:4093-4106.

Traub RD, Whittington MA, Buhl EH, LeBeau FEN, Bibbig A, Boyd S, Cross H, Baldeweg T (2001) A Possible Role for Gap Junctions in Generation of Very Fast EEG Oscillations Preceding the Onset of, and Perhaps Initiating, Seizures. Epilepsia 42:153-170.

Traub RD, Draguhn A, Whittington MA, Baldeweg T, Bibbig A, Buhl EH, Schmitz D (2002) Axonal gap junctions between principal neurons: a novel source of network oscillations, and perhaps epileptogenesis. Rev Neurosci 13:1-30.

Traub RD, Buhl EH, Gloveli T, Whittington MA (2003) Fast rhythmic bursting can be induced in layer 2/3 cortical neurons by enhancing persistent Na+ conductance or by blocking BK channels. Journal of Neurophysiology 89:909-921.

Traub RD, Bibbig A, LeBeau FE, Buhl EH, Whittington MA (2004) Cellular mechanisms of neuronal population oscillations in the hippocampus in vitro. Annual review of neuroscience 27:247-278.

Traub RD, Middleton SJ, Knopfel T, Whittington MA (2008) Model of very fast (> 75 Hz) network oscillations generated by electrical coupling between the proximal axons of cerebellar Purkinje cells. The European journal of neuroscience 28:1603-1616.

Tsuchiya N, Koch C (2005) Continuous flash suppression reduces negative afterimages. Nat Neurosci 8:1096-1101.

Tuladhar AM, Huurne Nt, Schoffelen J-M, Maris E, Oostenveld R, Jensen O (2007) Parieto-occipital sources account for the increase in alpha activity with working memory load. Human Brain Mapping 28:785-792.

Turner RW, Maler L, Deerinck T, Levinson SR, Ellisman MH (1994) TTX-sensitive dendritic sodium channels underlie oscillatory discharge in a vertebrate sensory neuron. The Journal of neuroscience : the official journal of the Society for Neuroscience 14:6453-6471.

Uhlhaas PJ, Linden DE, Singer W, Haenschel C, Lindner M, Maurer K, Rodriguez E (2006) Dysfunctional long-range coordination of neural activity during Gestalt perception in schizophrenia. The Journal of neuroscience : the official journal of the Society for Neuroscience 26:8168-8175.

van Kerkoerle T, Self MW, Dagnino B, Gariel-Mathis M-A, Poort J, van der Togt C, Roelfsema PR (2014a) Alpha and gamma oscillations characterize feedback and feedforward processing in monkey visual cortex. Proceedings of the National Academy of Sciences 111:14332-14341.

van Kerkoerle T, Self MW, Dagnino B, Gariel-Mathis MA, Poort J, van der Togt C, Roelfsema PR (2014b) Alpha and gamma oscillations characterize feedback and feedforward processing in monkey visual cortex. Proc Natl Acad Sci U S A 111:14332-14341.

van Welie I, van Hooft JA, Wadman WJ (2004) Homeostatic scaling of neuronal excitability by synaptic modulation of somatic hyperpolarization-activated Ih channels. Proceedings of the National Academy of Sciences of the United States of America 101:5123-5128.

Vanderwolf CH (1969) Hippocampal electrical activity and voluntary movement in the rat. Electroencephalogr Clin Neurophysiol 26:407-418.

VanRullen R, Reddy L, Koch C (2005) Attention-driven discrete sampling of motion perception. Proc Natl Acad Sci U S A 102:5291-5296.

VanRullen R, Macdonald JS (2012) Perceptual echoes at 10 Hz in the human brain. Curr Biol 22:995-999.

Vessey JP, Lalonde MR, Mizan HA, Welch NC, Kelly MEM, Barnes S (2004) Carbenoxolone Inhibition of Voltage-Gated Ca Channels and Synaptic Transmission in the Retina. Journal of Neurophysiology 92:1252-1256.

Viaene AN, Petrof I, Sherman SM (2011a) Synaptic properties of thalamic input to the subgranular layers of primary somatosensory and auditory cortices in the mouse. The Journal of neuroscience : the official journal of the Society for Neuroscience 31:12738-12747.

Viaene AN, Petrof I, Sherman SM (2011b) Synaptic Properties of Thalamic Input to Layers 2/3 and 4 of Primary Somatosensory and Auditory Cortices. Journal of Neurophysiology 105:279-292.

Vijayan S, Kopell NJ (2012) Thalamic model of awake alpha oscillations and implications for stimulus processing. Proceedings of the National Academy of Sciences of the United States of America 109:18553-18558.

Vijayan S, ShiNung C, Purdon PL, Brown EN, Kopell NJ (2013a) Biophysical modeling of alpha rhythms during halothane-induced unconsciousness. In: Neural Engineering (NER), 2013 6th International IEEE/EMBS Conference on, pp 1104-1107.

Vijayan S, Ching S, Purdon PL, Brown EN, Kopell NJ (2013b) Thalamocortical Mechanisms for the Anteriorization of Alpha Rhythms during Propofol-Induced Unconsciousness. The Journal of Neuroscience 33:11070-11075.

Vollebregt MA, Zumer JM, Ter Huurne N, Castricum J, Buitelaar JK, Jensen O (2015) Lateralized modulation of posterior alpha oscillations in children. NeuroImage 123:245-252.

von Stein A, Rappelsberger P, Sarnthein J, Petsche H (1999) Synchronization Between Temporal and Parietal Cortex During Multimodal Object Processing in Man. Cerebral Cortex 9:137-150.

Vorobyov V, Kaptsov V, Kovalev G, Sengpiel F (2011) Effects of nootropics on the EEG in conscious rats and their modification by glutamatergic inhibitors. Brain Res Bull 85:123-132.

Voytek B, Canolty RT, Shestyuk A, Crone NE, Parvizi J, Knight RT (2010) Shifts in gamma phase-amplitude coupling frequency from theta to alpha over posterior cortex during visual tasks. Frontiers in human neuroscience 4:191.

Waldhauser GT, Johansson M, Hanslmayr S (2012) alpha/beta oscillations indicate inhibition of interfering visual memories. The Journal of neuroscience : the official journal of the Society for Neuroscience 32:1953-1961.

Wang D, Jacobs SA, Tsien JZ (2014) Targeting the NMDA receptor subunit NR2B for treating or preventing age-related memory decline. Expert Opin Ther Targets 18:1121-1130.

Watrous AJ, Lee DJ, Izadi A, Gurkoff GG, Shahlaie K, Ekstrom AD (2013) A comparative study of human and rat hippocampal low frequency oscillations during spatial navigation. Hippocampus 23:656-661.

Wesnes K, Warburton DM (1983) Smoking, nicotine and human performance. Pharmacol Ther 21:189-208.

Westenbroek RE, Hell JW, Warner C, Dubel SJ, Snutch TP, Catterall WA (1992) Biochemical properties and subcellular distribution of an N-type calcium channel alpha 1 subunit. Neuron 9:1099-1115.

White JA, Banks MI, Pearce RA, Kopell NJ (2000) Networks of interneurons with fast and slow gamma-aminobutyric acid type A (GABAA) kinetics provide substrate for mixed gamma-theta rhythm. Proc Natl Acad Sci U S A 97:8128-8133.

Whittington MA, Traub RD, Jefferys JGR (1995) Synchronized oscillations in interneuron networks driven by metabotropic glutamate receptor activation. Nature 373:612-615.

Whittington MA, Stanford IM, Colling SB, Jefferys JG, Traub RD (1997) Spatiotemporal patterns of gamma frequency oscillations tetanically induced in the rat hippocampal slice. The Journal of physiology 502 (Pt 3):591-607.

Whittington MA, Traub RD (2003) Interneuron diversity series: inhibitory interneurons and network oscillations in vitro. Trends in neurosciences 26:676-682.

Whittington MA, Cunningham MO, LeBeau FE, Racca C, Traub RD (2011) Multiple origins of the cortical gamma rhythm. Dev Neurobiol 71:92-106.

Williams K, Russell SL, Shen YM, Molinoff PB (1993) Developmental switch in the expression of NMDA receptors occurs in vivo and in vitro. Neuron 10:267-278.

Wilson TW, Franzen JD, Heinrichs-Graham E, White ML, Knott NL, Wetzel MW (2013) Broadband neurophysiological abnormalities in the medial prefrontal region of the default-mode network in adults with ADHD. Hum Brain Mapp 34:566-574.

Womelsdorf T, Schoffelen J-M, Oostenveld R, Singer W, Desimone R, Engel AK, Fries P (2007) Modulation of Neuronal Interactions Through Neuronal Synchronization. Science 316:1609-1612.

Wrobel A, Bekisz M, Kublik E, Waleszczyk W (1994) 20 Hz bursting beta activity in the cortico-thalamic system of visually attending cats. Acta neurobiologiae experimentalis 54:95-107.

Wrobel A, Ghazaryan A, Bekisz M, Bogdan W, Kaminski J (2007) Two streams of attention-dependent beta activity in the striate recipient zone of cat's lateral posterior-pulvinar complex. The Journal of neuroscience : the official journal of the Society for Neuroscience 27:2230-2240.

Wu N, Hsiao C-F, Chandler SH (2001) Membrane Resonance and Subthreshold Membrane Oscillations in Mesencephalic V Neurons: Participants in Burst Generation. The Journal of Neuroscience 21:3729-3739.

Wu N, Enomoto A, Tanaka S, Hsiao C-F, Nykamp DQ, Izhikevich E, Chandler SH (2005) Persistent Sodium Currents in Mesencephalic V Neurons Participate in Burst Generation and Control of Membrane Excitability. Journal of Neurophysiology 93:2710-2722.

Yabuta NH, Callaway EM (1998) Functional streams and local connections of layer 4C neurons in primary visual cortex of the macaque monkey. The Journal of neuroscience : the official journal of the Society for Neuroscience 18:9489-9499.

Zarrinpar A, Callaway EM (2014) Functional Local Input to Layer 5 Pyramidal Neurons in the Rat Visual Cortex. Cerebral cortex (New York, NY : 1991).

Zauner A, Fellinger R, Gross J, Hanslmayr S, Shapiro K, Gruber W, Müller S, Klimesch W (2012) Alpha entrainment is responsible for the attentional blink phenomenon. NeuroImage 63:674-686.

Zhou ZL, Cai SX, Whittemore ER, Konkoy CS, Espitia SA, Tran M, Rock DM, Coughenour LL, Hawkinson JE, Boxer PA, Bigge CF, Wise LD, Weber E, Woodward RM, Keana JF (1999) 4-Hydroxy-1-[2-(4-hydroxyphenoxy)ethyl]-4-(4-methylbenzyl)piperidine: a novel, potent, and selective NR1/2B NMDA receptor antagonist. J Med Chem 42:2993-3000.